HYDROCARBON-AIR FUEL CELL

Report No. 8

Contract No. DA 36-039 AMC-03743(E)

ARPA Order No. 247

Task No. 7900.21.903.01.00.

Semi-Annual Report No. 4, 1 July 1965 - 31 Dec. 1965

Electronic Components Laboratory

U.S. Army Electronics Command

Fort Monmouth, New Jersey

ESSO RESEARCH AND ENGINEERING COMPANY

PROCESS RESEARCH DIVISION

LINDEN, NEW JERSEY

PcRD-2MGR-66

HYDROCARBON-AIR FUEL CELL

REPORT NO. 8

CONTRACT NO. DA 36-039 AMC-03743(E)
ARPA ORDER NO. 247
TASK NO. 7900.21.903.01.00.

SEMI-ANNUAL REPORT NO. 4, 1 JULY 1965 - 31 DECEMBER 1965

OBJECT: CONDUCT INVESTIGATIONS LEADING TO THE DEVELOPMENT OF HYDROCARBON AND METHANOL FUEL CELLS

Authored by:

Carl E. Heath
Hugh H. Horowitz
Barry L. Tarmy
Charles E. Morrell
James A. Wilson
William J. Asher
Morton Beltzer
Barret Broyde
George Ciprios
I-Ming Feng
Martin Lieberman
John M. Matsen
Eugene H. Okrent
Joseph A. Shropshire
Herbert H. Vickers
Elliot A. Vogelfanger
Abraham A. Zimmerman

The work performed under this contract was made possible by the support of the Advanced Research Projects Agency under Order No. 247, through the U.S. Army Electronics Command.

Esso Research and Engineering Company
Process Research Division
Linden, New Jersey

BLANK PAGE

CONTENTS

CONTENTS

ILLUSTRATIONS

TABLES

APPENDIX ILLUSTRATIONS

APPENDIX TABLES

SECTION 1

PURPOSE

The purpose of these investigations is to perform research on the basic components of fuel cells using electrolyte-soluble carbonaceous fuels and fuel cells using hydrocarbon fuels. One objective, which is a continuation of the work carried out under contracts DA 36-039 SC-89156 and DA 36-039 AMC-00134(E), is to improve the performance of methanol-air fuel cells and to incorporate improved components into multicell batteries to study the engineering problems of multicell operation. A second objective is to determine the feasibility of hydrocarbon-air fuel cells.

The major emphasis of the program is on the simultaneous research and development on all basic aspects of the cells to optimize performance of the entire cell and to take into account interactions between components.

This work is aimed toward the development of practical fuel cells using hydrocarbons or their partially oxygenated derivatives as fuels and air as oxidant. The fuels must be capable of reacting to carbon dioxide, be reasonably available, and pose no unusual corrosion, toxicity, or handling problems. Also, the cell must use a CO_2-rejecting electrolyte and operate at temperatures up to about 200°C. Other desired requirements include high electrical output per unit volume and weight, high efficiency, long life, high reliability, reasonable cost, particularly catalyst cost, and ruggedness.

The program is divided into seven parts. These are referred to as Tasks A through G in this report. Tasks A and D describe studies of catalysis and structure at the hydrocarbon and methanol electrodes, respectively. Air electrode research is discussed in Task E. Task B includes work on the construction of a liquid hydrocarbon-air demonstration battery. Task F deals with work on establishing the basic methanol cell design, especially with regard to the operation of all components in a single cell. Task G is concerned with the development of a self-contained Methanol Fuel Cell Battery Demonstrator. Finally, Task C describes exploratory studies aimed at new approaches to fuel cells.

BLANK PAGE

SECTION 2

ABSTRACT

2.1 Task A, Hydrocarbon Electrode

Work on the direct hydrocarbon electrode has continued to concentrate on studies of mechanism, catalysis and structure, aimed at improving the utilization of platinum or finding non-noble substitutes for it.

The mechanism studies were based on the finding during the previous period that the adsorption of saturated hydrocarbons occurred only on one of the two types of sites on the surface of platinum. Researchers at Baylor University had reported that it was possible to vary the ratio of the two types of sites by electrodepositing platinum from solutions containing different amounts of lead acetate. However, attempts to repeat this here produced no obvious effects on the relative sizes of the hydrogen peaks corresponding to the two types of sites in voltammetric scans. The total number of sites did vary, and the amount of butane adsorbed varied correspondingly. The ratios of the hydrogen, oxygen and butane peaks on the different electrodeposited blacks changed in a complex manner, but no pronounced advantage was found for any of the catalysts. More work would have to be done to learn how to vary the two kinds of sites and what affect this would have on butane performance.

Butane adsorption measurements were also made in phosphoric acid at 140° to determine whether the higher temperatures might not lead to stronger adsorption. It was found that adsorbed butane did cover a higher fraction of the sites available to hydrogen at the higher temperature. It was also more difficult to desorb by cathodization than it was at 80-90°C. These results explain why butane has poorer open circuit values but higher limiting currents in hot phosphoric acid than in sulfuric acid at the lower temperature: the butane adsorbs more strongly at the higher temperature but blocks some of the sites otherwise available for water discharge. Measurements of actual adsorption rates in hot phosphoric acid have not yet been successful, however.

The program to improve the utilization of platinum by using a support made considerable progress during this period. Butane limiting currents as high as 40 ma per mg of platinum were achieved at 150°C using a support of carbon treated with silica. Platinum black or platinum on untreated carbon gave only about 8 ma/mg under the same conditions. Part of the improvement was due to the impregnation procedure, which involves adsorption by the carbon of a surprisingly small amount of the platinum in the impregnating solution. Another factor was the silica content of the carbon, which was optimum at ten percent. The surface area of the carbon was also important since adsorption is being relied upon to implant the platinum. A low surface area carbon yielded a low activity catalyst. When oxidized with CO_2, however, the surface area increased, the platinum uptake rose and the catalytic activity improved. Raising the operating temperature to 190° increased the limiting current to over 80 ma/mg of platinum. Overall a tenfold improvement has been achieved, thus making the outlook for this program bright.

Some work was also done on the structure or fabrication of platinum black electrodes for use on liquid hydrocarbons, although most of the effort available had to be devoted to preparation of a demonstration cell stack. Fuel transport through decane electrodes is a recurring problem. The rate of fuel transport was found to

be independent of the activity of the electrode, varied by changing the Teflon sintering conditions. Thus, it is hoped to be able to reduce fuel transport without adversely affecting performance. Another structure problem had to do with separation of the fuel side Teflon barrier used to prevent fuel flooding. This problem was solved by finding a means of laminating a 3.5 mil porous Teflon film to the electrode without collapsing the pores. Variability in the quality of Teflon emulsion is a structural problem which remains to be faced in the future.

The non-noble catalyst program featured alloys, oxides, carbides and steam reforming catalysts. The alloy program concentrated on the development of a method for producing high surface area metals, which were truly alloyed in the sense of having altered lattice spacings in their X-ray patterns. A chemical reduction technique was found to be unsatisfactory as were initial attempts at making Raney alloys. After extraction of the aluminum the residues were found to be mixtures of the unalloyed metals or their oxides. However, true high surface area alloys could be prepared by annealing the Raney alloy, before extraction, at a temperature at which the binary phase diagram indicates a solid solution or intermetallic compound, and then quenching in water to retain the alloy in a metastable condition. While some of the alloys are active with hydrogen, none so far has shown activity on hydrocarbons. The method, however, appears to be very promising for future use.

In the oxide program the work on perovskites has been concluded and attention has been directed toward the closely related tungsten bronzes. Perovskites containing nickel and cobalt had been rendered conductive via the incorporation of vacancies in the oxide positions of the lattice. This conductivity, however, was lost rapidly on acid treatment. By analogy with the conductivity of lithiated nickel oxide, it was concluded that the conductivity of oxide deficient perovskites was due to oxidized species such as Co^{+++} which are known to be much less stable than the divalent ions. Hence the rapid conductivity loss as the unstable ions are extracted. Elements with more stable higher valence states such as manganese and chromium would be expected to form perovskites whose conductivity was acid stable. This proved to be the case. A good combination of acid stability and corrosion resistance was obtained with chromium and manganese perovskites. However, no catalytic activity toward hydrogen, oxygen, or hydrocarbons could be detected.

An attempt was made, therefore, to use achieve conductivity using the lower-than-normal valence states of the element molybdenum. However, there is apparently too little overlap between molybdenum orbitals in the perovskite structure. Satisfactory conductivity was not achieved and the approach was dropped.

The bronzes, however, look much more promising. These materials, utilizing the lower valence states of tungsten in a perovskite-like structure, are very acid resistant and have metallic conductivity. Unmodified they have no catalytic activity. It has been found possible to incorporate nickel into them, with some sacrifice in conductivity and acid stability, but with generally with a good combination of properties. The X-ray diagrams of these materials were extremely complex, indicating both mixed bronze phases and impurities. Therefore, improved compositions or means of preparation will have to be developed before an accurate assessment of their potential is possible. So far they have shown no catalytic activity, but only Ni^{++} ions have been incorporated. These do not have the d-10 configuration, which appears desirable for catalytic activity.

Mixed transition metal carbides are being investigated as fuel cell catalysts because they are more metallic in nature than the oxides, are highly conductive and in certain cases are corrosion resistant. It was first verified that commercially available grinding tool carbides were not catalytic, and that some "H"

phase carbides available at the University of Pennsylvania, and other simple carbides were not corrosion resistant. However, the so-called eta carbides appeared much more interesting. These combine group V and VI metals, which yield acid resistant carbides, and the first row transition elements into single phase carbides. A purchased sample of nickel-tungsten-carbide proved to be very impure, but the nickel in the actual eta phase was resistant to acid. Various apparatus are being set up to custom make these compounds at the desired compositions, stoichiometries and degrees of purity. It appears that a vacuum-induction furnace with a water cooled shield will be required.

Some time ago a means was found for fabricating non-noble steam reforming catalysts into conductive electrodes. These were active with hydrogen fuel but not with hydrocarbons. It was hypothesized that the presence of the reactants in the liquid phase might have inhibited the steam reforming function of the catalyst. To test this hypothesis steam reforming runs were carried out non-electrochemically in a pressure reactor, where the reactants, hexane or decane and water, could be main-in the liquid phase. Appreciable activity was obtained, limited only by diffusion rates. Thus, the presence of the reactants in the liquid phase did not damage the electrochemical performance of the catalysts. The presence of ions or the lower pressure must have been responsible.

2.2 Task B, Hydrocarbon Fuel Cell

Total cell studies were conducted to assess the engineering feasibility and system requirements of a direct liquid fuel-air fuel cell system. A liquid decane-air fuel cell was constructed with sufficient capability to allow evaluation of anticipated problem areas related to fuel transport and carbon dioxide rejection in the electrolyte space.

Tests in small (10 cm^2) single and multicell units indicated that cathode cracking and anode barrier separation could limit stack life. However, this problem was solved by laminating porous Teflon film directly to the sintered platinum-Teflon electrodes. Satisfactory life and performance were thus obtained. Unfortunately, chemical oxidation and cathode deterioration due to decane transport was observed in some multicell units. In addition, the small cell tests indicated a need for improved electrolyte venting to minimize carbon dioxide buildup and reduce cell resistive losses. Despite these problems, performance levels were quite satisfactory yielding 17-21 mw/cm^2 and 14-17 mw/cm^2 on oxygen and air respectively.

Based upon the information developed in the small scale cell tests a large (80 cm^2) five cell liquid decane-air multicell assembly and operating system was designed and constructed. Initial oxygen performance with Cyanamid AA-1 cathodes laminated to porous Teflon film agreed with that obtained in small cells. However, air performance showed an 80 mv debit due to decane transport to the cathode and system life was limited. Improvements in performance and life were obtained by using laminated porous Teflon film on sintered platinum-Teflon anodes and cathodes. A three cell assembly with these improved components has been run for over 400 hours. This same three cell assembly was run on a wide boiling range isoparaffinic jet fuel, yielding only about one third the liquid decane activity.

2.3 Task C, New Systems

The new systems effort has concentrated on intermediate temperature and buffer electrolytes, catalysts for buffer electrolytes and the catalyst-electrolyte slurry system.

The intermediate temperature electrolytes examined were pyrophosphoric and molten bisulfate mixtures. Work with low catalyst content electrodes in pyrophosphoric acid at 275°C has shown that high catalyst utilizations can be obtained. Butane could sustain 200 ma/cm^2 at 0.44 volts polarized, and oxygen, 500 ma/cm^2 at 0.38 volts polarized, on electrodes containing 5 mg/cm^2 of platinum. These activities are considerably greater than that attained by the equivalent electrode structures in 85% phosphoric acid at 150°C. The usefulness of an electrolyte that can operate at higher temperatures as a means of effecting higher catalyst utilizations has thus been demonstrated. Electrodes of still lower catalyst content, 2.5 mg/cm^2, exhibited a disproportionate activity decrease due to structural problems. It is anticipated that when suitable low catalyst density electrode structures are available, still further catalyst utilizations will be obtained using pyrophosphoric acid.

Molten alkali metal bisulfate electrolytes were studied to ascertain whether a system operating in the same temperature range as pyrophosphoric, but not as corrosive, was available. Hydrocarbon and oxygen activities in this medium on massive platinum electrodes were considerably lower than that obtained in pyrophosphoric acid. In addition, the electrolyte was not invariant, losing SO_3 at high temperatures and generating H_2S at reducing potentials. Molten salt fuel cell electrolytes must have anions which equilibrate with non-volatile and non-reducible oxides.

Silver cathodes exhibit appreciable activity in carbonate solutions, but the activity decreases with decreasing pH. A study was carried out to determine whether a carbonate solution could be kept above its equilibrium pH value when used as the electrolyte in a fuel cell where CO_2 is an anodic oxidation product. It was shown that carbon dioxide rejection from a carbonate solution into a flowing gas stream, such as would be available in an air electrode, was too slow to prevent rapid carbonation and return to the equilibrium pH.

Silver-palladium oxide catalyzed electrodes exhibited considerable activity on methanol in potassium hydroxide and potassium carbonate solutions. Limiting currents over 2000 ma/cm^2 were observed. Even butane showed evidence of some activity at these highly alkaline pH values. Raney gold and gold alloys were also shown to have some methanol activity in potassium hydroxide.

Further work with the slurry electrode system has shown that considerable performance improvement could be achieved with decane fuel by increasing the ratio of electrode area to volume and by improving the flow pattern. However, while the current density of the electrode was very high, the specific current density in ma/mg of catalyst was still so low that it is doubtful that catalyst utilizations better than that achieved in static systems could be obtained.

2.4 Task D, Methanol Electrode

Studies on the methanol electrode were continued, concentrating on further establishing the degree of stability and reliability of the ruthenium modified P-type catalyst, and on determining whether catalyst supports could be used to improve catalyst utilization. Single cell and half cell testing of the catalyst was completed. Anodes were tested for as long as 11,000 hours with non-recoverable losses of only 15 mv. In addition, reversible performance losses in cell performance ranging from 10 to 50 mv were found. These were recoverable by open circuiting the cell, changing the electrolyte, and/or overpolarizing the anode in the absence of methanol to 0.8 to 0.9 volts. Storage would not impair performance. However, copper was found to be an undesirable contaminant.

New techniques were developed for employing supports to effect reductions in catalyst loadings. Both silica-on-carbon and boron carbide were tested as supports. Catalyst utilization using the silica-on-carbon support amounted to only 0.12 ma/mg at 0.35 volts polarization. Studies of the impaired performance indicated a need to develop new washing procedures. Catalyst utilizations of 4.7 ma/mg were obtained using boron carbide as a support. Increasing the reduction temperature improved performance, with the best utilization obtained with hydrogen reduction at 225°C. Further improvements may be possible through changes in procedures for making the catalyst.

2.5 Task E, Air Electrode

Testing has continued on the development of cathode structures for methanol cells that do not require membrane backings to prevent gross water transport. Experiments were carried out using cathodes that were spray-coated with Teflon on the air side, to evaluate the performance during extended operation, and the effects of scaling them to practical sizes. It was found that these coated electrodes, when not heat-treated, would operate for about 900 hours with unimpaired performance. Furthermore, large 7.5 inch diameter electrodes could be prepared with performances comparable to the smaller 1 inch diameter electrodes. However, the electrodes leak electrolyte at small, but still unacceptably high, rates. As an alternative approach, sodium alginate was evaluated as a membrane substitute. Its performance in small electrodes was at least comparable to the conventional cathode. But scaled-up electrodes were 0.1 volt more polarized and also leaked. Thus, more work remains.

Research was also carried out on cathodes suitable for use in the hydrocarbon cell at 150°C in 14.7 M phosphoric acid. Several cathodes were developed. These included 50 and 10 mg/cm^2 sintered platinum-Teflon electrodes laminated to 3.5 mil porous Teflon films, and a carbon supported cathode containing 2.5 mg/cm^2 platinum. The electrode with the highest catalyst loading was polarized only 0.30 volt at 100 ma/cm^2. The 10 and 2.5 mg/cm^2 cathodes exhibit additional 70 and 160 mv polarizations, respectively. In addition, a high performance cathode using the silica-on-carbon support and containing only 1 mg/cm^2 of platinum presently is under test. This electrode exhibits over four times the catalyst utilization of the above mentioned electrodes.

2.6 Task F, Methanol Fuel Cell

Because of the high chemical oxidation rates occurring at the cathode in the 9" x 5-3/4" cells, further studies were carried out on techniques for reducing this loss. Dacron felt and Permaplex C-20 membrane barriers, installed between the electrodes in 4" x 4" half-cells and total cells, were found to substantially reduce chemical oxidation at the cathode. Performance was also improved. However, no improvements were obtained in the 9" x 5-3/4" cells using the same techniques. Baffling the anode chamber and the use of multiple injection ports were also tested in the 9" x 5-3/4" cell because this cell was not able to operate at low methanol concentrations at performance comparable to those obtained in 4" x 4" cells. However, no significant improvements were obtained.

A simplified cell was also tested using a wicking system to supply fuel, and natural breathing to supply air. The cell operated virtually unattended for 3000 hours. Thus, simplified cell operation without electrolyte circulation is feasible.

2.7 Task G, Prototype Development

A self-contained Methanol Fuel Cell Battery Demonstrator was designed, constructed, and tested briefly prior to delivery to the U.S. Army Electronics Command. Miniaturized, automatically controlled devices were developed to provide the essential auxiliary facilities required by the fuel cell module, with low parasitic power consumption. These include a corrosion-free high output pump for circulating sulfuric acid electrolyte, a low pressure drop system for supplying ambient air, facilities to provide adequate heat removal and recovery of product water and a simple acid concentration detector and controller. Also included was a methanol concentration controller to ensure an optimum addition rate of methanol. Power levels of about 80 watts at 6.0 volts regulated output were obtained during initial short-term testing of the integrated system. Subsequent testing of the fully-assembled Demonstrator gave power levels of 65 watts, but performance was not consistent, due to instability of the methanol control system.

SECTION 3

PUBLICATIONS, LECTURES, REPORTS, AND CONFERENCES

3.1 Lectures

Tarmy, B. L. and Ciprios, G. - The Methanol Fuel Cell Battery--International Conference on Energetics, Rochester, New York, August 20, 1965.

Shropshire, J. A., Okrent, E. H., and Horowitz, H. H. - Limiting Processes at Hydrocarbon Electrodes--Symposium on Hydrocarbon Air Fuel Cells at the 150th Meeting of the American Chemical Society, Atlantic City, New Jersey, September 12-15, 1965.

Okrent, E. H., and Tarmy, B. L. - Heat and Water Balancing of the Methanol-Air Fuel Cell--Fuel Cell Systems and Processes Symposium, Fifty-Eighth National Meeting of the American Institute of Chemical Engineers, Philadelphia, Pennsylvania, December 7, 1965.

3.2 Conferences

July 9, 1965 - Linden, New Jersey

Organizations represented: United States Army Electronics Command
Esso Research and Engineering Company

The meeting was a general review of program and plans for the methanol-air and hydrocarbon-air fuel cells.

August 4, 1965 - Fort Monmouth, New Jersey

Organizations represented: United States Army Electronics Command
Esso Research and Engineering Company

Specific areas of methanol-air and hydrocarbon-air fuel cell programs were reviewed.

September 24, 1965 - Linden, New Jersey

Organizations represented: United States Army Electronics Command
Esso Research and Engineering Company

Specific areas of methanol-air and hydrocarbon-air fuel cell programs were discussed.

November 19, 1965 - Linden, New Jersey

Organizations represented: United States Army Electronics Command
Esso Research and Engineering Company

Specific areas of methanol-air and hydrocarbon-air fuel cell programs were discussed.

3.3 Reports

This report is written in conformance with the detailed reporting requirements as presented in the Signal Corps Technical Requirement on Technical Reports (SCL-2101P, 18 February 1963) under the terms of our contract; these requirements differ from the usual requirements for reports issued within Esso Research and Engineering Company.

3.4 Publications

Shropshire, J. A., Okrent, E. H., and Horowitz, H. H. - Limiting Processes at Hydrocarbon Electrodes--Hydrocarbon Fuel Cell Technology, B. S. Baker, Ed., Academic Press, New York (1965) p. 539.

Tarmy, B. L. and Ciprios, G. - The Methanol Fuel Cell Battery--Engineering Developments in Energy Conversion, American Society of Mechanical Engineers, New York, 1965, p. 272.

SECTION 4

FACTUAL DATA

4.1 Task A, Hydrocarbon Electrode

The goals of the hydrocarbon electrode program remain as they were in the previous reporting period: to reduce the cost and increase the availability of the catalyst by increasing the utilization of platinum or by substituting a non-noble metal. The programs are thus divided into these two areas.

The platinum utilization problem is being approached through both long range mechanistic studies and direct short range catalyst modifications. Efforts in the former area concentrated on the extension of the chemisorption rate measurements which had led to the "two site" theory of platinum catalysis. Attempts were made to modify the nature and amounts of the two types of sites, and thereby affect electrocatalytic activity. The adsorption measurement techniques were also applied to phosphoric acid electrolyte at temperatures above 100°C, whereas they had previously been carried out only in 3.7 M sulfuric acid below 100°C. Results obtained previously indicated that at 80° to 100°C chemisorption would be rate controlling in the limiting current region, but not in the voltage sensitive or Tafel region. However, the energies of activation of the adsorption and electrocatalytic processes suggested that at higher temperatures the adsorption process would be rate determining in both regions.

The direct efforts to improve platinum utilization centered around the use of a carbon support. The advantageous use of silica as a co-support was developed further. When the surface area or porosity of the carbon was found to influence performance it was investigated. The effect of temperature variations were determined. Some electrode structure work involving the wetproofing technique was carried out, although most of the effort in this area was devoted to the preparation of a demonstration hydrocarbon-air cell stack (see Task B).

Research in the non-noble catalyst area is an extension of the previous work with some modification. Attention shifted from the conventional perovskites to modified tungsten oxide bronzes. These also possess the perovskite crystal structure, but due to an overlap of partially filled metal ion orbitals, possess a far superior combination of conductivity and acid resistance. The aim of the present studies was to determine whether catalytic metals could be incorporated into the bronzes with retention of their favorable properties. The alloy program now deals only with high surface area materials formed by a Raney technique. X-ray analysis has been used to determine whether alloys are actually formed by this procedure. Studies have been carried out to determine how to modify the Raney preparation technique to insure alloy formation. Metals chosen according to the principles previously outlined have been evaluated for catalytic activity. In addition, the silver-palladium noble metal system has been investigated. Finally, the investigation of mixed carbides has begun in the hope of combining the good conductivity and corrosion resistance properties of the Group IV and V carbides with the catalytic properties of the Group VIII metals.

Phase 1 - Modification of Two Types of Platinum Sites

As discussed in the previous report (7), the adsorption of butane on commercial platinum black in 3.7 M sulfuric acid is strongly indicated to occur only on about 50% of the catalyst surface, and based on the known differentiation of the

platinum surface with respect to hydrogen adsorption-discharge, the butane adsorption has been postulated to occur on a particular type of (hydrogen) site. As an extension and test of this concept, it would be very desirable to obtain a means by which the number and ratio of the two types of sites on the platinum surface could be varied in a consistent manner and the concomitant adsorption-oxidation of butane studied. Such a variation in the ratio of Type I to Type II hydrogen sites has been mentioned in publications by Franklin(8) and Will(9). Will obtained variations by cutting and polishing different faces of single crystals of platinum. Franklin produced different high surface area blacks by a variation in the current density and lead acetate concentration during the electrodeposition of platinum.

Following the latter lead, a brief study of the effect of potential and lead acetate concentration on the nature of platinum deposits was made and butane adsorption investigated on those deposits showing the most chance of alteration.

Part a - Effect of Platinizing Conditions on Subsequent Catalyst Deposits

A desirable range of platinization conditions was established by qualitative evaluation of voltage scans on nine electrodes prepared with 3% H_2PtCl_6 solution with a 100-fold variation in $Pb(Ac)_2$ concentration and 0.2 volt variation in deposition potential (0.04, 0.4, 4.0% $Pb(Ac)_2$; -0.25, -0.15, -0.05 volts vs S.C.E. 25°C). The highest lead concentration produced platinum deposits of low area with distorted voltage scans, probably indicating the presence of significant lead in the deposit. Most noticeable effects on catalyst area, in terms of oxide reduction peak, were found in the sample at 0.4% $Pb(Ac)_2$. Potential of deposition and, correspondingly, current density, appeared to have minor effects. On this basis, a closer look was taken at deposits produced at -0.15 volts vs S.C.E. with $Pb(Ac)_2$ concentration in 0.2% intervals in the range 0-1%. Electrodes were deposited on a total of 1/4 cm^2 platinum (sealed in glass) at a platinization level of 1 mg/cm^2. Voltage scans on the electrodeposited samples were run at 95°C in 3.7 M sulfuric acid from -0.15 v to 1.3 v vs S.C.E.

As shown in Figure A-1 and Appendix A-1 the surface area (in terms of oxide millicoulombs) varied widely over the range tested, going smoothly through a maximum area at about 0.5% $Pb(Ac)_2$ concentration. Even at the maximum level, however, the area, in mc oxide/mg, was only about equal to that found for typical commercial Pt blacks prepared by chemical methods. The ratio of total chemisorbed H· to oxide for most of these samples appears lower than that found for chemical blacks with a typical value of 0.38 mc H·/mc oxide at the lower surface areas (Appendix A-1). Unfortunately, uncertainty in distinguishing the dividing line between Type I and Type II hydrogen peaks on these samples made it appear undesirable to attempt to integrate the individual peaks. No obviously large differences in the appearance of the peaks with varying $Pb(Ac)_2$ concentration were observed, however.

Figure A-1

Effect of $Pb(Ac)_2$ on Surface Area

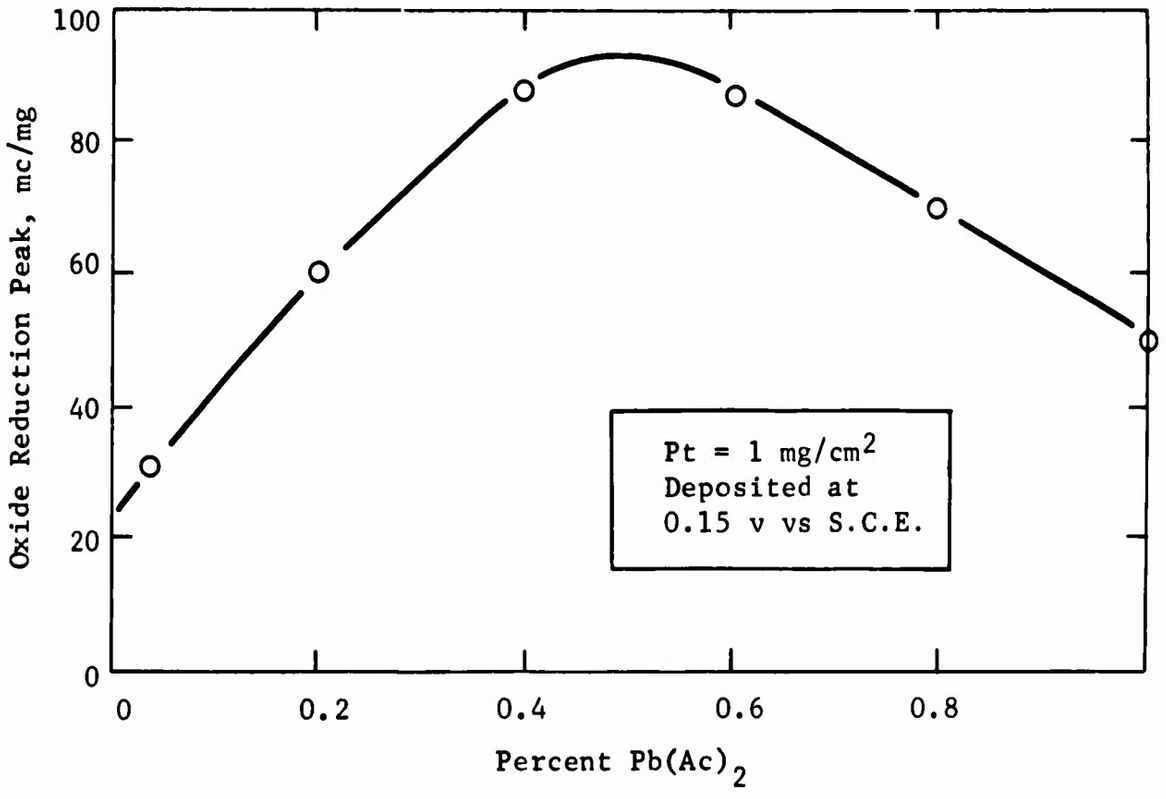

Part b - Adsorption of Butane on Electrodeposited Pt Samples

The series of electrodeposited platinum samples was investigated for saturation butane adsorption using the technique discussed in a previous report (6). Electrolyte wetted electrodes were held in vapor phase butane above a 3.7 M sulfuric acid solution saturated with the fuel at 95°C. The tip of the electrode was allowed to touch the solution in order to maintain potentiostatic control of the electrode during adsorption. Following a sixty minute exposure, electrodes were fully immersed and scanned from 0-1.3 v vs S.C.E. to obtain coulombs of fuel on the electrode and a measurement of oxide reduction peak area.

As shown in Appendix A-1 the ratios of millicoulombs of fuel at saturation to oxide millicoulombs for these samples were somewhat scattered within the extremes of 0.6 to 1.6. In contrast, previous experience with chemically prepared Pt blacks indicated a ratio of 1.58 $\pm$ 0.13 for thirteen samples (6). The present variation of the butane coverage could be explained in terms of millicoulombs of H· adsorbed on the various samples. Thus, as shown in Figure A-2, the total millicoulombs of fuel adsorbed correlated fairly well with total millicoulombs of H· found on the blank electrodes. The intercept on the abscissa suggests that a certain initial part of the electrodeposited material may not be effective for butane adsorption.

The slope of the mc fuel vs mc H· plot has a value of about 5 mc butane/mc total H·. This value is considerably higher than that found for commercial Pt black (e.g., 3.3 mc butane/mc total H·) and suggests considerably higher coverage with fuel than previously deduced for commercial Pt if we use the same assumptions (i.e., 26 electron fuel oxidation and 4 H· displaced per butane molecule).

Figure A-2

Fuel Adsorption Related To Total H·

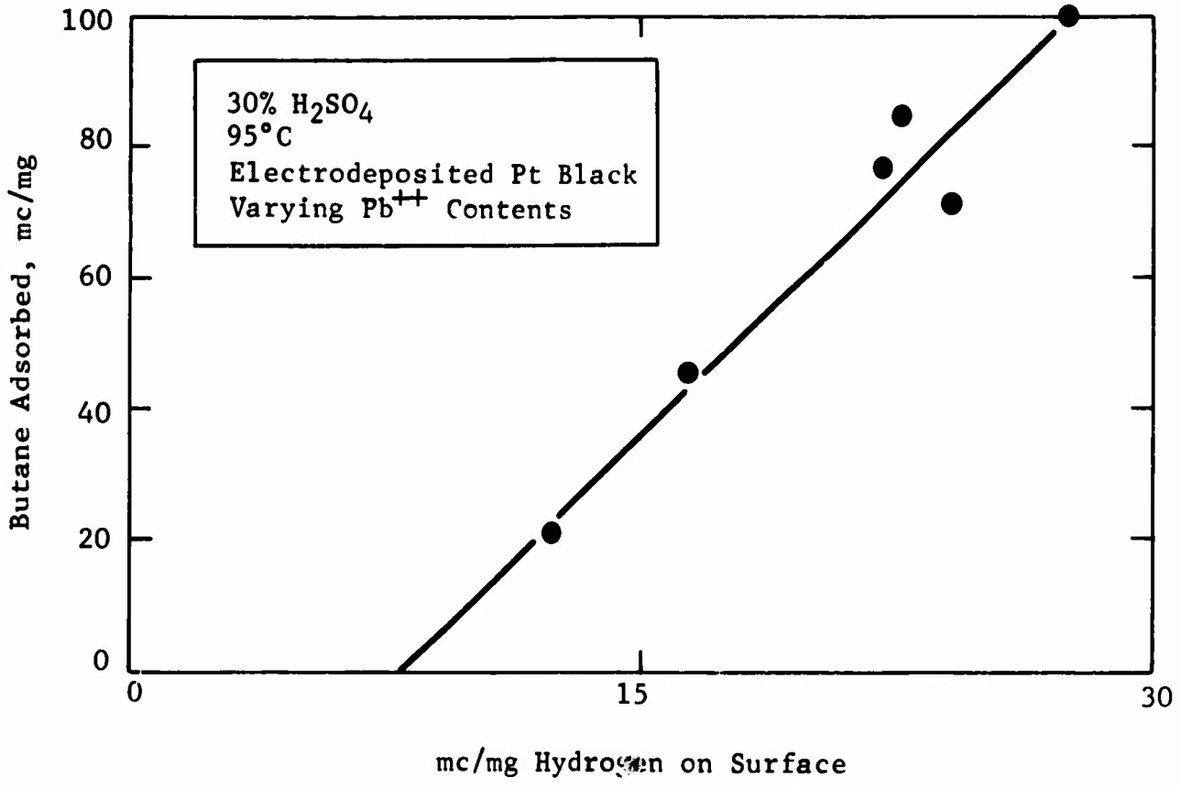

From the correlation with total H·, however, it does not appear that a variation in the ratio of sites has been effected by these techniques. Further studies will be necessary to determine if other variations in electrodeposition technique actually give the variations suggested by Franklin.

Phase 2 - Adsorption of Butane on Platinum Black in H_3PO_4 Solutions

It was pointed out in the previous report (7) that preliminary studies of butane adsorption on platinum black in H_3PO_4 solutions indicated behavior which differed significantly from that observed in H_2SO_4 solution. Since operation of practical hydrocarbon cells may necessitate the use of such high temperature electrolytes it seemed essential to extend the studies of fuel adsorption to H_3PO_4 electrolyte at temperatures in the range of 130 to 150°C. Studies were, therefore, carried out to define the equilibrium properties of the adsorption and desorption of butane on commercial platinum black under those and similar conditions, with an

eye to comparisons and contrasts with the previously discussed H_2SO_4 system. Equipment and procedures were the same as those described previously for obtaining equilibrium adsorption of butane in the H_2SO_4 system. Electrodes were 50 mg of Engelhard commercial platinum black mixed with 5 mg of Teflon 41 BX emulsion (du Pont) and pressed on smooth platinum flags.

Part a - Equilibrium Adsorption-Desorption of Butane on Platinum in 14.7 M H_3PO_4

Several experiments were carried out to define the saturation quantity of butane (in coulombs) on the platinum catalyst at equilibrium at 140°C. The saturation value in terms of Q_F/Q_o (millicoulombs fuel/mc oxide) was found to be 1.71 $\pm$.06 for seven samples at the 140°C level (Appendix A-2). The ratio of mc H·/mc oxide at 140°C used as a standardizing factor, however, varies in this system from that found in 3.7 M H_2SO_4 at 80-90°C. For the existing factor, $Q_H/Q_o(1.3) = 0.37$ at 140°C, saturation thus corresponds to $Q_F/Q_H \cong 4.62$.

If one assumes that butane displaces four H· as previously found in the H_2SO_4 system, the corresponding saturation coverage of platinum with butane in 14.7 M H_3PO_4 at 140°C is found to be $\sim$ 71% rather than the $\sim$ 50% of the (hydrogen available) surface found in H_2SO_4 solutions. Following our previous line of reasoning (7), it appears possible that butane in H_3PO_4 covers a significant quantity of Type I as well as Type II sites, possibly due to weaker solvent (anion) effects at the platinum surface in this system. It is possible that this higher coverage obscures too many (Type I) water discharge sites and results in the normally higher polarization observed for butane operation in H_3PO_4 electrolyte over that in H_2SO_4 systems (despite the temperature differential) (5)(6)(7).

Part b - Desorption in H_3PO_4 Systems

It was pointed out in the previous report (7) that butane adsorbed on commercial platinum black was rapidly desorbed as the electrode potential was moved cathodically into the region of Type I H· formation. Thus, 80% of complete desorption (from a saturation level) was accomplished in a 40 mv cathodic change from 0.0 to -0.04 v vs S.C.E. at 80°C. It was, therefore, of interest to determine if a similar desorption was as easily accomplished in H_3PO_4 solutions.

Desorption studies were carried out with butane, propane, and ethane at 140°C and butane at 100°C, using the technique described previously. The electrode was saturated with fuel in the vapor phase with the tip of the electrode touching the solution for continuity in the potential control circuit. Adsorptions were carried out at +0.05 v vs S.C.E. Then the electrode was fully immersed and equilibrated at the (more cathodic) potential of interest prior to obtaining the anodic voltage scan and integration of the fuel oxidation coulombs.

The data indicate that desorption of these fuels occurs much less readily in H_3PO_4 solution at 140°C than in the H_2SO_4 at 80°C. Thus, as shown in Figure A-3 (and Appendix A-2) the desorption of, e.g., butane in H_3PO_4 requires much more negative potentials and is never greater than about 80% complete even at hydrogen evolution potentials. Desorption of propane and ethane is even more difficult, in that order, and the comparison with butane-H_2SO_4 data, also shown in Figure A-3, makes it evident that the H_2SO_4 and H_3PO_4 systems differ significantly in their adsorption-oxidation characteristics for these fuels. The data also suggest that

information obtained on, e.g., ethane may be disturbingly inadequate to describe the behavior of butane and certainly fuels of much higher carbon number. It is of interest to note that desorption of butane in H_3PO_4 is relatively unaffected by the temperature difference between 100 and 140°C, thus confirming that the differences between H_2SO_4 and H_3PO_4 systems are largely solvent differences.

Figure A-3

Cathodic Desorption of Hydrocarbons

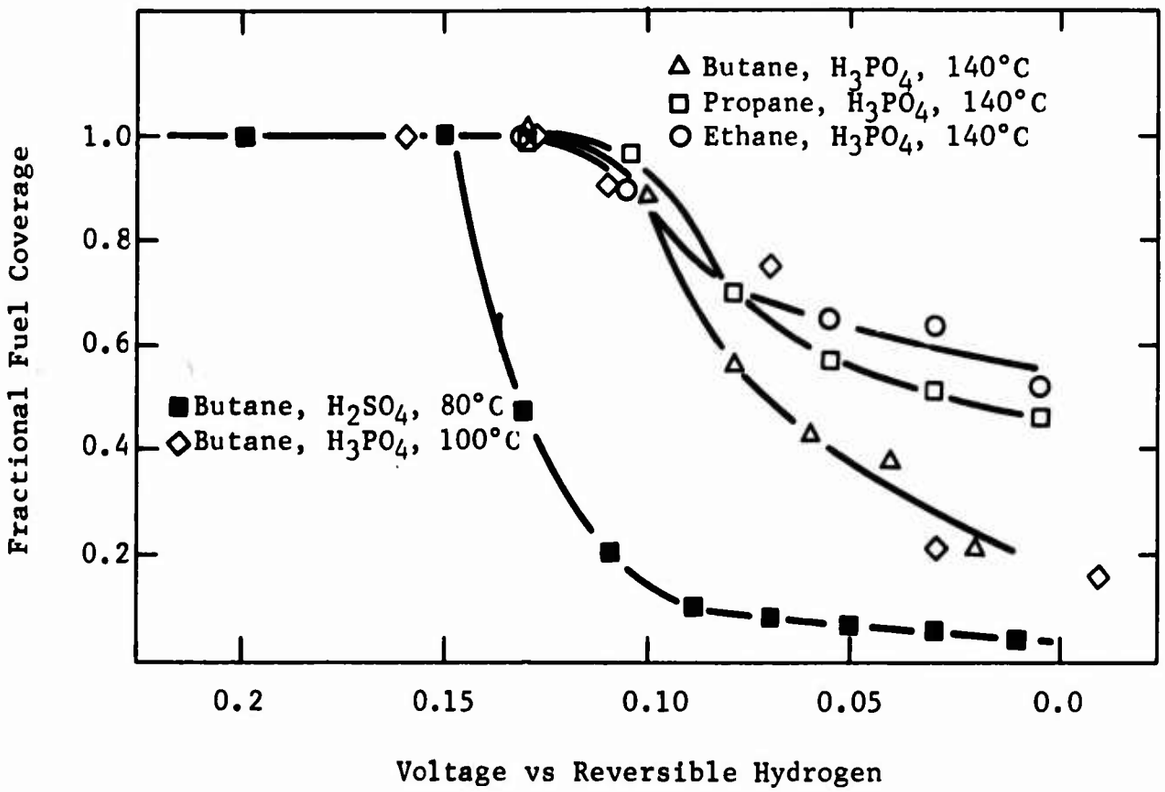

Part c - Adsorption at Temperatures Near the Boiling Point

It has been suggested in a previous paragraph that the equilibrium adsorption of butane fuel on platinum black in 14.7 M H_3PO_4 at 140°C may actually cover a greater number of surface sites than is desirable for optimum electro-oxidation. In addition, it has been found in actual practice that performance of hydrocarbon electrodes in 14.7 M H_3PO_4 electrolyte is optimum at about 150°C or water vapor pressure of about 600 mm (6)(7). It thus seemed desirable to qualitatively study the adsorption of fuel at temperatures approaching the boiling point of the electrolyte.

Adsorption tests were carried out in the manner described previously using electrodes with commercial platinum black. For comparison with the data in 85% H_3PO_4 (B.P. ~ 159°C), tests were also carried out in 96.5% H_3PO_4 (i.e., a significantly higher boiling point) and in 30% H_2SO_4 near its boiling point (~ 109°C).

The data, shown in Table A-1 (and Appendix A- 2), clearly indicate a sharp decrease in adsorption following a one hour period at temperatures approaching the boiling point of the respective acids. Thus, at 150°C, the adsorption in 85% H_3PO_4 is low and erratic while in 96.5% H_3PO_4 at the same temperature, values are equal to the values at 120°C. It is only at 160°C in 96.5% H_3PO_4 that the decreasing adsorption tendency is noted. Similarly, in H_2SO_4, only at a temperature 4°C below the boiling point can the decreased adsorption be noted.

Table A-1

Effect of Temperature on Relative Butane Adsorption

Engelhard Platinum Black
1 Hour Adsorptions

Temperature, °C	mc Butane/mc Oxide		
	14.7 M H_3PO_4	18 M H_3PO_4	3.7 M H_2SO_4
80	--	--	1.63
95	--	--	1.72
100	1.91	--	1.65
105	--	--	1.04
120	--	2.03	--
140	1.71	1.96	--
150	0.48,0.57,1.24 (erratic)	1.99	--
160	--	1.69	--

It is likely that this decreased adsorption is caused by lowered fuel transport at the decreased concentrations existing near the boiling point of the acid. Thus, at 150°C, 85% H_3PO_4 has a water vapor partial pressure of about 700 mm, and fuel concentration may undergo a tenfold change as the temperature is raised in such a system. It seems unlikely that the equilibrium nature of a chemisorption such as this would be severely effected by such a tenfold change.

An indication of transport control was obtained in a study of butane partial pressure effects at fixed temperature. In this experiment, carried out in 85% H_3PO_4 at 140°C, butane was diluted with argon over a 10:1 range and 1 and 2 hour adsorption exposures obtained on the platinum black electrodes. Results of these tests, shown in Figure A-4, indicate that a tenfold fuel dilution produces less than one-half the normal quantity of fuel adsorbed. However, the two hour exposures increase this value significantly, indicating that it is not an equilibrium effect.

Figure A-4

Effect of Partial Pressure
Relative Butane Coverage

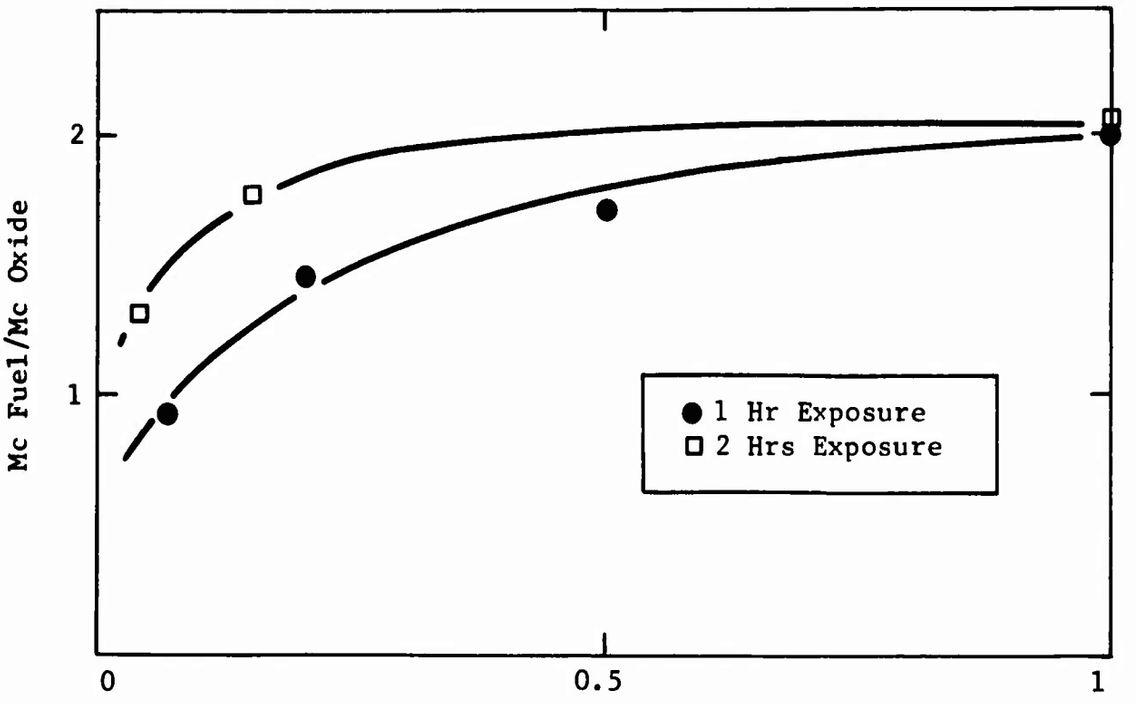

Despite the nature of the decreased adsorption, it is apparent that operation at low fuel partial pressures, near the boiling point, may have significant effects on the fuel available to the catalyst surface. Thus, if as postulated previously, the adsorption of butane from H_3PO_4 is normally too extensive for optimum performance, the observed optimization of these systems near the boiling point may involve optimization of fuel adsorption as well as water supply to the reaction. In addition, a similar argument may account for the ease of induction of potential oscillations by relatively minor temperature fluctuations under load.

Part d - Study of Adsorption Rates
in the H_3PO_4 System

Based on the adsorption rate data obtained previously using the flowing electrolyte technique in H_2SO_4 electrolyte, it seemed desirable to consider a measurement of adsorption rates in butane-Pt-H_3PO_4 systems at elevated temperatures. It is immediately obvious, however, that a somewhat different problem is posed. Thus, it is not at all apparent that sufficiently high electrolyte flow rates can be obtained in the porous tantalum plate system discussed in Report No. 7 to remove all transport effects and expose the adsorption limited rates for measurement

and study. For this reason it was decided to investigate the possibility of changing the system from a powdered Pt material supported on porous tantalum to a flow-through platinum screen arrangement upon which platinum black could be electrodeposited to desired levels. Sufficiently high flow rates should thus be more readily obtained for use with H_3PO_4 - 140°C electrolyte. At the same time, however, it was deemed advisable to investigate the identity of electrodeposited platinum versus commercial platinum black for fuel adsorption rates in the 3.7 M H_2SO_4 - 95°C system as a standard. This would provide a sound basis for extension to H_3PO_4 - 140°C using electrodeposited platinum.

Preliminary tests were carried out in the 3.7 M H_2SO_4 - 95°C flowing electrolyte system discussed previously using platinum electrodeposited on the platinum screen at a level of 4 mg/cm^2. After establishing blanks for the sawtooth scans with argon at 95°C, a series of butane adsorption experiments were run at -0.05, 0.0, +0.1 and +0.2 volts versus S.C.E. in the 3.7 M H_2SO_4 system. Coulombs of fuel accumulated versus wait time was plotted for maximum electrolyte flow conditions, about 200 cc/min.

Integration of these scans on electrodeposited platinum surprisingly indicated that the coulombs versus wait time plots were not nearly as linear for this system as they were for commercial platinum black. Non-linearity of the plots makes difficult the reliable estimation of adsorption rates and introduces a serious question as to the suitability of electrodeposited platinum as a research replacement for the commercial platinum black actually used for more practical electrode manufacture. It may be that real catalytic differences other than simple area considerations are present as is often speculated.

Further work will be necessary to establish if a workable system for adsorption rate measurements in high temperature H_3PO_4 can be found.

Phase 3 - Increasing Pt Utilization

In order to bring platinum performance with hydrocarbon fuels to practically feasible levels, specific current densities of several hundred ma/mg of platinum would have to be approached. Using bulk platinum, a maximum of 8 ma/mg has been obtained (butane, 14.7 M phosphoric acid, 150°C). It has been shown that about 10% of the Pt was present at the surface. The approach taken in the present study has been to use a support to make more of the platinum available in the surface and possibly to increase the activity of the atoms in the surface. A preliminary target of 80 ma/mg was set, it being felt that an improvement of this magnitude would justify further efforts toward the ultimate target.

Carbon is continuing to be used as the basic support material because of its conductivity, corrosion resistance, high surface area, and sorptive properties. It had been found earlier (7) that inclusion of a silica co-support gave a definite improvement in Pt utilization. Effort was concentrated on extension of this co-support approach.

Part a - Initial Benefit of Co-support

The co-support approach involved adsorption of ammonium chloroplatinate on carbon treated with freshly precipitated silicic acid gel (5% SiO_2 on carbon), followed by high temperature reduction and an activation step. The catalyst thereby obtained was reported (7) as having a utilization level of 16 ma/mg at a polarization of 0.40 volts. This was about twice the best level obtained on bulk Pt or on comparable impregnated Pt-on-carbon catalysts. It has now been determined that a fourfold improvement was actually obtained. Wet chemical analyses showed that the final catalysts contained 2.5 to 3% Pt instead of the 4 to 5% Pt estimated from a colorimetric determination of the unadsorbed Pt in the supernatant solution.

The discrepancy appears to have been due primarily to the formation of a colorless Pt(II) salt, not detectable colorimetrically, by reduction during the adsorption step. Some losses may also have occurred during the washing step. The revised data is shown in Table A-2.

Table A-2

Effect of 5% Silica on Platinum-on-Carbon Performance

Catalyst	Avg Performance, ma/mg @ η = 0.40 volts	No. of Replicates
Adsorbed 3% Pt/C-5SiO_2	28	5
Impregnated 6% Pt-10Ir/C	7	5

Thus, up to the start of this period a factor of four improvement in platinum utilization had already been achieved by means of the carbon support and silica co-support.

Part b - Co-support Optimization

Optimization studies on silica content using the co-support approach indicated that 10% by weight of SiO_2 (introduced as silicic acid gel) relative to carbon was optimum, and better than the 5% previously used. This is shown in Table A-3, taken from the complete data in Appendix A-3.

Table A-3

Effect of Added SiO_2 on Supported Pt Catalysts

% of Added SiO_2(1)	Pt Utilization, ma/mg @ η = 0.40 volts
0	15
5	28(2)
10	34(3)
15	24
50	10

(1) Weight relative to carbon.
(2) Average of 5 determinations.
(3) Average of 3 determinations.

Use of other co-supports was less effective than the silicic acid gel, though in some cases performance was better than carbon alone. See Table A-4.

Table A-4

Variation of Pt Activity with Nature of Co-Support

Adsorbed Pt Support	Best Pt Utilization, ma/mg, @ η = 0.40 volts(1)
Carbon	15
Carbon-20% Tungsten Bronze	7
Carbon-10% Calcium Silicate	13
Carbon-10% Acid-Treated Vermiculite	15
Carbon-10% Cabosil	23
Carbon-10% Aluminosilicate(2)	27
Carbon-10% SiO_2 (silicic acid gel)	38

(1) Several inferior runs felt to be limited by electrode structure or wetproofing not included. See Appendix A-3 for further details.

(2) Weight ratio of SiO_2:Al_2O_3 = 7:1.

Of these alternate co-supports, only the aluminosilicates appear to be worthy of further work. These are preparable in a variety of crystal structures and have often been used as supports for heterogeneous catalysts.

Part c - Colloidal Platinum on Silica Treated Carbon

An alternative approach which had been taken earlier involved adsorption of colloidal Pt rather than soluble chloroplatinate onto carbon to yield a 6% Pt catalyst. This method had given optimum utilizations (10 ma/mg) when carbon monoxide was used as reducing agent in the preparation of the colloid. By inclusion of 10% SiO_2 utilization was increased to 20 ma/mg. An attempt to increase utilization further by decreasing the catalyst concentration to 3% was unsuccessful. Nevertheless, the colloidal platinum is close enough in activity to the adsorbed soluble platinum in activity to be reconsidered in future studies. This result is remarkable in view of the relatively large particle size found for the colloidal platinum. This will be discussed in a later section.

Part d - Carbon Support Studies

The use of different batches of carbon revealed the importance of the structure of the carbon on the performance of the catalyst. Thus, one batch of carbon adsorbed 1.8 to 1.9% Pt as compared to 2.5 to 3% adsorbed by another under the same experimental conditions. Limiting currents decreased in the same order as platinum content. No improvement in performance was obtained with the poorer batch by modifying conditions to give greater Pt adsorption.

While both batches of carbon had been burned out with CO_2 at 1000°C for seven hours, the poorer carbon had only two-thirds of the surface area of the better carbon (110 vs 180 m^2/g). Additional burnout of the low surface area batch caused a 20% weight loss and increased its surface area to 192 m^2/g. Simultaneously the adsorption and performance levels improved, to equal those of the good batch. Further CO_2 reburnout to the extent of 28%, however, resulted in decreased surface area and substantial performance loss. See Table A-5.

Table A-5

Effect of Carbon Burnout on Performance

Carbon Batch	% Add'l Burnout (% wt loss)	Surface Area, m^2/g	% Pt Ads on C-SiO_2	Highest Limiting Current, ma/cm^2 (1)	Best Pt Utilization, ma/mg
1	--	180	2.9	45	37
2	--	112	1.9	20	25
2	20	192	2.8	45	39
2	28	172	2.7	23	20

(1) Polarization approximately 0.4 volts.

These results indicate that high surface area is an important attribute of a good carbon support. As found earlier, additional platinum forced on a platinum-saturated support is largely wasted. Burnout with carbon dioxide can increase surface area to some extent, but excessive burnout can decrease surface area and catalyst activity, probably by causing the pores to grow together and impurities in the carbon to concentrate. Thus, the use of carbons with higher initial surface areas appears to be warranted. Further information relating to the surface area and pore size distribution of these carbons is presented in Appendix A-4.

Part e - Effect of Temperature

Another approach that can be used to increase Pt utilization is to operate at higher temperatures. A preliminary examination was made of the effect of temperature increases up to 190°C. Results, shown in Table A-6 for the best catalysts-electrode combination tested, indicated that substantial performance improvements could be attained.

Table A-6

Effect of Temperature on Performance of 2.8% Pt on C-10% SiO_2

Operating Temperature, °C	Pt Utilization, ma/mg, @ Limiting Current (1)
150	39
175	70
190	87

(1) Polarization approximately 0.4 volts.

An activation energy of about 8 kcal/mole was determined for four series of tests in this temperature range, indicating a chemical rate limitation of some sort. Thus, the preliminary target has been attained by operation at higher temperatures. However, increased stability and corrosion problems (as well as water and heat balance problems not yet considered) make lower temperature operation seem more desirable.

Part f - Electron Micrograph Studies

In order to obtain some insight into the catalyst microstructure, electron micrographs were obtained down to a resolution of about 10 Å[1]. A high-quality micrograph of a representative Pt on carbon catalyst is shown in Figure A-5. These studies indicated the following:

- Adsorbed Pt on carbon catalysts had a dispersion of fairly uniform Pt particles in the 50-100 Å range.
- Adsorbed Pt on carbon + 5-10% SiO_2 catalysts showed a greater range of catalyst dispersion with Pt particles down to 10 Å; there was considerable non-uniformity, which was further increased by the additional carbon burnout.
- Before the reduction and activation steps, the adsorbed Pt was very highly dispersed, with particles not visible down to 10 Å. Hence, some particle growth or sintering is occurring during the reduction and/or activation steps.
- Colloidal Pt on C and SiO_2 catalysts primarily contained 100-300 Å Pt particles.

While the benefit of the silica may in part be accounted for in terms of increased dispersion, this is clearly not the entire effect, since the colloidal Pt catalyst (large particles) is also improved by SiO_2 addition. Other possible sources of benefit from silica are:

- Increased fuel adsorption or diffusion.
- Wetting or wetproofing effects.
- Shielding of Pt from deactivating sites on the carbon.
- Protective effects by selective adsorption of poisons or inhibitors.
- Separation of the carbon layers to increase accessibility.
- Creation of sites of higher activity.

Further work with the silica-carbon system should provide clues as to the true role of the silica and its ultimate potential benefit.

Part g - Attempts to Improve Stability Using Other Noble Metals

Two types of performance stability problems were encountered during electrode evaluations. In order to describe these it is necessary to review the testing procedure:

Polarizations were obtained at constant current initially with butane, then with oxygen, and finally again with butane. After determining oxygen performance, the electrodes were generally operated at 100 ma/cm^2 for 1/2 hour, before switching back to butane. As a rule, this oxygen treatment resulted in improved butane performance. The second butane run was made at a series of fixed current densities for a period of fifteen minutes each, and was terminated when rapid overpolarization was observed. Then the electrode was returned to the open circuit condition and longer term runs were made at selected current densities.

---

[1] Courtesy of Philips Electronic Instruments Company, Mt. Vernon, New York.

FIGURE A-5

ELECTRON MICROGRAPH OF 3% Pt ON CARBON CATALYST

Magnification ~ 2,000,000 X

100 Å

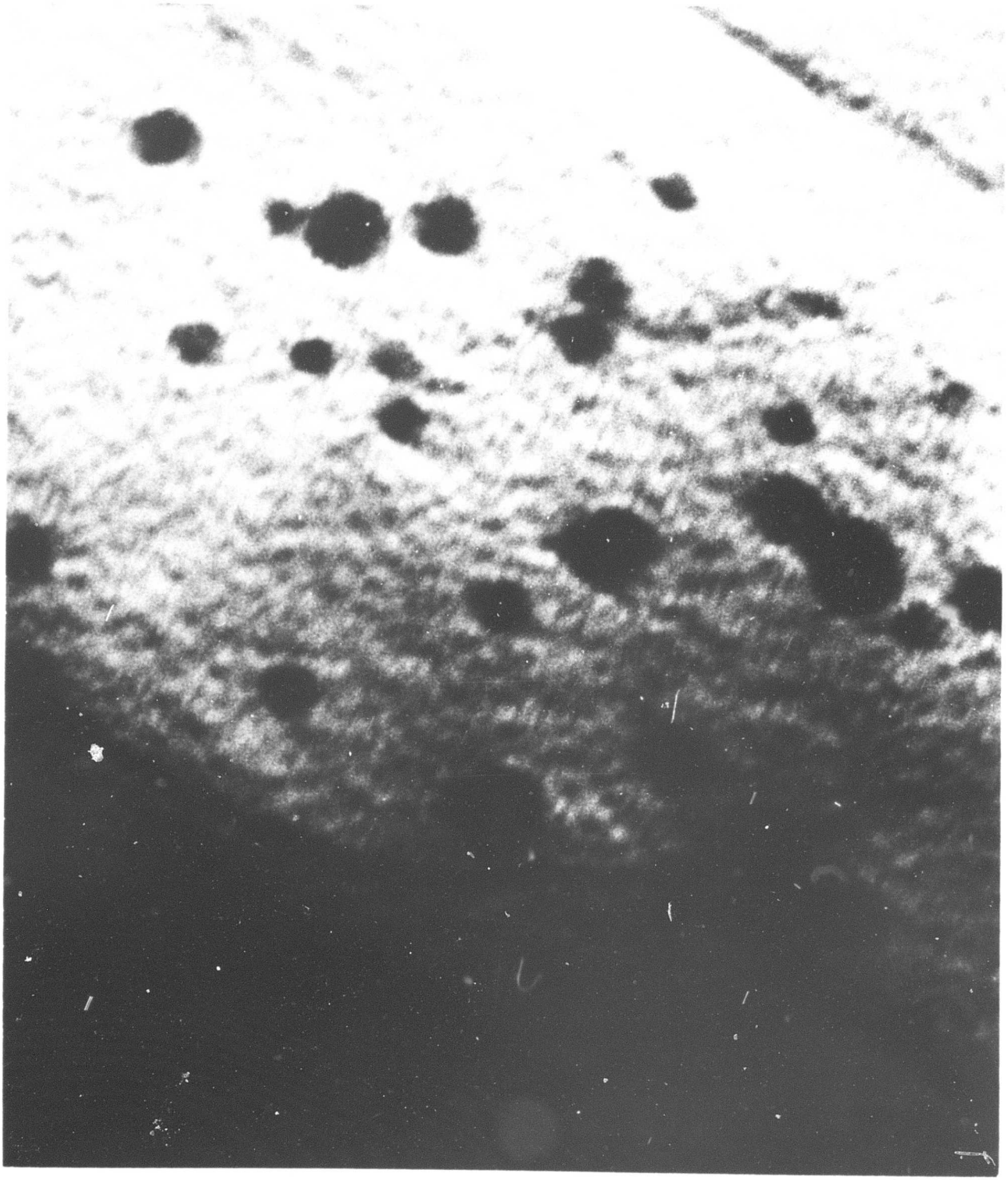

During this sequence two types of instability were noted, a reversible or "short term" and a permanent or "long term" increase in polarization with time.

(1) "Short-term" Stability

In the limiting current region, performance was only maintained for a limited time, rapid overpolarization occurring within one hour. After returning to open circuit, however, performance could generally be repeated, with a slightly improved level of operation following the first cycle. The short-term polarization may be accounted for by a slow build-up of impurities on the catalyst, which are removable by burnoff during overpolarization.

With the better catalyst-electrode systems, operation at about half the limiting current (20 ma/cm^2) was maintained for six to eight hours with no overpolarization. Polarization slowly increased during that period to a maximum of about 0.4 volts and then leveled off. A performance curve for a 3% Pt on C-10% SiO_2 catalyst is shown in Figure A-6.

Figure A-6

Change of Polarization with Time at 20 ma/cm^2

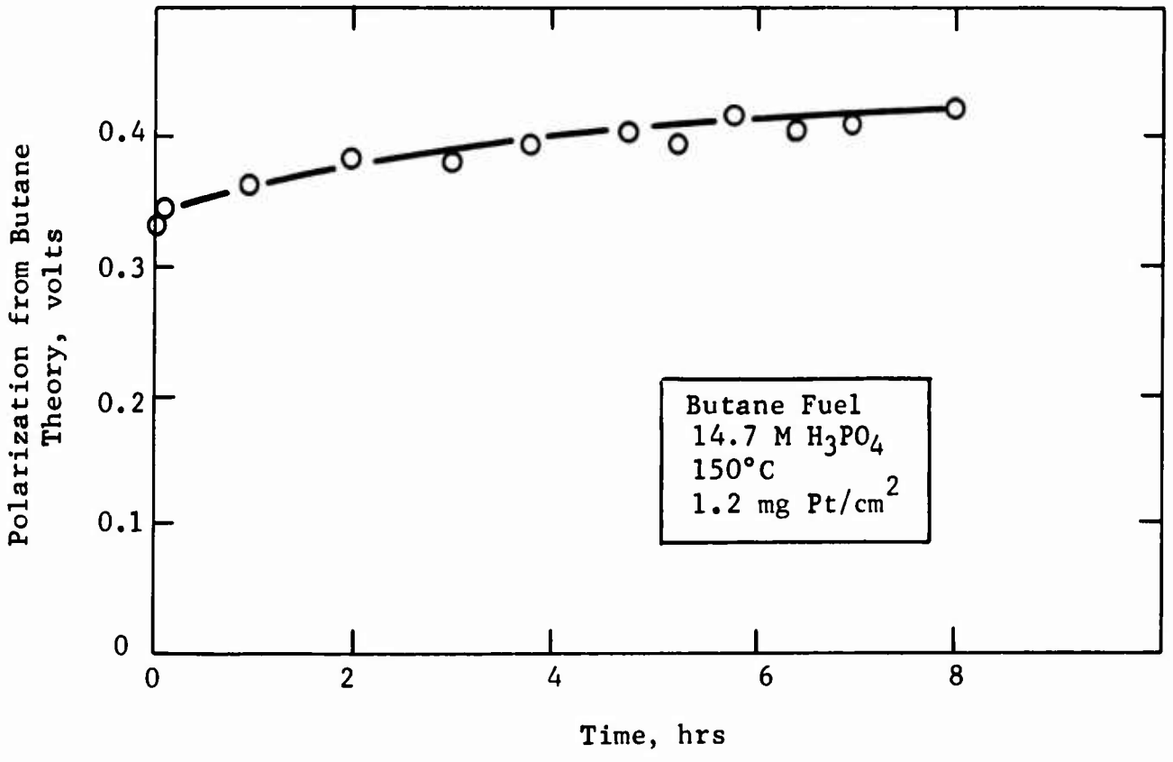

(2) "Long-term" Stability

During operation a gradual deterioration in electrode performance occurred at all current levels even when approached from open circuit. Considerable variation was observed: some electrodes had reproducible performance for several days, others already showed an irreversible decline (instead of the usual improvement) after the oxygen treatment.

Based on previous results, it was anticipated that the inclusion of Ir, Rh or Ru as co-catalysts with Pt would yield improved stability. However, the inclusion of these metals on silica treated carbon along with platinum decreased its activity, as shown in Table A-7.

Table A-7

Effect of Co-catalyst on Butane
Performance of 3% Pt on C-5% SiO_2

Co-catalyst (1)	Limiting Current ma/cm^2
Ru	15
Rh	20
Ir	30
--	40

(1) 10 wt % co-catalyst (based on Pt) in impregnating solution. Total noble metal content estimated to be 1.0-1.4 mg/cm^2.

The poor performance of the Ru and Rh systems was attributed to a precipitation of Ru and Rh compounds from the impregnating solution. Precipitate formation (detected in control runs without carbon) could have given very non-uniform distribution as well as blocking of the pores of the support. The better performance of the Ir system is accordingly attributed to its slower adsorption. This catalyst did in fact show improved long-term stability over Pt alone. Good reproducibility was obtained over a week of intermittent operation, as compared with two to three days for the Pt system. However, short-term polarization was not improved and the lower Pt utilization was a detracting feature. Future studies will attempt to optimize Ir content so as to obtain the best balance of effects.

Part h - Structural Aspects

A confounding feature in all of these studies has been the role of the Teflon in electrode performance. Variations have been encountered in performance not only from differences in Teflon content but also variations from one batch of Teflon emulsion to another, as shown in Table A-8.

Table A-8

Effect of Teflon on Electrode Performance

Teflon Batch No.	% Teflon	Limiting Current ma/cm^2
1	7.5	30
	10	45,45
	12.5	35
2	10	30,30

Comparisons of catalysts were, therefore, made under similar Teflon conditions wherever possible. In general, best results were obtained when the Teflon emulsion was allowed to sit undisturbed in a separatory funnel for at least several days to one week before use, and the bottoms were taken for electrode preparation.

The Teflon emulsion represents a source of variability which has not as yet been satisfactorily resolved. It is planned to rectify this situation in future electrode structure work.

In summary, limiting currents of up to 40 ma/mg of Pt on butane at 150°C have been achieved by optimization of the use of the carbon-silica support system. Operation at higher temperatures yielded specific current densities of over 80 ma/mg. Thus, the preliminary targets have been achieved. The studies of the carbon surface area and platinum particle size have indicated avenues along wich further strides toward the ultimate target may be taken. The electrode structure and stability problems remain to be solved before reliable cells can be built using supported platinum catalysts.

Phase 4 - Liquid Decane Electrodes

Liquid decane electrode structure research has been curtailed to allow for increased emphasis in the hydrocarbon total cell area. Consequently, liquid decane electrode testing has been keyed directly to supporting this effort. Primary emphasis was placed upon optimizing the 50 mg/cm^2 sintered platinum Teflon emulsion electrode structure through changes in fabrication conditions and Teflon content and the elimination of the barrier separation problem reported previously (6). During the course of this study, fuel transport rates were also determined with a view towards total cell design. In addition, some electrode materials testing work was required since a new batch of catalyst was required for the total cell electrodes, and variability was observed ir the Teflon 41BX emulsion obtained from DuPont.

Part a - Electrode Fabrication Modification

Work on the sintered platinum-Teflon electrodes reported previously (6), indicated that an increase of only 6°C in the sintering temperature produced a marked improvement in liquid decane performance. However, a complete optimization of the fabrication conditions was not attempted at that time, because the sintering process would give a complex pressure-temperature-time response surface even at a single Teflon level. Furthermore, since the sintering step is both beneficial to the electrode structure and detrimental to the catalyst, there should be a number of

equivalent pressure-temperature-time combinations with the same electrical performance. Fuel transport through the electrode is also a lingering physical problem. If it could be shown that fuel transport and electrode activity are independent of each other, then it should be possible to choose from among the above equivalent fabrication conditions the one that gives the least fuel transport. This would lead to an improvement in total cell efficiency and reduction in system complexity.

Consequently, a study was conducted to determine the effect of sintering conditions on electrode performance and fuel transport. As a first experiment, a series of 50 mg/cm^2 sintered platinum-Teflon emulsion electrodes was prepared using sintering temperatures which ranged from 326 to 359°C, and holding the fabrication pressure and sintering time constant (1100 psi, one minute). These electrodes were evaluated as decane anodes at 150°C in 14.7 M phosphoric acid using the standard half cell arrangement previously described (6). The results of this study are summarized in Figure A-7 (and Appendix A-5) which compares the current density at 0.45 volts polarized with fuel transport rate for various sintering temperatures. As anticipated from previous work, the sintering temperature critically determines the catalyst activity, a maximum being obtained at 349°C, the standard sintering condition. However, the fuel transport rate did not vary appreciably with either sintering temperature or current density even though the catalyst utilization showed a sevenfold variation. This is quite encouraging since it indicates that anode performance is independent of fuel transport rate. However, as indicated in Table A-9 below, reduction in Teflon content and increased sintering pressure and time so far have not reduced fuel transport. Alternate routes to fuel transport reduction will need to be examined in the future.

Table A-9

Effect of Fabrication Conditions
on Fuel Transport and Electrode Activity

Sintering Conditions			Fuel Transport, $cm^3/cm^2/min$	Current Density at 0.45 volts Polarized, ma/cm^2
Pressure, psi	Temp, °C	Time, min		
		10% Teflon		
1100	316	1	0.027	90
1100	349	2	0.028	45
8800	349	1	0.026	30
		15% Teflon		
1100	316	2	0.031	200
1100	349	1	0.026	200
8800	349	2	0.030	80

Figure A-7

Effect of Sintering Temperature
on Platinum Utilization and Fuel Transport

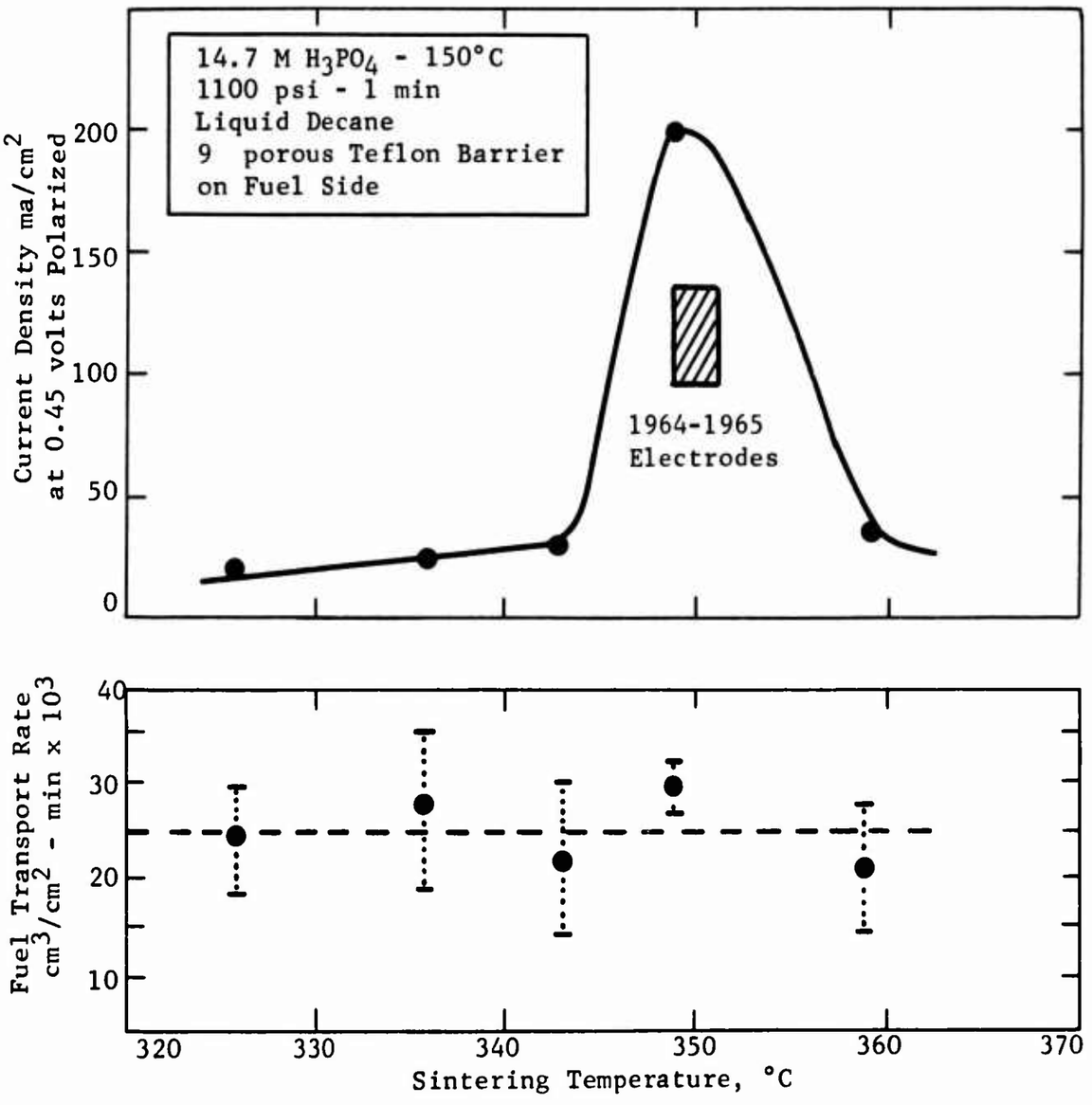

Table A-9 also serves to explore briefly the effect of sintering conditions on platinum activity. This data demonstrates the complexity of the sintering function and illustrates the trade off of sintering time and temperature. Notice that with 15% Teflon, electrodes sintered at 316°C for two minutes gave the same activity as those prepared at the standard 349°C - one minute condition while increasing sintering pressure was detrimental.

Part b - Materials Testing

Although the current densities indicated in Figure A-7 were higher than those obtained with the earlier standard electrodes this level could not be maintained in repeat preparations because of quality problems with subsequent samples of Teflon 41 BX emulsion even for samples of the same lot number. At the same time two lots of Engelhard platinum black catalyst were used, but the activity difference attributable to them was far smaller than that due to the Teflon, as illustrated in Table A-10.

Table A-10

Effect of Teflon Emulsion
History on Liquid Decane Performance

Date Received	Catalyst Lot No.	Polarization at Indicated ma/cm^2	
		40	100
Teflon Lot No. 4002			
6/15	10,004	0.36	0.40
7/15	10,004	0.32	0.50
8/15 (Tested 11/15)	11,909	0.32	0.48
Teflon Lot No. 4655			
9/15 (Tested 11/15)	10,004	0.42	0.60
9/15 (Tested 11/15)	11,909	0.39	0.57
10/15 " "	11,909	0.45	0.65
11/24(Tested 11/24)	11,909	0.41	0.56

Electrodes made with June batch of 4002 Teflon gave the high utilization, while material from the same batch obtained in July and August were inferior giving only the standard performance. Lot Number 4655, on the other hand, gave consistently poor performance; debits of 80 to 170 mv at 100 ma/cm^2 were observed. Attempts to improve the quality of the emulsion by filtration and pH adjustment resulted in even poorer performance levels. Additional work will be required to determine the source of the variability in electrodes fabricated with different batches of emulsion. Fortunately, a sufficient amount of Lot 4002 (8/15) was available to allow fabrication of the required 4" x 4" electrodes for the multicell assembly.

Part c - Barrier Separation Problem

Porous Teflon barriers, placed on the fuel side, have been found to be beneficial for liquid decane electrodes (5)(6) provided intimate contact between the barrier and the electrode is maintained. However, during extended operation gas buildup can force the 63 mil porous Teflon barrier away from the anode, reducing electrode efficiency by as much as a factor of two. Mechanical means can be used to minimize this problem in small electrodes but these are not too effective in the larger 4" x 4" system. The only solution is to make the barrier an integral part of the anode. Efforts to do this with the thick barrier have thus far been

unsuccessful because pressures as low as 100 psi result in altered barrier porosity. Exploratory studies with the thin porous Teflon film used in the cathode studies (reported in Task E) indicated that this could be laminated to the anode without loss in performance. The results of one such test are summarized in Table A-11 below. This electrode was prepared by removing the mold release agent from the screen side of the standard sintered platinum-Teflon electrode and pressing it to a 3.5 mil, 10 micron porous Teflon film at 8000 psi. As indicated, the performance of this cold laminated electrode was somewhat poorer than the standard electrode-barrier system.

Table A-11

Comparison of the Laminated Barrier
and Standard S.P.T.E. - Barrier System
(50 mg/cm^2 - 14.7 M Phosphoric Acid, 150°C)

Electrode	Barrier	Polarization from Decane Theory, at Indicated ma/cm^2, volts			
		0	10	40	100
Standard	63 mil, 9 micron Porous Teflon Placed on Anode	0.05	0.28	0.32	0.48
Laminated	3.5 mil, 10 micron Porous Teflon film, cold Laminated 8000 psi	0.07	0.27	0.40	0.55

This performance debit was believed to be due to the excessive pressure required to bond the film to the supporting screen. To correct this deficiency, a hot lamination procedure was devised which would allow lower lamination pressure. As in the previous experiment, a standard sintered platinum Teflon electrode was used. The mold release agent was removed from the screen side of the anode and a thin porous Teflon film was laminated in place by sintering at 349°C for 15 seconds at a pressure of 500 psig. Care was taken to place the film on the lower platen side of the sintering press to minimize catalyst sintering. A comparison of the performance of this electrode with the standard barrier system is shown in Figure A-8. This data indicates that the laminated barrier electrode is equivalent in performance to the older thick barrier system even when run with an additional 1/16" porous Teflon auxiliary barrier. This latter barrier is required as a spacer due to the fact that the design of the multicell stack was based upon the thick barrier.

Figure A-8

Effect of Laminated Barrier on Decane Performance

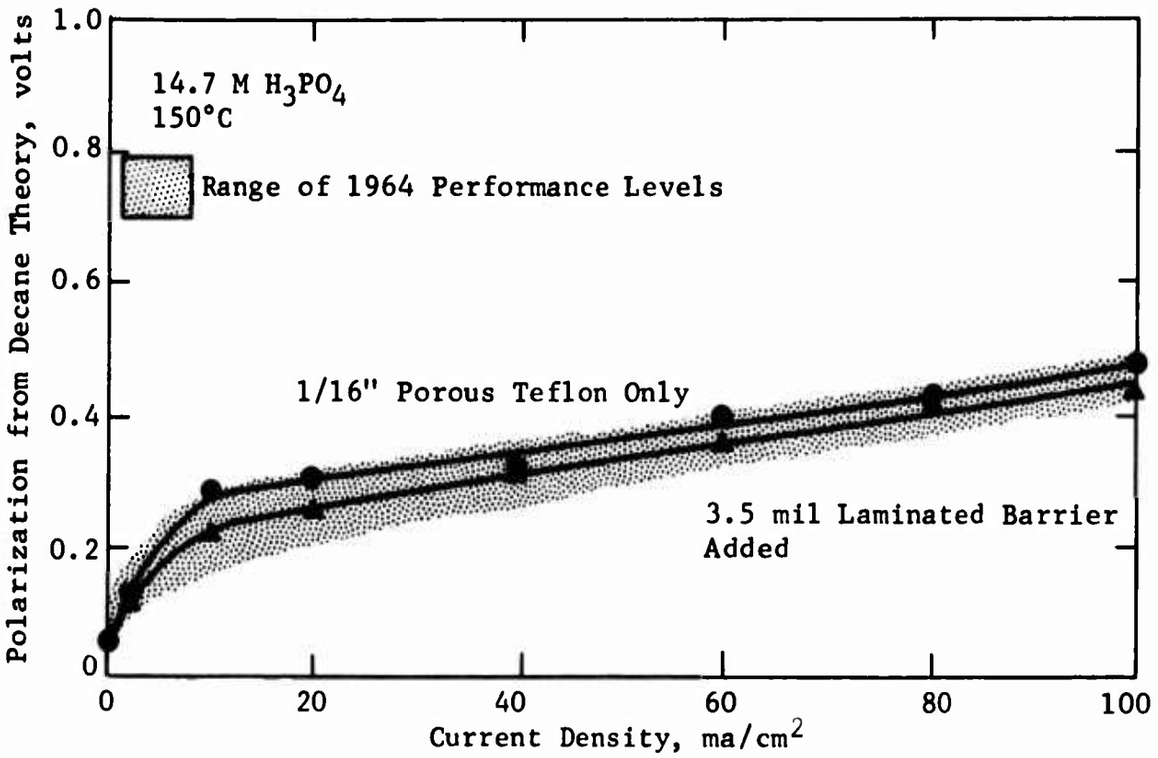

In short, a Teflon barrier has been made a integral part of the anode with no loss in performance. The barrier separation problem, therefore, should no longer exist. These electrodes were used in the total cell work reported in Task B.

Phase 5 - Alloy Catalysts

The program to replace the platinum catalyst with alloys of less noble metals has continued with emphasis on the preparation of alloys with high surface areas, chosen from the elements in the first long period and in Group IB, as outlined in the previous report.

Alloys prepared by a chemical coprecipitation and reduction technique had been found to be unsatisfactory. In extreme cases, the starting salts were not reduced and the end product was a fused mixture of the starting materials. Attention was then turned towards the Raney technique. This procedure is well known for preparing high surface area metal catalysts, but its applicability to alloy preparation had not been established. Work was, therefore, done to determine whether the high surface area metals prepared by the Raney technique were actually alloys, and, if not, to determine how alloys could be prepared by this technique.

Part a - Initial Alloy Preparation and Characterization

A number of metal alloys of the first row of transition elements with group IB metals and aluminum were prepared by melting in an arc furnace under helium. The solidified melt was milled and ground into a fine powder and extracted with 3 M potassium hydroxide under nitrogen. The resulting compositions including 60 atom % Fe-40 atom % Au, 40 Fe-60Au, 50Ni-50Au, 50Fe-50Au, 50Ni-50Cu, 50Co-50Cu, 50Mo-50Cu and 50Fe-50Ag were characterized by powder X-ray analysis, as listed in Appendix A-6. They were by and large, mixtures of the original alloying elements and not alloys in the form of solid solutions or intermetallic compounds. Some of the end products of these preparations were found to contain aluminum, and the iron composition also contained Fe_3O_4. This result was not unexpected because none of the phase diagrams of the alloys, except that of Ni and Cu, show a wide range of solid solutions at room temperature. In agreement with this, the 50Ni-50Cu composition was the only one found to contain a large percentage of Cu-Ni alloy, as a solid solution. Thus, the aluminum appears to be too poor a solvent for these transition metals to permit alloy formation by the arc melting technique, unless the phase diagram of the transition metal pair shows a stable alloy phase at room temperature at the ratio desired.

None of the poorly defined alloys prepared by simply melting and grinding was found to have any activity on hydrocarbons. The nickel-containing melts, since they contained Raney nickel, of course, showed activity on hydrogen, as documented in Appendix A-7. .

Part b - Raney Alloy Preparation
with Annealing and Quenching

Most of the binary phase diagrams of the alloys of Group IB metals and transition elements show a large single phase area somewhat below the melting point. Therefore, annealing the crude melt obtained from the arc furnace at a temperature in the single phase region would be expected to result in a homogeneous alloy. Then, a rapid quench in water should allow the alloy to return to room temperature without phase separation, in the form of a meta-stable solid solution. The important question then to be answered was whether extraction of the aluminum would leave a stable alloy or would result in separation into the thermodynamically stable two phase mixture.

In answering this question, special attention was given to the case of Fe-Au alloys, because in 1 to 1 atomic ratio, the calculated d-band vacancy based upon the band theory approached that of platinum. Furthermore, the lattice parameter of 50% iron in gold is also close to that of platinum. In the absence of Al-Au-Fe ternary phase diagrams, the annealing temperatures were chosen from the binary phase diagram. Annealing the 40Au-60Fe melt at 1100°C under argon followed by quenching in cold water and extraction with alkali produced a dark gray end product in extremely finely divided powder form. X-ray analysis indicated that it was a mixture of a solid solution and probably an intermetallic compound. This was in contrast to the rust colored mixture of Au and Fe_3O_4 obtained without the annealing and quenching steps.

The fact that true alloys may be formed by the Raney method is significant and the technique developed should be useful in the future for the preparation of high surface area alloys. A few other alloys were also prepared by this technique and the detailed information is included in Appendix A-6.

Part c - Electrochemical Activity of Alloys

The Raney catalysts all gave good to excellent performance initially. In particular, Raney alloys containing nickel invariably gave excellent performance even in the absence of a fuel. Under potentiostatic control, this current would gradually diminish with time. This behavior was attributed to interstitially dissolved hydrogen. Small amounts of residual aluminum might also contribute to the temporary activity. Very often, the initial temporary activity faded even in the presence of hydrogen as the fuel. Apparently, the interstitially dissolved hydrogen was readily available for electrochemical reaction yet difficult to replace. The reason for the difficulty to replace the initial hydrogen has not been investigated yet. Test procedures were developed in such a manner that the initial temporary activity would not be mistaken for the true activity.

All the alloy catalysts were evaluated potentiostatically throughout. Initially, they were run on N_2 without any fuel until a steady current density was reached. Butane was then introduced to replace nitrogen while the electrode polarization was held constant at various levels. After the butane test was completed, hydrogen was finally introduced to the electrode.

With the exception of Ni and Ni alloys which were active on H_2, none of the alloys tested showed any significant activity. They included poorly defined Raney alloys, annealed and quenched Raney alloys and commercial alloys. The performances of Raney gold, and annealed Raney 40Au-60Fe were typical. Raney gold showed no activity on butane and only insignificantly small activity or H_2. Alloying the gold with iron produced no significant change.

Table A-12

Typical Results with Raney Catalysts

3 M KOH, 80°C

	Current Density at 0.57 Volts Polarization from H_2 with Indicated Fuel (ma/cm^2)		
	N_2	C_4H_{10}	H_2
Raney Gold	0.4	0.5	6.0
Raney Annealed 40Au-60Fe	1.0	0.9	2.0

Thus, the non-noble alloy program has reached the point where a very promising method for high surface area preparations is available, but no hydrocarbon activity has yet been detected. The technique will have to be applied to Group IV, V, and VI metal alloys before a decision on its ultimate promise may be made.

Phase 6 - Mixed Perovskites

Part a - Background and Introduction

Earlier reports of this series (6)(7) have described the properties of a number of mixed perovskites of the general formula $A\ B'_x\ B''_{(1-x)}O_3$. A is a cation of large diameter (Cs, Ca, Sr, Ba or lanthanide element) included to obtain the proper lattice spacing. B' is the catalytic element, e.g. Ni, Co etc., and B'' is an element selected from Groups IV-VI of the Periodic Table to provide acid resistance. A wide range of elements have been used in these positions (see Table A-13).

Table A-13

Elements Used in Perovskite Studies

Group in Periodic System	I	II	III	IV	V	VI	VII	VIII
Ionic Position in Perovskite								
A	Li, Cs	Ca, Sr, Ba	La, Ce, Pr, Tl	Pb	Bi	--	--	--
B'	Ag, Cu	--	--	--	--	Cr	Mn	Fe, Co, Ni, Ru, Rh, Ir, Pt
B''	--	--	--	Ti, Zr, Sn, Hf	V, Nb, Sb, Ta	Mo, W	--	--

Many of the earlier compositions, especially those containing tantalum with a full complement of lattice oxygen (stoichiometric perovskites), showed excellent resistance to acid. However, these stoichiometric materials generally had poor electrical conductivities. Introduction of lattice oxygen deficiencies, both with and without doping, greatly increased electrical conductivity but lowered acid resistance to intolerable levels. Furthermore, it was shown that the relatively high electrical conductivities resulting from oxygen deficiencies were, in most cases, lost quite rapidly on contact with acid. In fact, loss of conductivity always proceeded more rapidly than dissolution of the catalytic metal from the solid perovskite by the acid.

It was demonstrated that the conductivities of nickel-containing perovskites having oxygen vacancies could be increased by changing the firing atmosphere from nitrogen to air. Also, inclusion of a small amount of cesium or lithium improved conductivity, especially in the presence of air. The similarity of these results to those observed with the simpler compound nickel oxide (10)(11) suggests a similar basis for the observed semi-conducting properties. By analogy with lithiated nickel oxide, the conductivity of the non-stoichiometric perovskites may be assumed to arise from the oxidation of a portion of the catalytic metal, Ni, Co, etc, to a higher-than-normal valence state, e.g. Ni^{III}, Co^{III} etc. Electrical semi-conductivity results from electron (or hole) exchange between these higher-valence-state atoms and the more numerous ones in the normal valence state. These effects are not observed in the stoichiometric perovskites since (1) the ideal stoichiometry of

these limits the degree of oxidation of the conductivity-producing ion and (2) the completely filled lattice lowers the mobility of the charge carriers.

This picture offers a plausible explanation of the rapid loss in conductivity with corrosion. The higher valence states of most of the transition elements considered here as potential catalysts are quite unstable in solution, the oxidized ions reacting rapidly with water to form oxygen. For these reasons, one would expect the higher-valence ions to react more readily with acid than those in the normal valence state. This would cause destruction of the charge carriers very early in the process of dissolution of the catalytic metal by acid and appears to explain very well the observed facts.

Two other observations support this general picture. In similar compositions, cobalt always gives higher conductivities than does nickel. This is attributed to the well established greater ease of oxidizing cobalt to higher valence states. Also, when non-stoichiometric perovskites in the more highly conducting range are treated with acid, visible gas evolution occurs. Presumably, this gas is oxygen, since iodine is liberated if acidic potassium iodide is used as corroding medium.

In order to obtain perovskites having conductivities which are stable to acids, it is obviously desirable to include--either as primary constituents or as doping agents--metals having higher valence states which are relatively stable toward acids. It was felt that manganese and chromium are most promising in this respect. For this reason, a portion of our work during this period was concerned with the study of perovskites doped with these metals in oxidized states (referred to generally as "oxidized state" compounds).

Another portion of the perovskite work during this period was concerned with a somewhat different approach, viz. an attempt to obtain high electrical conductivities by employing the "B" ion constituent, molybdenum, in mixed valence states. Two combinations, Mo^{V}-Mo^{VI} and Mo^{IV}-Mo^{V}, are possible and both have been studied. These are referred to as "reduced state" compounds, since oxidation must be rigidly excluded during firing.

Part b - Perovskites of High
Valence Manganese and Chromium

For the reasons explained in Part a, stoichiometric perovskites were prepared containing manganese or chromium at a nominal valence of four, to provide conductivity without the lattice deficiencies that would lead to acid instability. In agreement with the theory, the manganese and chromium did effectively raise the conductivities of perovskites containing nickel, cobalt, iron and copper. Examples are given in Table A-14, taken from the complete results given in Appendix A-8.

Table A-14

Improvement in Conductivity of
Perovskites Containing Manganese and Chromium

Nominal Formula	Conductivity, mho/cm
$SrCo_{.33}Ta_{.67}O_3$	2.6×10^{-10}
$SrCo_{.35}Ta_{.50}Mn_{.15}O_{2.9}$	1.1×10^{-6}
$SrCo_{.25}Ta_{.50}Mn_{.25}O_3$	4.2×10^{-6}
$SrCo_{.25}Ta_{.30}Mn_{.45}O_{2.9}$	4.3×10^{-5}
$SrCo_{.5}Mo_{.5}O_3$	1.2×10^{-10}
$SrCo_{.3}Mo_{.3}Cr_{.4}O_3$	6.0×10^{-5}
$SrNi_{.33}Ta_{.67}O_3$	7.1×10^{-9}
$SrNi_{.35}Ta_{.30}Mn_{.35}O_{2.8}$	2.7×10^{-5}

As shown in the above table additional doses of manganese produce little improvement over the initial benefit. The results with the nickel-tantalum combination were particularly gratifying since that one could not be rendered conductive via the oxygen deficiency route.

Conductivity appeared to improve slightly as the firing temperature was raised, up to an optimum point. Higher temperatures also caused a shrinkage of the cubic lattice spacing (see Table A-15 for one example). This result is logical since a decreased interatomic distance should promote greater orbital overlap and easier electron transfer between B atoms capable of changing valence.

Table A-15

Change of Conductivity and
Lattice Spacing with Firing Temperature

$SrNi_{0.35}Ta_{0.3}Mn_{0.35}O_{2.8}$

Firing Temp, °C	Conductivity mho/cm	X-Ray Spacing, Å(1)
1205	7.0×10^{-6}	7.953
1480	2.7×10^{-5}	7.817

(1) Average value from several peaks of disordered cubic perovskite powder pattern.

Attempts were made to improve the conductivity further by incorporating rare earth elements into the A position of the lattice at along with manganese in the B position. Rare earths such as lanthanium, cerium and praseodymium had earlier improved perovskite conductivity, but none of these benefitted the present manganese containing compositions. Thus, the best conductivity that could be reached was of the order of 10^{-4} to 10^{-5} mhos/cm--at or just under the conductivity target set for electrode use with an auxiliary conductor.

Perovskites made conductive with manganese or chromium had better acid stability than those of the same initial conductivity generated by oxygen deficiencies. The former were greatly superior with regard to the retention of conductivity after exposure to acid. In addition, they generally showed greater resistance toward extraction of the catalytic metal. The chromium compounds were not as good as the manganese. See Table A-16.

Table A-16

Acid Stability of Oxygen
Deficient and Mn and Cr Doped Perovskites

Nominal Formula	Log Initial Resistivity, mhos/cm	Acid Stability(1)		
		Hrs Tested	% Metal Lost	Log Final Resistivity
$SrCo_{.67}Mo_{.33}O_{2.66}$	4	8	77	10
$SrCo_{.25}Cr_{.45}Ta_{.30}O_{2.9}$	5	24	10	6
$SrNi_{.25}Mn_{.35}Ta_{.30}O_{2.9}$	4	24	7	5

(1) 3.7 M sulfuric acid, 86°C.

The greater acid stability is undoubtedly a consequence of the greater thermodynamic stability of the higher valence states of manganese and chromium, versus nickel and cobalt, as explained in Part a. In some cases, such as strontium cobaltmolybdate, the conductive manganese doped compound lost less cobalt in acid than the poorly conducting stoichiometric perovskite.

Several of the Mn-doped compositions containing Co, Ni and Fe were tested as both anode and cathode catalysts. Electrodes were prepared from tantalum powder, Teflon and the solids recovered from the acid stability tests. Tantalum screens were used as current collectors. This type of electrode was developed for testing for trace catalytic activities. For this purpose, it is free of many complications previously encountered with electrodes formed on platinum screens from carbon-catalyst mixtures.

These tests included hydrogen, ethylene and oxygen as reactants with 3.7 M H_2SO_4 at 100°C and with 85% H_3PO_4 at 150°C. In no instance was any significant degree of catalytic activity found.

Thus, oxidized Mn- and Cr-doped mixed perovskites show the best balance between electrical conductivity and acid stability properties of any group of high valence oxide compounds studied to date. They are still marginal in both these properties, however. Furthermore, they show no catalytic activity in either cathode or anode reactions. No further work on "oxidized state" perovskites as electrocatalysts is planned.

Part c - Reduced State Perovskites

Since mixed valence perovskites containing metals in a higher than normal valence state showed good properties but lacked catalytic activity, it was decided to investigate perovskites containing metals in a lower than normal valence state. Molybdenum was chosen as the B element because it is reducible from its normal hexavalent state to lower valences, because its reduced oxide, MoO_2, is highly conductive, and because cobalt and other molybdates are known industrial hydrogenation catalysts.

All the formulations were stoichiometric strontium-cobalt-molybdenum compositions containing three atoms of oxygen per atom of strontium, and one atom of combined cobalt plus molybdenum. The molybdenum was forced into a lower valence state, nominally five, by decreasing the ratio of cobalt to molybdenum. To prevent re-oxidation of the molybdenum the firings had to be done under nitrogen freed of water vapor and oxygen.

Unfortunately, the conductivities of the reduced valence molybdenum compounds, while better than the hexavalent molybdenum, never came close to the target value of 10^{-4} mhos/cm. See Table A-17, taken from the detailed data in Appendix A-9.

Table A-17

Conductivities of Reduced Molybdenum Perovskites

Nominal Formula: $SrCo_xMo_{1-x}O_3$

Atom Ratio Cobalt, X	% Reduced Mo	Conductivity mhos/cm
0.5	0	2.2×10^{-9}
0.417	57.2	2.9×10^{-7}
0.375	80	6.3×10^{-6}

Forcing the molybdenum valence further down to the IV to V, rather than the V to VI range, did not improve the conductivity further. It was interesting that the final products were very similar whether the initial reactants contained metallic molybdenum or MoO_2. The starting materials had vastly different conductivities but the final products were nearly the same (Table A-18).

Table A-18

Effect of Raw Materials on Mo Perovskite Conductivity

Nominal Formula $SrCo_{0.32}Mo_{0.68}O_3$

Starting Mo Compound	Log Resistivity, ohm cm, After Indicated Hrs Firing Time		
	0	3.8	21
Mo Metal	9	5	8
MoO_2	0	8	9

The X-ray spectra of all the compositions showed well developed perovskite structures of the ordered cubic type at all stages of firing. The lattice parameter was always 7.901 Å ± .005 (standard deviation), independent of the valence state of the molybdenum. The ordering, detected by additional lines in the cubic X-ray spectrum, indicates that the cobalt was incorporated firmly in the perovskite lattice.

The failure of the reduced molybdenum to achieve high conductivites prevented their meaningful testing as electrochemical catalysts. Their poor conductance must be attributed to insufficient overlap of the conductance orbitals of the molybdenum. Reduced tungsten and vanadium oxides (bronzes), on the other hand, have high, even metallic conductivity. Molybdenum bronzes are much more difficult to form. Attention therefore was focused on the tungsten bronzes rather than the reduced molybdenum perovskites.

Phase 7 - Oxide Bronzes

Part a - Introduction and Background

The oxide bronzes (not to be confused with metallic bronze alloys) are closely related structure-wise to the perovskites (12). The best known compounds of this type are based on tungsten and have the general formula A_xWO_3 (where A = Na, Li, K, Cu(I), Ag and Pb; and $x < 1.0$). The electrical properties of those containing alkali metals have been studied in detail (12) (13). Over wide compositional ranges, many of these materials are relatively good conductors of the metallic type. The conductivity is generated by the addition of electrons from the A metal into the empty conduction band of the "electron-less metal", WO_3. The tungsten is partially reduced to a valence state between five and six in the process. Tungsten bronzes also show exceptionally good resistance to attack by chemical reagents, especially acids. In fact, alkali metal ions in the A-position are highly inert to even the most corrosive acids such as HF.

It was not felt that the bronzes in the forms described in the literature would be very effective electrocatalysts. However, there is an important question in this connection which is not answered by the literature: can potentially catalytic metals such as Co or Ni be included in the bronze lattice by partial replacement of the tungsten according to the valence compensation principles used in the preparation of mixed perovskites?

It was hoped that a substitution of this type could be made without a great sacrifice in electrical conductivity. Also, it remained to be seen whether or not such "modified" bronzes could retain the catalytic metals in acids as well as the perovskites do.

The possibility of preparing "modified" bronzes of this type has been studied during the latter part of this period. Results reported here are preliminary in nature, since the program is still in progress.

Part b - Preparation of Bronzes

A study of the stoichiometry of such "modified" bronzes, using valence compensation principles, shows that allowable catalytic metal (Ni, Co) contents increase as the A-ion content increases. Maximum nickel contents would be desirable for catalysis, but increasing the nickel content reduces the amount of pentavalent tungsten, which provides the conductivity. The nickel content must, therefore, be kept below the value which reduces the tungsten V content to zero. The higher the A ion content the higher the tungsten V content and the higher the allowable nickel content. Table A-19 lists maximum and mid-range (W^V/Ni = 1/1) nickel contents, as dictated by valence compensation, for a range of mono- and di-valent metal contents in the A-position.

Table A-19

Nickel Content Allowed By Valence Compensation in Tungsten Bronzes

A ion Valence	Atom Ratio A	Atom Ratio Ni	
		Ni/W^V = 1	Max Ni (W^V = 0)
1	0.35	0.07	0.0875
1	0.8	0.16	0.20
2	0.35	0.14	0.175
2	0.8	0.32	0.40

Compositions chosen for initial study included:

(1) Simple bronzes, without catalytic metals, having a range of A-ion tents, both monovalent (Na) and divalent (Pb).

(2) Nickel "modified" compositions in the mid-range vicinity at two levels of A-ion contents ($A_{0.35}$ and $A_{0.80}$) for both monovalent and divalent A-ions. These mid-range compositions included Mo^V/Ni ratios of 0.5/1, 1/1 and 2/1. A priori thinking on this problem pictured Mo^V ions as a source of conducting electrons and Ni ions as a trap for them. Hence, the preliminary thinking attached some importance to these ratios.

Compositions studied so far in this program are listed in Appendix A-10 along with pertinent physical properties.

All firing compositions were compounded from dried starting materials, pilled, and the pills oven-dried in air at 240°F. The pills were wrapped in platinum foil and fired either under vacuum or in evacuated fused silica tubes. Both tungsten metal and tungsten dioxide were used, together with tungstates or tungsten trioxide, to obtain the lower valence states.

Part c - Conductivities of the Bronzes

The simple sodium bronzes were obtained in very pure form and showed conductivites and clear X-ray spectra in close agreement with literature values regardless of firing technique or starting materials (see Table A-20). The conductivities were about 10^5 times better than the manganese or chromium doped perovskites discussed in the previous phase.

Table A-20

Properties of Sodium Bronzes, Na_xWO_3

Value of x	Source of W	Firing Condition	Conductance, mhos/cm	X-Ray Spacing, Å
0.35	WO_2	Sealed Tube	1.23	3.810
0.32	---- Literature (14)----		--	3.813
0.80	W	Sealed Tube	11.8	3.852
0.80	W	Vac. Pump	6.07	3.852
0.80	WO_2	Sealed Tube	3.36	3.852
0.78	---- Literature (14)----		8.13	3.836

The simple lead bronzes were much lower in purity and contained appreciable amounts of lead tungstate. The conductivity decreased with increasing lead content (Table A-21), whereas the sodium bronzes showed an opposite trend.

Table A-21

Properties of Lead Bronzes, Pb_xWO_3

Value of x	Conductance, mhos/cm	X-Ray Spectrum
0.2	23.1	$PbWO_4$ plus two bronze phases: a = 3.86 Å and a = 3.78 Å
0.35	6.09	
0.45	1.65	
0.80(1)	1.77	

(1) Composition in the W^{IV-V} range, i.e. outside the usual W^{V}-W^{VI} range for bronzes. Comparison of X-ray spectra before and after acid treatment indicates presence of still other acid-stable phases of a non-perovskite nature.

The compositions containing added metals, e.g. nickel, were fired at the same conditions as the simple bronzes. Hence, the conditions used for the "modified" mixtures may not be optimum.

In both the sodium and lead series, conductivities of the fired materials decreased rapidly with increasing A-ion content (See Table A-22). X-ray data showed impurity phases of a non-bronze nature to be present in all these materials. All members of the $Na_{0.35}$ and $Pb_{0.35}$ series showed strong maxima characteristic of bronze structures, those for the former being more distinct. In fact, the spectra of both series gave strong indications of two different bronze structures, but the products were too impure to allow quantitative characterizations of these phases. Products of the $Na_{0.80}$ series were even more impure, although the X-ray spectra did indicate the presence of bronze phases.

Table A-22

Conductivities of "Modified" Bronze Compositions

Series	Conductivity Range, mhos/cm	X-Ray Spectra
$Na_{0.35}$	$5.2\text{-}7.9 \times 10^{-2}$	Impure but well-developed bronze structures present
$Na_{0.80}$	$2.4\text{-}42 \times 10^{-7}$	Very impure; bronze structure indicated present
$Pb_{0.20}$	0.508	--
$Pb_{0.35}$	$0.11\text{-}1.5 \times 10^{-4}$(1)	$PbWO_4$ present; two bronze structures present
$Pb_{0.50}$	2.1×10^{-2}	--
$Pb_{0.80}$	$2.1\text{-}5.5 \times 10^{-10}$	--

(1) For four composition containing nickel. Compositions containing Co, Fe^{II}, Mn and Cr are all in the 0.37-0.78 range with Fe^{III}, and Cu^{II} definitely lower, 5.0×10^{-2} and 8.0×10^{-5}, respectively.

Unfortunately, neither the X-ray data nor the conductivity data provide a definite answer to the general question of the state of combination of the added metal ions in these materials. Preparation of purer bronze phases, either by use of improved firing conditions or by treatment of the products with selective chemical agents to dissolve impurity phases, is necessary to answer this question.

Part d - Acid Stability of the Bronzes

The acid stability data, especially for the $Na_{0.35}$ series, provide some basis for believing that nickel may indeed be tied up in some very acid-stable phase such as a bronze. The acid stability tests (3.7 M H_2SO_4 at 86°C) were run in two steps:

(1) An initial step of 24 hours duration. It was felt that most nickel compounds of simple structure, e.g. binary oxides, salts, etc, would be completely decomposed by the acid during this period. On this basis, the undissolved nickel is that tied up in more stable complex structures, such as perovskites and bronzes.

(2) A second step of 72 hours. Nickel dissolved during this step is presumed to represent the corrosion rate of the more acid-stable phases present.

Many compositions in the $Na_{0.35}$, $Na_{0.80}$, and $Pb_{0.35}$ series showed good retention of nickel during the first step of the corrosion test. Those of the $Pb_{0.80}$ series were definitely poorer in this respect. However, losses of metal during the second step, by even those materials showing the greatest stability in the first step are relatively high, when compared to the stoichiometric perovskites. Typical data are given in Table A-23.

Table A-23

Acid Stabilities of "Modified" Tungsten Bronze Compositions

$A_xNi_yW_{1-y}O_3$

Nominal Composition		Cumulative % Nickel Extracted	
A-x	Ni:y	Step 1(1)	Step 2(2)
Na-0.35	0.058	1.4	57.7
Na-0.35	0.078	3.6	46.4
Na-0.80	0.16	13.0(3)	33.2(4)
Pb-0.35	0.14	13.0	69.1
Pb-0.35	0.17	3.1	36.6
Pb-0.80	0.16	38.8	57.0

(1) 24-25.5 hours at 86°C unless otherwise specified.
(2) 72 hours at 86°C unless otherwise specified.
(3) 66.1 hours.
(4) 114 hours.

Part e - Electrochemical Activity

A number of these "modified" materials (in the "as fired" state) in the higher range of conductivities were ground (agate mortar), mixed with Teflon, and formed into electrodes on tantalum screens. Limiting currents measured in both anode (H_2 and C_2H_4) and cathode (O_2) tests were not significantly better than those (< 0.02 ma/cm^2) found for blank electrodes (tantalum powder-Teflon on tantalum screen) under the same test conditions. Data are given in Table A-24.

Table A-24

Electrochemical Tests on
"Modified" Bronze Compositions, $A_{.35}Ni_yWO_3$

Composition		Limiting Current (ma/cm^2)			
		H_2		C_2H_4	O_2
A ion	Value of y	100°C(1)	150°C(2)	100°C(1)	100°C(1)
Na	0.06	<0.06	<0.06	<0.02	<0.02
Na	0.07	0.06	<0.02	0.06	--
Na	0.08	0.06	<0.06	0.1	<0.02
Pb	0.12	<0.06	<0.02	<0.02	<0.02
Pb	0.14	<0.02	--	<0.02	<0.02
Pb	0.16	<0.02	--	<0.02	<0.02

(1) With 3.7 M H_2SO_4.
(2) With 14.7 M H_3PO_4.

In summary, conductive tungsten bronzes containing prospective catalytic metals have been made. In certain composition ranges the materials conduct well enough to be used with or without an auxiliary current collecting powder. The acid stability data confirms the incorporation of the catalytic metals into a stable lattice. However, the compounds so far are too impure for us to determine how firmly the metals are held. So far the nickel containing products are electrochemically inactive. Other metals need to be examined. Even though the oxide bronzes are metallic conductors the added metal is present as an ion, rather than in the zero valent form which is used in conventional catalysis. It would be reasonable therefore, to choose ions such as Ag^+, Cu^+, Tl^{+3} whose outer electronic structure corresponds to Ni^o.

Phase 8 - Eta Phase Carbides

Certain carbides of the transition elements appear worthy of investigation as fuel cell catalysts because they are reported to combine corrosion resistance with high electrical conductivity. Transition metal carbides, sometimes called "hard metals", find wide use in special steels and are of considerable technological importance in that industry. Because of their importance simple (single metal) carbides are commercially available. For this reason this class of carbides was the first investigated here for use as fuel cell catalysts.

Unfortunately, it was found that the simple transition metal carbides do not show catalytic activity on either hydrogen or oxygen in either sulfuric acid or potassium hydroxide. Neither the pure carbides nor their solid solutions were active as electrodes. The electrodes tested were fabricated into high surface area structures with Teflon and ammonium carbonate as has been described in previous reports. The test results reported in Appendix A-11 were obtained in 30% sulfuric acid and 30% potassium hydroxide at 100°C. Chromium boride was also tested in this program. It was reported to be corrosion resistant and catalytic, but it possessed neither of these attributes.

As the simple carbides did not show catalytic activity and in many cases were not corrosion resistant, it was decided to investigate more complex structures. "H" phase carbides (15) and perovskite (16) structures of transition metals with post-transition metals and carbon were examined. Experiments showed that these materials were readily attacked in solution. They had very poor corrosion resistance. A study of η phase carbides was then begun. These are reported to possess extraordinary corrosion resistance.

There are two types of η phase carbides, those having the idealized formula A_3B_3C, called η_1, and those having the idealized formula A_2B_4C called η_2. Both these phases have a face centered cubic structure and belong to the space group Fd 3m. In this complex space group, octahedra of B atoms are arranged in a diamond-like lattice. Carbon atoms are located in the distorted octahedral holes between neighboring B octahedra. The remaining metal atoms are in tetrahedra distributed through the lattice. In the idealized formula of the η phases, A represents a first row transition element such as V, Cr or Mn, while B corresponds to a second or third row element such as Nb, Mo, W or Ta. It is expected that the first row element will impart catalytic activity to the carbide while the second or third row elements will provide corrosion resistance. A and B may be mixtures of elements. Indeed the literature shows that the number of η phases possibly increases if such mixtures are used (17) (18)

The investigation of the properties of η phase carbides was begun with a purchased sample of what was purported to be Ni_3W_3C obtained from Semi Elements of Saxonburg, Pennsylvania. It was found by X-ray diffraction to contain about 75% WC, some Ni_3C and the rest Ni_2W_4C, rather than 100% Ni_3W_3C. When this impure purchased carbide was treated with hot 30% sulfuric acid, the nickel carbide was removed from the system. However, the η phase structure retained its nickel component. Thus, it seems that this type of structure is acid resistant. An electrode prepared from the acid extracted sample did not show any catalytic activity. The acid resistance indicates that these phases should be investigated further, in more purified form.

As the purchased Ni_2W_4C sample was rather impure an attempt was made to prepare a tungsten η phase carbide in this laboratory by a rapid melting technique. A stoichiometric mixture of manganese (used because of its low melting point), tungsten and carbon, corresponding to Mn_3W_3C, was pelletized and then heated in a graphite mold to 1500°C and 3 tons/in^2 for a few minutes. After melting occurred, the sample was allowed to cool slowly. Its X-ray diffraction pattern indicated that WC was the principal product while a small amount of Mn_2W_4C and Mn_3C were also formed. This material, too, was acid stable although it corroded slowly in basic media.

Semi Elements is the only commercial supplier of η phase carbides. As their sample was quite impure and it was found that "quick and dirty" preparations in this laboratory did not produce pure η phases it was decided to attempt their preparation here by more careful means. Preparing these complex carbides in this laboratory not only will allow for close control of the purity of the product and completeness of the reaction but further will facilitate the production of a large number of samples of varying composition and stoichiometry. To this end, a vacuum induction furnace was assembled. It consisted of a stainless steel bell jar with quartz windows and a precisely machined lower edge, which formed a vacuum tight seal against a heavy steel base plate. Leads to a ten kilowatt induction unit and to a high capacity vacuum system came through the base plate.

In the first attempt at preparing an η carbide under carefully controlled conditions, a sample containing nickel, tungsten and carbon was pelletized and put in a graphite crucible, surrounded by the induction coil heater, a tantalum foil heat shield, and then an alumina crucible as another heat shield inside the vacuum chamber. Unfortunately, by the time the graphite crucible was degassed and heated to 1000°C the walls of the vacuum system got so hot that they began to buckle and the heating had to be discontinued. To prevent the heating of the walls during the second attempt a steel cylinder was used as a further heat shield between the alumina crucible and the vacuum chamber walls. This prevented the walls from heating but the connections on the induction heater got hot and vacuum was lost. Further the gasket at the bottom of the chamber also failed and lost vacuum. In order to avoid further heat shielding problems a water cooled bell jar has been designed. This should allow heating to high temperatures, with maintenance of vacuum, especially when lined with tantalum foil as a heat shield.

An all quartz vacuum system was also designed. Samples will be heated in vacuo to somewhat lower temperatures (up to 1000°C) within a quartz tube by means of an induction coil wrapped around it. Quartz was chosen as the furnace material because it adsorbs much less light than Vycor and thus would be heated much less by the glowing sample suspended in vacuum inside it. The first such furnace has been built and is currently being debugged. A third technique for making η carbides is also being tried. Pellets containing stoichiometric amounts of metals and carbon are being sintered in evacuated quartz tubes for several weeks. This procedure appears to be slow but sure, but product purity is questionable at this point.

It is expected to prepare many compositions of η phase carbides as soon as our water cooled vacuum shield is installed. These will be tested for electrochemical activity and for corrosion resistance.

If these materials do not give the desired results then other interstitial compounds will be made in the same apparatus and evaluated. The preliminary work with chromium boride indicates that complex structures will be needed here also to provide corrosion resistance.

Phase 9 - Hydrocarbon Reforming in the Liquid Phase

A non-noble metal catalyst for a hydrocarbon consuming fuel cell is, of course, highly desirable. Previous studies (5)(6) had shown that a non-noble metal steam reforming catalyst developed by Esso could be formed into an anode which was active with hydrogen fuel but not with hydrocarbons. In addition, this catalyst was active for the reforming of hydrocarbon and steam to form carbon dioxide and hydrogen from vapor phase reactants at fuel cell temperatures. Why the reforming to hydrogen and the subsequent consumption of the hydrogen at the anode did not occur in the fuel cell environment remained unanswered. It was hypothesized that the presence of the liquid phase reactants might have stopped the reforming reaction. To test this hypothesis reforming was attempted with both reactants, water and hydrocarbon, in the liquid phase.

These experiments were performed by passing liquid phase mixtures of hexane or decane and water up through a 13" long tube containing 3 1/8" diameter pills of catalyst. Temperatures of from 260 to 154°C were used with pressures of from 925 to 75 psig to keep the reactants in the liquid phase. Product analysis by mass spectrometry showed that reforming of hydrocarbons and water in the liquid phase was occurring at substantial rates. This, of course, shows the hypothesis that the presence of the liquid phases stopped the reaction is wrong.

The results of these tests show that increasing the flow rate increases the rate of reaction proportionately, as shown in Figure A-9 and Appendix A-12. This indicates the rate limiting step is mass transport rather than catalysis. The maximum reaction rates obtained were limited by the maximum flow rates of the pumps in test apparatus. The ultimate reaction rate at a very high flow rate and optimum geometry has not been determined.

Figure A-9

Effect of Flow Rate on Reaction Rate

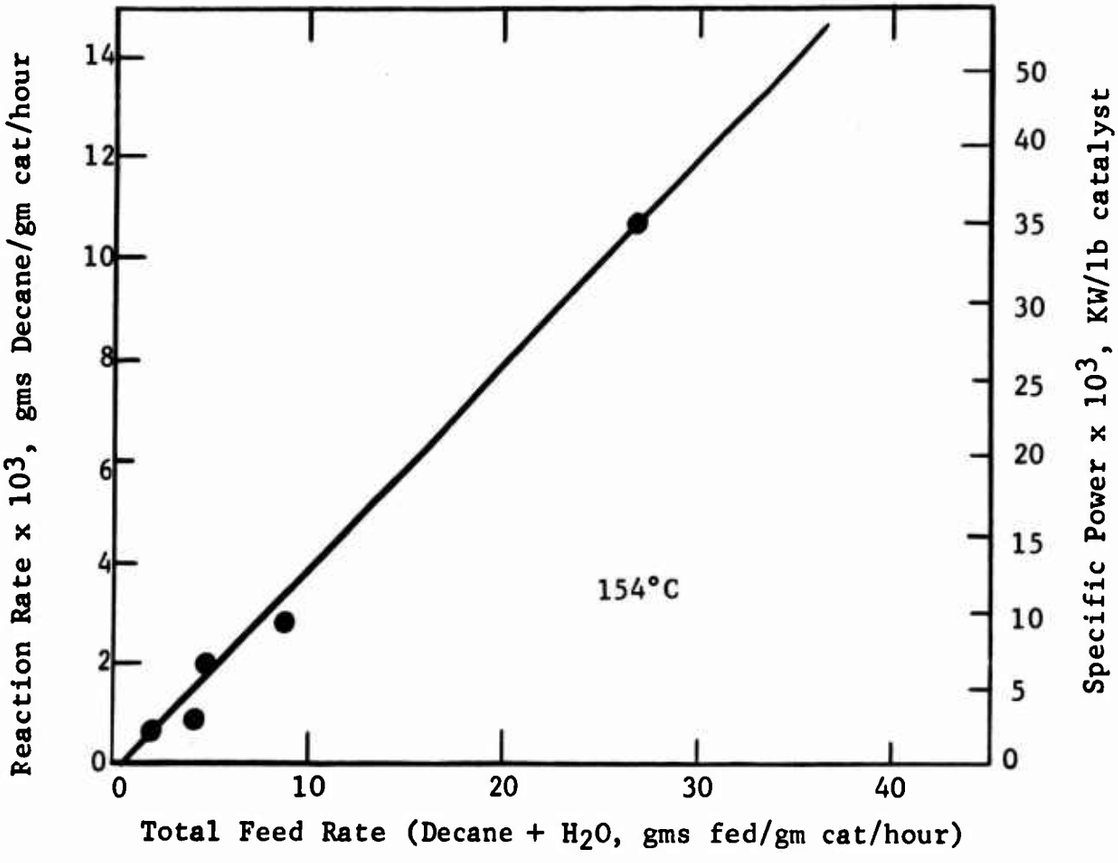

The rates of reaction obtained at maximum flow rate compared favorably to those previously obtained (5) in the vapor phase. The maximum measured rates of reaction with the liquid phase are nearly independent of temperature at a value of 10^{-2} weights of decane reacted per weight of catalyst per hour. This rate is about equivalent to the rate obtained in the vapor phase at 260°C, but nine times higher than the vapor phase rate at 154°C. The rates of reaction are shown in Figure A-10. This constant reaction rate, independent of temperature, confirms that the liquid phase reaction is mass transport limited. Thus, it has been shown not only that the presence of liquid phase reactants does not stop the reforming but that reaction rates with the liquid phase of up to nine times those in the vapor phase have been obtained Further, the ultimate liquid phase reaction rate in the absence of mass transfer limitation is even higher than the rates that have been obtained.

Figure A-10

Rates of Reforming at Low Temperature

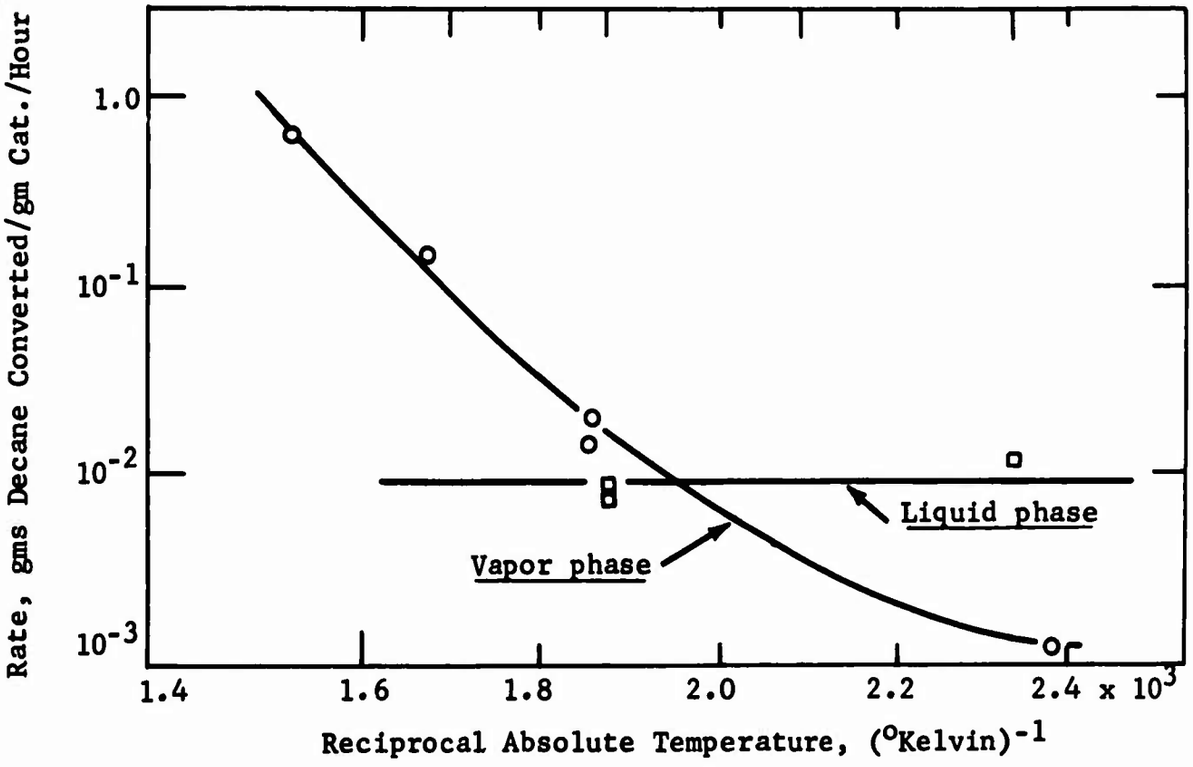

The outlook for a non-noble metal catalyst to be used at the anode of a hydrocarbon fuel cell has been brightened by the results of these experiments. Since it has been found that the presence of liquid phase reactants does not inhibit the reforming, only two additional conditions are present in the fuel cell that could stop the reforming reaction. These are the presence of the ions in the electrolyte, the pressure and the electrical potential between the catalyst and electrolyte. Conditions in a reformer can be made to successively approach those in fuel cell by adding electrolyte ions and imposing potentials on the catalyst. This type of study should identify why previous attempts to use this catalyst at an anode of a fuel cell failed. Once the reason is known, changes in the catalyst may be possible, so that the same non-noble elements of the reforming catalyst may be made to function as the anode of a hydrocarbon fuel cell.

4.2 Task B, Hydrocarbon Total Cell

The primary objective of the hydrocarbon total cell program is the evaluation of the engineering feasibility and system requirements of a direct liquid hydrocarbon-air fuel cell. To do this requires a total cell system with reasonable current capability. Consequently, research during this period has emphasized the development of a liquid decane-air fuel cell with sufficient capability to allow the evaluation of anticipated problem areas, such as operation with either fuel or oxygen transport into the electrolyte space, fuel recovery, chemical oxidation at the cathode, and temperature maintenance.

In addition, a second objective of this work has been the design, construction, and testing of a liquid decane-air total cell assembly for delivery to the U.S. Army Electronics Command at the end of the contract year. Test work on this unit has been completed.

Phase 1 - Studies in Hydrocarbon Fuel Cells

Tests were conducted in small (10 cm^2) liquid decane fuel cells to further explore the interaction of systems and electrode requirements. Particular attention is given to the problem of operation with fuel transport and carbon dioxide rejection in the electrolyte space. Previous studies (7) indicated that even for a 1 cm electrolyte chamber thickness decane could accumulate, causing a loss in performance at the cathode and increased IR. In addition, cathode system evaluation work was required because preliminary data indicated that the poor structural stability of the sintered platinum Teflon emulsion cathode could reduce cell life.

Part a - Small (10 cm^2) Cell Design

The liquid decane-air cell used in the initial phase of the engineering study, shown in Figure B-1, is basically the same as that used in the earlier sulfuric acid study (5). However, it was designed to function with 150°C, 14.7 M H_3PO_4 electrolyte in a temperature controlled oven using the operating system described in the previous semi-annual report (7). Operation in this oven allowed us to use the original Teflon cells without excessive thermal damage.

As indicated in Figure B-1, the unit cell consists of a central electrolyte chamber (0.109 inches thick) inserted between the air and fuel chambers. Fuel is fed by gravity into the bottom of the fuel chamber, then through the porous Teflon barrier to the anode. Some of the fuel is consumed at the anode electrochemically, however, the bulk of the fuel is transported through the anode into the electrolyte space. As a result, a significant electrolyte flow 0.5 cm^3/minute-cm^2, is required to sweep the decane upward out of the cell before it can inpinge on the cathode surface. However, this flow does not completely eliminate the impingement problem. Air enters counter current to the fuel and electrolyte flow.

As indicated previously, fuel transport can be a significant problem when operating at 150°C with oxygen since some cathodes are known to transport oxygen in much the same way as the anode transports fuel. Contact of oxygen and fuel on the hot platinum cathode can cause an explosion. Design changes in the 80 cm^2 multicell unit (discussed in Phase 2) have successfully minimized this hazard.

Figure B-1

Schematic of Liquid Decane Total Cell

(10 cm^2 Circular Electrode)

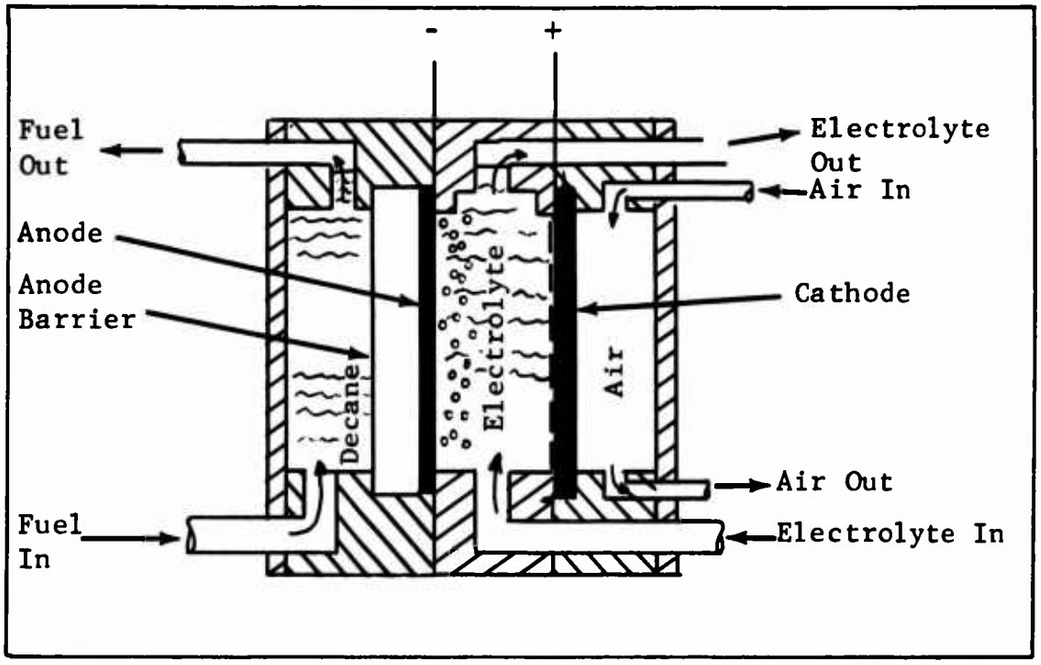

Part b - Cell Performance

Single and multicell tests have been conducted, using this 10 cm^2 cell, to evaluate component stability and compatibility prior to their incorporation into the 80 cm^2 assembly. Particular emphasis was given to the evaluation of improved cathode structures, since studies indicated that cathode cracking and checking could limit cell life. Therefore, a series of single and multicell tests were conducted varying the cathode structure while maintaining a constant anode configuration. Four cathode types were examined, including: (1) a standard 50 mg/cm^2 S.P.T.E. cathode coated with 6-8 mg/cm^2 Teflon spray coating, (2) a standard S.P.T.E. cathode covered with a 3.5 mil porous Teflon film, (3) a commercial Cyanamid AA-1 cathode laminated to a 3.5 mil porous Teflon film, and (4) the sintered carbon Teflon electrode. The results of this study are summarized in Appendix B-1. Analysis of this data indicates that except for the sintered carbon Teflon cathode, all of the electrodes gave the same initial performance levels despite the fivefold variation in catalyst loading. The average cell performance obtained in these single and multicell tests are shown in Figure B-2. For the five systems tested the average cell performance fell essentially on a single curve with a peak power capability of 17 mw/cm^2 on oxygen and 14 mw/cm^2 on air. However, the best three cell stack gave 21 mw/cm^2 on oxygen and 17 mw/cm^2 on air. Since all of the potential cathodes gave the same total cell performance, selection was based upon the ability to maintain performance and interface control after prolonged exposure to environmental temperature. The effect of exposure to

Figure B-2

Initial Performance of Liquid Decane Cells
(10 cm^2 Unit)

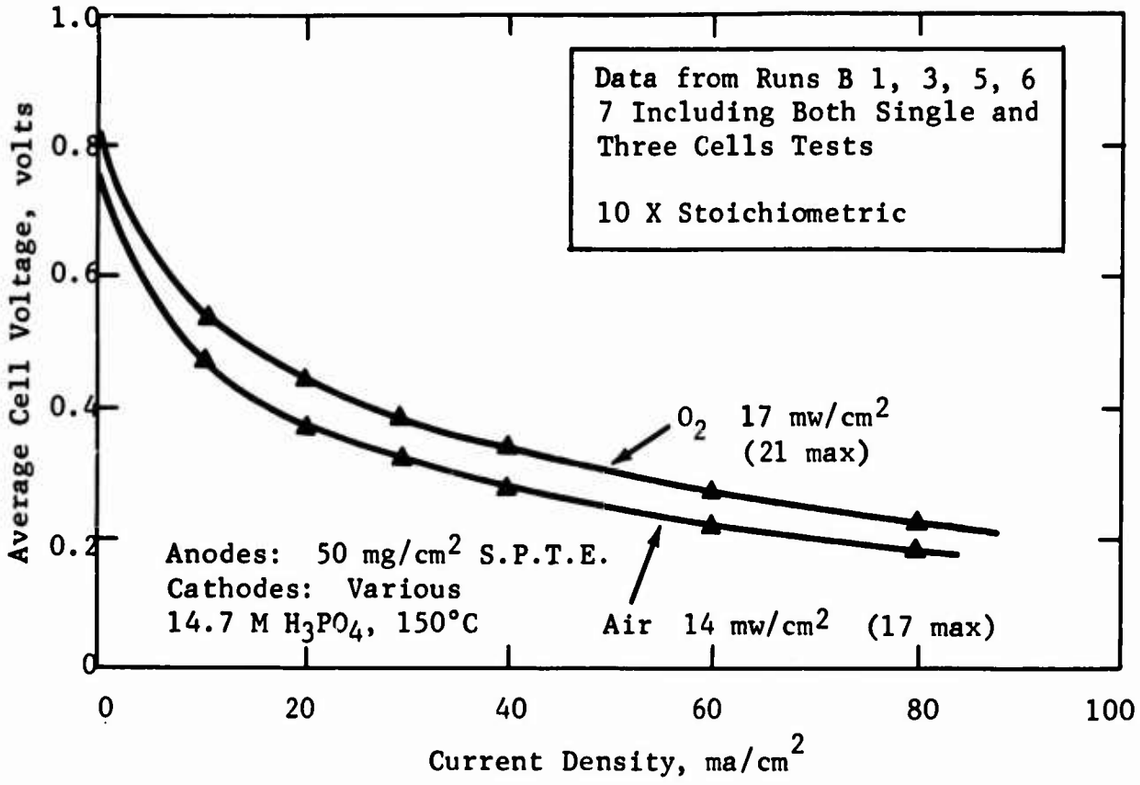

elevated temperature on cathode performance is shown in Figure B-3, which is a plot of hours at temperature (not load) versus total stack output voltage at 25 ma/cm^2. Of the three electrodes tested, only the clad sintered platinum Teflon electrode was able to maintain performance and interface control throughout the test period, suffering only a 0.1 volt loss in performance in the last six hours due to a system upset which allowed excessive quantities of decane to reach the cathode and some barrier separation. This cladding separation problem was corrected by lamination of the porous Teflon film to the cathode at elevated temperature (see Task E, Phase 2). On the other hand the laminated American Cyanamid AA-1 electrode failed to maintain cell performance despite the fact that interface control was good throughout the test. This poor performance was most probably due to decane poisoning (or flooding).

In view of these findings, the 80 cm^2 multicell system will use the 50 mg/cm^2 S.P.T.E. electrode laminated to a thin porous Teflon film.

Figure B-3

Effect of Exposure to
Temperature on Decane Air Performance

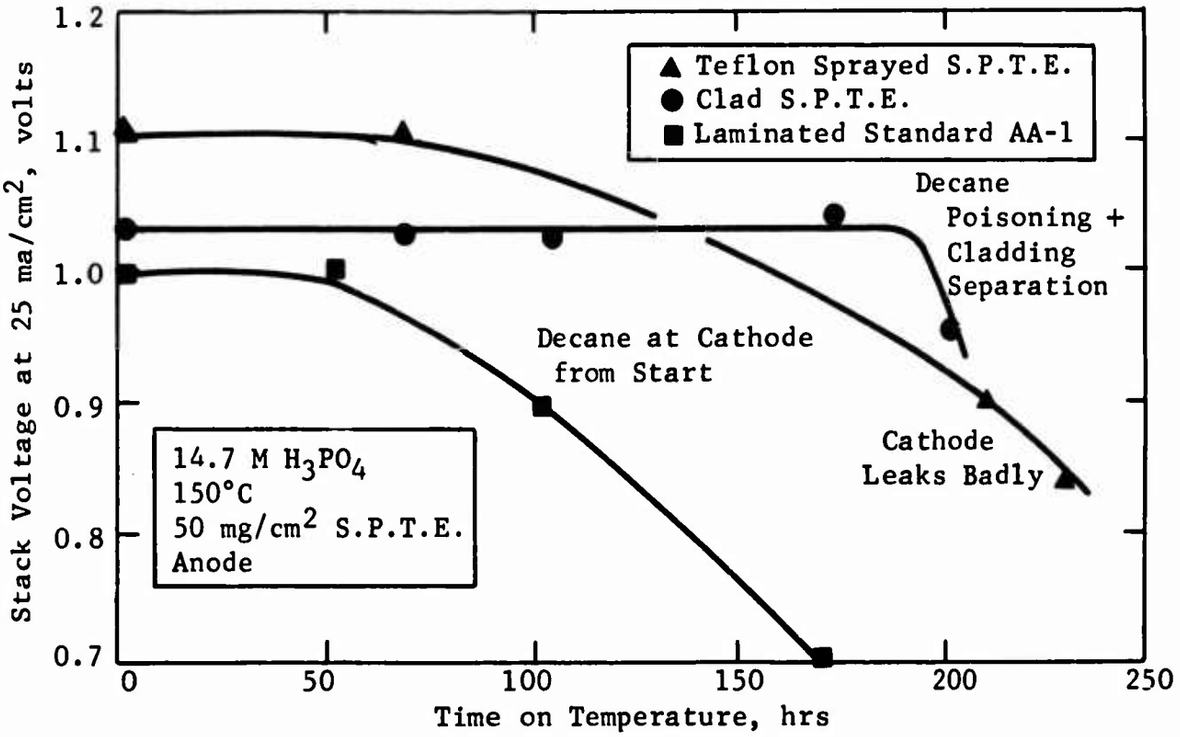

Part c - Gas Rejection and Resistance Losses

One of the multicell assemblies was tested on butane prior to operation on liquid decane to evaluate the effect of CO_2 rejection in the electrolyte space on cell IR loss. The results of this study, shown in Figure B-4, indicate that the 10 cm^2 cell does not have adequate gas release capability. Ideally, the IR current density curve should be a perfect straight line through the origin. Figure B-4 is almost linear up to 60 ma/cm^2, however, for currents greater than 60 ma/cm^2. CO_2 rejection from the intercell space becomes limiting and increased IR is observed. These data indicate that an improved venting system will be required in the 80 cm^2 unit.

In the course of this IR investigation a butane performance curve was also determined to see how well the half cell measurements predict total cell performance. The performance data shown in Figure B-5 indicates good agreement yielding 31 mw/cm^2 on oxygen compared to 35 mw/cm^2 predicted from half cell data. Air data were equally good and a peak power of 19 mw/cm^2 was obtained.

Figure B-4

Effect of CO_2 Evolution on Cell Ohmic Loss

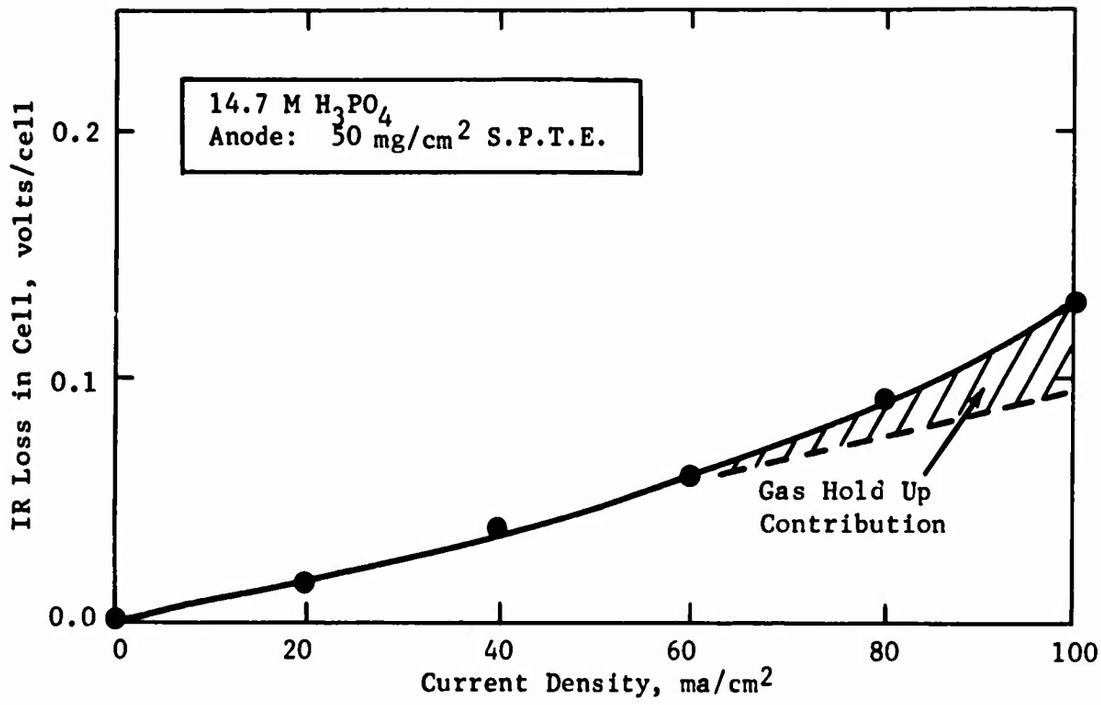

Figure B-5

Butane Performance

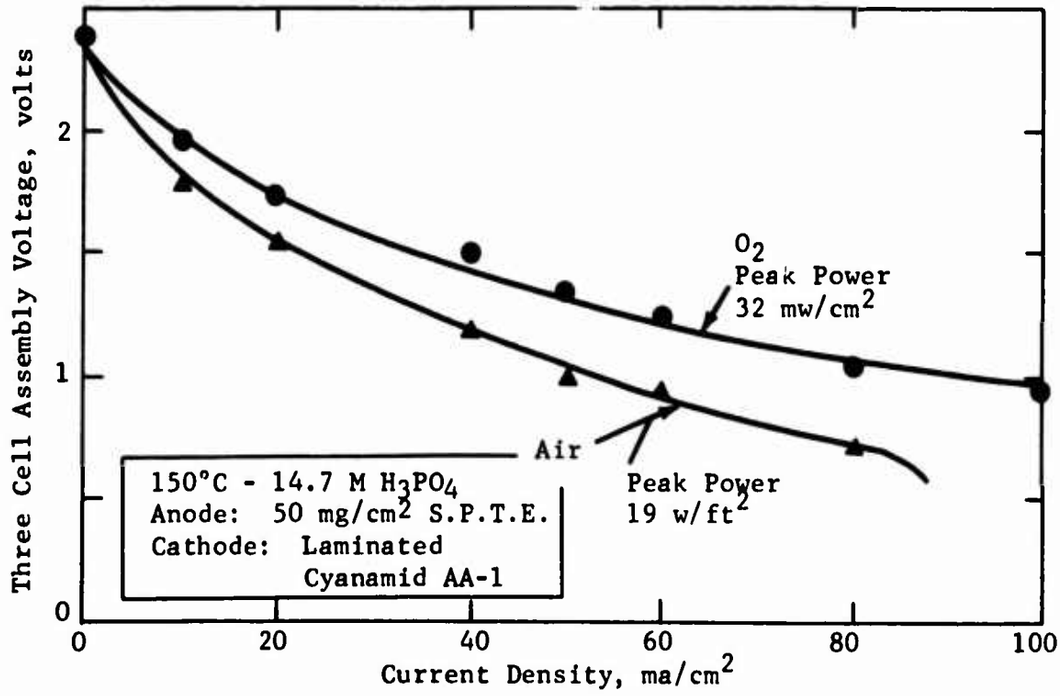

Part d - Engineering Evaluation

Operating experience with the small multicell assembly pointed up a number of cell and operating system defects which were corrected in the final 80 cm^2 multicell assembly and operating system. Table B-1 lists these problem areas and the recommended correction procedure.

Table B-1

Problems with 10 cm^2
Cell and Operating System

Defect	Recommendations
Operating System	
Gravity feed electrolyte circulation system unreliable and difficult to balance.	Go to pump feed-gravity return system rather than a pump return used in the operating systems.
Fuel cracking and coking in heater electrolyte tank.	Use ambient temperature tank with decane removal weir rely on preheater to maintain electrolyte temperature.
	Provide a fuel recovery and purification system.
The Cell	
Mechanical pinning not adequate to prevent anode barrier separation	Laminate the barrier to anode.
Fuel contacting the cathode	Provide electrode free residence space for decane at the top of the electrolyte chamber (especially important when operating on oxygen (see below)).
Electrolyte venting poor, CO_2 not released rapidly enough	Modify the vent system to provide for independent liquid and gas exits to minimize back pressure on gas release ports.
Explosion possible when operating on oxygen.	Provide vent gas purge on all vent lines for oxygen operation, install effective electrolyte exit weir to insure positive electrolyte head.

Phase 2 - Engineering Studies in the
4" x 4" Liquid Decane Multicell Assembly

The information developed in the study of cell and systems requirements with 10 cm^2 liquid decane-air cells (Phase 1) was used to design and construct a sealed up (4" x 4") fuel cell assembly and multicell operating system. Details of the modified unit cell are discussed in Appendix B-3 and the improved operating system (5 cell) is described in Appendix B-4.

A five cell fuel cell assembly is shown in Figure B-6. Its overall dimensions are 6-1/4 x 6-3/4 x 4-1/2 including end plates and spring closure, requiring approximately 0.45 inches per cell.

Figure B-6

LIQUID DECANE-AIR FUEL CELL
FIVE CELL ASSEMBLY

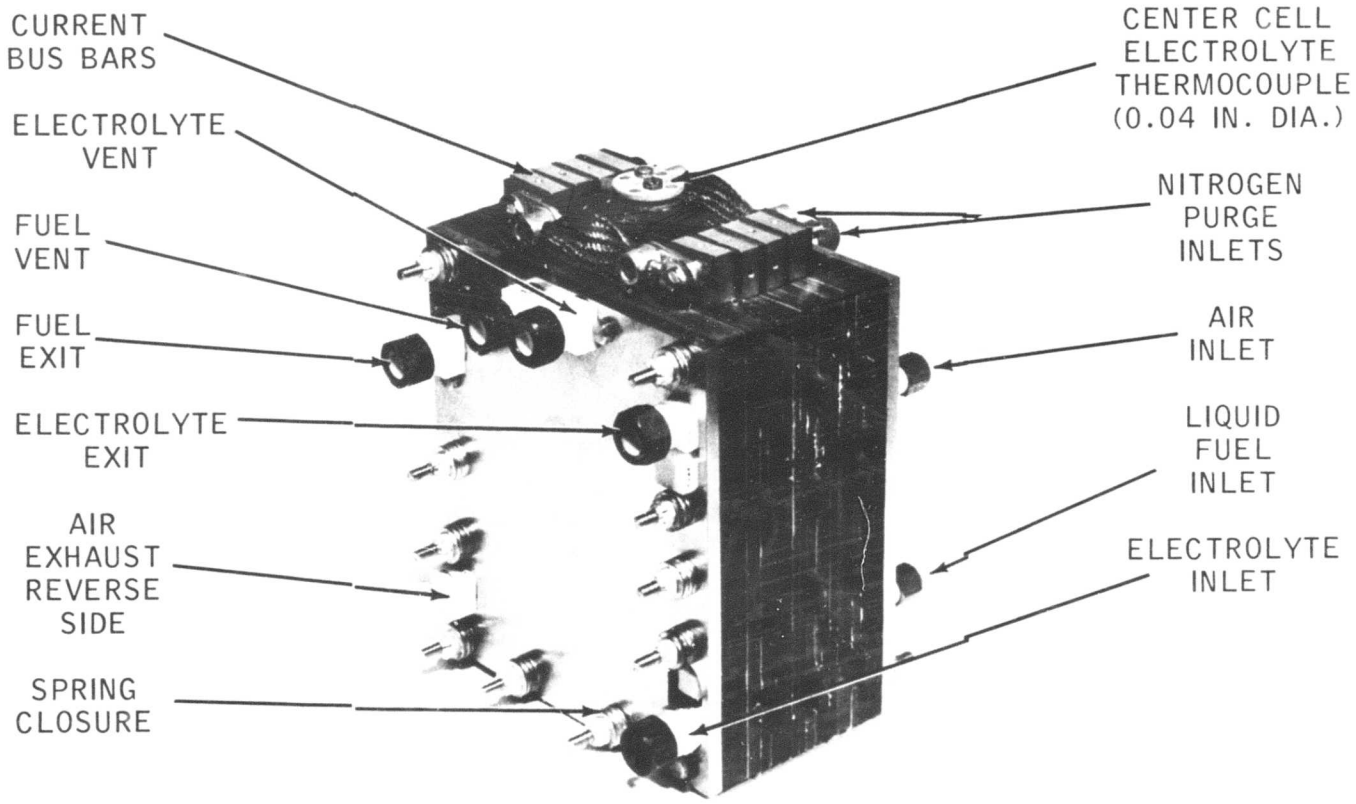

Figure 1 shows the feed and exhaust connections for the fuel, air and electrolyte, the nitrogen purged vent system, the current collector bus bars and the special Belleville spring closures required to prevent leakage on temperature cycling. The order of assembly for this series convected five cell stack is shown in Appendix Figure B-2.

Part a - Performance Evaluation

Tests were made with this liquid decane-air multicell system using 14.7 M phosphoric acid electrolyte to study the effects of system scale-up on cell operation and electrode life. Two individual unit cell configurations were used. In

the first tests the anode barriers were not bonded to the 50 mg/cm^2 S.P.T.E. electrodes and clad Cyanamid AA-1 cathodes were used. However, in subsequent work laminated 50 ma/cm^2 S.P.T.E. anodes and cathodes were evaluated.

In the initial tests, the performance of the individual cells proved to be sensitive to electrolyte flow distribution. This was corrected by opening the electrolyte balance pressure line to both end plate electrolyte input manifolds in order to feed each cell from both ends of the stack. The initial performance curves obtained with unlaminated S.P.T.E. anodes and clad Cyanamid cathodes are shown in Figure B-7 and Appendix B-2, along with a predicted performance curve based up the average 10 cm^2 system previously tested. The oxygen performance is in good agreement with the predicted values. However, the air data indicates a 0.40 volt (80 mv/cell) debit due to decane transport across the electrolyte chamber. This decane transport to the cathode caused a continuous performance loss, so that after 100 hours on test (34 on load) the stack output was reduced from 3 to 1.5 watts, while after 200 hours the power level was only 1.3 watts. Failure occurred at 240 hours due to cathode barrier rupture.

Figure B-7

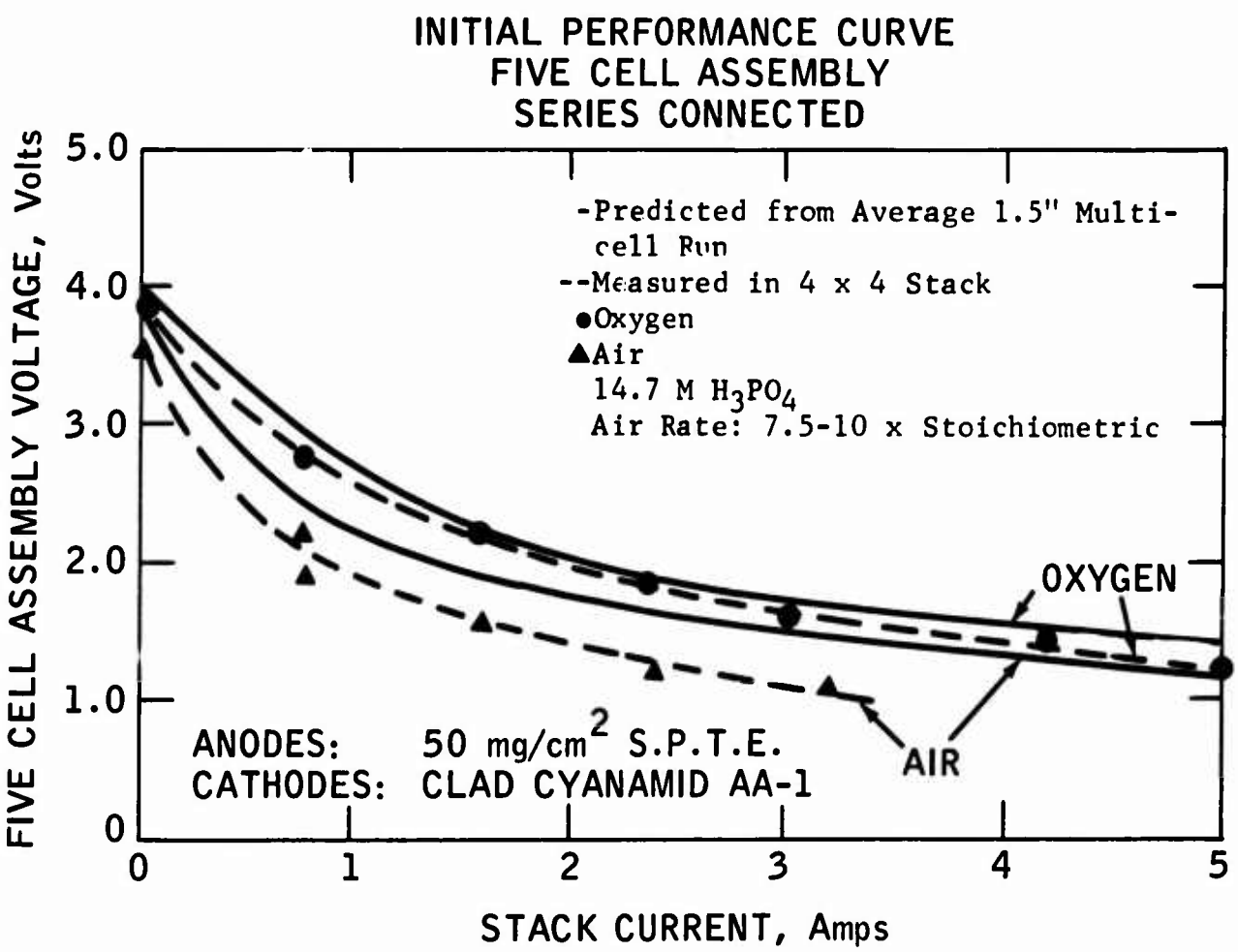

Next a three cell assembly was run to evaluate the improved laminated electrodes and check on the operation of the delivery test unit since a faulty relay had previously resulted in the loss of the second five cell assembly. This loss of components forced a reduction in the number of cells used in subsequent test assemblies in order to save enough for a five cell delivery unit.

The results of this laminated electrode test is summarized in Figure B-8, which compares the average cell voltage on oxygen for both the clad and laminated structures. As indicated the oxygen performance compares quite favorably with the anticipated value despite the fact that the cathodes were prepared using an older technique than currently used. This latter technique is known to produce 100 mv more polarization per cell on air than the optimum clad material. However, the major advantage obtained with this system is found in improved electrode life, maintaining a stack power (3 cells) of 1.1 watts for over 400 hours on test including three cold shutdowns and a run on a wide boiling range jet fuel (Esso OTF-90).

Figure B-8

Initial Oxygen Performance Multicell Assembly

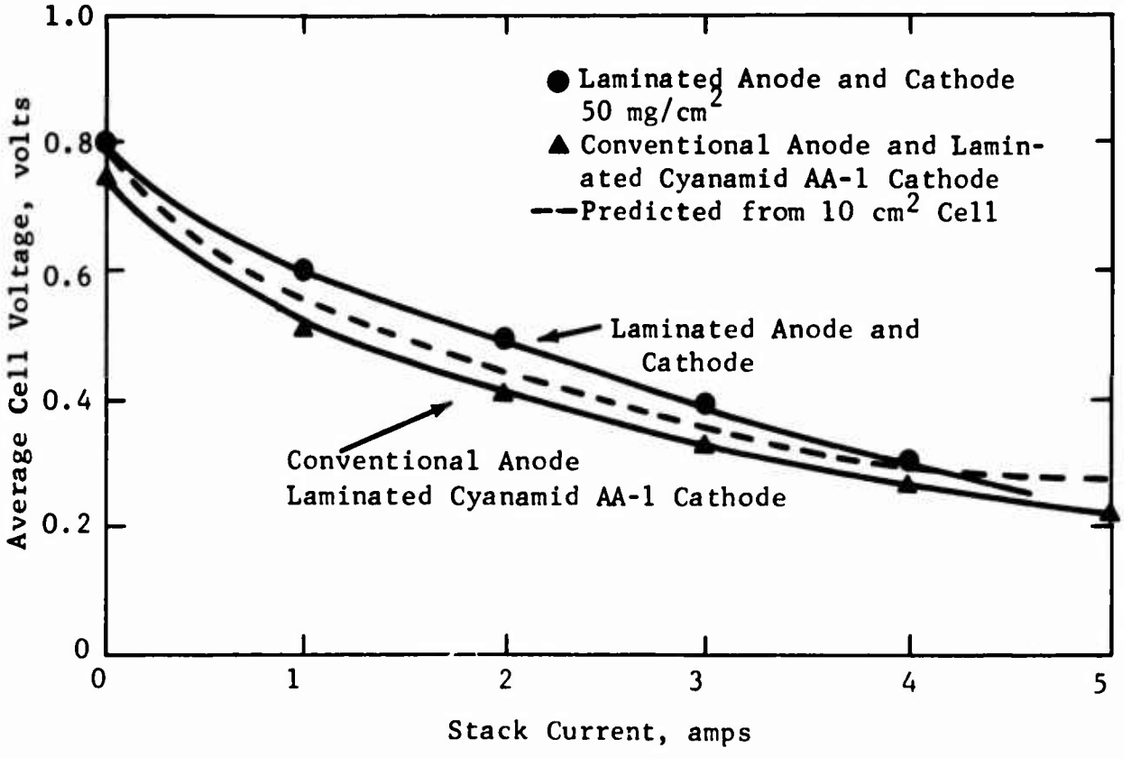

Part b - Performance Evaluation
Wide Boiling Range Fuel

The use of wide boiling range fuels was briefly examined using the three cell assembly just discussed to determine what new problems were introduced when opeating with realistic fuel systems. A special low sulfur isoparaffinic turbo fuel (supersonic jet fuel-90, boiling range 195°C to 290°C) was silica gel percolated and fed to the cell through the normal fuel feed system. The results shown in Figure B-9 indicate a threefold reduction in power capability with this isoparaffin fuel. Inspection of the operating system indicated that this was due to increased fuel transport through the anode with resultant increased cathode poisoning. Thus, solution of the fuel transport problem should also improve performance on wide boiling range fuels. No other system or cell operating difficulties were observed with this fuel.

Figure B-9

Effect of Wide Boiling Range
Fuel on Stack Performance-Oxygen

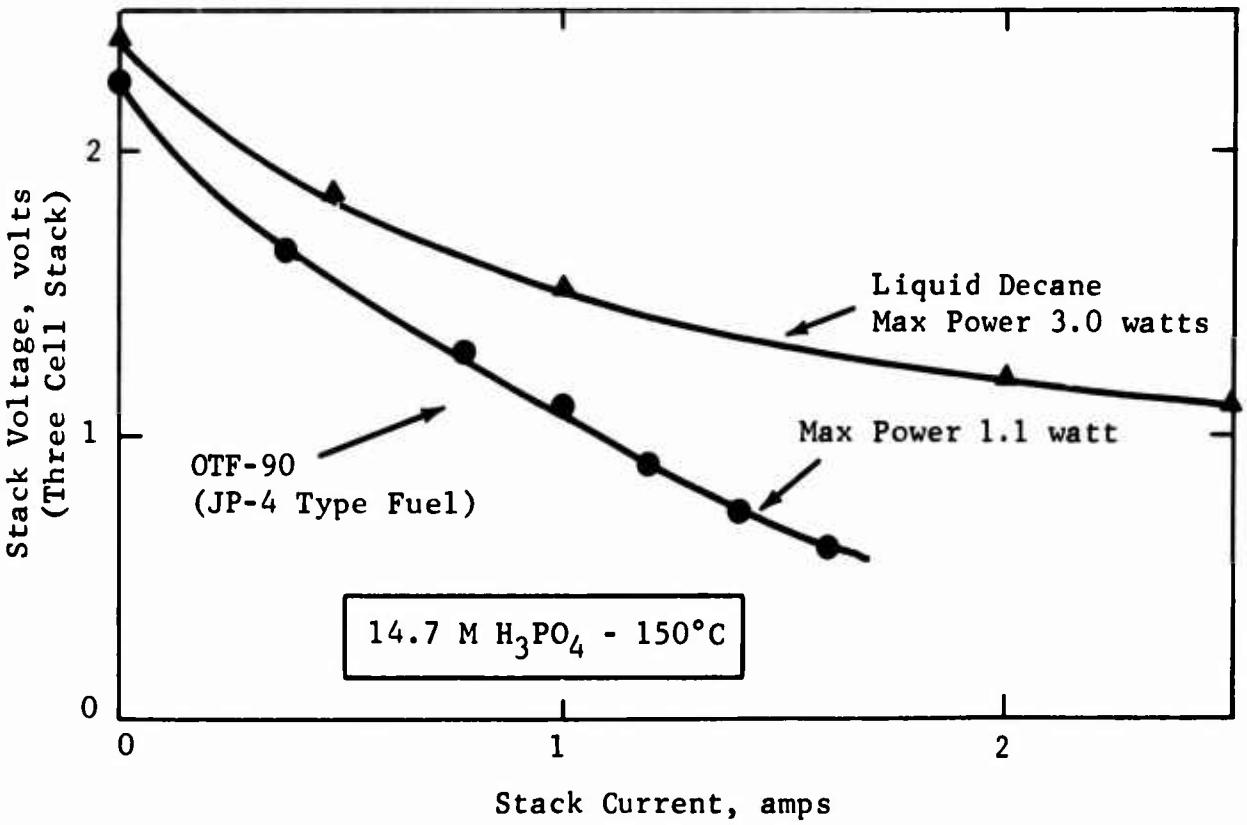

4.3 Task C, New Systems

In addition to the conventional work on electrocatalysis, electrode structure and total cell development, effort is also being expended on new electrolytes and new electrode configurations. The electrolyte work has emphasized temperatures of about 100°C above normal. The aim here is to decrease platinum catalyst requirement to practical levels or permit the use of less active non-noble metals such as nickel without approaching the very high temperature levels of the molten carbonate (600°C) or the solid zirconia (1000°C) fuel cells. Pyrophosphoric acid considered previously, was examined further and molten bisulfates were also investigated. The carbon dioxide rejecting properties of carbonate electrolytes were also determined to learn how alkaline a buffer would still be invariant. Some work was done on methanol catalysts showing activity in buffer electrolytes. Finally, the slurry electrode configuration was studied further to determine its ultimate potentialities.

Phase 1 - Catalyzed Carbon Electrodes in Pyrophosphoric Acid

In previous studies (7) pyrophosphoric acid was shown to be an excellent electrolyte for hydrocarbon fuel cells. With butane as test fuel current densities of over 400 ma/cm^2 were obtained at 250°C. The oxygen or air electrode had nearly theoretical open circuit polarizations and the former was polarized as little as 0.08 volts at 100 ma/cm^2. The next point to be ascertained was the extent to which the platinum quantity, initially at 50 mg/cm^2 could be reduced by the use of this electrolyte. Platinum supported on carbon at a level of 5 mg/cm^2 was used as the electrode catalyst, initially with poor and irreproducible results. The work reported here was aimed at improving this performance.

Part a - Anode Performance

The first step taken to improve the performance of platinum-on-carbon catalysts in pyrophosphoric acid electrolyte involved a change in the impregnation technique. When relatively high platinum contents are used (6 wt %) much of the chloroplatinate ion in the impregnating solution is not adsorbed by the carbon, but merely absorbed by it. Upon reduction the adsorbed chloroplatinate is probably converted simply to platinum black. Therefore, the impregnation was carried out in two steps with an intervening reduction with borohydride, in order to decrease the probability of reducing non-adsorbed platinum. The results obtained with these electrodes appeared to be sensitive to subtle differences in what was ostensibly the identical procedure for preparing the platinum-on-carbon catalyst. Since the cause of the activity differences has not been determined, it is being ascribed for purposes of reporting to minor differences in technique of two operators, labeled in this report as A and B.

As shown in Figure C-1, the double impregnation was inferior to the single impregnation, but the unexplained technique differences produced a large improvement in butane performance. Limiting currents went from 50 ma/cm^2 to over 200 ma/cm^2. Specific current densities of 40 ma/mg of platinum were reached. These are very promising at this early stage of development.

Figure C-1

Improvement of Pt-On-C
Electrodes with Impregnation Technique

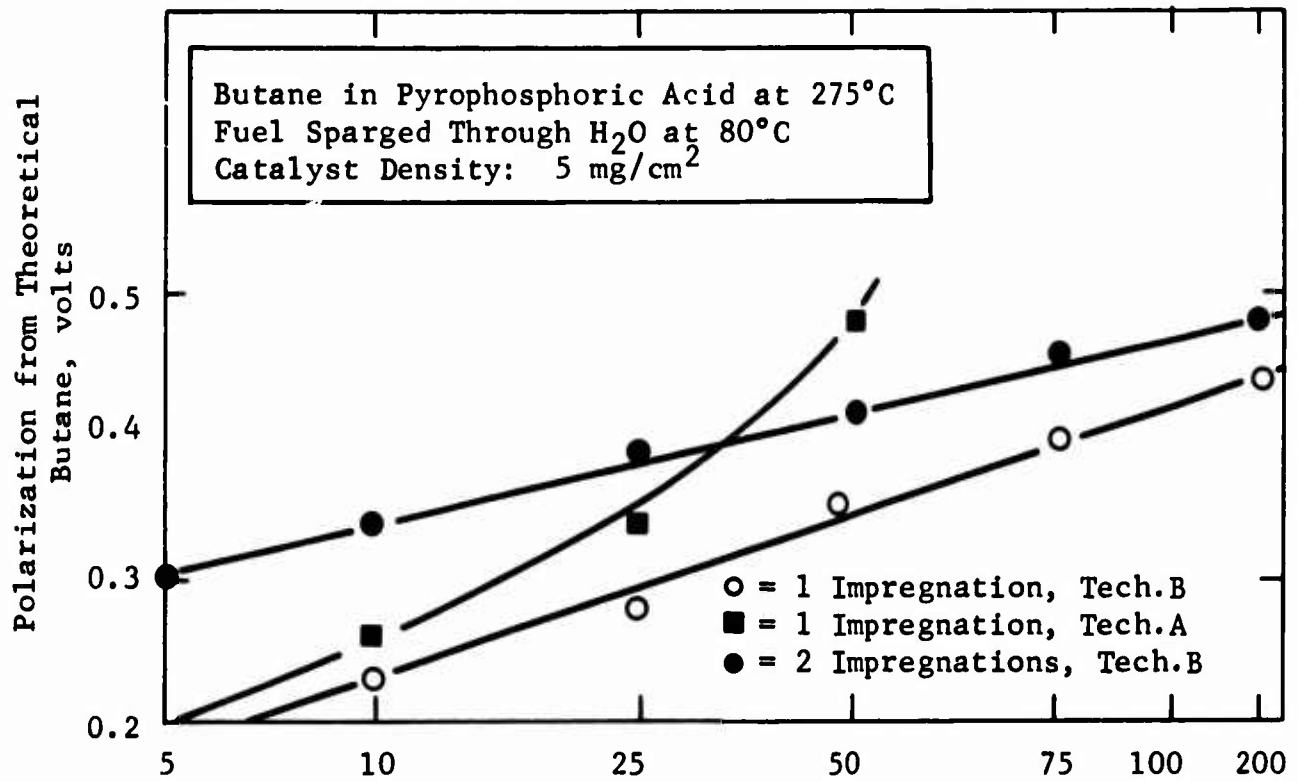

The differences in the techniques which produced this large improvement may involve the severity of the washing step after the second reduction. Excessive washing with acid or washing with alkali leads to a poor result. Chloride ion is probably the most important material removed by washing. Therefore, studies to determine the effect of small amounts of chloride, and other halide ions, on platinum performance are warranted.

The electrode porosity was also varied using the best impregnation and washing technique and was found to have a significant affect. As shown in Figure C-2, high porosity electrodes outperformed low porosity electrodes with one or two step impregnation procedures. The result suggests that further work on electrode structure is required to realize the full potential of the pyrophosphoric acid.

Figure C-2

Activity Increases with Electrode Porosity

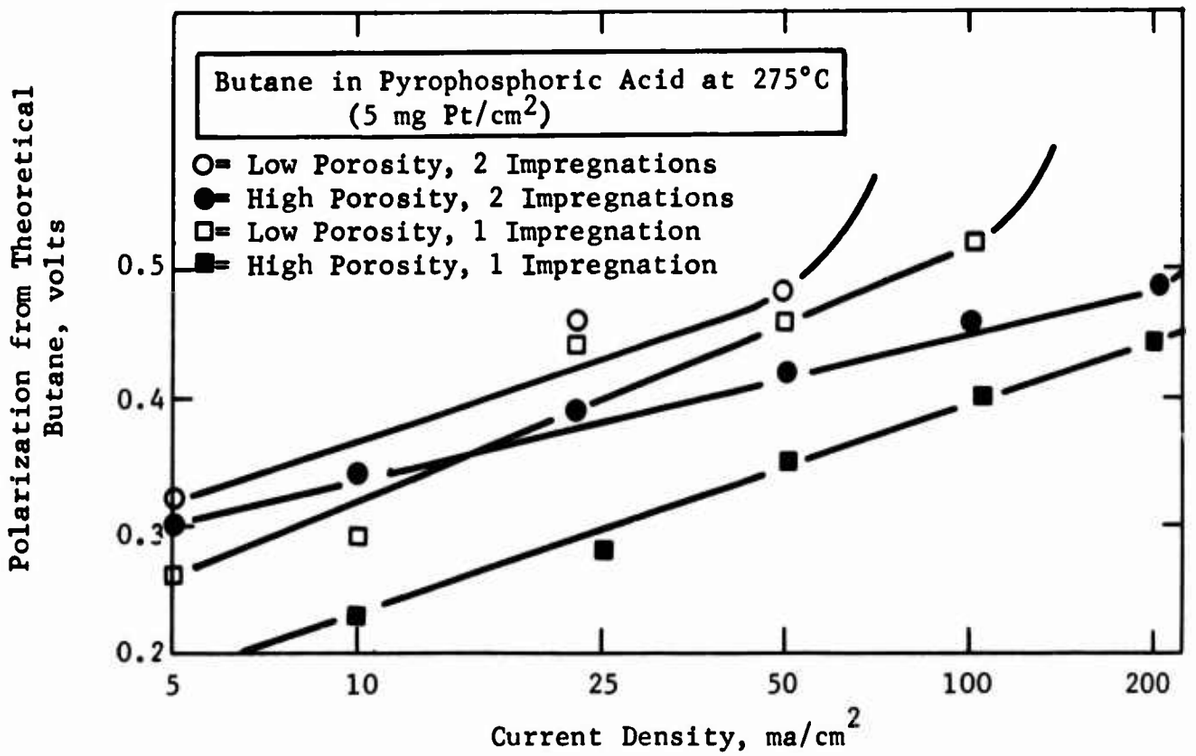

A number of high porosity, doubly impregnated catalyzed carbon electrodes having a catalyst density of only 2.5 mg/cm^2 were also tested with butane in pyrophosphoric acid. They were prepared by simply using half the quantity of catalyst carbon. With one exception, all exhibited low and unstable activity, severe polarizations occurring at current densities under 25 ma/cm^2. The exceptional structure could sustain 125 ma/cm^2 or 50 ma/mg of platinum as shown in Table C-1.

Table C-1

Butane Activity on
Catalyzed Carbon Electrode(1)

2.5 mg Pt-Ir/Carbon Electrolyte Temp 275°C
Fuel Sparged Through Water at 80°C

Polarization from Theoretical Butane at Indicated ma/cm^2, volts					
5	10	25	50	100	125
0.26	0.30	0.43	0.45	0.49	0.58

(1) See Appendix C-1 for detailed hydrocarbon performance data.

Decreasing catalyst density merely by reducing the thickness of the electrode does not seem to be the optimum means of improving platinum utilization. Apparently, difficulties in maintaining a suitable interface with the reduced quantity of carbon harms performance. This was confirmed by the low activity exhibited by these electrodes on oxygen and hydrogen. Oxygen activities on catalyzed carbons in pyrophosphoric acid are dealt with in the following part of this report.

The ability of pyrophosphoric acid to permit the generation of 50 ma/mg of platinum with butane fuel is certainly very promising in view of the relatively small amount of electrode and catalyst development work done using this electrolyte. Such work is definitely warranted in the future. Specific current densities of 100 ma/mg of platinum may be anticipated from this system.

Part b - Oxygen Activity on Catalyzed
Carbons in Pyrophosphoric Acid

Oxygen was tested only with the high porosity, doubly impregnated carbon electrodes. The activity was quite high (0.33 volts polarized at 100 ma/cm^2), and as shown in Figure C-3, quite reproducible. The detailed data are given in Appendix C- 2.

Figure C- 3

Oxygen Activity on Catalyzed
Carbon Electrodes in Pyrophosphoric Acid

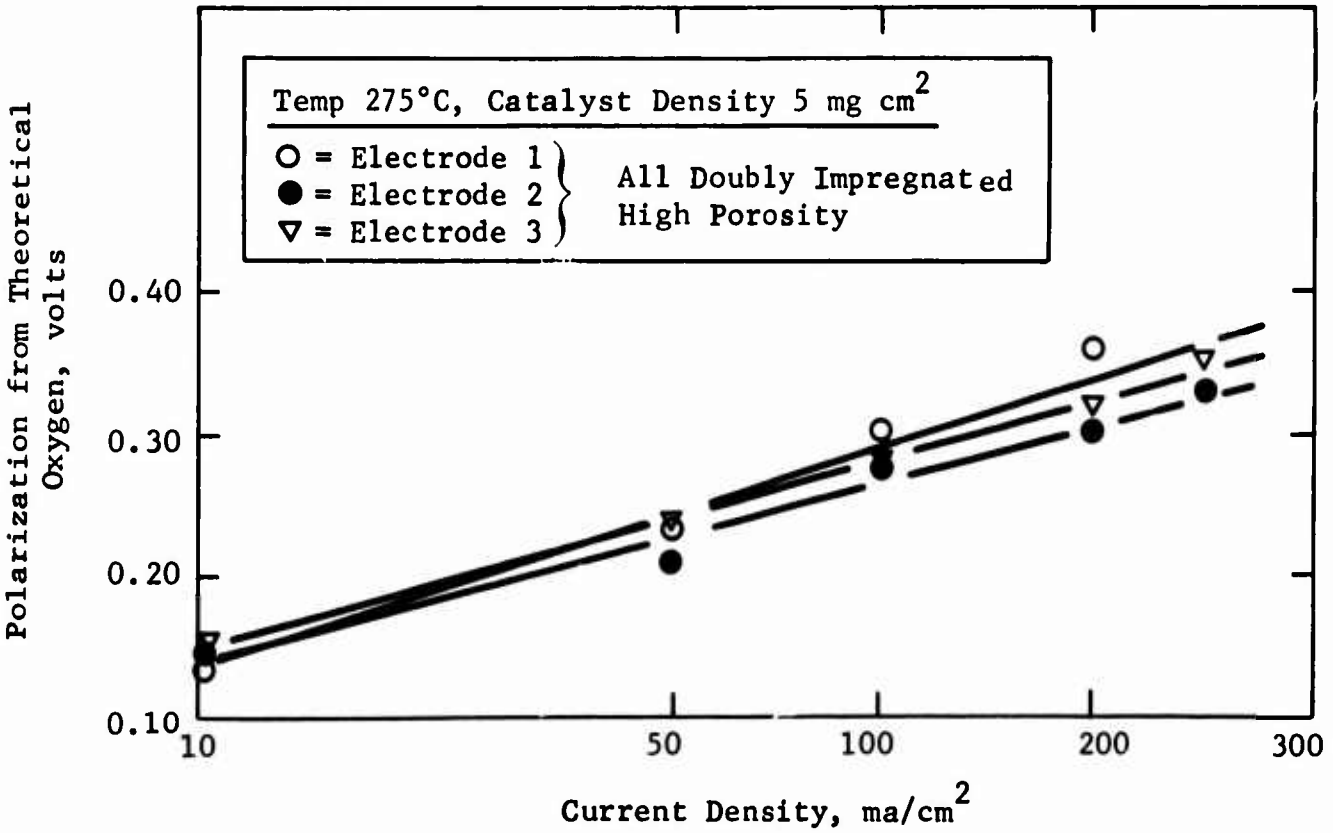

An electrode having a catalyst density of 2.5 mg/cm^2 was tested with oxygen at 275°C in pyrophosphoric acid. Performance was poor and deteriorated on continued testing as shown in Table C-2.

Table C-2

Oxygen Activity in Pyrophosphoric Acid at 275°C

	Polarization from Theoretical Oxygen at Ind. ma/cm^2, volts					
	5	10	25	50	100	150
Initial	0.18	0.19	0.24	0.34	0.49	0.64
Final	0.23	0.28	0.41	0.62	--	--

Again the decrease in activity of these electrodes relative to those having 5 mg/cm^2 of catalyst may be attributed to structural changes resulting from reduction of the total amount of all components that go into the electrode. The need for reducing the quantity of catalyst without damaging the structure is thus re-emphasized.

Phase 2 - Molten Alkali Metal Bisulfate Electrolytes

Promising electrochemical activity has been obtained with saturated hydrocarbons at 150°C in 85% phosphoric acid. This was achieved, however, with massive platinum electrodes. Catalyst loading could be decreased by operating at higher temperatures where activation-limited processes are rapid. High temperatures do introduce materials and start-up problems. Consequently, the benefits of enhanced activity must be compared with these debits. To determine the feasibility of this approach, investigation of electrolytes that could be used at 200°C and for a considerable range above this temperature, e.g. 350°C was required. It had been demonstrated that molten pyrophosphoric acid electrolyte allows operation at temperatures ranging from 200 to 275°C and higher if necessary (7). As has been shown above, increased catalyst utilizations were obtained using this electrolyte. Pyrophosphoric acid thus shows great promise. However, its extreme corrosiveness makes it difficult to obtain suitable inert materials for construction of a fuel cell employing this electrolyte. Glass, for example is readily attacked by pyrophosphoric acid above 200°C.

Thus, an investigation of still other electrolytes was warranted. These systems would operate at the same temperatures as pyrophosphoric acid and hopefully be less corrosive. Molten alkali metal bisulfates were chosen for investigation as a possible fuel cell electrolyte. These bisulfate melts can be used over approximately the same temperature range as pyrophosphoric acid. While sufficiently corrosive to preclude the use of non-noble metal catalysts, the molten bisulfates do not react with the wide spectrum of materials as does pyrophosphoric acid. Glass, for example, does not corrode in bisulfate melts at temperatures well above 300°C.

Molten potassium bisulfate melts at about 210°C, and has adequate ionic conductance above its melting point. The specific resistance ranges from 20 ohm-cm just above the melting point to 7 ohm-cm at 300°C(19). It is known that hydrogen on

platinum black acts as a reversible electrode in this melt[20]. If desired to operate below 200°C, low melting, mixed alkali metal bisulfate eutectics can be made[19]. Thus, an electrolyte having an operating temperature range extending from about 150°C to several hundred degrees centigrade is possible.

In addition to being conductive, any fuel cell electrolyte must be invariant and have adequate buffering capacity. In this study these properties were investigated and electrochemical performance with hydrocarbons and oxygen evaluated.

Part a - Chemical Stability of Molten Bisulfates

Studies were made to determine if molten bisulfate is an invariant electrolyte at the contemplated operating temperatures. Initial work with this electrolyte at 220 and 250°C had shown that sulfur trioxide slowly evolves from molten $KHSO_4$. This can only result from electrolyte decomposition which is supposed to occur by the following steps:

$$(1)\quad 2\ HSO_4^- \longrightarrow S_2O_7^{-2} + H_2O$$

$$(2)\quad S_2O_7^{-2} \longrightarrow SO_4^{-2} + SO_3$$

The electrolyte is, therefore, not invariant. The addition of water to the hydrocarbon feed which is necessary for activity might suppress reaction (1) and therefore also help maintain the electrolyte composition.

This concept was tested as follows. In two separate experiments a stream of nitrogen gas was sparged through the melt, which was maintained at 250°C. In one case, the gas stream was sparged through a water reservoir at 60°C before entering the melt, and in the second case dry hydrogen was used. In both cases, sulfur trioxide was detected in the effluent gas stream, and on a qualitative basis, in about the same amounts. This would indicate that feeding moist fuel to the cell would not keep the electrolyte invariant. These studies were repeated at a lower temperature, 220°C, but the thirty degree temperature reduction did not appear to reduce the extent of electrolyte decomposition.

While the electrolyte may not be invariant at these conditions, the decomposition rate under fuel cell conditions may be low enough for this electrolyte to be employed. Sparging through the melt pushes the equilibrium of the decomposition reaction to the product side, and even under these conditions, the extent of reaction was very small.

It is conceivable that in a fuel cell, sulfur trioxide could be fed in with the air or oxygen stream, and water in the hydrocarbon feed. Of course, analogous measures are taken in molten carbonate fuel cells with success. The addition of both these components could suppress decomposition. This was not tested.

Thus, bisulfate electrolytes are not sufficiently invariant at high temperatures; however, they might possibly be of interest at lower temperatures. In another experiment, a eutectic of 53.5% $NaHSO_4$, 46.5% $KHSO_4$ was evaluated at 150°C with dry and moist nitrogen. After three times as much sparging as in the higher temperature runs, sulfur trioxide was barely detectable. At 150°C, the decomposition rate is apparently low enough so that the bisulfate is in effect a stable electrolyte.

This eutectic was studied with butane and oxygen using sintered platinum Teflon electrodes at 150°C. The reference electrode was a Luggin containing a melt consisting of 97 wt % of the mixed alkali metal eutectic, plus 3 wt % silver sulfate, into which a silver plated gold wire was immersed.

The butane was sparged through a water reservoir at 80°C. Current densities of 200 ma/cm^2 were achieved. The voltages measured exhibited slow oscillations at all current densities, but at no time was the electrode irreversibly polarized. The results are shown in Table C-3.

Table C-3

Activity of Butane in Molten
Alkali Bisulfate Eutectic at 150°C

Current Density, ma/cm^2	Polarization from Theoretical Butane, volts
0	0.09-0.12
5	0.27-0.31
10	0.37-0.43
50	0.42-0.47
100	0.50-0.56
200	0.44-0.56

The open circuit voltage of a butane-oxygen couple in this eutectic melt would be only 0.48 volts.

Two electrodes were investigated using oxygen. One exhibited much greater activity than its duplicate, but both exhibited poor performance. At a potential of 0.58 volt with respect to a hydrogen electrode, hydrogen sulfide was generated. Finally, at higher current densities, the better performing structure exhibited lower polarizations. The results are shown in Table C-4.

Table C-4

Activity of Oxygen in Molten
Alkali Bisulfate Eutectic at 150°C

Current Density, ma/cm^2	Polarization from Theoretical Oxygen, volts	
	Run 1	Run 2
0	0.48	0.48
10	0.56	0.58
25	0.58	0.66
50	0.58	--
100	0.54	--

Because of the erratic behavior and low activity exhibited by oxygen in this medium at 150°C, further work with molten bisulfates was carried out at temperatures above 200°C and will be described in the next section. If electrochemical activity at the higher temperature level warranted, the problem of electrolyte decomposition could then be examined in more detail, particularly the possibility of continually recirculating the decomposition products.

Part b - Butane Activity in Bisulfate Medium

The performance of butane in molten potassium hydrogen sulfate (potassium bisulfate), was quite sensitive to the partial pressure of water in the fuel feed. This was controlled by passing the fuel through a water reservoir prior to entering the cell. Figure C-4 shows the activity of butane as a function of the fuel feed water vapor content. The polarization at the lower current densities decreases with increasing water temperature, up to a water temperature of 90°C.

Figure C-4

Water Vapor Influence on Butane
Activity in Molten Potassium Bisulfate

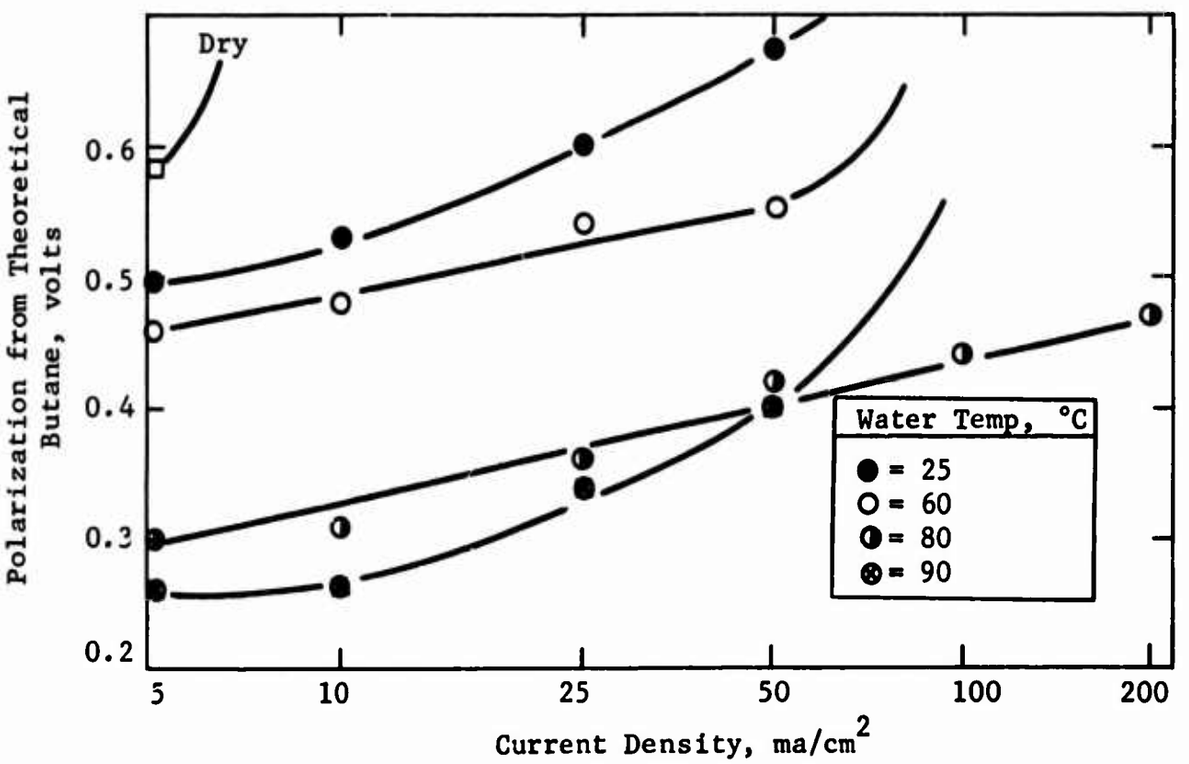

The lowest polarization at 100 ma/cm^2 is 0.44 volts. The limiting current increases up to a maximum of 200 ma/cm^2 at a water temperature of 80°C, falling off sharply above this temperature. The detailed data are given in Appendix C-3.

The activity of butane in molten bisulfate as a function of fuel water vapor content markedly resembles that in pyrophosphoric acid. This is shown in Figure C-5, where the limiting current for butane in each electrolyte is plotted against the water vapor pressure. The absolute activity of butane in the molten bisulfate is much lower than in pyrophosphoric acid.

Figure C-5

Effect of Water Vapor
on Butane Limiting Current

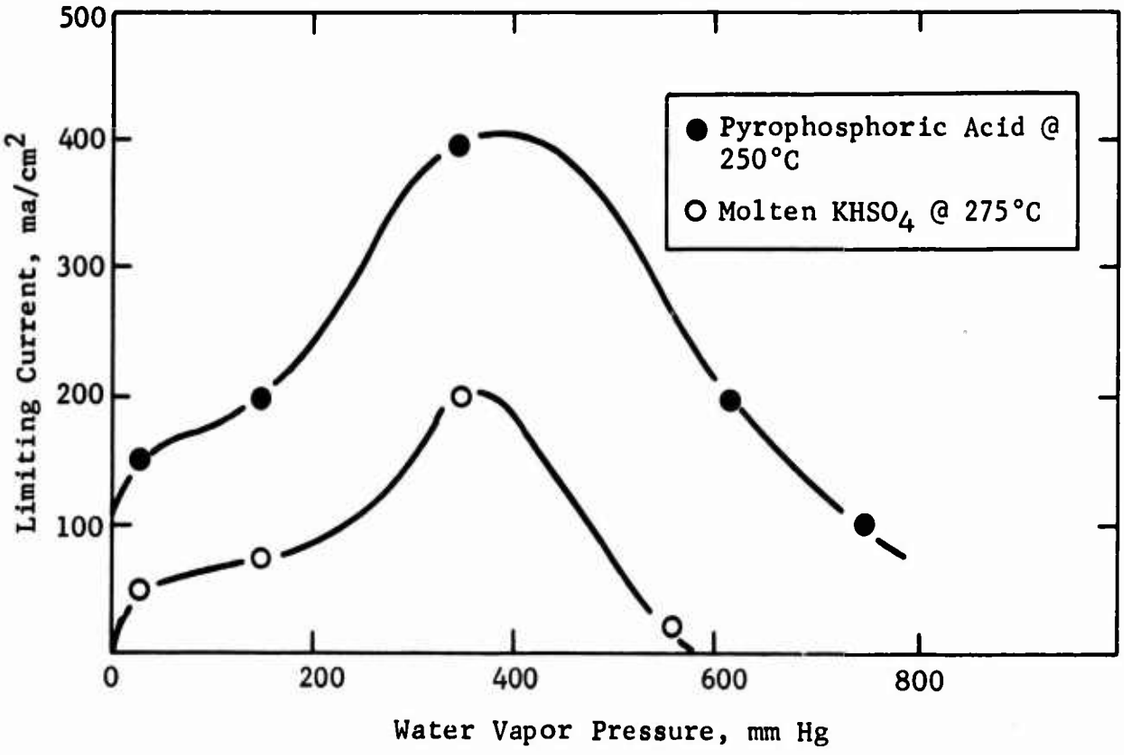

The importance of the proper water supply with both electrolyte, and the parallel behavior over a wide range of water vapor pressures strongly suggests that the same mechanism is operating in both electrolytes. That the performance is poorer in the bisulfate medium could be due to a variety of reasons. Competitive adsorption between fuel molecules and the ions of the electrolyte may be greater in the bisulfate melt. In addition, unlike pyrophosphoric acid or phosphates in general, sulfate ion is an oxidizing agent. Thus, it may undergo reduction at the anode, giving rise to a mixed potential. Either or both of these factors may be responsible for the poorer open circuit voltages and the lower activity in bisulfate melts. Butane activity in molten potassium bisulfate at 275°C was poorer than that in 85% phosphoric acid at 150°C. This would apparently eliminate molten bisulfates as a medium, allowing increased catalyst utilization by operating the fuel cell over 200°C.

It was of interest to determine whether the low anodic activity in this medium is peculiar to butane or a general property of saturated hydrocarbons. Ethane was, therefore, tested in molten bisulfate to see if it would exhibit greater activity than butane. As with butane, the fuel was sparged through a water reservoir. The reservoir was maintained at 80°C, on the assumption that this would also be the region of maximum activity with ethane. As shown in Table C-5, the activity of ethane is considerably lower than that of butane in this medium.

Table C-5

Comparative Hydrocarbon
Activity in Molten Bisulfate at 275°C

Current Density, ma/cm^2	Polarization from Theoretical Hydrocarbon, volts	
	Ethane	Butane
5	0.32	0.30
10	0.39	0.31
25	--	0.36

Considering the operating temperature, the low reactivity of saturated hydrocarbons in bisulfate melts is probably a general phenomenon. Despite these disappointing results, this electrolyte was tested further. Oxygen activity was studied to determine if cathode performance improvements could be obtained in this medium. Studies of still higher temperatures were undertaken to determine if any beneficial affects on activity occurred. Finally, low catalyst density electrodes were tested in this medium.

Part c - Oxygen Activity in Bisulfate Medium

Oxygen performance tests were carried out on a number of platinum electrodes in molten potassium bisulfate at 275°C. One structure exhibited extremely low activity, but similar electrodes tested showed improved and comparable activities. It was thought that further improvements in activity by using an electrode containing Teflon, but which was not sintered could be obtained. Oxygen activity on this structure was comparable to that exhibited on the better sintered electrodes. The results are shown in Figure C-6, the detailed data in Appendix C-4.

Oxygen activity in this medium is much lower than that obtained on the same electrode structure in pyrophosphoric acid at the same temperatures. It is probable that the redox properties of bisulfate, which generate a mixed potential that lowers the activity of fuels in this medium relative to that in pyrophosphoric acid, also decrease cathode activity.

Figure C-6

Oxygen Activity in Molten Potassium Bisulfate

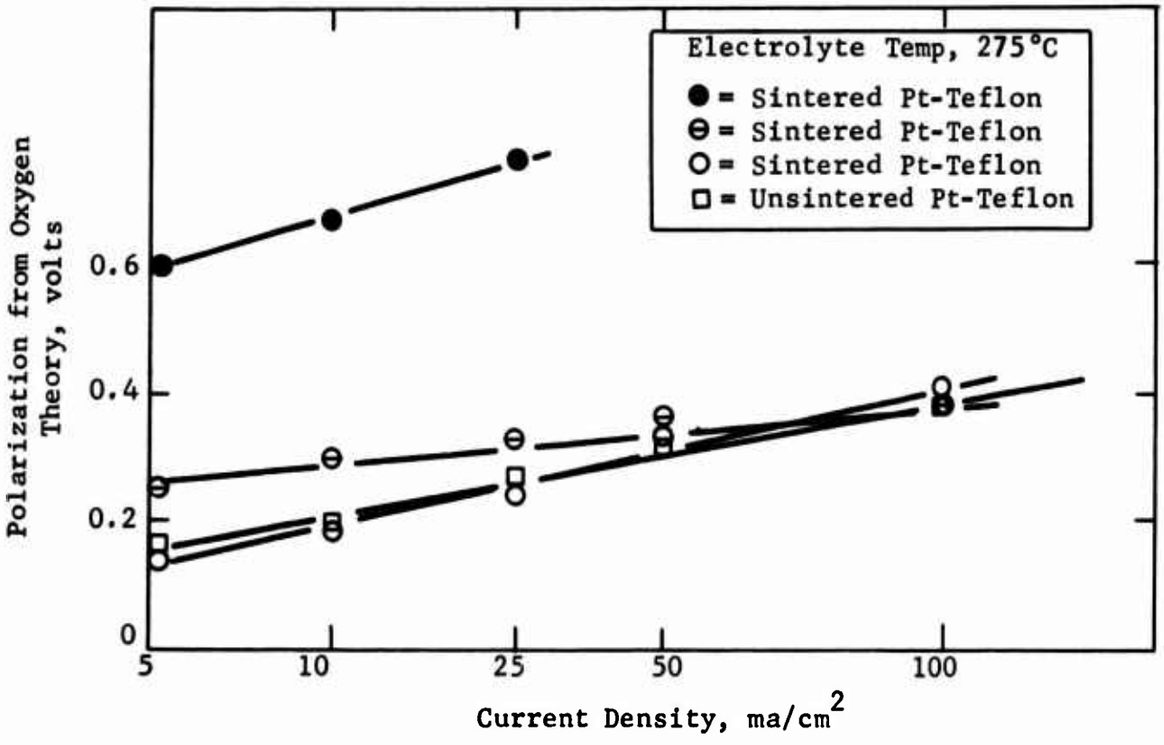

Part d - Activity in Molten Bisulfate at 350°C

The activities of butane on oxygen in the bisulfate melt are considerably lower than that obtained in pyrophosphoric acid at comparable temperatures. By operating at temperatures above 300°C, it was hoped that performance improvements would be such that the resultant activity would be equal to or surpass that in pyrophosphoric acid. As the solubilities of gases in ionic melts generally increase with increasing temperature, it should also be possible to extend the limiting current regions.

Butane and oxygen electrodes were studied in molten potassium bisulfate at 350°C. Contrary to expectations, both reactants as shown in Table C-6 exhibited poor activity. The butane in particular gave much poorer activity at 350°C than at 275 or 150°C.

Table C-6

Performance in Molten
Potassium Bisulfate at 350°C

Current Density, ma/cm^2	Polarization from Theoretical, volts		
	Oxygen		Butane
	(1)	(2)	(3)
0	0.20	0.23	0.31
5	0.26	0.30	0.33
10	0.29	0.32	0.40
25	0.36	0.38	0.75
50	0.43	0.44	--
100	0.64(4)	0.48	--

(1) Sintered platinum Teflon electrode.
(2) Unsintered platinum Teflon electrode.
(3) Fuel sparged through water at 80°C.
(4) Electrode became flooded due to leakage.

The poor activity of butane at 350°C could be due to a mixed potential system. The competing cathodic reaction, i.e., reduction of bisulfate ion, may improve to a greater extent at higher temperatures than is the anodic oxidation of hydrocarbon. If this is the case, bisulfate would be an unsuitable electrolyte at temperatures above 300°C.

Still another reason for the poorer activity at 350°C could be the sintering of the Teflon in the electrodes at that temperature. To test this possibility, these electrodes were then tested on oxygen in 85% phosphoric acid at 150°C. The performance of these structures was comparable to the standard sintered platinum Teflon electrode. Since the activity of these structures is sensitive to the sintering temperature during formulation, it may be safely assumed that little or no sintering of the Teflon occurred during the work at 350°C. The lower activity at 350°C cannot, therefore, be attributed to physical changes occurring in the electrode.

Part e - Activity on Catalyzed
Carbons in Molten Bisulfates

It was of interest to ascertain the activity decrease in going from 50 to 5 mg/cm^2 of catalyst using bisulfate electrolytes. As shown elsewhere in this report, the studies with pyrophosphoric acid showed that high catalyst utilizations were obtained although they were still short of target. Based on previous results, it was not expected that low catalyst density electrodes run in molten bisulfates would match the performance obtained in the pyrophosphoric acid medium. However, the possibility existed that the activities obtained would exceed that exhibited by the same structures in 85% phosphoric acid at 150°C.

Studies of butane and oxygen activity on a dual impregnated noble metal alloy catalyst, high porosity carbon electrode (5 mg/cm^2 catalyst) were carried out. Both reactants gave reduced activity relative to the high catalyst content electrodes as shown in Table C-7. Butane was inactive. This could be due to a combination of factors such as a decrease simply due to a reduction in catalyst density, the possibility of a mixed potential, and the affect of the catalyst support in this medium, that is, the chemical reduction of bisulfate on carbon which is known to occur at higher temperatures.

Table C-7

Performance of Catalyzed Carbon
Electrodes in Molten Potassium Bisulfate

Temp 275°C, Fuel Sparged Through Water at 80°C

Current Density, ma/cm^2	Polarization from Theoretical, volts	
	Oxygen	Butane
0	0.34	0.33
1	0.50	0.78
5	0.52-0.59	--
10	0.56-0.62	--
50	0.69	--
100	0.55	--
200	0.49	--

The oxygen activity was poor and erratic in that at higher current densities, the polarization started to decrease. This was not investigated further. The inactivity of the fuel on this structure in this medium, in addition to the activity being lower than that obtained at lower temperatures in phosphoric acid is sufficient justification to rule out further work with bisulfate electrolytes.

Part f - Other Chemical Properties of Bisulfate Melts

Although not reported in the literature, it has been found that when hydrogen is brought to a platinum electrode in contact with a bisulfate melt, hydrogen sulfide is generated. This is not the case when a saturated hydrocarbon is in contact with platinum in the melt. Despite the presence of hydrogen sulfide, hydrogen on platinum does act as a reversible hydrogen electrode in this melt. This enables the establishment of theoretical potentials of a given reactant in this melt against a reference electrode. The reference electrode used was a silver wire immersed in a melt composed of 3 weight percent silver sulfate in 97 weight percent of whatever bisulfate salt was employed.

Phase 3 - Carbon Dioxide Absorption by Carbonate Electrolyte

Silver appears to be a promising non-noble metal cathode in high pH electrolytes such as carbonates. In addition to lowering catalyst cost, silver has an additional advantage over platinum cathodes in a fuel cell employing a soluble fuel. No chemical oxidation of methanol occurs on silver cathodes in carbonate solutions containing as much as 9 volume percent methanol. There is also no increase in cathodic polarization from the fuel-free values over this range of methanol concentrations, either at open circuit or under load.

Part a - Carbon Dioxide Rejecting
Properties of Carbonates

Since the silver catalyzed air electrode activity improves with increasing pH, it was of interest to determine if the kinetics of the carbonate to bicarbonate conversion would allow operation at a pH higher than the equilibrium value of 10.2.

The ability of potassium carbonate solutions to reject carbon dioxide was measured as follows: carbon dioxide was added to a 2 molar carbonate solution at 95°C, at a rate equivalent to about 100 ma/cm^2. The potential between a hydrogen electrode in this solution and a calomel reference electrode was followed with time. The decrease in pH was calculated from the potential decrease, and in turn, the extent of the equilibrium reaction.

$$CO_2 + CO_3^{-2} + H_2O \longrightarrow 2\ HCO_3^{-1}$$

As shown in Figure C-7 , carbon dioxide addition resulted in a rapid pH drop. The final pH was about two units lower than the initial level corresponding to that of a carbonate-bicarbonate buffer.

An attempt was also made to remove the added carbon dioxide and restore the high initial peak by sparging with nitrogen at the same temperature, in the hope that the negligible partial pressure of carbon dioxide in the gas stream would reverse the equilibrium. The pH increase, shown as the lower line in Figure C- was very slow. The pH rose to 10.5 after 90 minutes and to 11.6 after twelve hours from an initial value of 10.2.

Thus, there is no advantage to using a carbonate electrolyte in place of an equilibrated carbonate-bicarbonate buffer. Improvements in silver cathode performance will require structural and catalytic advances, rather than operation at difficultly maintainable higher pH levels.

Figure C-7

Regeneration of Carbonate is Difficult

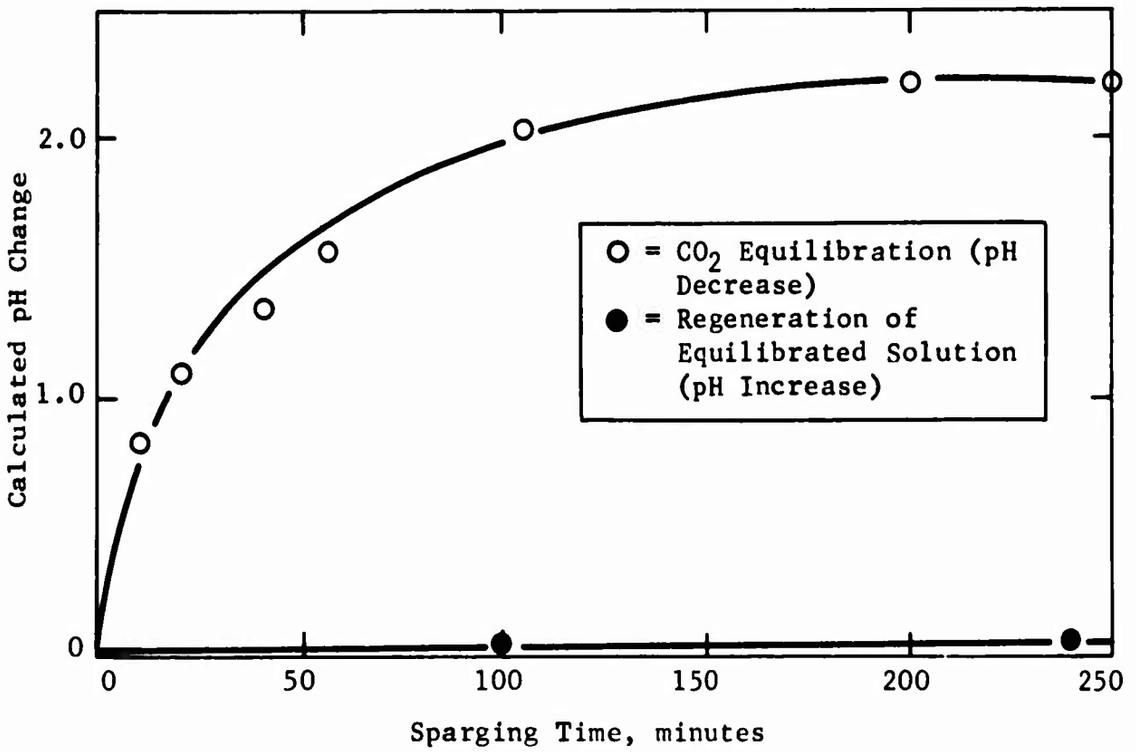

Phase 4 - Methanol Catalysts for Base or Buffer

Two catalysts which may be considered as less noble than platinum were developed as offshoots of the hydrocarbon catalysis alloy program and were tested on methanol in non-acidic electrolytes, with promising results. One was Raney gold, available as a base case from the Raney alloy program. The second was a mixture of palladium oxide and silver representing a combination of a group IB metal with a second row, rather than first row, transition element.

Part a - Silver-Palladium Catalyst

Mixtures of powdered palladium oxide and metallic silver were tested as methanol catalysts in potassium hydroxide and potassium carbonate electrolyte. While the palladium was used in the oxide form, it was undoubtedly reduced to the metal with a high surface area by the time open circuit potentials were reached. The best electrode gave very impressive performance reaching a limiting current of 2000 ma/cm^2 in alkali and a polarization of only 0.12 volts at 100 ma/cm^2. In carbonate electrolyte performance was inferior, though still noteworthy for an electrode containing no platinum. Corrosion currents were not observed below 0.9 volts polarization. See Figure C-8 and Appendix C-5 for details.

Figure C-8

Methanol Performance of
Silver-Palladium in Bases

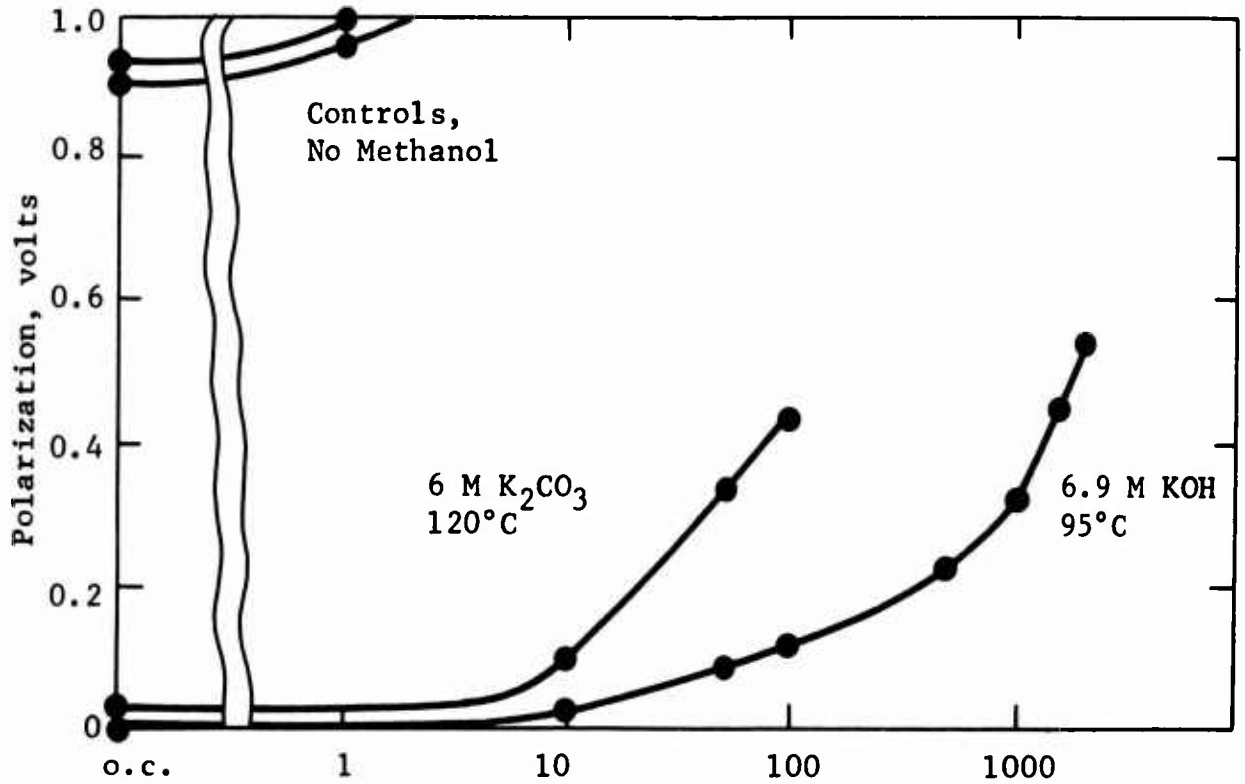

The initial runs were made with sintered metal mixture for greater mechanical strength, but it was found that unsintered mixtures gave better performance. Sintered palladium-gold mixtures also gave appreciable performance but were not as good as the catalysts containing silver.

The catalyst also gave some apparent activity with butane as the fuel in carbonate electrolyte. While limiting currents were relatively small, 5 to 10 ma/cm^2, the performance curve was notable because open circuit and low current density polarizations were near or actually below the theoretical butane potential. This was also characteristic of the methanol performance. The palladium may be serving as a steam reforming catalyst with the hydrogen being consumed as the fuel. Palladium is a known steam reforming catalyst.

Thus, palladium appears promising as a catalyst base in non-acidic media. While by no means non-noble, its ultimate potentiality in terms of ma/mg or ma/dollar is unknown and could conceivably exceed that of platinum. Its activity remains to be demonstrated in a true carbon dioxide rejecting electrolyte, rather than the carbonate actually used. Electrode structure problems may be limiting its hydrocarbon performance and must be further investigated.

Part b - Gold and Gold Alloy Catalysts

Powdered gold and gold alloys had been shown to have some methanol activity in previous experiments. Since they were made available in connection with hydrocarbon alloy catalyst program, Raney gold and gold alloys were tested for methanol activity in 6.9 M KOH at 90°C and their performance was compared with that of 325 mesh gold powder.

The comparison of electrical performance indicated that Raney gold produced 30 to 50 fold increase in current, very likely from its high surface area. Alloying Au with Fe caused a big loss in methanol activity.

Table C-8

Methanol Performance of Gold Catalysts

6.9 M KOH, 90°C

Catalyst	Polarization from Methanol Theory at Indicated ma/cm^2, volts			
	0	10	100	300
325 mesh gold powder	0.15	0.66	0.94	--
Raney gold	0.12	0.36	0.50	0.65
Raney annealed 40 Au-60Fe	0.16	0.88	--	--

Thus, gold is by no means inactive on methanol in non-acidic media and deserves to be investigated further. Polarizations with it are higher than with platinum in alkali probably because the gold surface oxide forms at more anodic potentials than the platinum surface oxide. Adsorbed or co-precipitated redox agents may help alleviate this problem.

Phase 5 - Slurry Catalyst Electrodes

Previous work demonstrated the feasibility of utilizing as a decane electrode system a slurry of suspended catalyst in a mixture of electrolyte and fuel. The slurry was stirred by a rotating conductive paddle which kept solid catalyst particles mechanically in suspension and collected current from the catalyst particles during collision. However, the catalyst utilization was not high enough to be of practical application and the magnitude of the stirring energy requirement relative to the system power output was unknown. The following studies were carried out to determine the stirring energy requirement and to learn whether physical changes giving increased current collection efficiency could improve the catalyst utilization.

Part a - Separation of Current Collection from the Stirrer

The seemingly attractive approach of using a rotating conductive paddle to serve as a stirrer and at the same time as a current collector has two major undesirable features. First the size, shape, and velocity requirements for optimum

stirring and turbulence do not necessarily coincide with and may even be opposite to those for current collection. Secondly, an inconvenient sliding electrical contact is necessary for utilizing the rotating stirrer as a current collector.

A simple modification was made and stationary current collectors were added to the previous test set-up illustrated in Figure C-1 of Report No. 5. The mercury pool which served as the sliding electrical contact was eliminated. Furthermore, the stirring paddle was changed from a rectangular into a helical shape. The helical stirrer created more eddy flow which in turn increased the collision frequency between the catalyst particles and the stationary collectors, resulting in improved electrical performance as illustrated in Figure C-9 . The detailed results are tabulated in Appendix C-6. All tests included in this Appendix were carried out at 1500 rpm with 35 cc decane and 35 cc electrolyte.

Figure C-9

Performance Improvement Due to Helical Stirrer

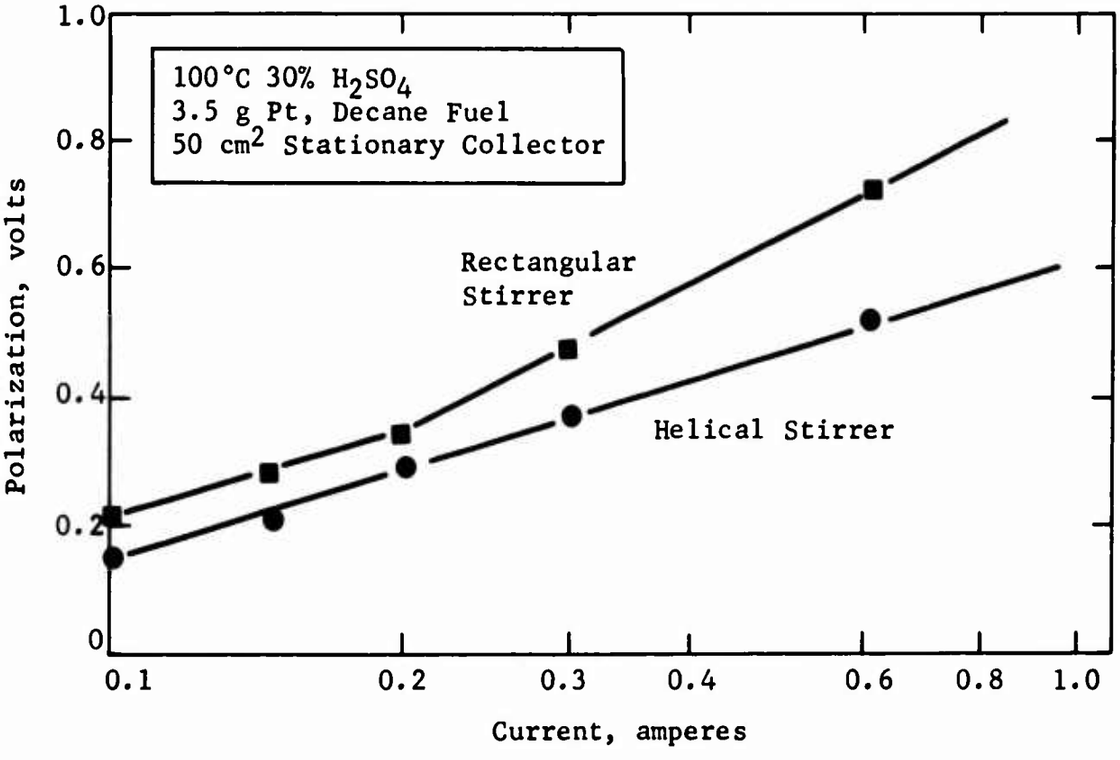

Part b - Stirring Power Consumption

The slurry system involves an additional parasitic power consumption for stirring the slurry. As previously reported, attempts had been made to minimize this power requirement by taking different approaches to suspending the slurry. However, none was successful. For example, experiments were conducted to suspend platinum black and other catalysts by sparging decane through the electrolyte.

However, this could only produce weak turbulence, not sufficient to maintain collision between catalyst particles and current collector. Thus, direct mechanical stirring inside or outside the collector seemed unavoidable. Measurements were made to determine the stirring power consumption with a helical stirrer. Since the optimum stirring speeds had been found to lie within the range of 1200 to 1800 rpm, speeds of 1200, 1500, and 1800 rpm were chosen. Other conditions were identical to the test conditions of Part a. The results as tabulated in Appendix C-7 show a stirring power consumption of the order of 0.4 watt. The frictional power consumption arising from the motor itself, and measured at no load conditions, was much higher because of the oversize bearings supporting the stirrer. With improved designs of the motor and bearing support, the frictional power consumption can be reduced. These results indicate that the level of power consumption, although high, is still of the order of magnitude of the output that might be obtained from a cell at present performance levels. Since practical applications would depend upon improvements in cell geometry and catalyst activity giving several orders of magnitude improvement in performance, it can be expected that stirrer power consumption would not be a major problem in the light of such advances.

Part c - Effect of Collector Area on Performance

The effect of stationary collector area was studied in two different electrolytes at two temperatures. This was made possible by having three stationary collectors in the new arrangement, each with a surface area of 25 cm^2, counting both sides. During the experiment, the test area was varied in steps of 25 cm^2 by disconnecting one or two collectors. The test data obtained by varying the collector area as tabulated in Appendix C-6 were obtained galvanostatically. From the performance curves, the currents at fixed polarizations were obtained and compared for three different collector areas in Figures C-10 and C-11. They showed that the current increased with increasing collector area, but at a rate dependent upon the polarization. Thus, separation of the current collection and stirring functions did permit the freedom to optimize each independently, and led to sizable performance improvements.

The temperature effect was looked into in one experiment with phosphoric acid as the electrolyte and a 75 cm^2 current collector. By raising the temperature from 150 to 175°C, the current at 0.27 volt polarization was increased from 0.28 to 2.0 amperes. At 0.46 volt polarization, the slurry electrode could carry 4.8 amperes current. The improvement in performance with temperature would correspond to a limiting process with an activation energy of 30 kcal/mole. The fact that a value this high has never before been observed suggests that the improvement was due to added turbulence caused by the boiling of the decane. The system could be operated practically in this way only if a source of heat and cooling water were available. However, the result does demonstrate how much improvement can be obtained from increased contact between the particles, the decane and the electrode. These results are consistent with the analysis given in Appendix C-11 of the last report (7). When the average time a particle spends between collisions with current collector (t_s) is large, as appears to be the case in this situation, the current, I, is given by equation 8 of that analysis as:

$$I = \frac{C_1}{t_s} \ln \frac{t_s}{C_2} + \frac{C_3 \eta}{t_s}$$

where the C's are system constants, and η is the polarization of the stationary electrode. The average time between collisions must be roughly inversely proportional to the electrode area, although the precise relation would depend on the hydrodynamics of the system. It will be seen that the first term on the right

Figure C-10

Effect of Stationary Current
Collector Area in Sulfuric Acid

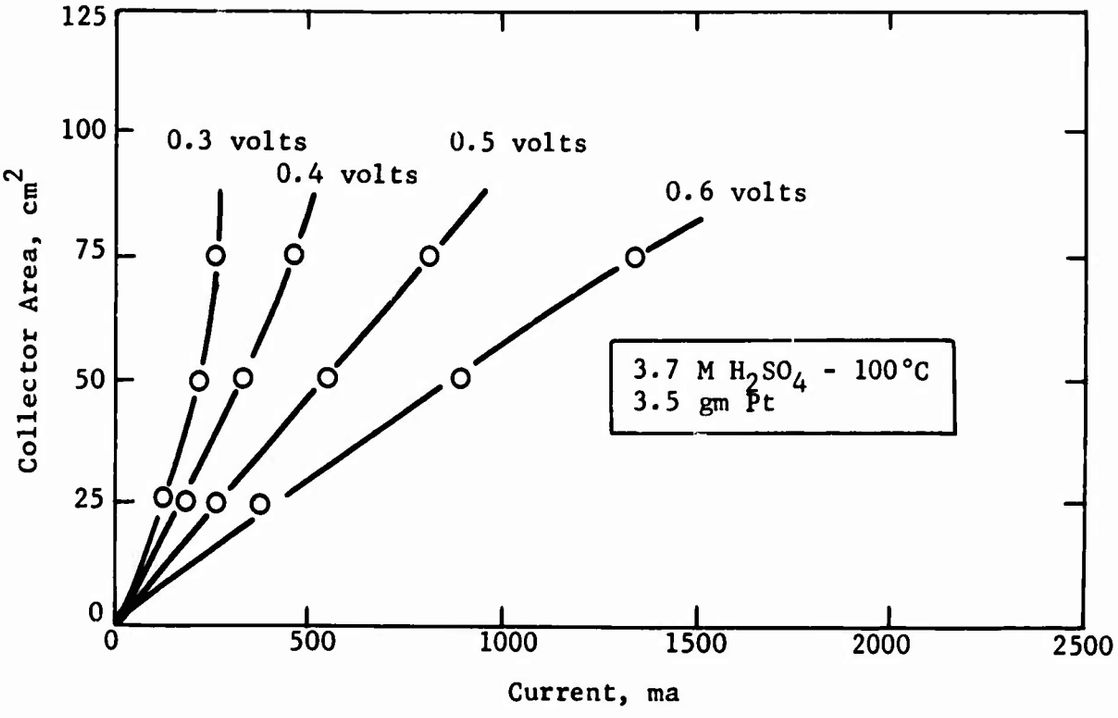

Figure C-11

Effect of Stationary Current
Collector Area in Phosphoric Acid

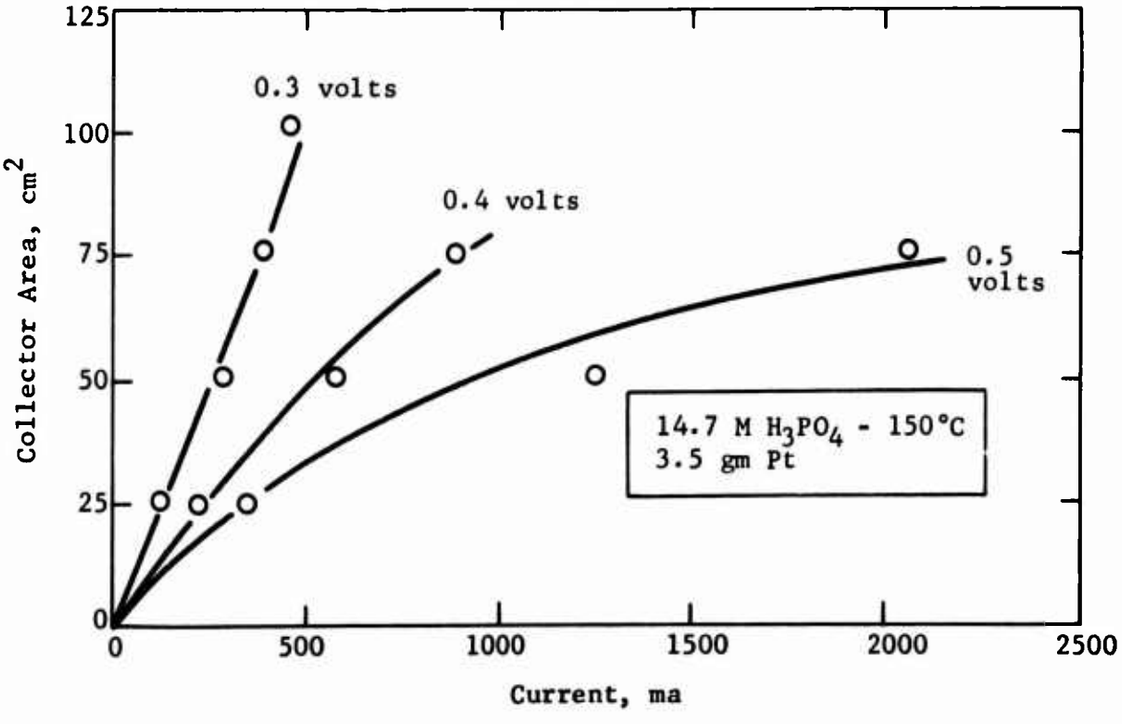

varies less than linearly with electrode area, t_s appearing in both a numerator and a denominator. The second term, containing the polarization, does vary linearly with area. Therefore, the increase in current with collector area should be most pronounced at high polarizations as observed.

Theoretically it should be possible to estimate the constant parameters in the above equation, use the data to determine t_s, and thereby have enough information to estimate the ultimate performance of the system. Unfortunately, since the relation between t_s and electrode area is unknown t_s would have to be estimated from the curvature in the voltage-current relation for each electrode. The data is not good enough to permit this to be done with any accuracy. Very roughly the results suggest that t_s is in the range of 5 to 25 seconds. This means the system is still quite inefficient and capable of considerable further improvement at larger electrode area to volume ratios. The shape of the curves in Figures C-10 and C-11 and the temperature effect certainly support this.

Further performance improvements could be made, for example, by eliminating the measuring probes in the test set-up so that the volume and catalyst quantity could be reduced without decreasing the collector area. A circular electrode chamber 0.5 cm in diameter and 10 cm long having a volume of 2 cc could be designed with a finned cylindrical collector of 50 to 75 cm^2 surface area. This would provide a much higher surface to volume ratio, a lower t_s and hence an improved catalyst utilization.

However, since the quantity of catalyst in the present experiments was so high, the specific current density at 150° was of the order of 0.5 ma/mg at best. It is, therefore, doubtful that the levels achieved with a static system, about 6 ma/mg, could be matched with the slurry system. Furthermore, the chances of improving the system still further to reach practical levels of 100 ma/mg seem very remote.

Since the actual current levels for this small volume are relatively high, in the ampere range, the system seems to be well suited for the evaluation of new catalysts, especially non-noble ones available in large quantities.

4.4 Task D, Methanol Electrode

Studies on the methanol electrode have concentrated on further establishing the degree of stability and reliability of the ruthenium modified P-type catalyst. In addition, experiments were carried out to determine whether the silica-on-carbon and boron carbide supports could be used to increase catalyst utilization.

Phase 1 - Studies of Ruthenium Modified P-type Catalyst

The ruthenium-modified P-type catalyst is the main catalyst presently used in multicell studies. Therefore, the testing of this catalyst under widely varying conditions has been carried out to establish its basic characteristics under more controlled conditions than those obtainable in multicell units.

Part a - Life Testing of the Ruthenium Modified P-type Catalyst

The half-cell life testing of ruthenium modified P-type catalyst carried out during the past year was continued. The data are summarized in Appendix D-1. These cells were operated continuously except for a daily 15 minute open circuit. Polarization readings were recorded every 30 minutes after current was restored. The cells were occasionally reactivated by flushing and overpolarizing in methanol-free acid.

Two electrodes made using borohydride reduced catalyst were tested to 11,000 hours. These showed an average loss of only 15 mv. Two electrodes of hydrogen reduced catalyst showed a similar 15 mv loss after 4400 hours. These losses are not primarily time dependent. Indeed, the above electrodes showed a marginal performance gain at the time of the previous report (7). Instead these losses are believed to be due to chance contamination by halides, accidental methanol starvation, and other random upsets.

A few runs were made to pin down various sources of contamination and deactivation. Run 1a, using cell 5, indicated that use of distilled water instead of deionized water could cause a moderate but definite performance loss. This was retested in run 2a, cell 5 with no loss resulting. Contamination has previously been experienced in the distilled water distribution system, and this is presumed to have occurred in run 1a.

Various metals such as aluminum and copper, which have been contemplated for use in the methanol battery may be the source of contamination. It is therefore necessary that if any chance exists of metal corrosion products entering the battery electrolyte, then these products must not poison the electrodes. In run 26, cell 5 aluminum was added to the life test cell. This metal dissolved readily in the warm sulfuric acid electrolyte, but electrode performance was unaffected. In runs 2a, cell 4 and 2c cell 5, copper metal and copper sulfate were added. Both of these caused immediate and serious electrode performance loss and hence have to be completely isolated from the circulating electrolyte in a battery. Hence, distilled water transferred through copper pipes is suspect.

Total cell life testing also was continued. A departure from the normal operating procedures was made in the storage tests (cell 3 and 4). These were initiated at the time of the last report (7). In these tests, the cells were stored at open circuit at room temperature after being filled with 1 M methanol in 3.7 M sulfuric acid. Twice a week, fresh 0.5 M methanol was added and the cells were operated for about half an hour to check their performance level. They were then

refilled and returned to storage. This mode of operation was a simulation of conditions a battery might be subjected to during intermittent use and storage under field conditions. These cells showed an initial performance gain during their first few days of operation and then maintained the high performance level for 4000 hours of testing. These were quite good cells, and a spot check at 60°C showed them capable of 0.50 and 0.51 volts at 46 ma/cm^2. There appears to be no problem in storage of methanol fuel cells in the manner described.

All series of life tests in 5 cm^2 and 10 cm^2 cells reported to date have now been terminated. The results may be briefly summarized as follows:

1. Anodes lose 20 to 40 mv over a 24 hour period, and performance may be regained by brief open circuiting. This is attributed to trace amounts of impurities (halides) which slowly deposit on the electrode and are desorbed at open circuit.

2. There is an additional slow deactivation which may range from 10 to 50 mv over the period of a month. This can be reversed by rinsing the electrode in fresh electrolyte and overpolarizing it briefly to about 0.8 to 0.9 volts in the absence of methanol. This deactivation is attributed to the adsorption of minute traces of partial oxidation products, and the overpolarization seems to burn off these products.

3. Except for these reversible poisoning effects there seems to be no performance loss associated with normal operation or storage of anodes over long periods of time. Deactivation can apparently result from contamination or improper operation, and of course such mishaps are more likely to occur in long term tests.

Part b - Operation of Methanol Electrodes at High Current Densities

Polarization of methanol anodes as a function of current densities and methanol concentration was investigated in the last report (7) at current densities up to 400 ma/cm^2. Although higher current densities are of no foreseeable interest in an operating methanol-air total cell, electrode behavior in that region might give added insight to phenomena of electrode behavior. Results are given in Figure D-1 and Appendix D-2. They strengthen earlier conclusions that mass transport from the bulk solution to the electrode surface is excellent. In 1.0 M methanol, concentration polarization at 1000 ma/cm^2 causes only a 20 mv debit in electrode polarization. Thus, it would seem that electrode structure in present methanol electrodes is excellent and is not a serious cause of polarization.

The transition from Tafel behavior in the low current region to limiting current is continuous. There is no evidence of a double Tafel slope region which has been derived or observed by several authors (e.g. Austin, L. G.(21))for porous flooded electrodes. This indicates either that the methanol electrodes are too thin for such a region to become predominant, or that CO_2 evolution from the electrode surface changes the nature of the transport process from simple diffusion to a convective type of transport.

It is also encouraging to note, that even at the high current densities with very vigorous gas evolution, there was no sign of electrode disintegration or flaking off of catalyst particles.

Figure D-1

Anode Polarization at High Current Density

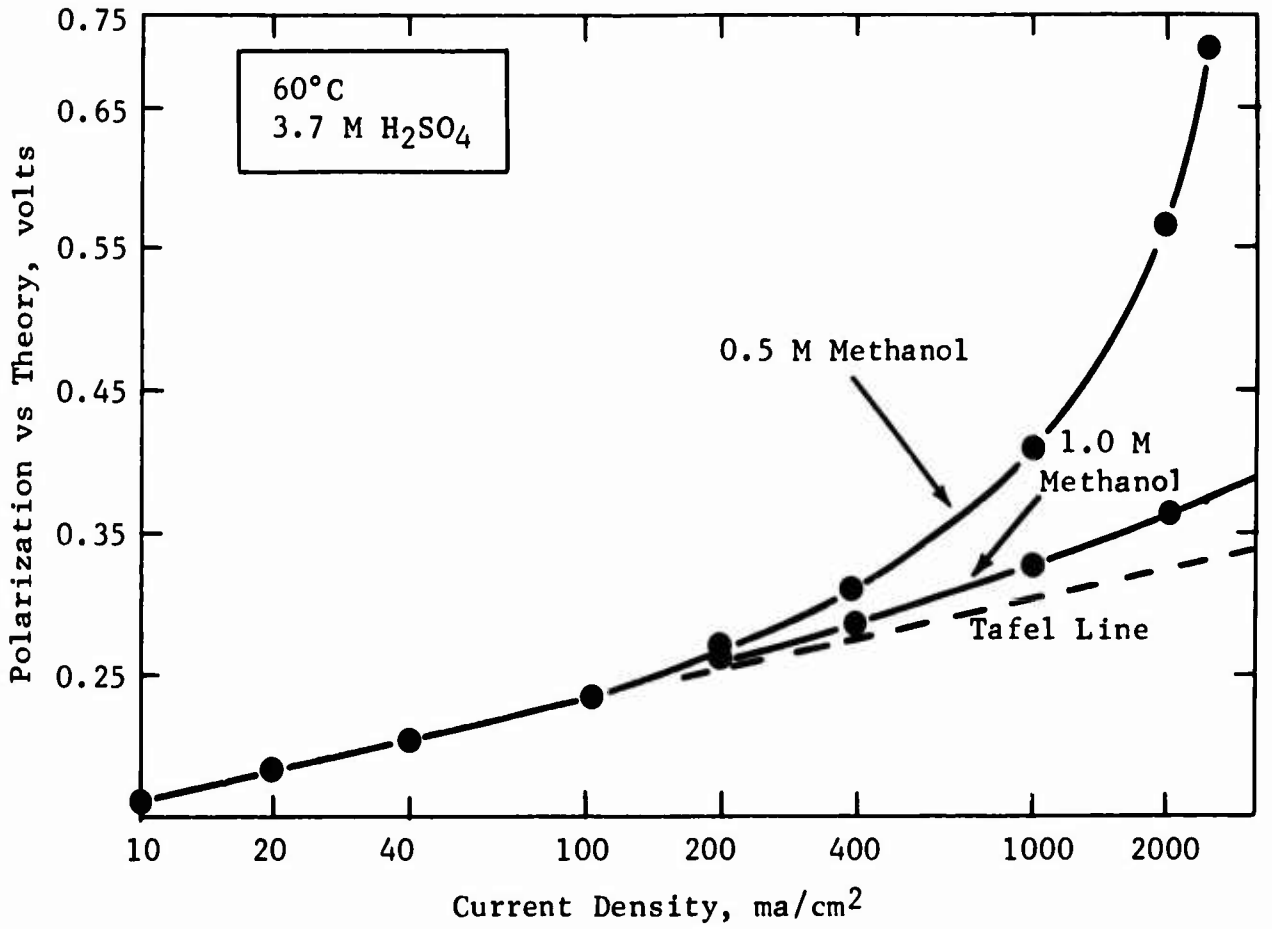

Phase 2 - Use of Supports for the Ruthenium Modified P-type Catalyst

The ruthenium modified P-type catalyst is presently an unsupported catalyst. Studies are now under way to determine whether supports could be used to decrease catalyst loading without impairing efficiency.

Part a - Silica on Carbon

An evaluation was made of the use, in the methanol electrode, of the silica-on carbon support. This support, developed for hydrocarbon electrodes, was discussed in Task A. Ten percent silica on carbon was used as the support for the ruthenium modified P-type catalyst. Reduction was carried out using both potassium borohydride at room temperature or hydrogen at 225°C.

The prepared electrodes were tested using 1 M methanol in 3.7 M sulfuric acid. Their performances were very poor, the electrodes being polarized more than 0.35 volts, at open circuit. Therefore, experiments were carried out to determine the causes of the difficulties. The major areas considered were electrode fabrication procedures, carbon quality, and silica loading.

Faulty fabrication could impair performance, primarily as a result of inducing mass transport limitations. This was not the case, since increasing the methanol concentration did not markedly improve performance. Carbon quality was not a problem, since carbon electrodes prepared without silica gave the expected catalyst utilization, 4.5 ma/mg at 0.35 volts polarization. Thus, the presence of silica is contributing to the performance loss.

One reason for this could be the changes in washing procedures required when silica is used. The procedures used to prepare the hydrocarbon electrodes are too severe for this catalyst, while the potassium hydroxide washing treatment employed with this catalyst would leach out silica. Therefore, several washing techniques for chloride removal were tried. These included, dilute 0.001 N potassium hydroxide, and 90% saturated solutions of potassium sulfate and potassium chlorate.

The use of these washing procedures directionally improved performance. However, their levels were still extremely low. The best of these employed potassium sulfate. The utilization in this case was 0.12 ma/mg at 0.35 volts polarization compared with 0.024 ma/mg originally obtained using only a water wash. These results are shown in Table D-1 and detailed in Appendix D-3.

Table D-1

Effect of Washing Technique on Utilization

Wash Solution	Concentration	Utilization at 0.35 volts Polarized ma/mg
H_2O	--	0.024
KOH	0.001 N	0.080
$KClO_4$	90% Saturated	0.090
K_2SO_4	90% Saturated	0.120

It is not known whether the new washing procedures were effective in removing all the chloride ions or had any other deleterious effect. Therefore, further work is needed to establish whether washing remains a problem or whether some other problem associated with the silica is operative.

Part b - Boron Carbide

In other tests of new supports, ruthenium modified P-type catalyst was supported on a boron carbide (B_4C). Previous studies (7) have shown that good performance could be obtained using 800 mesh B_4C particles. The good performance obtained with this low surface area support suggests that there might be a positive interaction between the support and the catalyst giving improved performance.

This was tested in experiments using varying catalyst loadings and several reduction procedures. The results obtained with the different catalyst loadings indicate that there may be an interaction with the support, but a negative rather than a positive one. The average utilizations at 0.35 volts polarized, obtained with 20, 5 and 1 wt % catalyst, respectively, were 3.2, 1.1, and 0.37 ma/mg. This could be due to an interaction between some of the catalyst and the support making that portion of the catalyst inactive.

The catalyst also showed improvement at more severe reduction conditions. The utilization increased from 2.0 to 4.7 ma/mg by using hydrogen at 225°C rather than borohydride reduction. This is shown in Table D-2 and Appendix D-4.

Table D-2

Effect of Reduction Conditions on
Performance of B_4C Supported Catalyst

Reducing Agent	Temp, °C	Utilization at 0.35 volts Polarization, ma/mg
KBH_4	25	2.0
H_2	120	2.9
H_2	225	4.7

The fact that the utilization increases rather than decreases with increasing temperature shows that the impregnation of the catalyst on the boron carbide suppresses sintering. Thus, more severe reduction conditions should be further evaluated.

A unique feature in these results is the fact that the curves of polarization versus current density on semi-log coordinates show sharp changes in the Tafel slopes at about 10 ma/cm^2. This is shown in Figure D-2. The slope below 10 ma/cm^2 was 0.08 and the slopes at higher current densities ranged from 0.13 to 0.16. The higher slope and higher current densities do not appear due to fuel mass transport limitation, since increasing methanol concentrations from 1 M to 2 M reduced the polarization only marginally (10-20 mv). Furthermore, the increased slope is not ohmic in form. Therefore, further efforts are needed to determine the cause of this change in slope and to find ways for maintaining the lower (0.08) slope at higher current densities. However, so far, no advantage in catalyst utilization for using supports has been found for this catalyst system.

Figure D-2

Tafel Slope Change
Boron Carbide Supported Catalyst

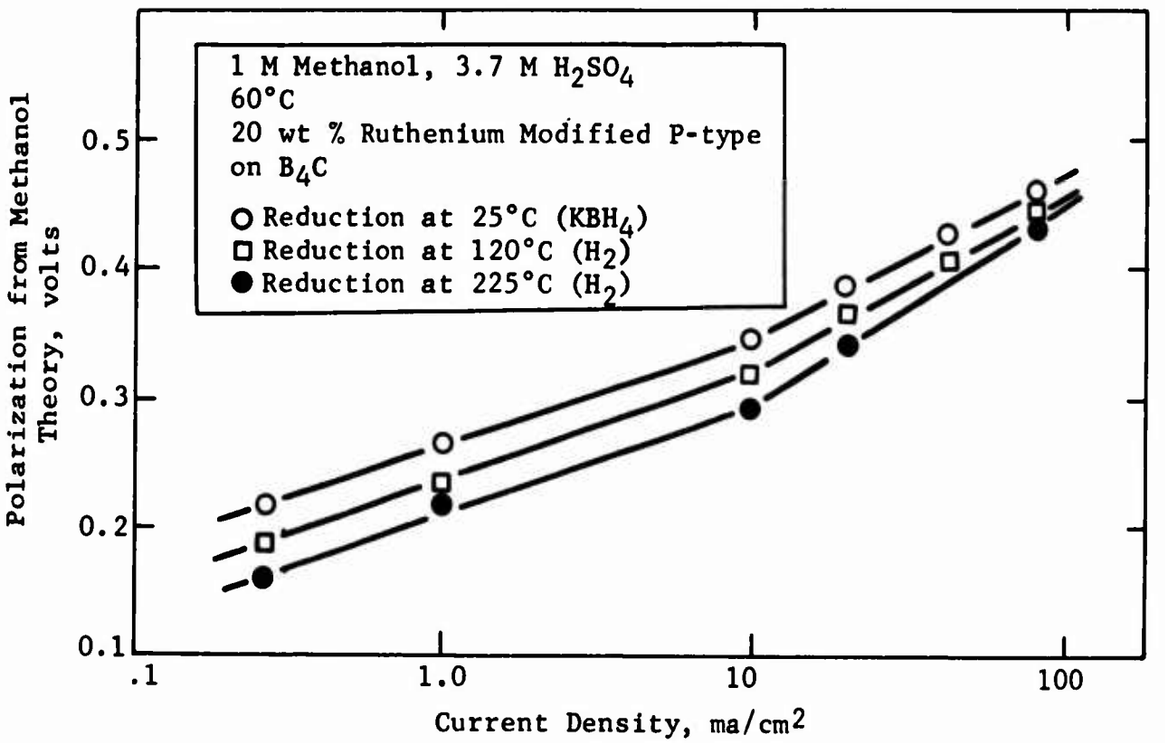

.5 Task E, Air Electrode

Studies were continued on the development of cathode structures that do ot require the use of membrane backings. This work primarily covers the perform- nce and scale-up of Teflon spray-coated and sodium alginate coated electrodes. hese coatings on the electrode serve to prevent gross water transport through the merican Cyanamid AA-1 platinum-Teflon electrodes, and thus replace the Permion embrane presently being used. Work was also carried out on air electrodes capable f operating at high temperatures for use with phosphoric acid electrolyte. These ncluded various coated metal and carbon based electrodes.

Phase 1 - Teflon Coated Cathodes

The previous report (7) indicated that small 1" diameter electrodes, spray oated with "Fluoroglide" Teflon emulsion, could produce electrodes with perform- nces comparable to those obtained with membrane backed electrodes. These tests howed that gross leakage rates of electrolyte into the air chamber could be kept o tolerable low levels. Therefore, experiments were carried out to determine whether performance could be maintained for extended periods of operation with larger sized electrodes.

Part a - Life Testing of Teflon Coated Electrodes

A set of these small electrodes were operated continuously until failure at 50 ma/cm^2 in 3.7 M sulfuric acid in the presence of 1 M methanol. The electrodes were subjected to a 6" electrolyte head. To impart better uniformity to the coat- ings, two of the finished electrodes were heated to 150°C for 15 and 120 minutes, respectively. The test apparatus is shown in Appendix E-1.

The best performance and longest life were obtained with the electrode that was not heat treated. This electrode operated at about 0.5 volt polarization for 900 hours and then abruptly failed. The heat treated electrodes performed some- what better initially, but continuously lost performance at a rate of about 15 mv/ 100 hours. This is shown in Figure E-1.

Figure E-1

Performance of Teflon Coated Electrodes During Life Test

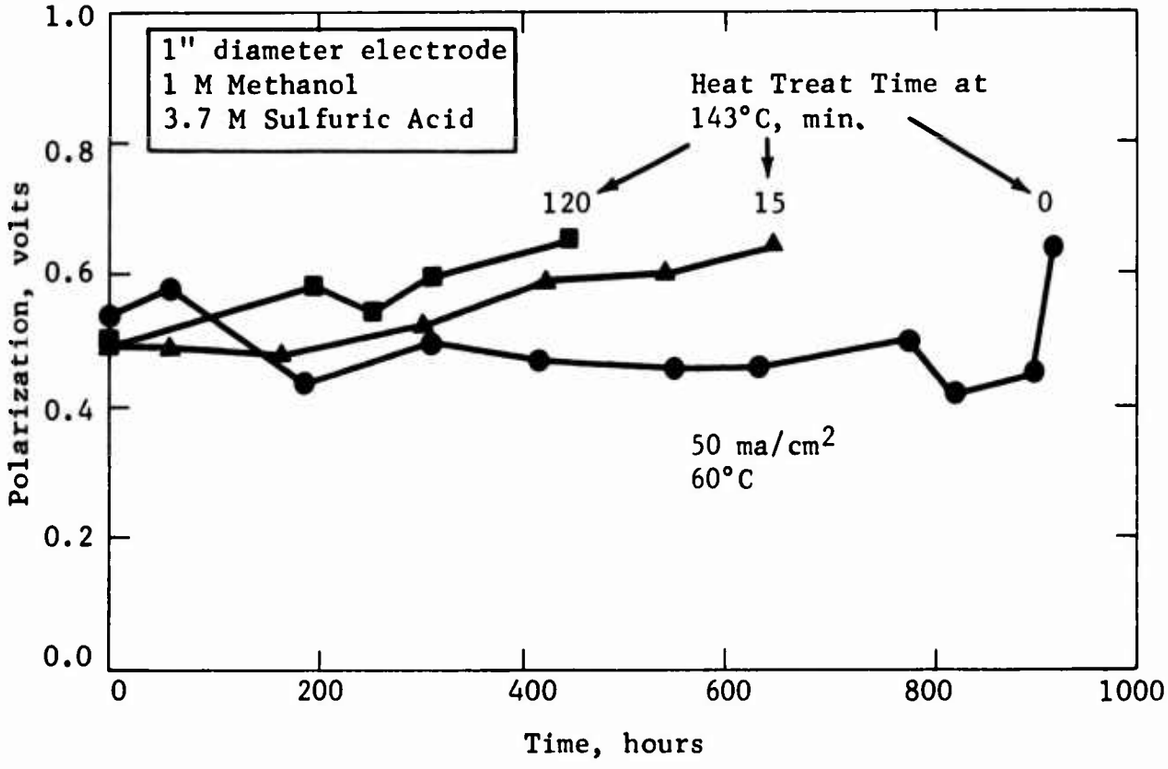

More testing is required before any conclusions can be drawn regarding the causes of failure and the reasons for the slow, continuous decline in performance of the heat treated electrodes.

Part b - Scale-Up of Teflon Spray Coated Electrodes

To determine the problems arising in scaling up this process, a 7.5" diameter Teflon spray coated Cyanamid AA-1 electrode was tested in a half cell apparatus depicted in Appendix E-2. The performance of this electrode was studied in methanol-free electrolyte at 60°C. For comparison, a conventional Permion membrane clad cathode was also examined in the same apparatus and under similar conditions. Because there was some variation in potential over the electrode surface, the reported polarizations represent the average of fourteen readings taken over the face of the electrode.

The results of the test are shown in Figure E-2. The performance of the scaled-up Teflon sprayed electrode proved to be better than that of the membrane clad electrode. Polarization of this electrode was about 50 mv lower than those of the membrane clad electrode over a wide current density range. However, the Teflon spray coated electrode leaked electrolyte into the air chamber at an unacceptably high rate, 0.005 $cm^3/min\text{-}cm^2$ of electrode area.

Figure E-2

Performance of Scaled-Up Teflon Coated Cathodes

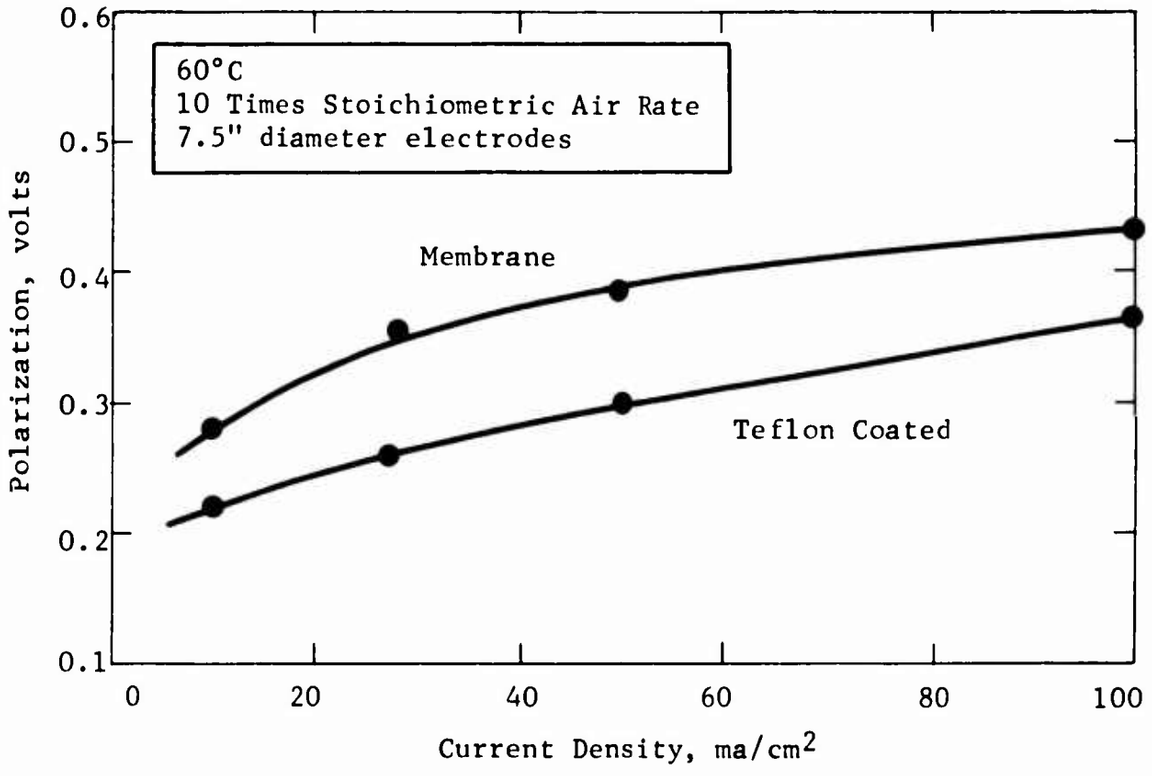

Thus, although performance is excellent, further efforts or techniques for preparing leak-free coatings on large electrodes are still needed.

Phase 2 - Sodium Alginate Coated Electrodes

As an alternative approach, sodium alginate, a polyuronic acid derived from seaweed, was used to control the electrolyte seepage of 1" diameter membraneless electrodes. Formulations of alginate and deionized H_2O were prepared and pressed into Cyanamid AA-1 electrode substrates.

Part a - Performance of Small Sodium Alginate Electrodes

Because the resulting coating is hydrophilic, it was placed on the electrolyte side. The electrochemical performance of these structures was evaluated in methanol-free electrolyte and electrolyte containing 1 M methanol. The performances at 50 ma/cm^2 are presented below in Table E-1. More complete data may be found in Appendix E-3.

The performance of the alginate coated electrode was comparable to the conventional Permion membrane clad structure and to the Teflon spray coated electrode. Furthermore, this benefit in performance was found to be somewhat better with 1 M methanol present. At 50 ma/cm^2, the polarization of this electrode with methanol present was 0.47 volt, compared to 0.53 volt for the conventional cathode.

Table E-1

Performance of Alginate Coated 1" D Electrodes

Electrode Description	Methanol Concentration of Electrolyte, M	Polarization at 50 ma/cm^2
Sodium alginate 17 wt % in H_2O pressed to Cyanamid AA-1	0	0.45
	1	0.47
Conventional Permion-Cyanamid clad AA-1	0	0.47
	1	0.53
Teflon spray coated Cyanamid AA-1	0	0.48
	1	0.56

Tests conducted in 30 wt % H_2SO_4 at 60°C using air at 10 x stoichiometric

Part b - Performance of Scaled Up Alginate Electrode

The alginate-water formulation with the best performance in tests using 1" diameter electrodes was then used to fabricate a large 9 x 5-3/4" electrode. A mixture containing 17 wt.% sodium alginate was pressed into a Cyanamid AA-1 screen at 500 psi, forming the acid insoluble barrier. The electrode was incorporated into the half-cell test facility, and compared with a standard methanol anode.

The performance of the scaled-up alginate barrier electrode was poorer than its smaller 1" diameter counterpart. The cathode polarization was about 0.1 volt higher at comparable test concentrations. Electrolyte leakage occurred in tests with 1 M MeOH. Table E-2 summarizes the results of these scale up tests.

Table E-2

Performance of Scaled-Up Sodium Alginate and Electrode

MeOH Conc, M	Cell Voltage, volts	Polarization at 40 ma/cm^2, volts		IR at 100 ma/cm^2, volts
		Anode	Cathode	
0.50	0.20	0.38	0.53	0.215
0.75	0.16	0.40	0.55	0.215
1.0	0.13	0.40	0.58	0.215

Test Conditions - Air Rate: 10 x stoichiometric
Fuel Feed: 50% Conversion/pass
Temperature: 60°C

Phase 3 - High Temperature Structures

Research on high temperature cathode structures has been conducted in support of the liquid decane-air total cell development effort. The prime objective of this program was to develop a workable air electrode for inclusion in the final multicell assembly. In addition, attempts were made to reduce total catalyst loading. These cathodes were designed to operate at 150°C in 14.7 M phosphoric acid electrolyte, a more stringent requirement than that encountered in low temperature cells. As a result, these electrodes must be interface-maintaining even after repeated temperature cycles. Furthermore, oxygen or air transport through the electrode into the electrolyte space cannot be tolerated.

Part a - Laminated Cathodes

Tests already reported in Task B indicated that the 50 mg/cm^2 sintered platinum Teflon electrodes failed to maintain the air electrolyte interface after operating in the 1.5" diameter cells for 100 hours. The use of Teflon spray coating improved this life to 160 hours. Examination of these electrodes indicated that this failure was due to severe checking and cracking of the electrode surface, necessitating some auxiliary interface control device.

Preliminary experiments in 14.7 M phosphoric acid, indicated that a porous Teflon film applied to the air side of the cathode could provide the interface control without loss in electrode performance. Indeed, with a properly bonded coating, significant performance improvements could be obtained. The data are summarized in Table E-3.

Table E-3

Air Performance of Clad Cathodes

(14.7 M H_3PO_4-150°C, 3.5 mil Porous Teflon-10 Micron Pores)

	50 mg/cm^2 S.P.T.E.		10 ma/cm^2 Cyanamid AA-1	
	Polarization from Theoretical Oxygen at Indicated ma/cm^2, volts		Polarization from Theoretical Oxygen at Indicated ma/cm^2, volts	
	50	100	50	100
No cladding	0.35	0.45	--	--
Placed film	0.35	0.45	0.37	0.44
Laminated film(1)	0.27	0.30	0.32	0.37

(1) Lamination procedures differed for the two electrodes.

Note that the best laminated Cyanamid AA-1 cathode was only 70 mv poorer than the higher loaded sintered platinum Teflon structure.

To further optimize this effect, a study of the effect of film pore diameter and porosity on air and oxygen performance was conducted using the 14.7 M phosphoric acid electrolyte (see Appendix E-4). To do this, porous Teflon films, obtained from Chemplast Inc., were laminated to the catalyst rich side of the Cyanamid AA-1 electrode by cold pressing at 1500 psi. The results of this study, shown in Figure E-3, indicate that porosity per se (in the range of 50-90%) does not appear to affect cathode polarization. However, pore diameter appears to be critical, with a pore diameter of 10-20 microns being optimum on oxygen, while the best results on air were obtained with 10 micron pore diameter material. Furthermore, scale-up to larger (4" x 4") electrodes presented no problem. Because of the more severe sintering conditions used in the 50 mg/cm^2 sintered platinum Teflon cathode, the simple cold press lamination procedure could not be applied to making large electrodes, although cold lamination of 1.5" diameter electrodes was possible. These cold laminated cathodes were prepared by removing the mold release agent from the screen side of the previously formed cathode and pressing the screen side to the porous Teflon film. The resultant 1.5" diameter electrode gave 0.27 and 0.24 volts polarization at 50 and 100 ma/cm^2, respectively. Larger (4" x 4") cathodes could not be prepared by this technique, because the Teflon-screen bond was inadequate to maintain a stable configuration even with pressures as high as 8000 psi. At this latter pressure, a performance debit of 100 mv was observed. An alternate lamination

Figure E-3

Effect of Cladding Pore
Diameter on Cathode Performance

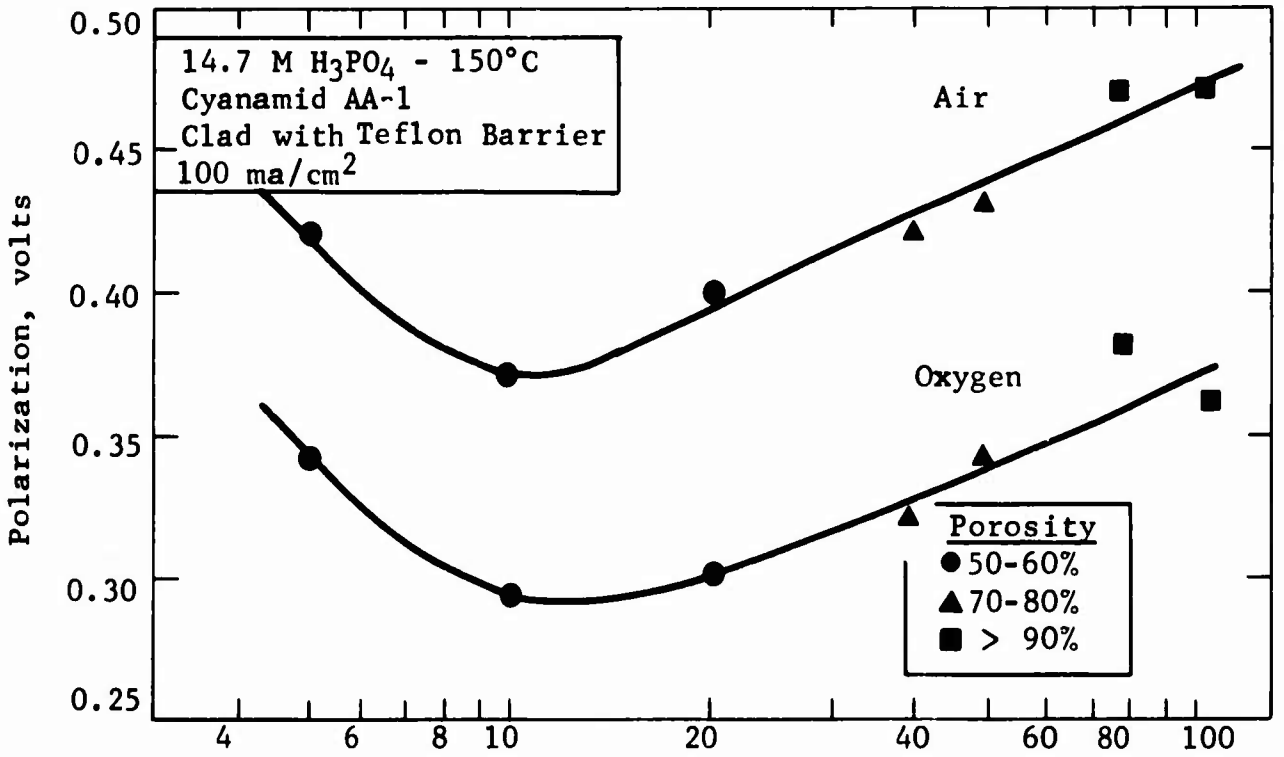

procedure was developed for the large electrode, which was similar to the barrier cladding technique used in anode preparation. It consisted of sintering the film to the precleaned screen side of the cathode at 349°C and 1100 psi for one minute. The resultant electrode was 0.30 volts polarized on air at 100 ma/cm^2. From the anode work, it now appears that adequate laminates can be obtained by sintering at 500 psi for only 15 seconds, provided the film is placed in contact with the lower heated platen, thus avoiding any sintering of the electrode.

Part b - Sintered Carbon Teflon Cathode

Efforts to reduce cathode catalyst loading have centered about the use of the sintered carbon Teflon emulsion electrode structure previously developed for butane anodes. Early work (4) with carbon supported cathodes indicated that a 1.3 mg/cm^2 Pt loading was possible with sulfuric acid electrolytes. Preliminary data obtained during oxygen activation of the butane anodes indicated that a 90 wt % platinized carbon 10 wt % Teflon emulsion electrode could yield good oxygen and air performance in phosphoric acid. Consequently, the effect of sintering temperature on air performance was examined between 313 and 360°C, using a sintering pressure of 2200 psi of one minute duration. The results of this study (Figure E-4 and Appendix E-5) indicated that the optimum sintering temperature was 349°C. However, the reponse surface was somewhat flatter than that obtained with the sintered platinum Teflon electrodes.

Figure E-4

Effect of Sintering Temperature on Cathode Performance

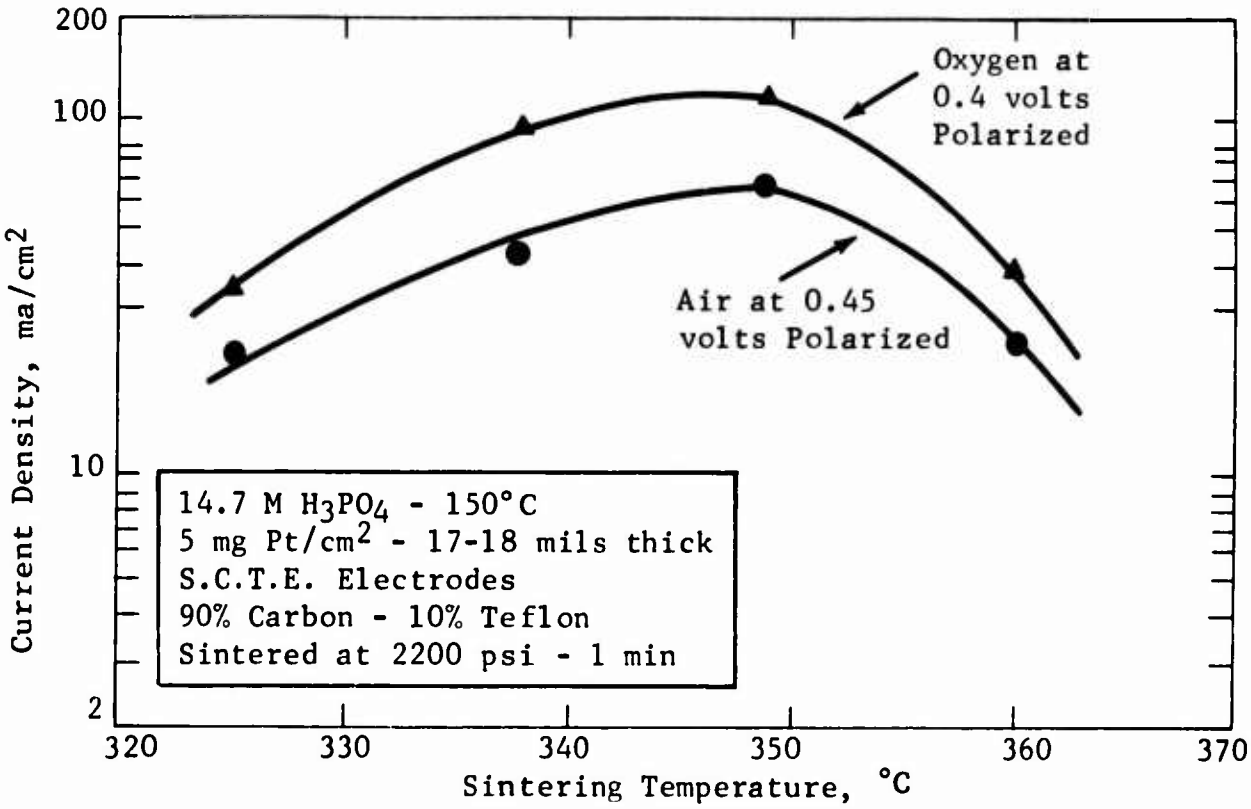

The effect of catalyst thickness was examined in separate experiments using catalyst zone thicknesses of 0.016 and 0.029 cm. These thicknesses were obtained using catalyst concentrations ranging from 6 to 24 wt %. The results of these experiments, summarized in Table E-4, indicate that thickness is not an important parameter.

Table E-4

Effect of Catalyst Thickness on Cathode Performance

(14.7 M H_3PO_4, 150°C)

Loading mg Pt/cm2	Catalyst Thickness, cm	Pt Utilization at Indicated Polarization, ma/mg	
		Oxygen (0.35 volts)	Air (0.45 volts)
2.5	0.016	24.0	38.0
	0.029	20.2	20.2
5.0	0.016	10.5	12
	0.029	14	13

However, the 2.5 mg/cm^2 thin carbon electrode did give somewhat higher air utilization than anticipated from oxygen performance, indicating that more work in this area is required. A plot of oxygen utilization versus catalyst loading, shown in Figure E-5, indicates that for catalyst loadings greater than 1 mg/cm^2, utilization decreases monotonically with loading. Included in this figure are data for both platinized carbon (6-24%) and platinum on silica treated carbon (1-4%). Air utilization response was similar except for the 2.5 mg/cm^2, 12% platinized catalyst.

Figure E-5

Effect of Catalyst Loading on Platinum Utilization

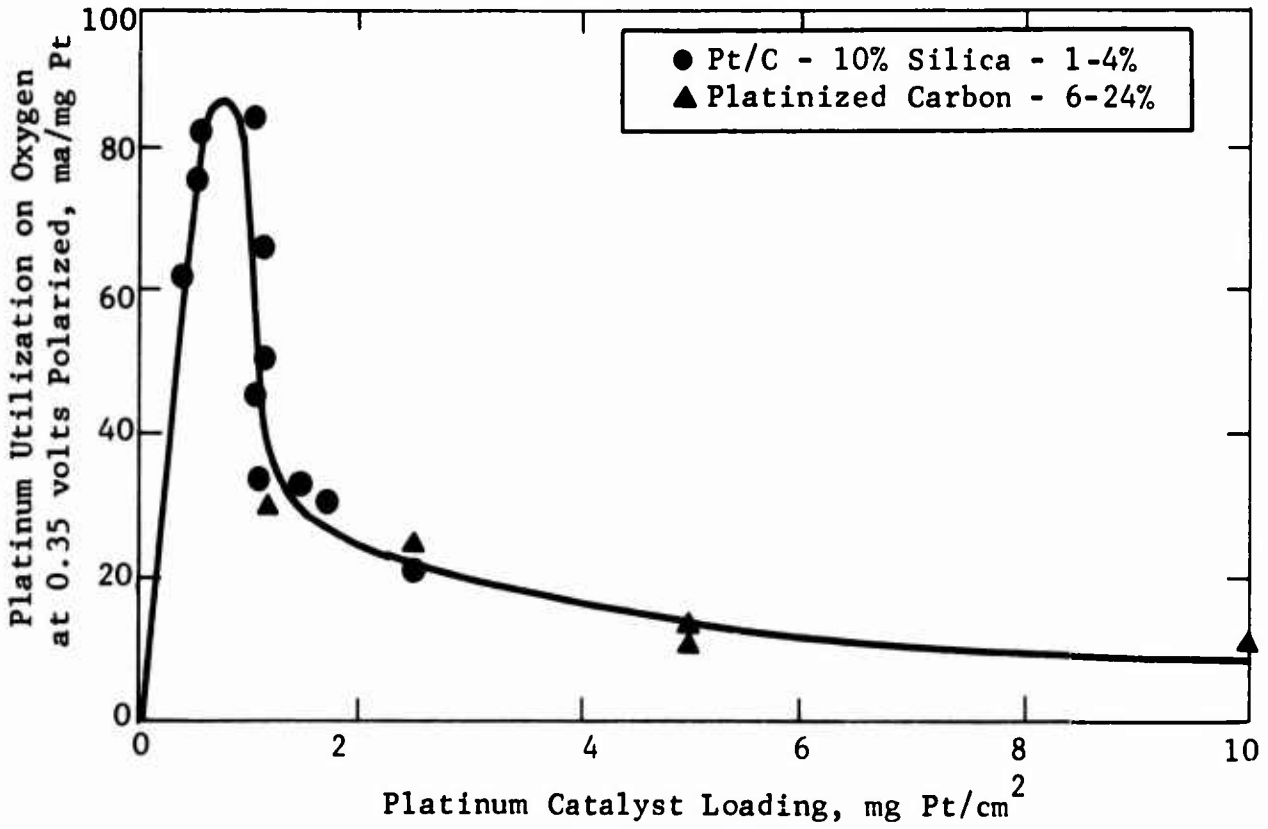

Part c - Cathodes for Hydrocarbon-Air Cell

As a result of studies discussed in Parts a and b above, three potentially useful cathode systems have been developed for the hydrocarbon-air total cell system. These include (1) a 50 mg/cm^2 sintered platinum Teflon electrode laminated to a 3.5 mil porous Teflon film, (2) a 10 mg/cm^2 American Cyanamid AA-1 electrode laminated to a porous Teflon film and (3) a 2.5 mg/cm^2 sintered carbon Teflon electrode structure. The air performances of these three systems are shown in Figure E-6.

Figure E-6

Air Performance of Candidate
Cathodes for Hydrocarbon-Air Cell

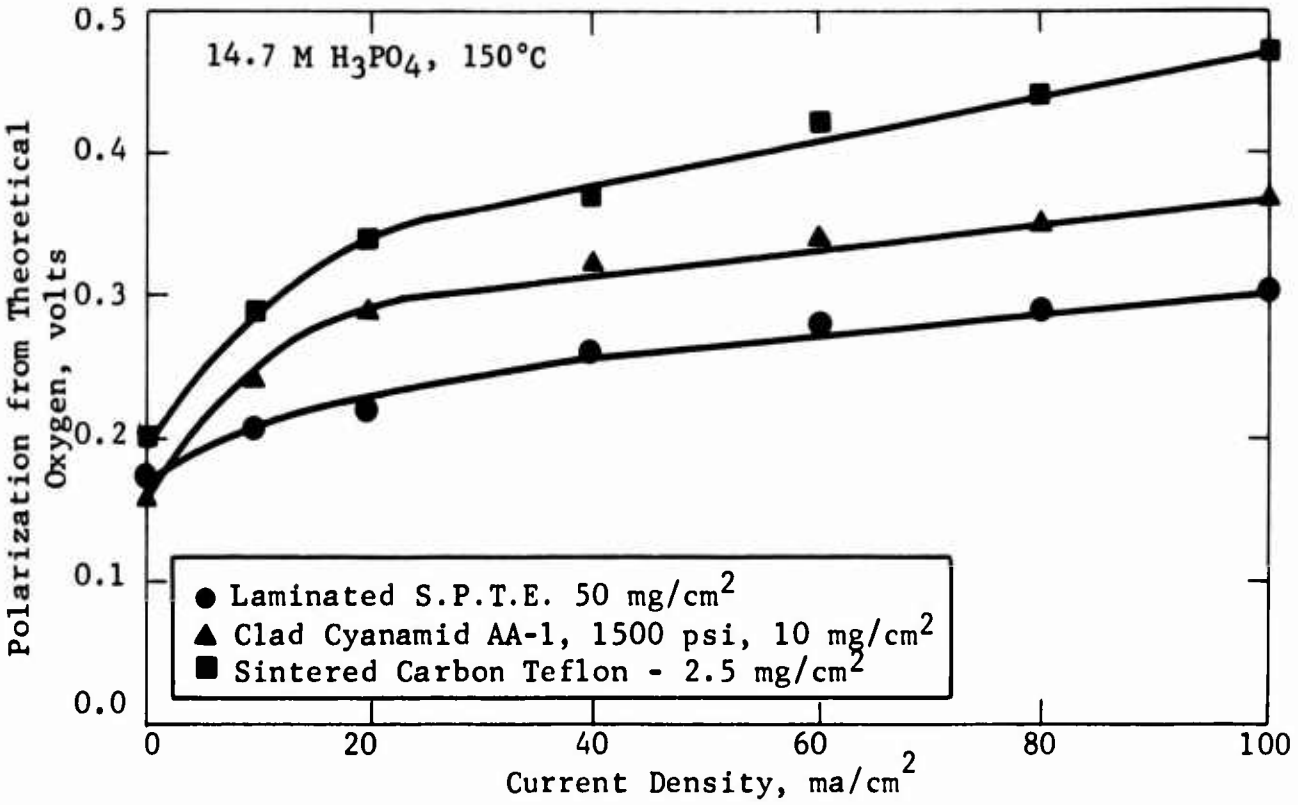

As expected, the highest loaded cathode gives the best performance, yielding 0.3 volts polarization at 100 ma/cm^2. However, the fivefold reduction in catalyst loading obtained in going from the laminated S.P.T.E. electrode to the laminated Cyanamid AA-1 structure resulted in only a 70 mv debit at 100 ma/cm^2, while further reduction to 2.5 mg Pt/cm^2 produced an additional 90 mv debit. Total cell tests leading to the final selection were discussed previously in Task B.

4.6 Task F, Methanol Fuel Cell

Further testing of single cells have primarily concentrated on the problems of reducing the chemical oxidation rates in the large 9" x 5-3/4" cells. Emphasis was placed on evaluating the effectiveness of barriers placed between the anode and cathode to reduce methanol migration, and on decreasing the methanol concentration required at the anode to the levels permissible with the smaller cell design. In addition, work was carried out on a simplified low power direct feed cell.

Phase 1 - Use of Cathode Diffusion Barriers for Reducing Direct Chemical Oxidation

Work in the preceding period(7) indicated that the use of felt or gel barriers between the anode and cathode of a total cell could reduce chemical oxidation of methanol at the cathode. Since operating conditions, such as methanol concentration and temperature, are not easily controlled or measured in a total cell, the barrier effect was therefore examined under better-defined conditions using a half cell. The tests were repeated in total cell operation.

Part a - Felt Barriers

The half-cell tests were carried out with the cathode and barrier clamped to the side arm of a well-stirred cell described previously(5). Electrolyte volume was large enough that negligible changes in methanol concentration occurred during the test period. Resistance-free polarizations were measured with calomel reference electrodes connected in an interrupter circuit. Direct comparison runs were made with and without felt diffusion barriers to eliminate variation between electrodes, errors in meter calibration, etc. Complete data are in Appendix F-1.

The tests showed that the addition of Dacron felt barriers substantially reduces direct oxidation by about 30%. Two types of felt were used, #5290 and #54. The less permeable felt, #54, showed a slight, 10% advantage over the more open felt, (#5290) in this respect. Some scatter in the data occurred at the lower current densities due to experimental problems. These results are shown in Figure F-1.

Figure F-1

Effect of Felt Barrier on Direct Oxidation

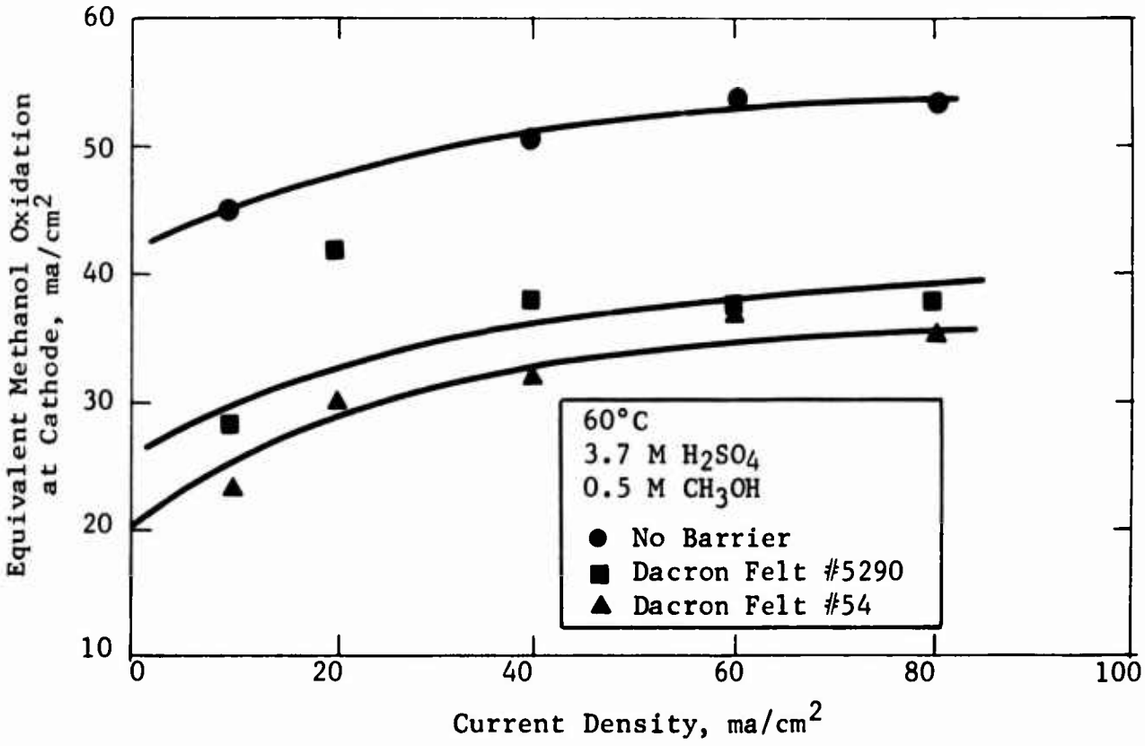

As shown in Figure F-2, the felt barrier also substantially improves electrical performance of the cathode by reducing the methanol concentration at this electrode. This is in contrast with the somewhat equivocal results with barriers in a total cell(7). The felt-protected electrode performed electrically as if it were carrying 30 ma/cm^2 less current and is actually operating at 15 ma/cm^2 less direct oxidation. This suggests that a given rate of direct oxidation uses twice as many cathode sites (for methanol as well as oxygen) as the corresponding electrochemical consumption of oxygen.

Figure F-2

Effect of Felt Barrier on Polarization

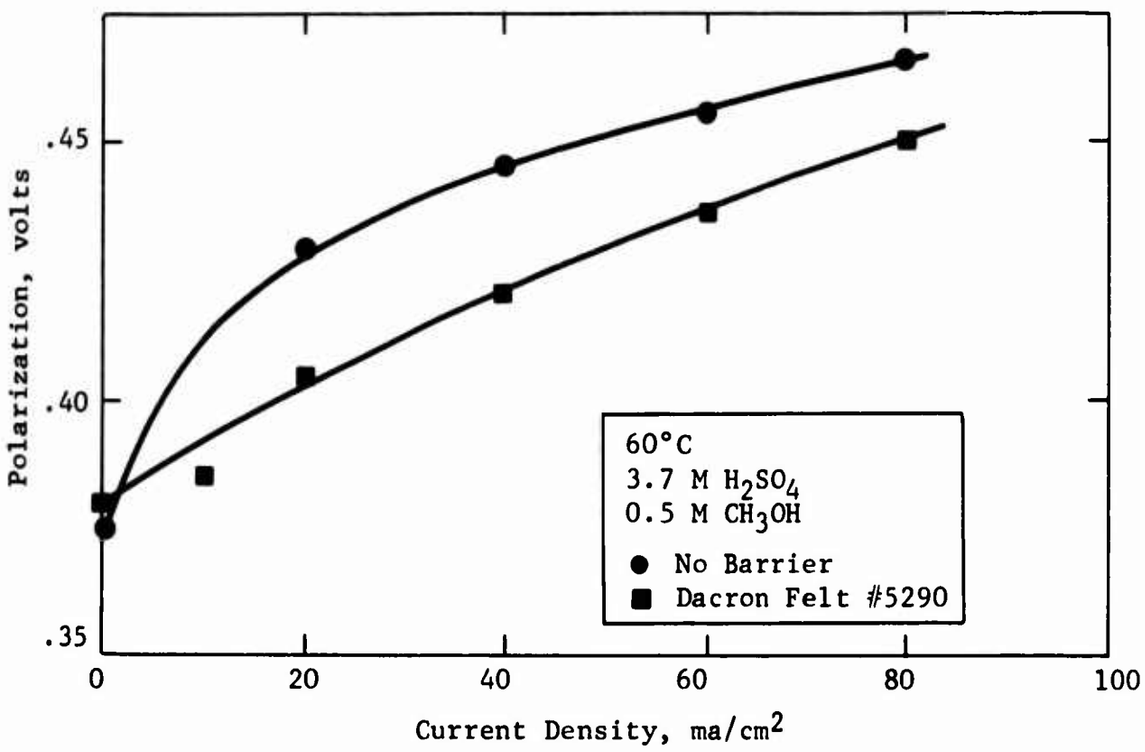

Part b - Membrane Barriers

Several experiments were also carried out to determine if a Permaplex C-20 membrane could substantially reduce methanol diffusion and direct oxidation. This is a 20 mil thick cation exchange membrane manufactured by Permutit. This was changed from the sodium to the hydrogen form by equilibrating in acid for several hours and was then pressed to the Cyanamid AA-1 cathode. Figure F-3 shows that this substantially reduced direct oxidation to about a third of that with felt or, a fifth of that with no barrier. Electrical performance was comparable to the control, that is, without the Permutit membrane in the absence of methanol, and was better than the control with methanol present. Complete data are presented in Appendix F-1.

Figure F-3

Effect of Permaplex Membrane on Direct Oxidation

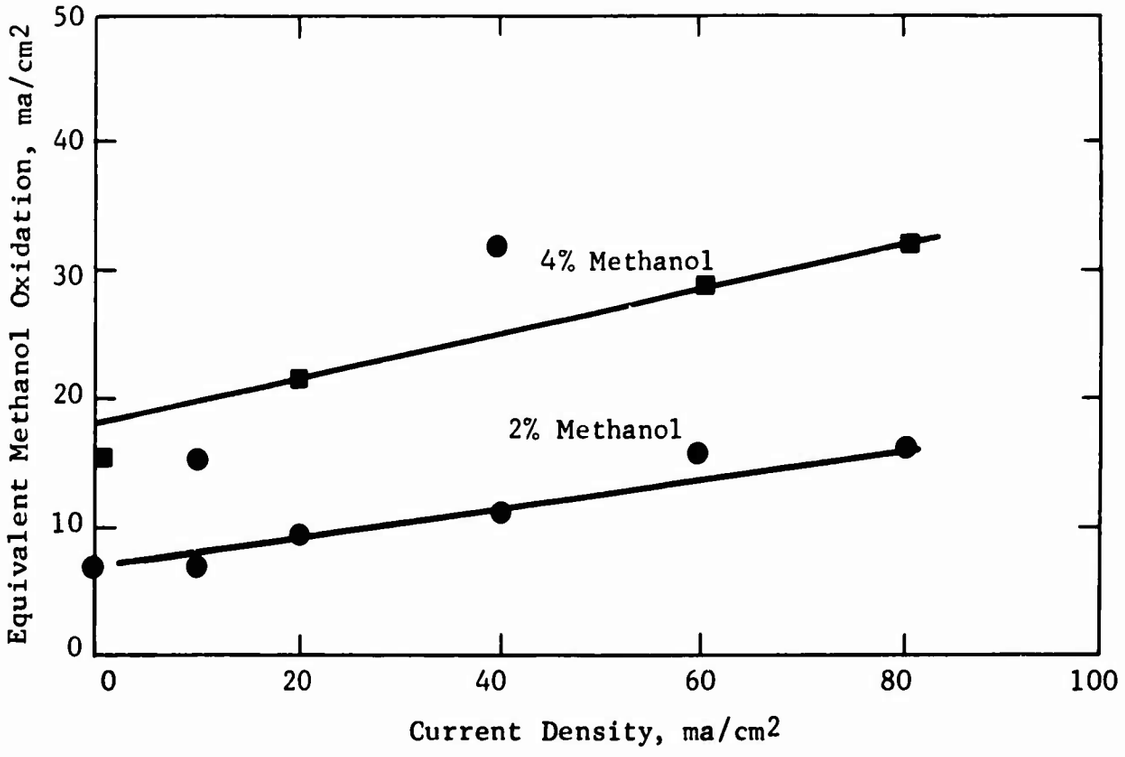

Part c - Barriers in Total Cells

Having examined the effect of barriers in a half cell, studies were conducted again in a total cell. Figure F-4 shows that again the barrier was quite effective in reducing chemical oxidation. Here, chemical oxidation was reduced by about a factor of three. Complete data are given in Appendix F-2. However, the effect on electrical performance was less clear in this case, because of inconstancy of anode polarization, possibly caused by gas entrapment in the felt barrier and a change in cell temperature and temperature gradients. Cathode polarization was generally slightly higher in runs in which felt was used. This was more than offset by the lower chemical oxidation. Thus the use of these barriers holds promise for significantly reducing direct methanol oxidation at the cathode.

Figure F-4

Effect of Barrier in Total Cell Operation

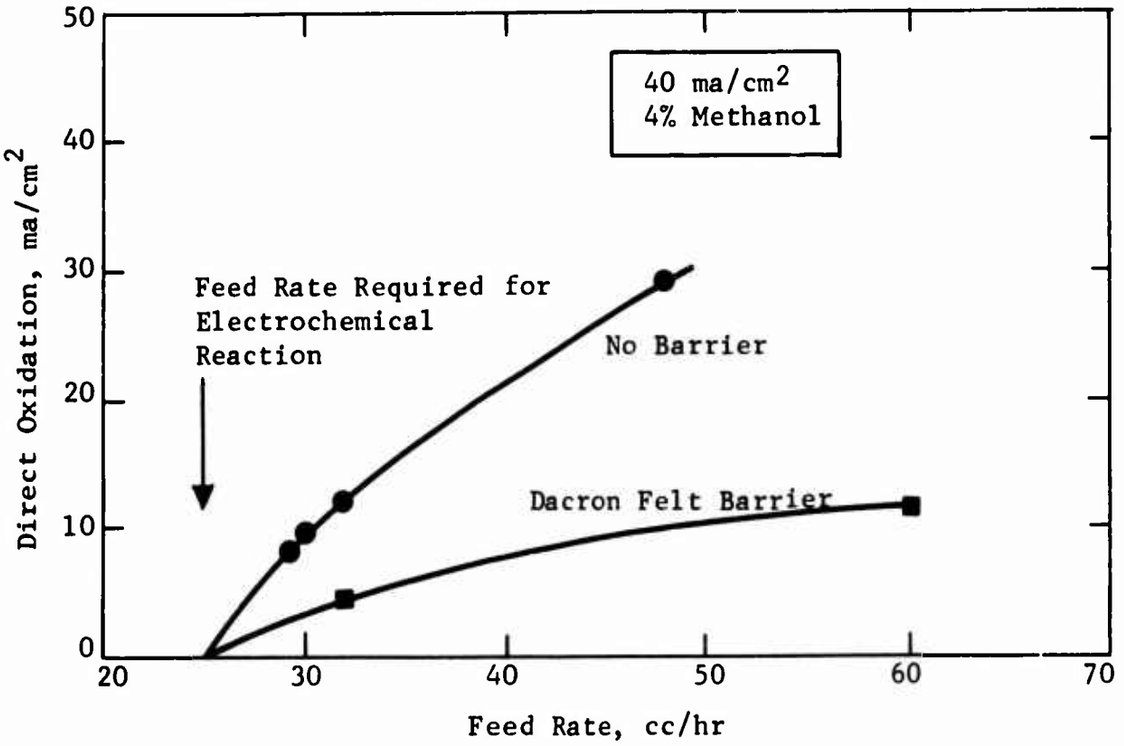

Phase 2 - Application to Large Cells

The studies on methods for lowering the rates of chemical oxidation were also extended to the large 9" x 5-3/4" cells. This work was done in conjunction with other tests aimed at reducing the required methanol concentration in these cells. These experiments were prompted by the finding that, in the larger cells, fuel distribution problems existed which resulted in impaired performance at low methanol concentration.

Part a - Use of Baffles in the Anode Chambers

A series of experiments was carried out to determine whether additional baffling within the anode chamber would improve anode performance. In initial preliminary experiments, the chamber was simply packed with glass beads. Subsequently, Dacron felt baffles were installed. The types of baffling configurations employed are shown schematically in Figure F-5.

Figure F-5

Schematic of Dacron Baffling Arrangement

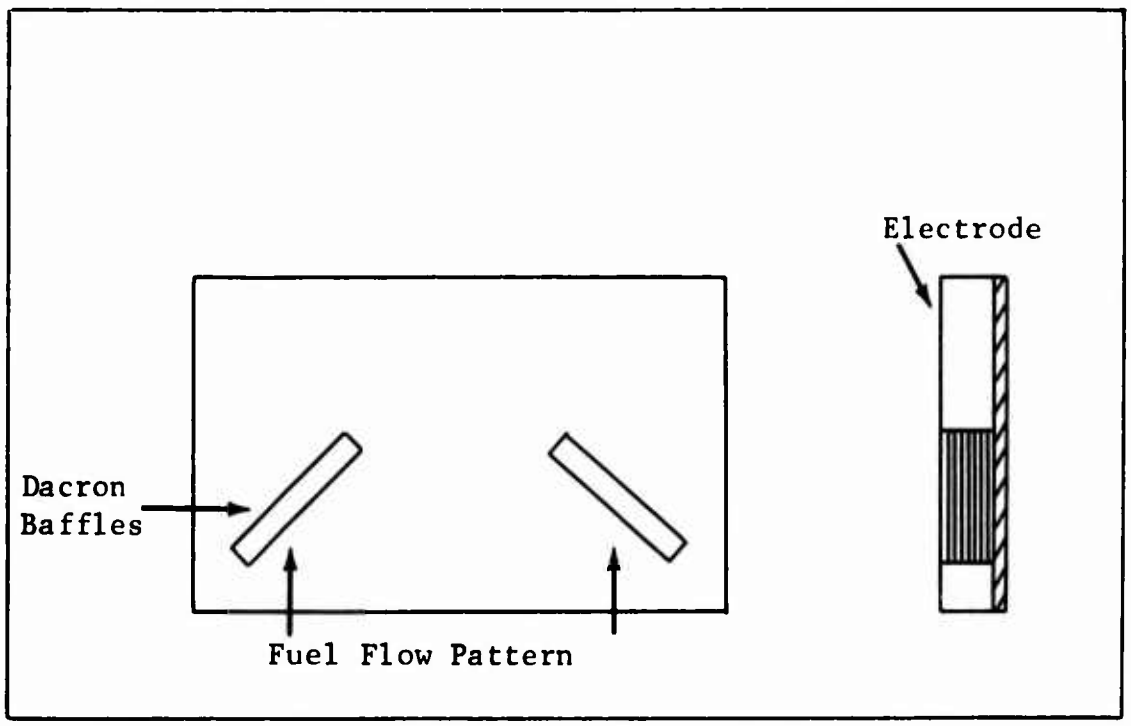

The use of glass beads, while impractical because of the high pressure drop required to pump electrolyte, demonstrated that baffling could improve anode performance at low methanol concentrations. For example, with 1 vol % methanol and 12% conversion per pass, anode polarization was only 0.31 volts. However, the addition of the more practical Dacron baffles resulted in no change in performance. These data are presented in Appendix F-3. Thus, more work on baffle design is still needed.

Part b - Internal Multiple Injection Ports

As an alternative approach to improving the fuel distribution over the anode, polypropylene tubes were extended into the anolyte chamber, thus permitting internal fuel distribution over the anode face. A schematic of the design is presented in Figure F-6.

Figure F-6

Internal Multiple Injection Ports

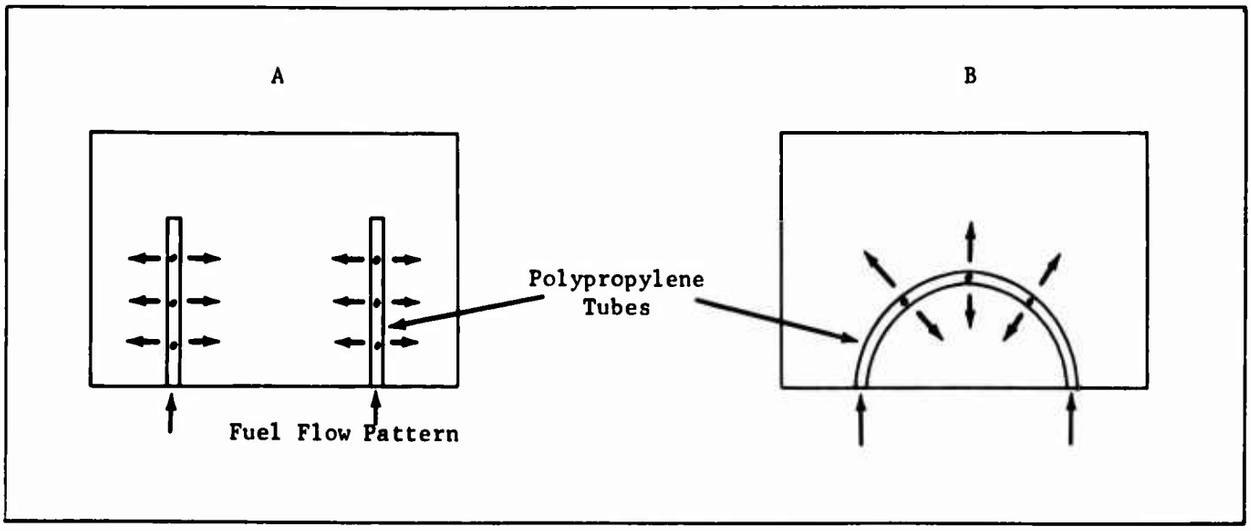

Table F-1 summarizes some of the salient test results of two internal multiple injection designs. No significant improvement in either anode or cathode polarizations, or cell IR was observed when the data were compared with the performance of the standard configuration. Complete data, which include repeated tests of this cell modification, are presented in Appendix F-3. These data further substantiate the conclusion that no significant improvement was made.

Table F-1

Performance of Multiple Injection Systems

Configuration	Methanol Conv., vol %	Conversion Per Pass, %	Cell Voltage, volts	Polarization at 40 ma/cm^2, volts	
				Anode	Cathode
A	2	50	0.38	0.38	0.36
	3	50	0.40	0.34	0.38
B	2	50	0.38	0.37	0.38
	3	25	0.32	0.37	0.44
Standard	2	50	0.40	0.39	0.35
	3	50	0.38	0.38	0.37

Part c - Double Portless Anode System

In another approach to reducing chemical oxidation, a test configuration consisting of two conventional anodes, with a gold current collector sandwiched between them, and a Permion membrane clad Cyanamid AA-1 cathode was tested in the 9" x 5-3/4" cell. The anode nearest the cathode contained carbon dioxide rejection ports; carbon dioxide was rejected through slits cut in a gasket separating anode and cathode.

The initial results of tests using this cell design were encouraging. Table F-2 summarizes some test results. Anode and cathode polarizations were lower than that derived from the standard configuration. On the other hand, the cell internal resistance was also higher, resulting in a total cell voltage which was about the same as that obtained in the unmodified cell. However, further tests carried out with this configuration gave less impressive results. These are presented in Appendix F-3.

Table F-2

Performance of Double Portless Anode Test Configuration

Conversion* Pass, %	Cell Voltage, volts	Polarization at 40 ma/cm^2, volts		Ohmic Loss, volts
		Anode	Cathode	
12.5	0.40	0.34	0.38	.095
25.0	0.40	0.35	0.38	.095
50.0	0.40	0.33	0.37	.095

*Methanol concentration, 3 vol %.

Part d - Performance of Systems Incorporating Methanol Diffusion Barriers

Attempts to use the previously discussed barriers to reduce chemical oxidation at the cathode were made during the past interim. Combinations of 32 mil Dacron felt (with and without bubble disengaging spacers) and Nalfilm membranes were tested. In addition, a system consisting of two Permion membranes was also evaluated. Appendix F-4 depicts a schematic of the barrier set-ups. The results of this study are presented in Table F-3. More complete information may be found in Appendix F-5.

In all of the configurations tested, total cell performance was poorer than for the conventionally assembled cell at comparable conditions. Most of the performance loss in the barrier systems appeared to come from higher internal resistance. Chemical oxidation was not significantly decreased as indicated by the carbon dioxide content in the spent air stream. This is illustrated in Table F-3.

Table F-3

Systems Incorporating Barriers

Added Barrier	MeOH Conc, vol %	Cell Voltage, volts	Polarization, volts		Ohmic Loss, volts	Equivalent Chemical Oxidation Current, ma/cm^2
			Anode	Cathode		
None	3	0.40	0.35	0.37	0.08	16
Dacron felt	3	0.34	0.42	0.34	0.10	17
Dacron felt + Spacer	3	0.37	0.39	0.33	0.11	--
Dacron felt + Spacer + Nalfilm	2	0.0	0.36	0.64	0.20	7
Two Permion membranes	2	0.27	0.35	0.48	0.120	17

These differences in results between the 4" x 4" and 9" x 5-3/4" cells indicate that the nature and type of baffling or barriers used to reduce chemical oxidation depend on details of the actual cell design used. Thus, the reduction in chemical oxidation in the large 9" x 5-3/4" cell will require extensive design changes to make this system operate as efficiently as the smaller unit.

Phase 3 - Simplified Low Power Methanol Fuel Cells

In the previous report (7), a description and performance curves were given for a methanol cell which had its cathode directly exposed to the air. This permitted operation without an auxiliary blower for air supply. The cell has now been further modified to eliminate electrolyte circulation or methanol feed pumps. It is being run with direct methanol feed via a wicking system. The cell is thus a completely self-contained system having no auxiliaries or moving parts.

Part a - Cell Operation

The cell was operated for 3000 hours unattended except for bi-weekly refilling of the fuel tank and occasional electrolyte addition to make up for evaporation and leakage. The load, a demonstration flashing buoy light, consumed 60 ma (0.6 ma/cm^2) at 0.6 volts. The methanol feed rate was 0.86 cc per day for a stoichiometric requirement of 0.36 cc per day. The excess was directly oxidized at the cathode. The wicking system used was not suitable for closer control at these low flow rates, hence the higher chemical oxidation rates. However, this cell does demonstrate the feasibility of low power systems without auxiliaries for long term unattended operation.

4.7 Task G, Prototype Development

Engineering research has continued on the development of a methanol-air prototype fuel cell battery. Emphasis was placed on improving the operation of multicell stacks and on the development of the auxiliary and control systems required for the self-sustained operation of the fuel cell battery.

Phase 1 - Operating Characteristics of the Sixteen Cell Stack

Additional testing of the sixteen cell stack containing 9" x 5-3/4" electrodes was conducted to define the effect of time on performance and to evaluate modifications for improving stack operation.

Part a - Performance of Sixteen Cell Stack With Time

Testing of the sixteen cell stack was extended to 485 hours on current load over a seven month period. Only a moderate decline in performance was noted during the first 275 hours on load, from 7.3 volts to 6.8 volts at 40 ma/cm^2. However, performance declined to 5.2 volts after 485 hours of operation, as shown in Figure G-1. The maximum power output decreased correspondingly, from 120 watts initially to 68 watts at the end of the test period.

Figure G-1

Performance Stability with Time

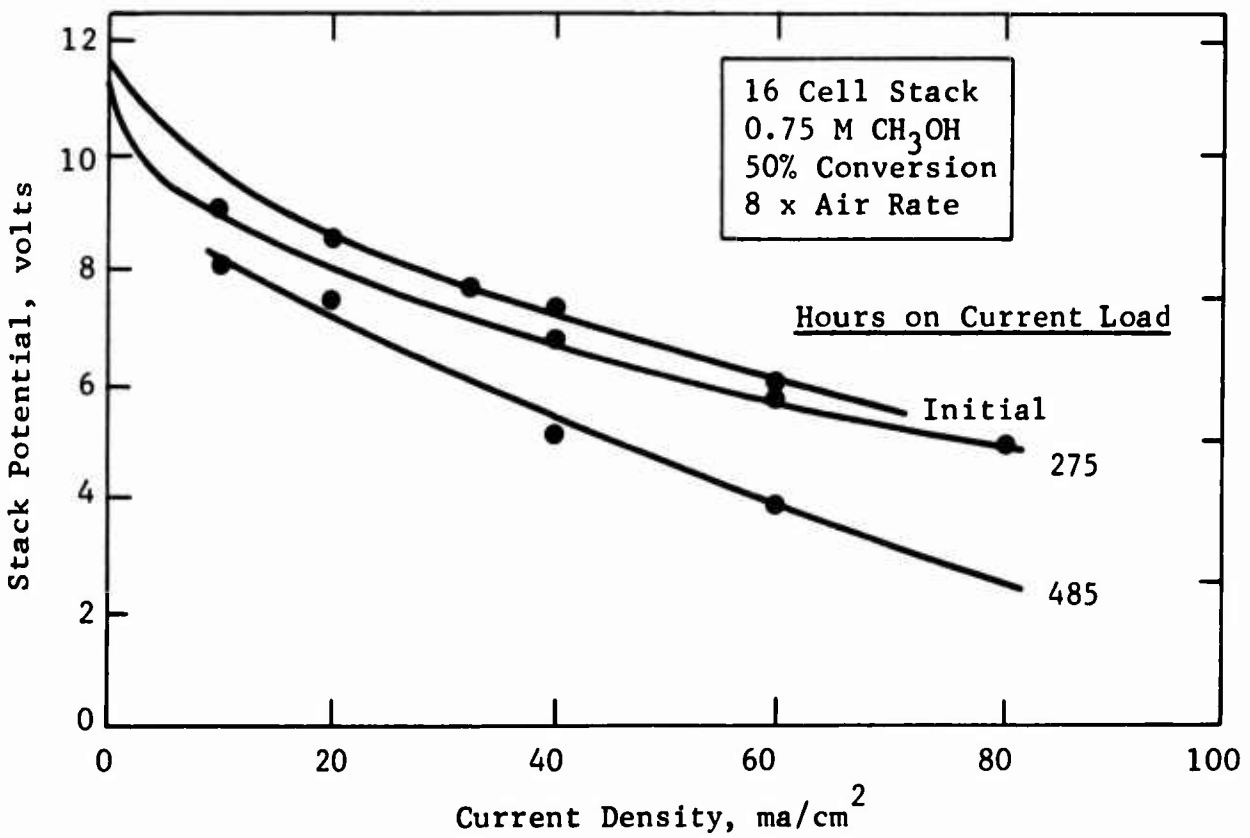

Most of the performance loss occurred after 400 hours of testing, as shown in Figure G-2.

Figure G-2

Effect of Time on Cell Voltage

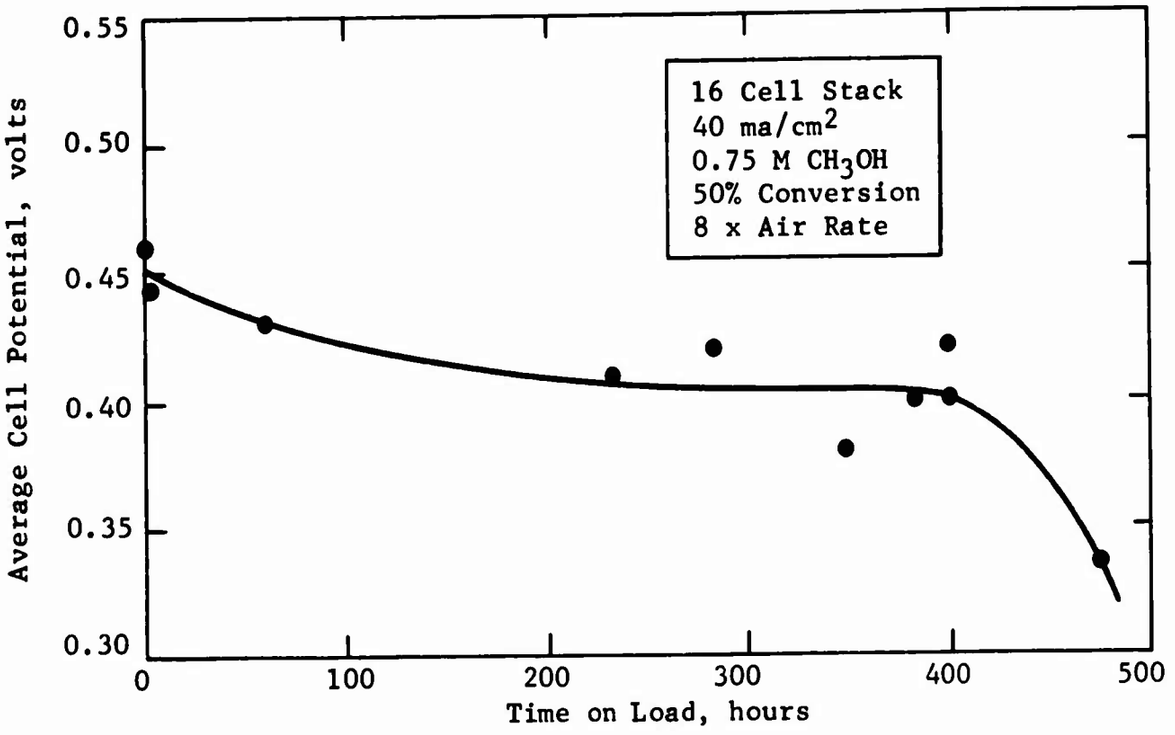

A detailed study of electrode performance showed that increased anode polarization was responsible for most of the performance loss. Anode polarization increased significantly after 485 hours of testing, from 0.29 volts to 40.0 volts at 40 ma/cm^2, as shown in Table G-1. Slightly increased ohmic losses were also noted.

Table G-1

Effect of Time on Average Cell Performance

Voltage	Time on Current Load, hrs	
	1	485
Cell Voltage	0.44 ± 0.03	0.34 ± 0.02
Anode Polarization, volts	0.29 ± 0.05	0.40 ± 0.03
Cathode Polarization, volts	0.43 ± 0.05	0.40 ± 0.03
Ohmic Loss, volts	0.05 ± 0.00	0.07 ± 0.02
16 Cell Stack; 0.75 M CH_3OH in 3.7 M H_2SO_4; 50% Conversion; 8 times stoichiometric air rate; 60-70°C.		

The decline in performance after 400 hours is attributed to severe upsets that occurred during the development of the integrated methanol addition control system described below in Phase 2. These upsets resulted in frequent periods of prolonged methanol starvation, resulting in anode overpolarization and electrolyte discoloration. Also, excessive amounts of methanol were occasionally fed to the stack, resulting in temperatures in excess of 90°C. Thus, the performance losses noted above are not regarded as typical of those to be expected from routine operation of the methanol-air fuel cell system.

Inspection of the anodes showed that catalyst retention on the 9" x 5-3/4" anodes was, in general, excellent. Only one anode showed signs of marked catalyst loss. The remaining fifteen anodes contained minor pin holes. These pin holes apparently had no effect on the rate of methanol transport through the anodes into the electrolyte chamber adjacent to the cathodes. Thus, chemical oxidation levels were essentially the same throughout the test period. For example, operation at 40 ma/cm^2 with 0.75 M methanol at 50% conversion per pass gave chemical oxidation rates of about 20 to 25 ma/cm^2, independent of stack history.

Similarly, the cathodes appeared intact. Although the Permion 1010 membranes were discolored, they remained firmly bonded to the cathode surface. Operation at excessive temperatures may have collapsed some membrane pores, resulting in the moderate increase in cell ohmic losses noted earlier.

Additional data are presented in Appendix G-1 to G-3. Complete details of the stack components and assembly procedures were reported earlier (7).

Part b - Thermal Characteristics of the Sixteen Cell Stack

Previous studies showed that wide temperature distributions existed within the sixteen cell stack (7). These were caused primarily by the introduction of electrolyte into one side of the stack through the parallel-flow manifold system. The electrolyte picked up heat from the manifold walls and entered succeeding cells at higher temperature, so that the interior cells approached the 90°C ceiling temperature imposed by the use of polypropylene frames.

Therefore, the electrolyte flow path through the sixteen cell stack was altered. A dual-entry system was provided. This was done by inserting plugs in the feed inlet manifolds between the center cells, as shown schematically in Figure G-3.

Altering the flow path markedly improved the temperature distribution within the sixteen cell stack. As illustrated in Figure G-4, individual cell temperatures under typical operating conditions ranged from 57 to 68°C using the dual-entry feed manifold, compared with a range of 46 to 75°C obtained with the older, single-entry manifold. The new temperature distribution remained flat, even at more severe operating conditions. Complete data are given in Appendix G-4.

Figure G-3

Schematic Comparison of Feed Inlet Systems

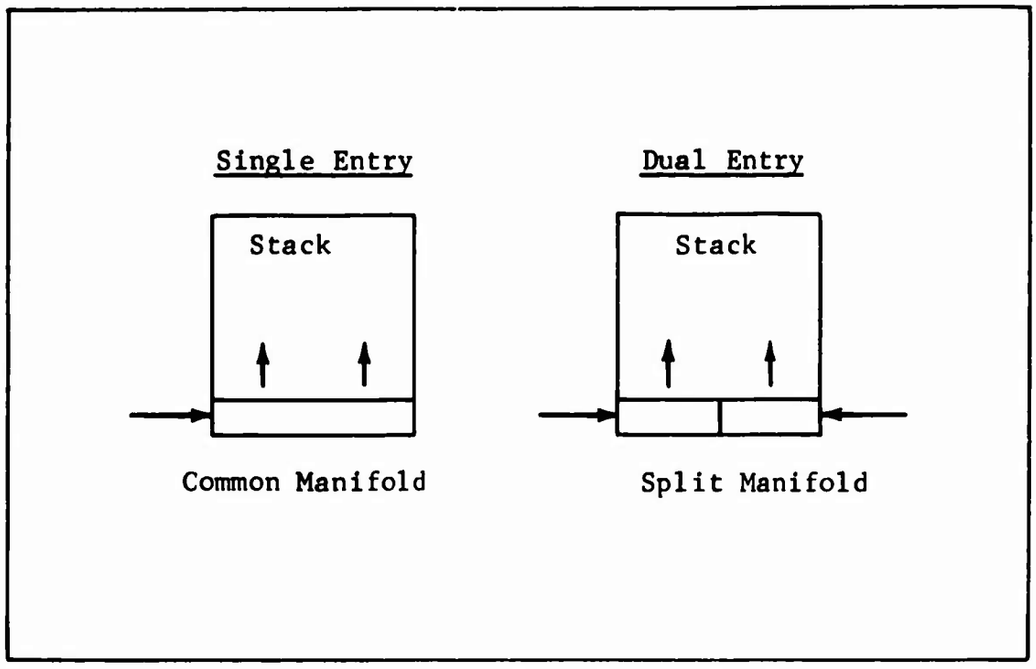

Figure G-4

Effect of Fuel Manifold Type on Temperature Distribution

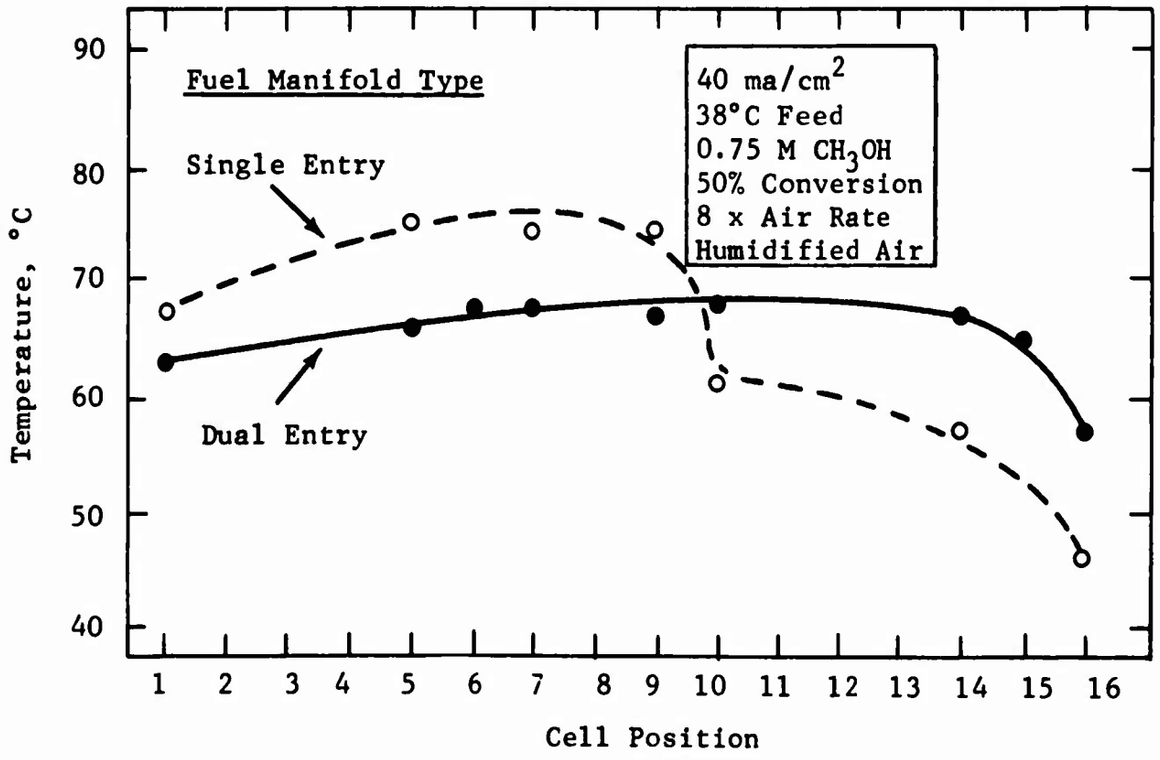

Feed distribution remained unaffected by the change-over to the dual-entry system. Thus, average cell performance and anode polarization were essentially the same in either half of the sixteen cell module, as shown in Table G-2. Complete data are presented in Appendix G-5.

Table G-2

Effect of Dual-Feed System on Cell Performance

Cell Group	Cell Potential, volts	Anode Polarization, volts
1 to 8	0.38 ± 0.05	0.40 ± 0.03
9 to 16	0.41 ± 0.04	0.39 ± 0.02
40 ma/cm^2, 0.62 M CH_3OH in 3.7 M H_2SO_4 at 50% Conversion, 8 times Stoichiometric Air Rate		

Part c - Miscellaneous Sixteen Cell Stack Studies

Evolution of carbon dioxide causes the displacement of electrolyte from within the anolyte chambers of the methanol fuel cell. Provision must be made for storing this displaced electrolyte during operation and for its return prior to shutdown. Previous studies have shown that prolonged storage of exposed electrodes can result in performance debits (7). Therefore, a study was made of the extent of electrolyte displacement from within the 9" x 5-3/4" cells of the sixteen cell stack. Both steady state and transient data were obtained.

Steady state displacements of up to 400 cc were noted for operation at maximum gas evolution rates, as shown in Figure G-5. About 10 minutes at high current loads and 20 minutes at low loads were required to achieve steady state. Subsequent studies showed that pump rates of 200 cc/min could be obtained from the proposed electrolyte gear pump being developed for the integrated methanol battery system. Therefore, a pump-back time of about two minutes appears feasible for refilling the multicell stack prior to shutdown. Complete data are listed in Appendix G-6.

Figure G-5

Effect of Current Load on Electrolyte Displacement

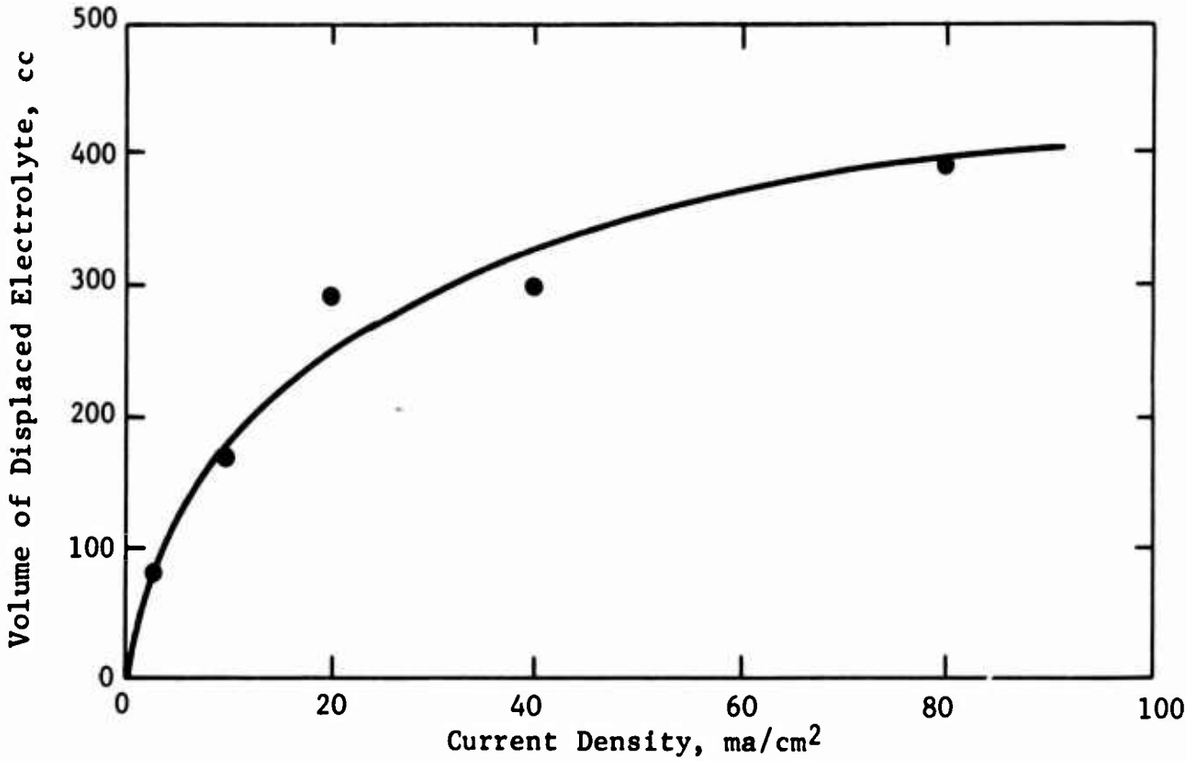

Phase 2 - Development of Auxiliary and Control Systems for the Methanol Fuel Cell Battery Demonstrator

An extensive development program was conducted to design, construct and test the necessary compact auxiliary equipment required for the operation of the integrated Methanol Fuel Cell Battery Demonstrator. These auxiliaries included the electrolyte circulation and concentration control systems, the air supply system, the methanol concentration control system, and the associated electronic control systems.

Part a - Electrolyte Circulation System

The development of a compact, low-power, corrosion-free, electrolyte gear pump was described in a previous report (7). This submerged-type pump is used to circulate electrolyte from the battery reservoir or sump system to the fuel cell stack. The pump was incorporated into an assembly that included an E. V. Hill pump motor, a rotameter to monitor the flow rate, and a check valve to prevent backflow from the elevated stack assembly. A 2/1 reduction ratio gear box was used to augment the torque output of the motor, thus improving reliability at low flow rates. A picture of the assembly is shown in Appendix G-6.

The pump delivered more than 200 cc/min against a 12 inch electrolyte head with power consumption levels of 0.10 to 0.36 watts. The pump was operated without difficulty for several hundred hours, both in separate test assemblies and as part of an integrated battery system. Additional details are given in Appendices G-8 and G-9.

Part b - Water Addition System

Previous studies showed that more water leaves a fuel cell module via the exhaust air stream than is produced by the oxidation of methanol (7). Some, but not all, of this excess will be recovered by the air auxiliary system described below. Thus, provision must be made to add water to the circulating electrolyte to maintain the acid concentration at the desired level of 3.7 M sulfuric acid.

The approach of using the electrolyte level within the system to control water balancing suffered from the fact that the apparent liquid volume increases with increasing current, because of the large amounts of carbon dioxide produced at the anode and rejected through the electrolyte. Because of this factor, a hydrometer was developed for controlling acid concentration.

The hydrometer consists of a spherical float attached to a metal core at the bottom and suspended by several weighted chains. This device is depicted in Figure G-6 and Appendices G-7 and G-9. As the acid becomes concentrated, the float rises and readjusts to a new equilibrium as a result of its picking up some of the chain weight. The change in density of the float with temperature compensates for the density change of the electrolyte.

Figure G-6

Acid Hydrometer for Water Balancing

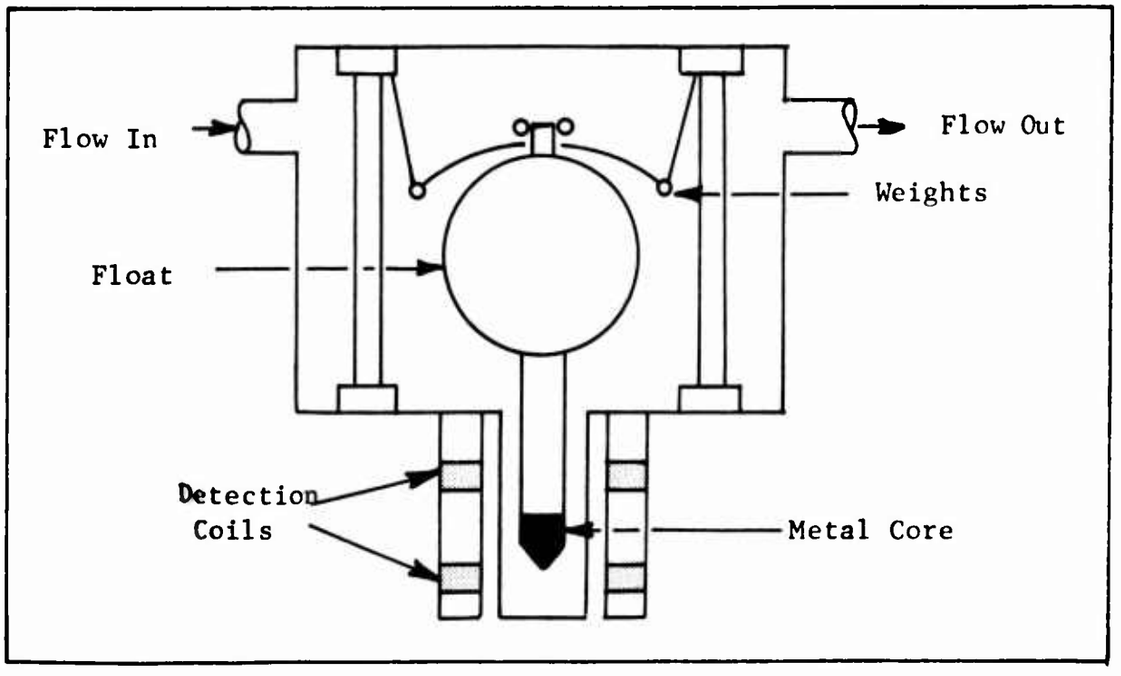

Acid concentration is controlled by adding water through a motor-driven valve so that the maximum sulfuric acid concentration is about 4.2 M. A Globe Model No. 98A102-8 motor and 495/1 reduction ratio gear box were used for this purpose. The water valve is actuated by a controller which detects the position of the metal core below the float by means of radio-frequency coils. An upper coil

controls water addition, while the lower coil activates a signal light indicating that the acid has been diluted to about 3.3 M. About 0.25 watts of parasitic power are required to operate the valve motor. Details of the control system are presented in Appendix G-13.

The make-up water supply is obtained from the main water tank. This tank releases water on demand, using a self-actuated air displacement principle, closely resembling the action of the constant-level feeding system used with kerosene heaters. A drawing of the main water tank is given in Appendix G-9. Additional details of the final flow systems are presented later in Phase 3.

Part c - Air Auxiliary System

Ambient air must be provided to the fuel cell stack. In addition to its function as a reactant, flowing air may be used to control stack temperature by adjusting the rate of water removal from the cells. However, most of this water must be recovered to maintain a reasonable water balance. Therefore, work was conducted to develop such a system.

A survey of available blowers, and their associated power demands, quickly showed that only a low pressure drop air auxiliary system would allow operation at low parasitic power levels. These studies indicated that pressure drop should not exceed 0.26 inches of water. An estimated pressure drop distribution among the proposed air auxiliary system components is given in Table G-3.

Table G-3

Estimated Pressure Drop Distribution

Flow Path	Estimated Maximum Allowable Pressure Drop, inches H_2O[1]
From Blower through Water Economy Unit	0.02
Through Stack	0.05
Through Knock-out Pot	0.02
Through Air Condenser	
Tubes	0.10
Expansion and Contraction	0.05
Through Water Economy Unit to Final Exhaust	0.02
Total	0.26

(1) At 70,000 cc/min maximum anticipated air rate.

A modified Lytron Model 4515 condenser, consisting of twelve 5" unfinned aluminum tubes connected in parallel, was selected to recover the water in the exhaust air stream leaving the fuel cell stack. Initial tests with an unmodified condenser having internal extended-surface tubes showed that pressure drop through the unit would be excessive, about five inches of water at 40,000 cc/min air flow rate. The modified unit, on the other hand, gave 0.04 inches of water pressure drop at the same air rate. A photograph of the modified condenser is presented in Appendix G-7.

The condenser performed satisfactorily in bench-scale tests. Simulated, wet, stack exhaust air flowing at 20,000 cc/min, was cooled from 56°C to 33°C. Cooling air at 26°C was supplied by a small four-bladed fan operated with an E. V. Hill motor. About 0.7 watts of parasitic power were consumed. Addition test data are given in Appendix G-10

The exhaust air from the stack may contain entrained acid droplets that have leaked through defective membranes within the fuel cell stack. Therefore, a knock-out pot was included between the stack exhaust duct and the air condenser to prevent excessive corrosion of the aluminum condenser tubes. This was done primarily to extend the service life of the condenser, rather than to prevent a buildup of aluminum sulfate in the electrolyte. Earlier studies had shown that anode performance was unaffected by the presence of this salt.

A membrane humidity exchanger, or water economy unit, was developed to remove additional water from the cooled exhaust stream leaving the air condenser. The device consists of a Nalfilm 30 membrane separating two polypropylene air passages in which fresh, ambient air and exhaust air flow countercurrently, as shown in Figure G-7. The membrane is permeable to moisture and permits the exhaust air to transfer water and heat to the fresh air stream, thus leaving the battery at temperatures and humidities approaching ambient conditions. The membrane has high water permeability, via a pore condensation mechanism, and is acid-resistant.

Figure G-7

Water Economy Unit

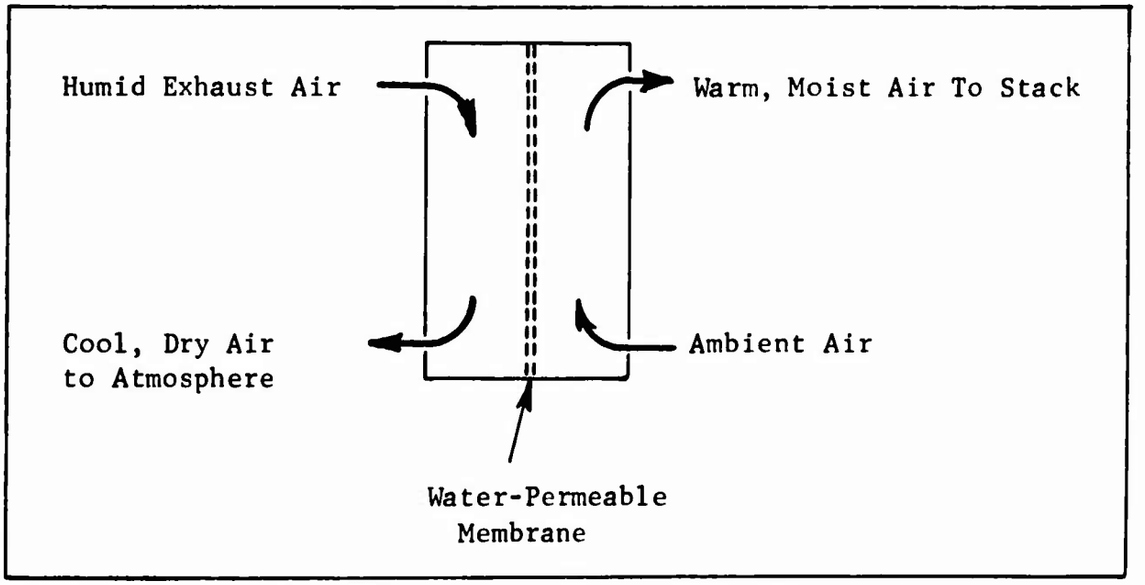

Two models of the water economy unit were evaluated. The model selected for use in the Battery Demonstrator was chosen on the basis of its lower pressure drop, less than 0.02 inches of water at 40,000 cc/min air flow rate. Although the rejected model gave higher water transfer rates, its pressure drop was excessive for this application. Performance data on these units is given in Appendix G-11. A drawing of the final unit is presented Appendix G-9.

In addition to the air condenser and the water economy unit, an electrolyte cooler was developed to provide additional means for dissipating stack heat. The cooler was constructed from tantalum tubing. Stainless steel extended surfaces were used to increase heat transfer rates. The unit was integrated with the air condenser, thus using a common blower to supply cooling air. Additional details are given in Appendices G-7 and G-9.

Part d - Methanol Addition System

Methanol concentration control represents a critical system in the Battery Demonstrator. Close control of the methanol concentration within relatively narrow limits is essential to the maintenance of both good performance and long life. The approach taken to provide this control was to develop a methanol analyzer employing a new detection concept (7). This technique, in essence, measures the current of a small electrode under conditions where methanol transport to this detecting electrode is limited by a membrane rather than by the catalyzed reaction. In this situation, the current is essentially independent of factors causing changes in catalyst activity or electrode performance.

An alternative approach was to develop a feed pump that would add programmed amounts of methanol to the circulating electrolyte, based on battery load. However, it was felt that the latter control scheme would lack flexibility, and that it would be difficult to construct a reliable, low power pump for delivering very low flow rates.

The methanol control system was evaluated in conjunction with the sixteen cell stack. Integration of these systems proved troublesome. The major problem areas that induced control instabilities were identified as system dead time and analyzer anode reliability. Response studies showed that minimum time lag was required between the methanol injection point and the detecting analyzer. Considerable effort was also directed toward developing a long-lived anode.

Successful operation was finally achieved and resulted in maximum methanol concentration limits of about $\pm$ 0.1 M about the desired control point of 0.75 M. The system appeared stable during load changes between 0 and 80 ma/cm^2. The power requirement to operate the feed valve was about 0.25 watts. Additional details of the methanol control system are presented in Appendix G-12.

Part e - Electronic Control Systems

Integration of the process subsystems described above is required for the operation of a self-sustained battery system. Therefore, compact electronic controls were developed to ensure a successful meshing of these systems. The process functions to be controlled included the electrolyte and air flow rates, and the methanol and water addition rates. In addition, a series-regulation circuit was devised to regulate the voltage output of the Battery Demonstrator at 6.0 $\pm$ 0.1 volts. Complete details of the control systems are given in Appendix G-13.

Phase 3 - Self-Contained Methanol Fuel Cell Battery Demonstrator

A self-contained Methanol Fuel Cell Battery Demonstrator was designed and constructed using the technology discussed in this and previous reports (1 through 7). This Demonstrator, while not meeting the standards of a prototype, will help to evaluate the problems inherent in the operation of a completely integrated methanol fuel cell system. As such, the unit must be considered a research tool. The Demonstrator was tested briefly prior to delivery to the U.S. Army Electronics Command in January, 1966.

Part a - Description of the Battery Demonstrator

The demonstrator, shown in Figure G-8, consists of a finished piece of hardware containing the essential elements for the self-sustained operation of the methanol fuel cell.

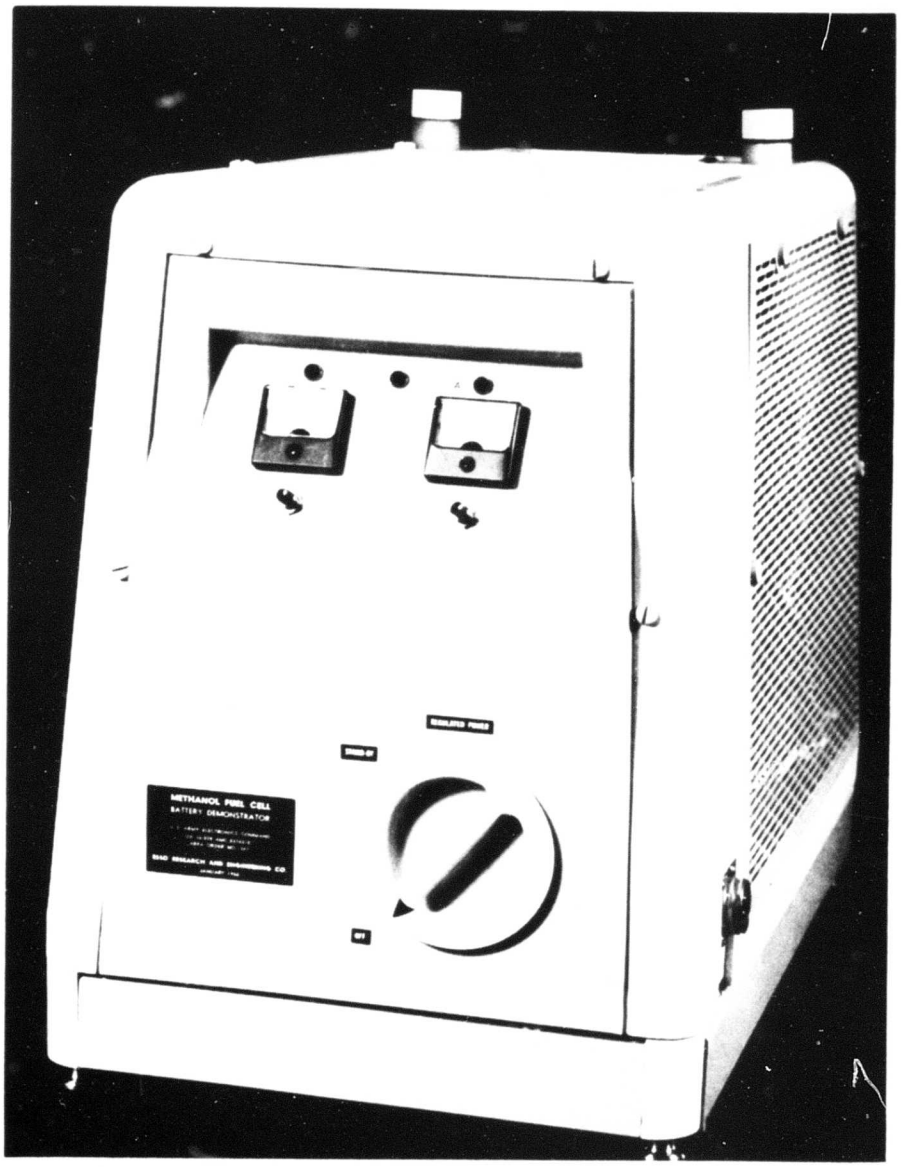

Included in the aluminum case are the stack assembly, methanol feed and water make-up tanks, an air blower, electrolyte circulation pump, a heat and water system, and the necessary controls. The interrelationships among these components are schematically shown in Figure G-9, and in greater detail in Appendix G-14.

In this system, methanol and water are added to the electrolyte that circulates through the stack assembly and the heat and water balance system. Air is also fed to and vented from the battery assembly through the heat and water recovery system. Provision is made for regulating the electrical output of the Demonstrator at 6.0 $\pm$ 0.1 volts.

Figure G-9

Simplified Schematic Flow
Plan of Complete Methanol Battery

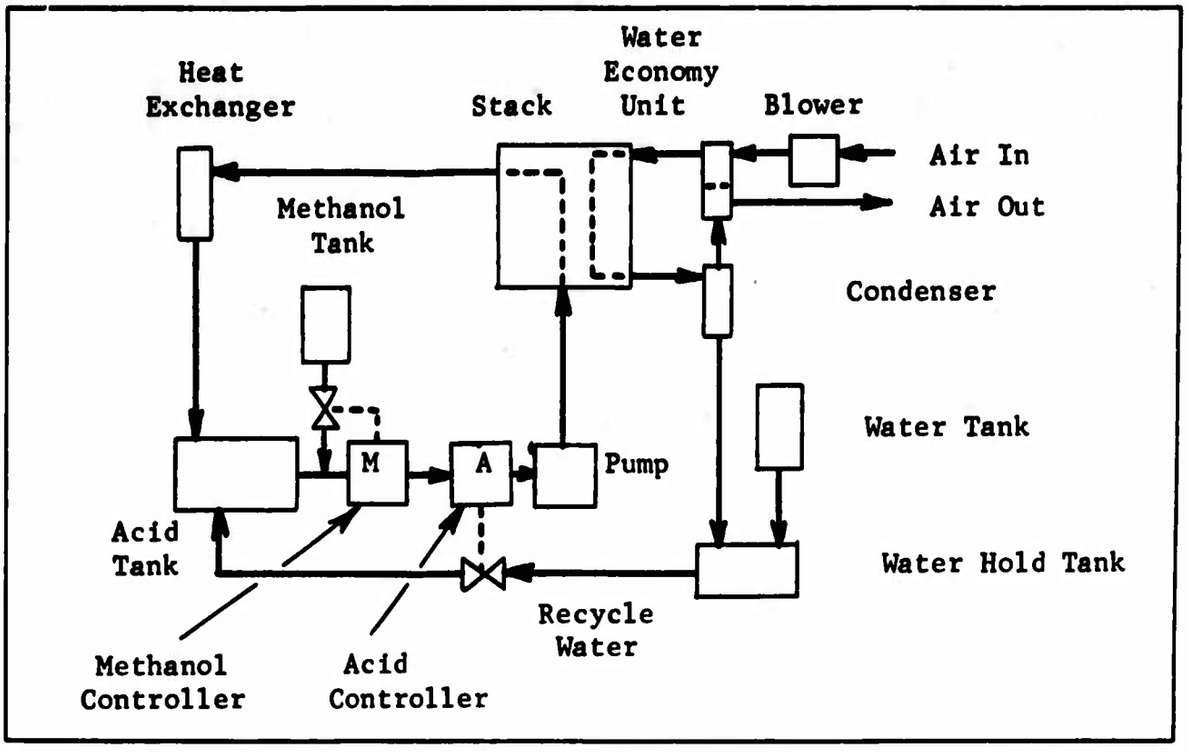

As delivered, the unit weighed 94 lbs and occupied 3.5 cu ft. No attempt was made to optimize the weight of the system components, or to assemble an overly compact device. Rather, in keeping with the research character of the Demonstrator and the timing requirements involved, the unit was designed to be accessible for inspection and maintenance. In addition, a Performance Monitor was provided to help diagnose the operation of the key Demonstrator subsystems. The Monitor is described in Appendix G-13.

Part b - Components of the Battery Demonstrator

A twenty cell stack containing 9" x 5-3/4" electrodes provided the main electrical power for the Demonstrator. Standard components and assembly procedures were used, as described in previous reports (6,7). Modifications included the use of redesigned air inlet and outlet manifolds to reduce pressure drop through the stack, and sturdier electrolyte outlet manifolds to reduce leakage. The modified components are shown in Appendix G-7, Figure G-8. The dual-entry feed manifold was also used, as described in Phase 2. Finally, several cells contained hydrogen reference electrodes and temperature-indicating thermistors to aid in performance evaluation.

Preliminary tests were conducted on the stack assembly itself to ascertain its performance. These tests were conducted using once-through electrolyte containing 0.75 M methanol, fed with a Mace diaphragm pump, and laboratory air. Initial average cell performance was slightly below that obtained in the best sixteen cell stack, as shown in Figure G-10. Thus, cell voltage at 40 ma/cm^2 was 0.41 volts compared with 0.46 volts for the smaller stack. Reactant distribution problems may account for the difference. Initial anode polarizations, in general, were higher for the twenty cell stack. Complete data are given in Appendix G-15.

Figure G-10

Comparison of Initial Performance in Multicell Stacks

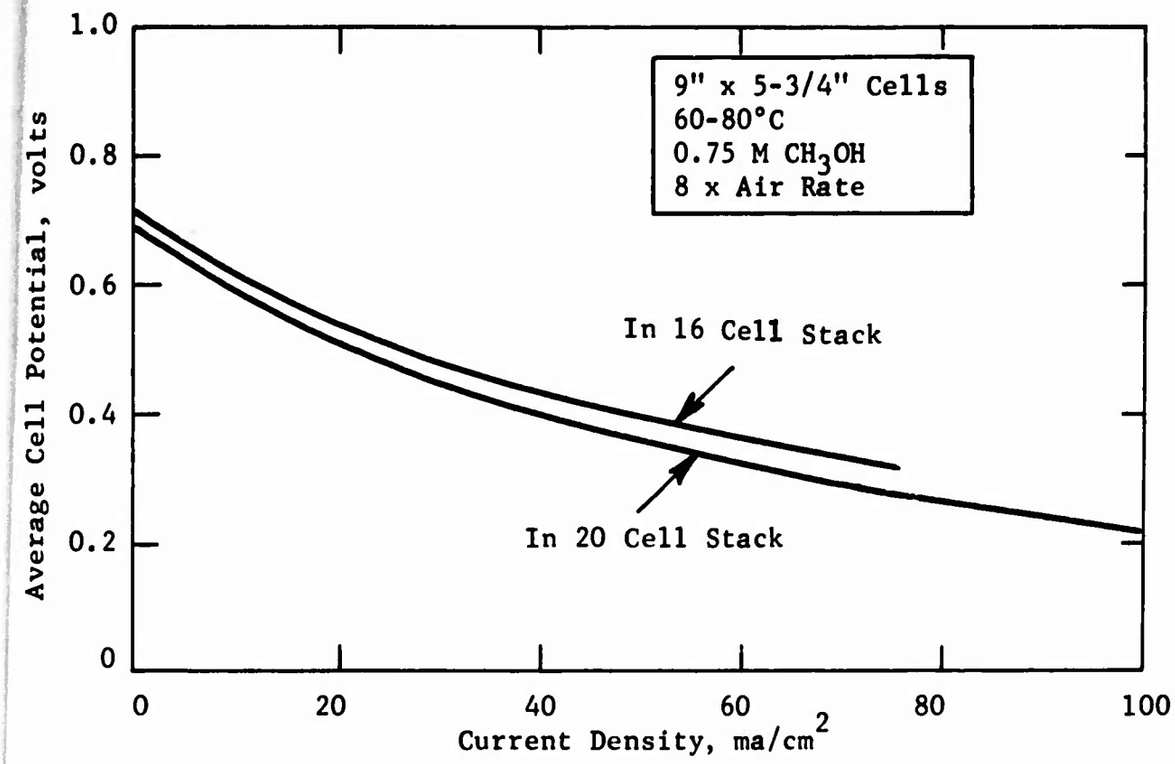

The design and construction of the auxiliary subsystems was discussed in Phase 2 of this Task. The units were connected together mainly with polypropylene tubing and fittings. Most of the electrolyte lines were treated with graphite mold-release powder to improve their wetting and flow characteristics.

Part c - Operation of the Battery Demonstrator

The Demonstrator was designed to be self-operating, requring minimum operational adjustments. A three-position master switch controls the Demonstrator. The positions are OFF, STAND-BY, and REGULATED POWER. In the STAND-BY position, power to operate the various subsystems is supplied by internally mounted mercury dry cells. During start-up conditions in STAND-BY, the fuel cell stack is activated for subsequent use. During shutdown, this switch position permits the electrolyte circulation system to displace carbon dioxide gas from the fuel cell stack. About two to three minutes are required for either function.

In the REGULATED POWER position, the Demonstrator is truly self-operating, with the fuel cell stack supplying all power, both for internal parasitic needs and for the external 6 volt regulated output circuit. Additional operating details are given in Appendix G-16. Use of the Performance Monitor as a diagnostic tool is also discussed.

Part d - Performance of the Battery Demonstrator

Construction of the Demonstrator was completed only recently and consequently few test results are available. Initial testing of the integrated assembly was performed with the electronic control panels mounted externally. Performance was good during these short-term tests. Regulated power outputs of up to 82 watts at 6.0 volts and 13.3 amps were obtained, as shown in Figure G-11. Corresponding stack performance was 99 watts at 7.0 volts and 14.1 amps. Additional data are given in Appendix G-17.

Figure G-11

Initial Performance of Integrated System

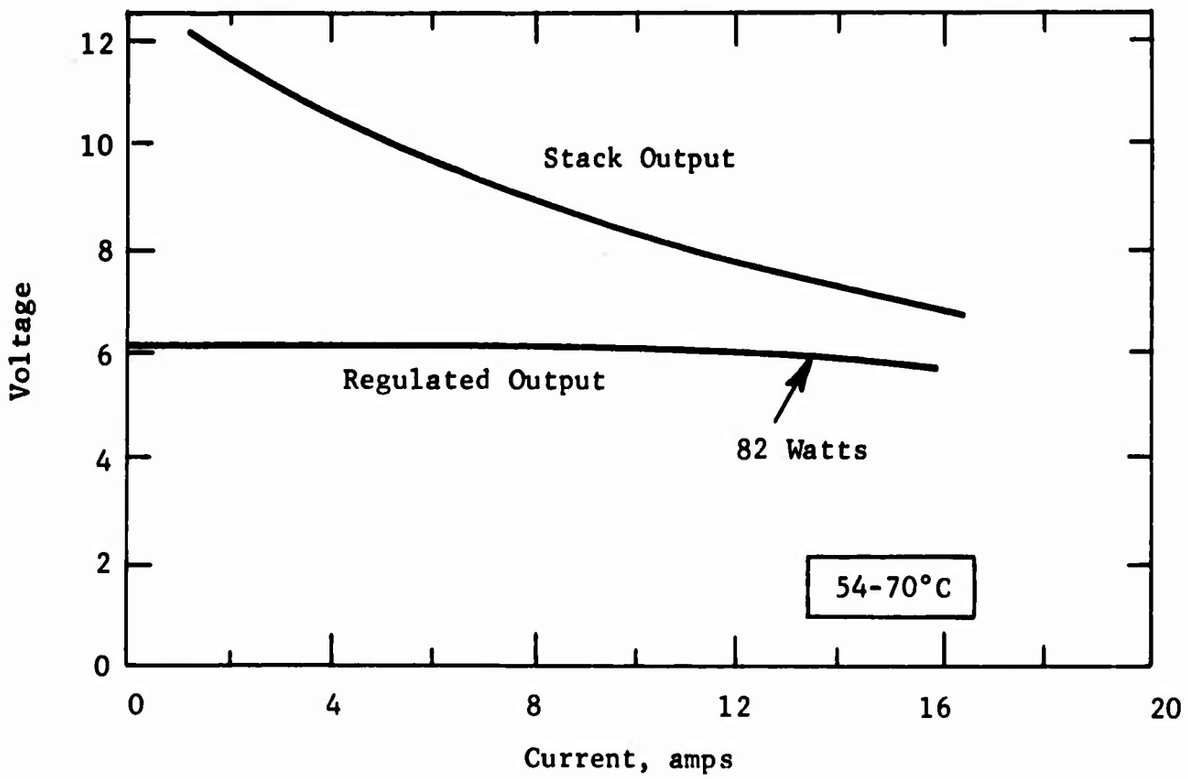

Cell voltage distribution data, taken at this time, showed that performance in several cells was much lower than average, as depicted in Figure G-12. Diagnostic tests did not clearly identify the cause of this poor performance, but faulty cathodes were suspected. During subsequent tests, cell 20 failed completely and was reconnected in parallel electrically with adjacent cell 19. Complete cell distribution data are given in Appendix G-18

Figure G-12

Distribution of Cell Voltages in Twenty Cell Stack

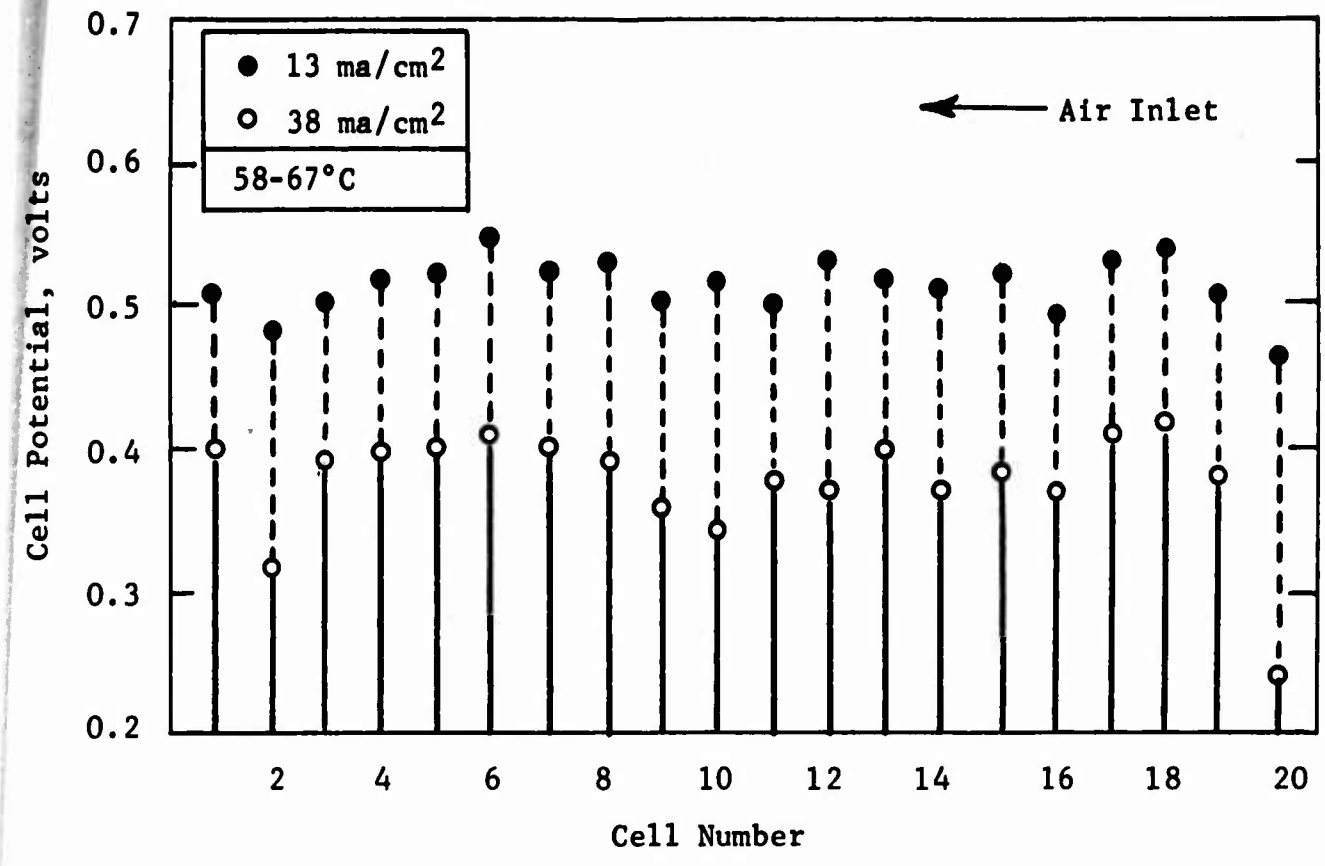

An estimate was made of the distribution of parasitic power losses in the Demonstrator. As shown in Table G-4, most of the losses were associated with the voltage regulation circuits.

Table G-4

Typical Distribution of Power Output

Stack Performance	99 watts(1)
Demonstrator Output	82 watts(2)
Power Losses	17 watts

System	Motor Losses, watts	Control Circuitry Losses, watts
Air Blower	0.23	0.25
Electrolyte Pump	0.40	0.40
Cooling Fan	1.10	0.16
Acid Concentration Control	0.25(3)	0.25(3)
Methanol Control	0.25(3)	0.25(3)
Current Shunts	--	1.80
Output Voltage Regulator	--	12.70
Total	2.23	15.81

(1) 7.0 volts at 14.1 amps.

(2) 6.0 volts at 13.1 amps.

(3) Intermittent Operation.

The completely integrated Battery Demonstrator was tested briefly prior to delivery to the U.S. Army Electronics Command. Performance levels had declined to a maximum regulated output of 65 watts at 6.0 volts, as shown in Figure G-13. This decline is attributed to successive imbalances in feed methanol concentration caused by an unstable methanol addition system. As a result, the fuel cell stack was frequently starved or subjected to excessive temperatures, depending on the level of methanol concentration. Further testing is required to uncover the source of this instability and to determine the ultimate effectiveness of the other Demonstrator subsystems.

Figure G-13

Performance of Assembled Battery Demonstrator

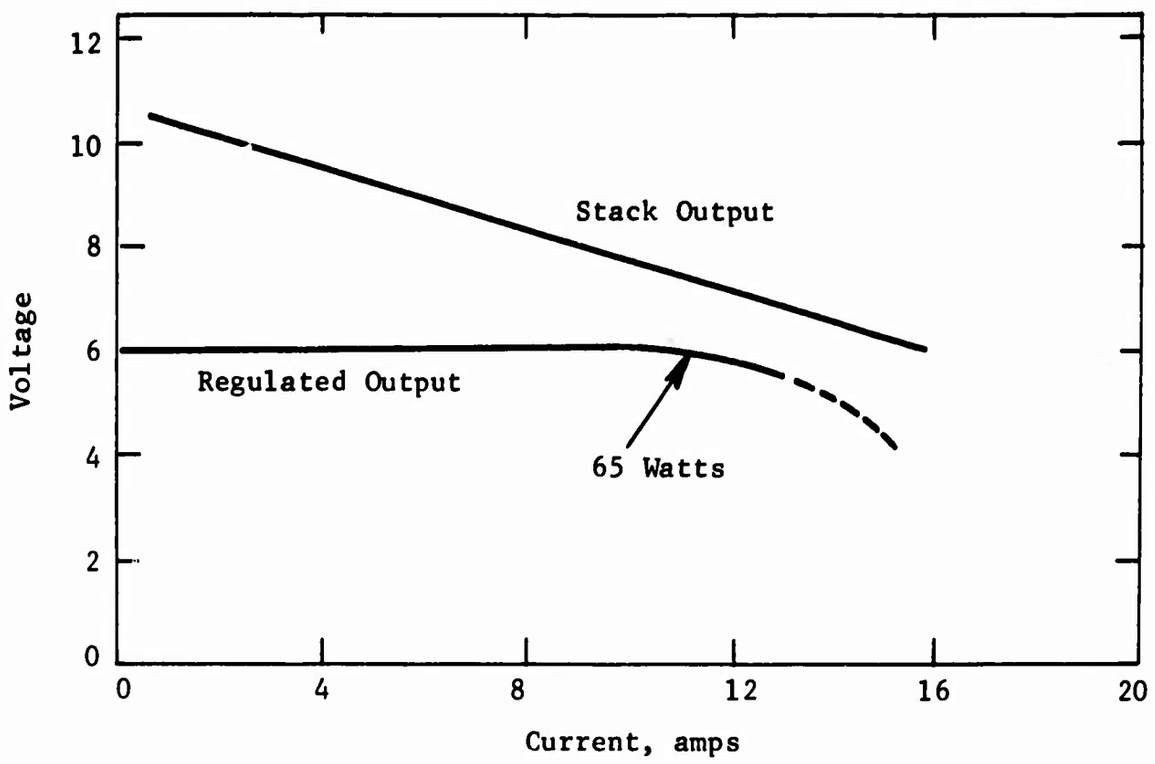

SECTION 5

CONCLUSIONS

5.1 Task A, Hydrocarbon Electrode

Phase 1 - Modification of Two Types of Platinum Sites

No profound changes in the nature of butane adsorption on platinum black due to variation in the concentration of lead acetate in the platinizing solution have yet been detected. The lead acetate concentration changed the platinum black surface area by a factor of four. The optimum was reached at 0.4 wt %. However, the shape of the hydrogen peaks did not vary significantly, contrary to a report in the literature. The total amount of butane adsorbed varied linearly with the platinum surface area. At this point it is not known whether the report in the literature is incorrect or whether it would take more detailed work to find the effect. However, since F. Will has shown that the ratio of the two types of hydrogen sites depends on the crystal plane exposed, it is still probable that this ratio could be varied by additives in the depositing solutions.

Phase 2 - Adsorption of Butane on Platinum Black in H_3PO_4 Solutions

As might be expected the adsorption of butane on platinum at 140° is more tenacious than at 80°C. A greater fraction of the sites available for hydrogen are occupied by the butane and its cathodic desorption is more difficult to effect. Decreasing the partial pressure of butane by diluting it with argon or by raising the electrolyte temperature and partial pressure, decreased the rate of butane accumulation, but this was probably a solubility effect. The equilibrium butane coverage was independent of partial pressure, indicating that the adsorption is substantially irreversible. Experimental difficulties have so far prevented adsorption rate measurements in hot phosphoric acid. The adsorption picture will be incomplete until these measurements are made.

Phase 3 - Increasing Platinum Utilization

The use of supports and co-supports for platinum has provided significant improvements in its specific activity and continues to look promising for the future. The impregnation of silica treated carbon by adsorption, followed by activation, has given specific current densities in ma/mg of platinum five times as high as platinum black. Raising the temperature from 150 to 190°C doubled the activity and emphasized the potentiality of higher temperature operation. Supported catalysts are known to resist sintering at high temperatures.

The structure of the carbon support has been shown to affect activity. It was possible to control the surface area of the carbon, the amount of platinum adsorbed, and the activity of the catalyst by adjusting the extent of "burnout" with carbon dioxide at 1000°C. Control of initial surface area via burnout of the carbon should be an important preparative tool in the future. Electron micrographs showed that adsorbed platinum on carbon ranged in particle size from 10 to 100 Å, the range being increased by silica treatment of the carbon. Further optimization of particle size distribution should be possible. B.E.T. and porosimetry measurements indicated that most of the carbon pore volume is in large (ca 1000 Å) pores whereas most of the pore surface is in small (~100 Å) pores. Improvements in catalyst location should therefore be possible.

The stability of the catalytic activity in the limiting current region is still a problem, which needs further work. The variability of the wetproofing afforded by different batches of Teflon emulsion also remains a continuing annoyance.

Phase 4 - Liquid Decane Electrodes

The activity of platinum-Teflon electrodes was confirmed to be extremely sensitive to the sintering variables: pressure, temperature, time and Teflon content. Complete optimization has not been possible due to the effort required for total cell fabrication. The fact that the rate of fuel transport through the electrode was independent of its activity is a promising result. It suggests that fuel transport may be reduced or eliminated without hurting activity. The sintering of a Teflon barrier directly to the electrode face represents an important improvement in electrode structural stability.

Phase 5 - Alloy Catalysts

The addition of annealing and quenching steps to the Raney alloy procedure has provided a means of preparing true alloys of high surface area. The finding that meta-stable alloys retain their chemical configuration even when a third component, aluminum is extracted is significant. Even though none of the alloys has shown electrochemical activity the method should be useful in future work.

Phases 6 and 7 - Perovskites and Oxide Bronzes

An explanation for the rapid loss of conductivity of the oxide deficient perovskites upon acid treatment essentially eliminated them from further consideration as acid fuel cell catalysts. The explanation assumed that the conductivity arose in a manner similar to that of lithiated nickel oxide, wherein part of the nickel becomes trivalent. Such higher valence ions are chemically unstable and are rapidly lost in acid. In line with this, perovskites containing manganese and chromium, whose higher valence ions are stable, had a better combination of acid resistance and conductivity than did the nickel and cobalt perovskites. However, the failure of these to show any catalytic activity effectively concluded the perovskite program.

The tungsten oxide bronzes, on the other hand, are very promising as catalyst bases. These have the perovskite lattice structure but rely on reduced valence states of tungsten for their conductivity. Samples that were easily prepared in an inert atmosphere showed excellent conductivity and acid resistance. Attempts to incorporate nickel into these have so far yielded complex materials of reduced, though still acceptable, conductivity and acid resistance. However, the area has just begun to be explored and many other metals remain to be incorporated into the oxide bronzes at varying stoichiometries.

Phase 8 - Eta Phase Carbides

Eta phase carbides such as Ni_3W_3C seem worthy of further examination as fuel cell catalysts. The results of an initial examination of an impure commercial sample was favorable in that it demonstrated the acid resistance of the nickel present in the eta phase. The conductivity of the transition metal carbides is well known. The need for controlled composition and stoichiometry, the failure of "quick and dirty" preparative methods, and the impurity of purchased commercial carbides, makes it imperative that an apparatus for custom preparation of these carbides be set up. The vacuum induction furnace should fill this need.

Phase 9 - Hydrocarbon Reforming in the Liquid Phase

Steam reforming catalysts were active when the reactants, water and hexane or decane, were present as liquids. The earlier failure of steam reforming catalysts to yield anode activity with liquid phase decane fuel, therefore, must be attributed, not to the presence of the liquid phase, but either to electrolyte dissolved in the water or to the low pressures used in the fuel cell anodes. The present finding provides an incentive determining the effect of electrolyte and pressure and re-examining the anodic activity of steam reforming catalysts under different conditions. It also may lead to a more efficient reformer-fuel cell combination.

5.2 Task B, Hydrocarbon Total Cell

Phase 1 - Studies in Hydrocarbon Fuel Cells

Studies in small scale single and multicell liquid decane-air fuel cell assemblies have shown that operation with fuel transport into the electrolyte space is feasible. However, decane transport to the cathode can impair performance and result in chemical oxidation. Tests with improved cathode structures indicate that significant reductions in cathode catalyst loading might be obtained if decane transport could be reduced or eliminated. The laminated 10 mg Pt/cm^2 Cyanamid AA-1 cathode gave the same initial performance as the 50 mg/cm^2 S.P.T.E. electrode. However, decane transport caused a marked reduction in cell output after 160 hours of testing. Decane transport was also responsible for the poor performance of a 2.5 mg/cm^2 sintered carbon Teflon electrode. Thus, only the laminated 50 mg/cm^2 porous Teflon film-sintered platinum Teflon electrode could operate for over 200 hours without excessive performance loss. Consequently, this anode system was selected for the final scaled-up five cell assembly. Operating experience with the small multicell unit pointed up a number of cell and system defects which were corrected in the final large scale design. These defects included inadequate electrolyte venting and barrier separation. Despite these problems performance levels with liquid decane were quite good, yielding 17 and 14 mw/cm^2 with oxygen and air respectively.

Phase 2 - Engineering Studies in the 4" x 4" Liquid Decane Multicell Assembly

A five cell direct liquid decane-air multicell assembly and operating system was constructed, capable of 6 watts with oxygen and 3.7 watts on air. Tests with this system indicate that except for previously discussed heat and water balance problems, there do not appear to be any engineering obstacles to the development of a high power density direct liquid hydrocarbon-air fuel cell battery. However, electrode components are quite sensitive and life is limited. Improved laminated anodes and cathodes have resulted in stack life of over 400 hours. However, significant performance losses have been noted. These can amount to up to 50% of the initial performance especially if cold shutdown are required.

Tests with wide boiling range commercial fuels (isoparaffins) indicate that operation with these materials is feasible, but performance is imparied due to increased fuel transport through the anode, which results in an increased cathode debit.

5.3 Task C, New Systems

Phase 1 - Catalyzed Carbon Electrodes in Pyrophosphoric Acid

Operation at higher temperatures as a means of increasing catalyst efficiency has been amply demonstrated with pyrophosphoric acid. Butane is considerably more active in this electrolyte at 275°C than in phosphoric acid at 150°C on carbon electrodes containing as little as 5 mg/cm^2 of platinum. With oxygen, the activity at the higher temperature on a catalyzed carbon is greater than that exhibited by a 150°C electrode having ten times the platinum loading. Electrodes of lower catalyst densities (2.5 mg/cm^2) have so far performed poorly, although one allowed a utilization of 50 ma/mg on butane. The problems at this low loading are due primarily to the difficulties involved in fabricating a suitable electrode structure, and should be surmountable.

Phase 2 - Molten Alkali Metal Bisulfate Electrolytes

The activities of butane and oxygen on massive platinum electrodes in molten potassium bisulfate at 275°C are considerably lower than that obtained in phosphoric at 150°C. Operation at 350°C in the bisulfate medium further reduces activity. Finally, butane exhibited no activity on catalyzed carbon, and oxygen activity was poor and erratic with these structures. The inherently lower activities obtained in the bisulfate melts and almost complete lack of activity in catalyzed carbons are attributed to the oxidizing properties of this electrolyte.

Although generally less corrosive than pyrophosphoric acid, bisulfate melts are not promising as intermediate temperature fuel cell electrolytes. It is concluded that molten salt fuel cell electrolytes must have anions which equilibrate with non-volatile and non-reducible oxides.

Phase 3 - Carbon Dioxide Absorption by Carbonate Electrolyte

Silver cathodes can match the activity of platinum catalysts if the electrolyte pH levels are not lower than twelve. A study of the absorption and desorption of carbon dioxide by carbonate solutions indicates that it is not feasible to maintain a carbonate solution above its equilibrium pH, even when one side is exposed to a carbon dioxide free air stream.

Phase 4 - Methanol Catalysts for Base or Buffer

Silver-palladium oxide catalyst shows considerable promise for use in basic and perhaps in buffer solutions. Limiting currents of over 2000 ma/cm^2 were observed with methanol in base and there was evidence of some activity with butane. Activity in CO_2 rejecting buffers remains to be demonstrated. Raney gold alloys also show sufficient activity in base to warrant further investigation.

Phase 5 - Slurry Catalyst Electrodes

The slurry electrode system responded quite well to increases in electrode surface area and to changes in electrolyte and fuel (liquid decane) flow pattern. Stirring power requirements were not prohibitive for this stage of development. However, the specific current density in ma/mg of catalyst was still so low that it is doubtful that catalyst utilizations better than that achieved in static systems could be obtained. The high current density per unit electrode area may make the slurry electrode suitable for catalyst testing.

5.4 Task D, Methanol Electrode

Phase 1 - Studies of Ruthenium Modified P-type Catalyst

Single cell and half cell testing of the ruthenium modified P-type catalyst has demonstrated its long-life capability. In half cell tests, the anodes lost only 15 mv after 11,000 hours of operation. In total cells, the anodes lost 20 to 40 mv during a day. However, performance may be regained by open-circuiting for brief periods. There is an additional slow deactivation of 10 to 50 mv occurring over a month's time. This is reversible by changing electrolyte and overpolarizing the anode to 0.8 to 9 volts in the absence of methanol. There appear to be no losses associated with storage. However, trace contaminants such as copper can reduce performance.

Phase 2 - Use of Supports for the Ruthenium Modified P-type Catalyst

The use of the silica-on-carbon and boron carbide as supports has not improved utilization of the ruthenium modified P-type catalyst. However, the initial results were susceptible to improvement through modification in the washing procedure. The best utilization achieved was 0.12 ma/mg at 0.35 volts polarization using potassium sulfate in the washing solution. Catalyst utilization using boron carbide as the support could be increased to 4.7 ma/mg when the hydrogen reduction was carried out at 225°C. Further increases in the severity of reduction may lead to increased utilization.

5.5 Task E, Air Electrode

Phases 1 and 2 - Teflon Coated Cathodes; Sodium Alginate Coated Electrodes

Interface maintaining cathodes, backed by a Teflon coating applied to the air side, can be operated for extended periods of time and scaled-up to practical sizes without loss of performance. However, further work is needed to minimize electrolyte leakage through the larger sized electrodes. Good performance is also possible using sodium alginate coatings instead of the membrane. However, a scale-up debit exists, and leakage of electrolyte is excessive, so that further work is also necessary for this structure.

Phase 3 - High Temperature Structures

Several types of electrodes have been developed that are suitable for use in a hydrocarbon cell operating at 150°C with 14.7 M phosphoric acid as the electrolyte. These include platinum-Teflon structures containing 50 and 10 mg/cm^2 of platinum and laminated to 3.7 mil porous Teflon films, and a carbon supported cathode containing 2.5 mg/cm^2 of platinum. In addition, cathodes using carbon and silica as the support can be made using only 1 mg/cm^2 of platinum. These have four times the catalyst utilization of the electrodes having higher catalyst loadings.

5.6 Task F, Methanol Fuel Cell

Phases 1 and 2 - Use of Cathode Diffusion Barriers for Reducing Direct Chemical Oxidation; Application to Large Cells

Chemical oxidation at the cathode can be reduced without loss in electrical performance by using interelectrode barriers, such as Dacron felt or Permaplex C-20 membranes. However, these reductions were only affected in the 4" x 4" cells. Improving fuel distribution by baffling or adding multiple injection ports to the 9" x 5-3/4" did not correct the loss in anode performance at low methanol concentrations.

Phase 3 - Simplified Low Power Methanol Fuel Cells

The feasibility of operating the methanol fuel cell with direct feed, without electrolyte circulation was demonstrated in a 3000 hour test.

5.7 Task G, Prototype Development

Phase 1 - Operating Characteristics of the Sixteen Cell Stack

The operation of the sixteen cell multicell unit confirmed the long-life characteristics of the methanol fuel cell found in previous studies. A moderate decline in performance was noted for the first 400 hours of operation, about 50 mv per cell at 40 ma/cm^2 during a seven month period. Subsequent testing, performed during the development of the methanol control system, produced severe imbalances in operation. This resulted in considerable performance loss, mainly at the anode. Use of a new dual-entry feed manifold eliminated the wide temperature distribution noted previously within multicell modules. A temperature range of only 11°C was noted at 40 ma/cm^2, compared with 29°C for the older, single entry manifold system. Fuel distribution was unaffected by the manifold change. Displacement of electrolyte within the sixteen cell stack, caused by the evolution of carbon dioxide, amounted 400 cc at 80 ma/cm^2, thus requiring the use of an external electrolyte reservoir during operation.

Phase 2 - Development of Auxiliary and Control Systems for the Methanol Fuel Cell Battery Demonstrator

Low power auxiliary components required for the self-sustained operation of the Methanol Fuel Cell Battery Demonstrator were designed, constructed and tested. A small, corrosion-free gear pump was integrated into the electrolyte circulation system. The pump performed well during several hundred hours of testing. An acid concentration control system was devised, using a temperature-compensated hydrometer float. The float position was used to control the addition of water to maintain about 3.7 M sulfuric acid concentration. Low pressure drop auxiliaries were devised to perform necessary heat and water balancing within the Demonstrator. An air condenser performed satisfactorily, reducing the temperature of a typical stack exhaust air stream by 23°C. Additional quantities of water were recovered by using a membrane water economy unit. However, pressure drop limitations required the use of a less effective model of the economy unit. An integrated methanol control system was developed, utilizing the diffusion-controlled analyzer. Stable operation was attained after considerable difficulty. Methanol concentration was controlled at 0.75 $\pm$ 0.1 M. The essential electronic controls were constructed for all systems of the Battery Demonstrator, including a series-regulation circuit for producing an output voltage of 6.0 $\pm$ 0.1 volts.

Phase 3 - Self-Contained Methanol Fuel
Cell Battery Demonstrator

The feasibility of operating the methanol fuel cell system was demonstrated by constructing and testing the first self-contained Methanol Fuel Cell Battery Demonstrator. The Demonstrator contained a 20 cell stack using 9" x 5-3/4" electrodes, together with the essential auxiliary components required for self-sustained operation. Although the Demonstrator was primarily a research tool, initial testing of the integrated system gave power outputs of up to 82 watts at a regulated 6.0 volts. Parasitic power losses were low, about 17 watts, mostly associated with the control system circuitry. Subsequent testing of the completed Demonstrator produced regulated-voltage power outputs of about 65 watts, but performance was not consistent due to instability of the methanol control system.

SECTION 6

PROGRAM FOR NEXT INTERVAL

Catalyst cost,or availability, remains the primary obstacle to the development of a practical direct hydrocarbon-air fuel cell. A considerable portion of our research effort has been devoted to this problem in the past and has led us into relatively complex realms of inorganic chemistry. However, a large effort was also devoted to the construction of batteries and demonstration units. This involved the solution of engineering problems which must at present be considered secondary to the main problem. In the future the size of the effort under this contract will be reduced and the engineering work will be almost completely eliminated. Essentially all the future work will be directed toward the solution of the catalysis problem. The goal will be activity with saturated hydrocarbons, but other fuels such as hydrogen, methanol and olefins will be examined to provide clues to the solution of the problem. There will be no further work on methanol catalysis as an end in itself. New catalysts will also be checked for cathode activity with oxygen and air. Since higher temperatures may help solve the catalysis problem, electrolytes permitting such temperatures will continue to be sought.

Thus, the percentage distribution of effort in the future will be quite different than it has been in the current period:

		Effort Expended, %	
			Projected
Task	Title	July-Dec, 1965	Jan-June, 1966
A	Hydrocarbon Electrode	39	80
B	Hydrocarbon Fuel Cell	8	2
C	New Systems	11	15
D	Methanol Electrode	4	0
E	Air Electrode	1	3
F	Methanol Fuel Cell	5	0
G	Prototype Development	32	0

The specific projects to be investigated are outlined below.

6.1 Task A, Hydrocarbon Electrode

Work on all phases of the hydrocarbon electrode will constitute the majority of the research effort in 1966. This will include noble metal catalyst improvements, electrode structure improvements, the search for non-noble catalysts and mechanism studies.

The mechanism studies will focus on variables affecting the chemisorption rates of saturated hydrocarbons on platinum. Attempts will be made to measure these rates in hot phosphoric acid, to determine whether liquid decane behaves in the same way as gaseous butane and to measure the effects of acid strength and buffer type on hydrocarbon adsorption. In addition, experiments will be run to modify the platinum surface to improve its adsorption rates or oxidation potentials.

Elucidation of the cause of lack of adsorption in at neutral pH values might shed clues on the nature of the adsorption processes which could lead to rate improvements. Any improvements obtained would be incorporated into the noble metal catalysis program.

To achieve further improvements in the utilization of noble metal catalysts more of the details involved in the use of supports will be investigated. Other co-supports will be looked at. Variations in the surface area, particle size, hydrophilicity, porosity, and ash and sulfur contents of the carbon supports will be studied. In particular, ozone treatment of the carbon to improve its pore structure and wetting properties will be tried. The catalyst impregnation and activation techniques will be altered. Attempts will be made to minimize catalyst sintering during activation while maintaining the benefits of the activation treatment. Alloying of the platinum will be studied to improve stability and to promote activity.

Electrode structure work will concentrate on the adaptation of carbon based electrodes to liquid fuels and the prevention of gas breakthrough through the anode. Layered and bonded structures with varying wetting properties, particle sizes or compositions will be constructed. Quality control and reproducibility problems relating to the electrode wetproofing technique will also be attacked. Electrode structures may be fabricated as required to suit the electrolyte program. Satisfactory electrodes will be checked for ease of scaling to larger sizes and for operating life.

The non-noble metal catalyst program will continue to be divided into the areas of alloys, oxides and carbides, with a small effort being devoted to steam reforming catalysts. The alloys to be prepared will be of high surface area prepared either by the Raney alloy technique or by chemical methods. The metals will be chosen from the first row transition elements, the group IB elements or the refractory metals of groups IV, V and VI B. Some of the heavier members of groups III to V A may be included. The metals will be blended as their phase diagrams permit. In addition to electrochemical measurements the alloys will be tested chemically, for hydrogenation and steam reforming activity, and physically, for their geometric and electronic structure. It is hoped in this way to convert practical results into a general picture which will be of more lasting value than a purely exploratory program.

The oxide program will be concerned with modified bronzes. Attempts will be made to obtain pure compounds containing silver, nickel, copper, and other metals felt to be able to provide catalytic activity. Tungsten is the favored component of the oxide structure, which provides the conductivity and acid resistance, but other elements such as tantalum will be considered on the basis of literature reports that they form bronzes. Some of the bronzes will contain alkali metals at the corners of the tungsten oxide octahedra, but many will be made with nothing but the catalytic metal in this position. The preparative technique will be varied as required for optimum purity of each preparation. Purity will be established principally by analysis of X-ray powder diagrams. Conductivity and acid stability measurements will also be made on each sample. Electrochemical evaluation will include several fuels, such as hydrogen, oxygen, unsaturated and saturated hydrocarbons and methanol. Potentiostatted corrosion tests will also be run under an inert atmosphere. Some of the catalysts will be tested for chemical reactivity as mentioned under the alloys program.

Transition metal carbides principally of the eta phase crystal structure will be prepared for the most part in a newly designed water cooled vacuum furnace. However, a quartz tube furnace and sealed tube lower temperature firings will also

be looked at. The carbides will contain first row transition elements combined with second and third row group IV to VI B refractory metals. Surface areas will be increased by grinding, although in some cases aluminum may be incorporated and leached out using the Raney method. The carbides will be analyzed primarily by the powder X-ray method. They will be evaluated for chemical and electrochemical corrosion. Conductivity should be no problem. Electrochemical testing will be similar to that of the alloys and bronzes.

Work on steam reforming catalysts will be aimed primarily at determining the causes of their failure to catalyze the oxidation of hydrocarbons even though they would react to produce hydrogen and would electrochemically consume hydrogen. Steam reforming reactions will be carried out in the liquid phase to determine whether electrolyte dissolved in the water was responsible for the catalyst failure. If so the particular electrolyte component at fault may be determined.

6.2 Task B, Hydrocarbon Fuel Cell

Emphasis will again be shifted away from total cell work to allow for increased efforts to improve cell components. Consequently, no total cell engineering work is planned during the next interval. However, some total cell tests may be conducted if warranted by improvements in cell components.

6.3 Task C, New Systems

Considerable further work will be done on new medium temperature electrolytes. The pyrophosphoric acid system is very promising. Consideration will be given to new electrode structures and cell materials for use with it. No further work will be done on the bisulfate system due to its numerous shortcomings. Other systems containing anions which equilibrate with oxides that are non-volatile and have no redox properties will be looked at intensively. Phosphates and phosphonates are prime candidates. In each case conductivity, stability, handling properties, redox activity and electrochemical activity on hydrogen, oxygen and hydrocarbons will be determined.

The promising palladium based catalysts will be examined further in basic and buffered electrolytes. The effects of temperature, pH and buffer composition will be explored with the present silver-palladium oxide catalyst using both methanol and hydrocarbons as fuels. Other palladium based compositions will also be examined with a view toward determining the optimum specific current density in ma/mg that can be achieved. Supported palladium compositions will also be examined.

The slurried catalyst system will no longer be examined as a practical electrode but may be used for catalyst evaluation in specific cases.

6.4-6.7 Tasks D, E, F and G

No further work will be done on methanol batteries or total cells under this contract. Methanol will be used where applicable as a test fuel for providing additional information on potential hydrocarbon catalysts. Similarly there will be no program devoted specifically to air electrodes, but new catalysts will be tested routinely for oxygen or air cathode activity.

BLANK PAGE

SECTION 7

IDENTIFICATION OF PERSONNEL AND DISTRIBUTION OF HOURS

7.1 Background of New Personnel

Carl E. Heath (Ph.D., Chemical Engineering, University of Wisconsin) has returned as Section Head responsible for all fuel cell research activities within Esso Research. For biography see Report No. 1 of this series, Section 7.1.

William J. Asher (M.S., Chemical Engineering, Ohio State University) joined Esso Research in 1958. Most of his experience with the company has involved the study of the engineering and physical chemistry aspects of new separation techniques to determine their technical feasibility and the development of some of these techniques. He has eight patents and patent applications in this area. Presently, he is working on a study to a non-noble metal catalyst for hydrocarbon electrodes.

Barret Broyde (Ph.D., Physical Chemistry, Polytechnic Institute of Brooklyn) has been with Esso Research since he completed two years of post-doctoral work in molten salt chemistry at New York University in February, 1962. His doctoral dissertation was on photochemistry and radiation chemistry in rigid matrices. At Esso he has investigated hydrocarbon-water interfacial phenomena and worked on the development of aviation lubricants. Presently, he is working on non-noble metal catalysts for hydrocarbon electrodes. He has three publications and one pending patent.

7.2 Distribution of Hours

The following are the technical personnel who have contributed to the work during the report period 1 July 1965 - 31 December 1965 and the approximate number of hours of work performed by each:

William J. Asher	779
Morton Beltzer	880
Barret Broyde	711
George Ciprios	996
James Colthart	304
William R. Epperly	517
I-Ming Feng	836
Carl E. Heath	133
Eugene L. Holt	341
Hugh H. Horowitz	747
Duane G. Levine	459
Martin Lieberman	824
John M. Matsen	696
Eugene H. Okrent	824
Joseph A. Shropshire	348
Barry L. Tarmy	754
Charles E. Thompson	136
Herbert H. Vickers	824
Elliot A. Vogelfanger	296
James A. Wilson	386
Abraham A. Zimmerman	848
Total	12,639

SECTION 8

REFERENCES

(1) Heath, C. E., Tarmy B. L., et al, Soluble Carbonaceous Fuel-Air Fuel Cell, Report No. 1, Contract DA 36-039 SC-89156, 1 Jan. 1962 - 30 June 1962.

(2) Tarmy, B. L., et al, Soluble Carbonaceous Fuel-Air Fuel Cell, Report No. 2, Contract DA 36-039 SC-89156, 1 Jan. 1962 - 31 Dec. 1962.

(3) Tarmy, B. L., et al, Soluble Carbonaceous Fuel-Air Fuel Cell, Report No. 3, Contract DA 36-039 AMC-00134(E), 1 Jan. 1963 - 30 June 1963.

(4) Tarmy, B. L., et al, Soluble Carbonaceous Fuel-Air Fuel Cell, Report No. 4, Contract DA 36-039 AMC-00134(E), 1 Jan. 1963 to 31 Dec. 1963.

(5) Heath, C. E., Holt, E. L., Horowitz, H. H., Levine, D. G., Tarmy, B. L., et al, Hydrocarbon-Air Fuel Cell, Report No. 5, Contract DA 36-039 AMC-03743(E), 1 Jan. 1964 - 30 June 1964.

(6) Heath, C. E., Holt, E. L., Horowitz, H. H., Levine, D. G., Tarmy, B. L., et al, Hydrocarbon-Air Fuel Cell, Report No. 6, Contract DA 36-039 AMC-03743(E), 1 July 1964 - 31 Dec. 1964

(7) Epperly, W. R., Holt, E. L., Horowitz, H. H., Levine, D. G., et al, Hydrocarbon-Air Fuel Cell, Report No. 7, Contract DA 36-039 AMC-03743(E), 1 Jan. 1965 - 30 June 1965.

(8) Franklin, T. C., and McClelland, D. H., J. Phys. Chem., 67, 2436 (1963).

(9) Will, F. G., J. Electrochem. Soc., 112, 451 (1965).

(10) Wagner and Grünewald, Zeit. Phys. Chem., B40, 455 (1938).

(11) Verwey Haayman and Romeyn, Chem. Weekblad, 44, 705 (1948).

(12) M. J. Sienko, Advances in Chemistry Series No. 39, Nonstoichiometric Compounds, 1963, page 225.

(13) H. R. Shanks, P. H. Sidles and G. C. Danielson ibid, page 237.

(14) G. Hägg, Zeit. Phys. Chemie., B29, 192 (1935).

(15) W. Jeitschko, et al, J. Less Common Metals, 7, 133 (1964).

(16) H. Nowotny, et al, Planseeberichte, 12, 31 (1960).

(17) K. Kuo, Acta Metallurgica, 1, 301 (1953).

(18) L. K. Borusevich, et al, Zh. Strukt. Khim., 6, 313 (1965).

(19) S. E. Rogers and A. R. Ubbelohde, Trans. Far. Soc., 46, 1051-1061, 1950.

(20) A. J. Arvia et al, Electrochimica Acta, 10, 33 (1965).

(21) L. G. Austin, Trans. Far. Soc., 60, 1319 (1964).

APPENDIX A-1

EFFECT OF VARIATIONS IN LEAD ACETATE CONCENTRATION DURING PLATINIZATION ON ADSORPTION PROPERTIES OF BLACK(1)

	Conc $Pb(Ac)_2$ wt %	Ads Time, min(2)	H· or ΔH· (mc)(3)	Mc Fuel	Mc Oxide	Mc Fuel / Mc Oxide	Mc H· / Mc Ox
A	0.0(4)	60	3.3	39.5	27.6	1.43	--
	0.04	Blank	3.1	--	8.17	--	0.38
B	"	60	--	5.41	8.12	0.67	--
	"	"	--	4.60	8.57	0.54	--
	0.2	Blank	5.68	--	14.99	--	0.38
C	"	60	2.81	21.04	13.29	1.585	--
	0.4	Blank	6.75	--	21.83	--	0.31
D	"	"	7.09	--	20.64	--	0.343
	"	60	4.91	24.95	18.12	1.38	--
	0.6	Blank	5.33	--	21.77	--	0.25
E	"	"	5.62	--	19.69	--	0.29
	"	60	(5.43)	19.48	21.19	0.92	--
	0.8	Blank	5.81	--	17.46	--	0.33
F	"	"	6.22	--	15.48	--	0.40
	"	60	3.82	17.79	14.46	1.23	--
	1.0	Blank	3.83	--	12.70	--	0.30
G	"	"	4.31	--	11.69	--	0.37
	"	60	2.20	11.08	9.14	1.21	--
H	0.4(4)	60	11.85	11.02	83.8	1.32	--

(1) Microelectrode 0.25 cm^2; 1 mg Pt/cm^2 deposited at 0.15 volts vs S.C.E., at 25°C, from a chloroplatinate solution containing 3 wt % Pt.

(2) Time for exposure to butane in 3.7 M H_2SO_4 at 95°C.

(3) For no fuel adsorption, value indicates millicoulombs in hydrogen peak. With fuel adsorbed, value indicates decrease in hydrogen peak relative to blank.

(4) Four mg/cm^2 plated instead of one.

APPENDIX A-2

STUDIES OF HYDROCARBON ADSORPTION ON PLATINUM BY VOLTAGE SCAN TECHNIQUES

Engelhard Pt Black

Fuel	Electrolyte	Temp, °C	Adsorption Time, min	Potential of Adsorption, volts vs S.C.E.	Potential of Equil After Adsorption volts vs S.C.E.	Mc Fuel / Mc Oxide	Remarks
Butane	14.7 M H_3PO_4	140	60	+0.05	Same as adsorption	1.63	First five duplicated from Report No. 7.
"	"	135	30	0.00	"	1.70	
"	"	135	180	0.00	"	1.66	
"	"	140	60	+0.05	"	1.76	
"	"	140	120	+0.05	"	1.80	
"	"	140	60	+0.05	"	1.71	
Butane	"	140	60	+0.05	"	1.60	Chronological sequence. Slight decay with time of operation.
"	"	140	60	+0.05	"	1.56	
"	"	140	60	+0.05	"	1.57	
Butane	14.7 M H_3PO_4	140	60	+0.05	+0.05	1.70	
"	"	140	60	+0.05	+0.02	1.51	
"	"	140	60	+0.05	0.0	0.98	
"	"	140	60	+0.05	-0.02	0.73	
"	"	140	60	+0.05	-0.02	0.70	Q_H/Q_o = 0.36 @ 140°C.
"	"	140	60	+0.05	-0.04	0.61	
"	"	140	60	+0.05	-0.04	0.67	
"	"	140	60	+0.05	-0.06	0.35	
"	"	140	60	+0.05	-0.08	0.29	
Butane	14.7 M H_3PO_4	100	60	+0.05	+0.05	1.91	
"	"	100	60	+0.05	0.0	1.73	
"	"	100	60	+0.05	-0.04	1.43	
"	"	100	60	+0.05	-0.08	0.41	
"	"	100	60	+0.05	-0.12	0.33	
Ethane	14.7 M H_3PO_4	140	60	+0.05	+0.05	0.63	
"	"	140	60	+0.05	+0.025	0.57	
"	"	140	60	+0.05	0.0	0.44	
"	"	140	60	+0.05	-0.025	0.41	
"	"	140	60	+0.05	-0.05	0.40	
"	"	140	60	+0.05	-0.075	0.33	
Propane	14.7 M H_3PO_4	140	60	+0.05	+0.05	0.61	
"	"	140	60	+0.05	+0.025	0.59	
"	"	140	60	+0.05	0.0	0.43	
"	"	140	60	+0.05	-0.025	0.35	Q_H/Q_o = 0.37 @ 140°C.
"	"	140	60	+0.05	-0.05	0.32	
"	"	140	60	+0.05	-0.075	0.28	
Argon	14.7 M H_3PO_4	80	--	-0.16 (1)	--	0.664 (2)	
"	"	100	--	-0.11	--	0.595	
"	"	110	--	-0.10	--	0.547	
"	"	120	--	-0.095	--	0.501	
"	"	130	--	-0.08	--	0.410	
"	"	140	--	-0.07	--	0.374	
"	"	150	--	-0.05	--	0.275	

(1) This and six following are potentials used as E_{H_2} for determining total Q_H/Q_o, on hydrocarbon free electrodes. Determined from bubble point or voltage where cathodic current vanishes.

(2) These and six following are $Q_H/Q_{o(1.3)}$ rather than Q_F/Q_o.

APPENDIX A-2 (CONT'D)

STUDIES OF HYDROCARBON ADSORPTION ON PLATINUM BY VOLTAGE SCAN TECHNIQUES

Fuel	Engelhard Electrolyte	Temp, °C	Adsorption Time, min	Potential of Adsorption, volts vs S.C.E.	Potential of Equil After Adsorption volts vs S.C.E.	Mc Fuel / Mc Oxide	Remarks
Butane	14.7 M H_3PO_4	150	60	+0.05	--	0.48	
"	"	150	120	+0.05	--	0.57	
"	"	150	60	+0.05	Same as adsorption	1.27	Same electrode consecutive set.
"	"	150	60	+0.05	"	1.24	
"	"	150	60	+0.05	"	1.24	
Butane	18 M H_3PO_4	120	60	+0.05	Same as adsorption	2.03	Q_o (relative area) decreases by factor of 2 during runs.
"	"	140	60	+0.05	"	1.96	
"	"	150	60	+0.05	"	1.99	
"	"	160	60	+0.05	"	1.69	
Butane	3.7 M H_2SO_4	80	60	0.0	Same as adsorption	1.63	
"	"	95	60	0.0	"	1.72	
"	"	100	60	0.0	"	1.65	
"	"	105	60	0.0	"	1.04	
							Relative Butane Concentration.
Butane	14.7 M H_3PO_4	140	60	+0.05	Same as adsorption	2.00(3)	1.00
"	"	140	60	+0.05	"	1.70	0.50
"	"	140	60	+0.05	"	1.45	0.19
"	"	140	60	+0.05	"	0.91	0.07
"	"	140	120	+0.05	"	2.04	1.0
"	"	140	120	+0.05	"	1.77	0.15
"	"	140	120	+0.05	"	1.31	0.04

Argon Diluted Butane

(3) This set of internally consistent, high values may be due to water loss and electrolyte concentration from long term sparging to equilibrium.

APPENDIX A-3

SUPPORTED PLATINUM CATALYSTS

Reference	Catalyst(1)	Carbon Surface Area, m^2/g	Pt Loading(2) mg/cm^2	Run Type(3)	Butane Performance, 14.7M H_3PO_4, 150°C — Polarization from Theory at Indicated ma/cm^2, Volts: 0	5	10	15	20	25	30	35	40	45	50	Pt Utiliz'n(4)	O_2 Performance: Polarization from Theory at Ind ma/cm^2, Volts: 0	50	100
3943-8	3.5% Pt on C	180	1.5	A	.165	.32	.375	.42	.485	Dead	--	--	--	--	--		.24	.35	.43
				B	.18	.295	.34	.38	.405	.435	Dead	--	--	--	--	15			
				C	.185	--	.335	.37	.39	.415	Dead	--	--	--	--				
3934-14	3.0% Pt on C - 5% SiO_2	"	1.2	A	.16	.28	.335	.37	.40	.41	.44	Dead	--	--	--		.23	.33	.39
				B	.15	.26	.30	.33	.35	.365	.39	.40	.435	Dead	--	32			
				C	.13	.24	.28	.305	.325	.345	.365	.38	.41	.42	Dead				
4311-41	" " " " "	"	"	B	.135	.27	.32	.36	.38	.415	Dead	--	--	--	--	25	.20	.35	.44
				C	.13	--	--	--	--	--	.405	Dead	--	--	--				
4311-46	" " " " "	"	"	B	.18	.28	.34	.37	.41	.43	Dead	--	--	--	--	20	.26	--	.48
				C	.16	--	--	--	--	.41	Dead	--	--	--	--				
3943-28	4.0% Pt on C - 15% SiO_2	"	1.7	A	.15	.28	.335	.37	.395	.415	.45	Dead	--	--	--		.24	.35	.43
				B	.14	.24	.29	.325	--	.37	.39	.42	Dead	--	--	23			
				C	.13	--	--	--	--	--	--	--	.405	.425	Dead				
3934-8	2.4% Pt on C - 33% SiO_2	"	1.0	B	.18	.35	.405	Dead	--	--	--	--	--	--	--	10	.24	.40	.50
				C	.17	--	.405	.45	Dead	--	--	--	--	--	--				
3943-31	3.6% Pt on 10% SiO_2 - C(5)	"	1.5	A	.16	.27	.34	.39	.42	Dead	--	--	--	--	--		.25	.35	.41
				B	.15	.28	.33	.37	.405	--	--	--	--	--	--	23			
				C	.14	--	--	--	--	.355	--	.405	.44	Dead	--				
4312-22	3.1% Pt on C - 8% SiO_2(6)	172	1.3	B	.18	.37	Dead	--	--	--	--	--	--	--	--	8	.26	.66	--
				C	.20	--	.395	Dead	--	--	--	--	--	--	--				
4312-24	" " " " " (6)	"	"	A	.175	.35	.42	Dead	--	--	--	--	--	--	--	7	.27	--	.40
				B	--	.36	.43	Dead	--	--	--	--	--	--	--				
4312-29	" " " " " (6)	"	"	A	.15	.36	.44	Dead	--	--	--	--	--	--	--		.26	--	.43
				B	.16	--	.385	--	Dead	--	--	--	--	--	--	10			
				C	.17	--	--	.41	Dead	--	--	--	--	--	--				
4631-9	" " " " " (6)	"	"	A	.18	.47	--	--	--	--	--	--	--	--	--	6	.26	.46	--
				B	.17	.37	.475	Dead	--	--	--	--	--	--	--				

(1) Reduction of Pt salt with carbon monoxide, followed by activation step.
(2) Sintered carbon - Teflon electrode prepared using Teflon 41 EX emulsion (7.5-15%)
(3) A. Butane Performance before oxygen treat
B. " " after " "
C. " " " overpolarization
(4) Highest specific current density, ma/mg, at 0.4 volts polarized.
(5) Pt salt adsorbed on SiO_2 before carbon added.
(6) Preparation apparently was contaminated with iron oxide during reduction step.

APPENDIX A-3 (CONT'D)

SUPPORTED PLATINUM CATALYSTS

Reference	Catalyst(1)	Carbon Surface Area, m^2/g	Pt Loading(2) mg/cm^2	Run Type(3)	Butane Performance, 14.7M H_3PO_4, 150°C — Polarization from Theory at Indicated ma/cm^2, Volts: 0	5	10	15	20	25	30	35	40	45	50	Pt Utiliz'n(4)	O_2 Performance: Polarization from Theory at Ind ma/cm^2, Volts: 0	50	100
3934-39	2.8% Pt on C - 10% SiO_2	180	1.17	A	.17	.285	.35	.38	.405	.425	.45	Dead	--	--	--		.21	.30	.36
				B	.17	.265	--	--	.33	.365	.38	.40	.42	.46	Dead	34			
				C	.13	--	--	--	--	--	--	--	.40	.425	.45				
3934-45	" " " " "	"	"	A	.195	.30	.345	.385	.405	.43	Dead	--	--	--	--		.23	.29	.35
				B	.14	.26	.305	.32	--	.36	.38	.40	Dead	--	--	38			
				C	.135	--	.29	--	.335	--	.35	--	.38	.40	Dead				
3934-50	" " " " "	"	"	A	.22	.32	.355	.40	.42	.425	Dead	--	--	--	--		.22	.29	.35
				B	.18	.285	--	.36	--	.39	.415	.45	Dead	--	--	30			
				C	.14	.28	.31	.345	.36	.375	.38	.40	.415	.44	Dead				
3943-39	3.9% " " " " (7)	110	1.6	A	.145	.29	.36	.415	.46	Dead	--	--	--	--	--		.24	.35	.42
				B	.115	.25	.30	.36	.40	Dead	--	--	--	--	--	19			
				C	.09	--	--	--	--	.39	.405	Dead	--	--	--				
3943-42	3.8% " " " " (8)	"	"	A	.115	.305	.375	.42	.47	Dead	--	--	--	--	--		.27	.42	.49
				B	.12	.255	.30	.34	--	.425	Dead	--	--	--	--	14			
4311-12	1.0% " " " " (9)	"	0.4	A	.16	.395	Dead	--	--	--	--	--	--	--	--		.24	.42	.50
				B	.15	.355	.42	Dead	--	--	--	--	--	--	--	23			
4311-14	1.5% " " " " (10)	"	0.6	A	.185	.345	.41	Dead	--	--	--	--	--	--	--		.23	.37	.43
				B	.17	.314	.385	Dead	--	--	--	--	--	--	--	23			
				C	--	--	--	.41	Dead	--	--	--	--	--	--				
4311-31	1.9% " " " "	"	0.8	A	.21	.36	.405	Dead	--	--	--	--	--	--	--		.23	.38	.45
				B	.155	.36	.41	Dead	--	--	--	--	--	--	--	18			
				C	.135	--	--	.41	Dead	--	--	--	--	--	--				
4311-33	" " " " "	"	"	A	.205	.35	Dead	--	--	--	--	--	--	--	--		.27	.43	.57
				C	.15	--	--	.35	.40	Dead	--	--	--	--	--	25			
				B	.14	.27	.33	.38	.44	Dead	--	--	--	--	--				
4311-36	" " " " "	"	"	A	.15	.305	.36	Dead	--	--	--	--	--	--	--		.29	.44	.52
				B	.12	--	.315	.35	Dead	--	--	--	--	--	--	28			
				C	.08	--	--	--	.345	Dead	--	--	--	--	--				

(1) Reduction of Pt salt with carbon monoxide, followed by activation step.
(2) Sintered carbon - Teflon electrode prepared using Teflon 41 BX emulsion (7.5-15%)
(3) A. Butane Performance before oxygen treat
B. " " after " "
C. " " " overpolarization
(4) Highest specific current density, ma/mg, at 0.4 volts polarized.

(7) Prep contained 2X usual amt of Pt salt.
(8) " " 4X " " " " "
(9) " " ½ of usual amt of Pt salt.
(10) " " ½ " " " " " "

APPENDIX A-3 (CONT'D)

SUPPORTED PLATINUM CATALYSTS

Reference	Catalyst[1]	Carbon Surface Area, m^2/g	Pt Loading[2] mg/cm^2	Run Type[3]	Butane Performance, 14.7 M H_3PO_4, 150°C — Polarization from Theory at Indicated ma/cm^2, volts											Pt Utilization[4]	O_2 Performance: Polarization from Theory at Ind. ma/cm^2, volts		
					0	5	10	15	20	25	30	35	40	45	50		0	50	100
4312-36	2.8% Pt on C-10% SiO_2	192	1.17	A	.155	.34	.39	.43	.465	Dead	--	--	--	--	--		.22	---	.40
				B	.16	.30	.35	.39	.41	.425	Dead	--	--	--	--	34			
				C	.135	--	--	--	--	--	--	--	.40	.42	Dead				
4213-39	" " " "	"	"	A	.165	.30	.36	.40	.42	.46	Dead	--	--	--	--		.23	---	.40
				B	.16	--	.31	--	.355	--	.405	.435	Dead	--	--	30			
				C	.16	--	--	--	--	--	--	--	.44	Dead	--				
4565-25	" " " "	"	"	A	.15	.28	.33	.36	.385	.405	Dead	--	--	--	--		.24	---	.43
				B	.15	.28	.325	.36	.40	.42	Dead	--	--	--	--	25			
				C	.14	--	--	--	--	--	.41	Dead	--	--	--				
4565-26	" " " "	"	"	B	.145	.285	.32	.36	.39	.41	.43	Dead	--	--	--	28	.245	---	.40
				C	.13	--	--	--	--	--	--	.42	Dead	--	--				
4565-13	2.9% " " "	"	1.2	A	.17	.315	.365	.37	.42	.42	.46	Dead	--	--	--		.24	---	.38
				B	.165	.26	--	.32	--	.36	--	.40	.415	--	--	33			
				C	.145	--	--	--	--	--	--	.38	.40	Dead	--				
4565-16	" " " "	"	"	A	.155	.29	.35	.375	.40	.42	Dead	--	--	--	--		.25	---	.55
				C	.13	--	--	--	--	--	.435	.45	Dead	--	--	20			
				B	.145	.26	--	.355	.39	.43	Dead	--	--	--	--				
4565-43	" " " "	"	0.6	A	.185	.37	.42	Dead	--	--	--	--	--	--	--		.24	.36	.44
				B	.17	.365	.37	.405	Dead	--	--	--	--	--	--	33			
				C	.155	--	--	--	.405	.43	Dead	--	--	--	--				
4630-24	" " " "	"	1.2	A	.14	.29	.34	.36	.39	.43	Dead	--	--	--	--		.26	---	.39
				B	.14	.275	.32	.345	--	.38	.405	Dead	--	--	--	33			
				C	.135	--	--	--	--	--	--	.385	.41	.41	Dead				
4630-47	" " " "	"	"	A	.18	.31	.37	.39	.42	.45	Dead	--	--	--	--		.24	.34	.44
				B	.145	.27	--	.355	--	.405	.42	Dead	--	--	--	25			
				C	.13	--	--	--	--	--	.405	Dead	--	--	--				
4631-5	" " " "	"	"	B	.13	.26	--	.35	.39	Dead	--	--	--	--	--	17	.26	.39	.49
				C	.12	--	--	--	.41	.44	Dead	--	--	--	--				
4311-18	1.75% Pt on C-10% Cab-O-Sil	110	0.7	A	.19	.36	.40	Dead	--	--	--	--	--	--	--	15	.24	.39	.47
				B	.19	.33	.39	Dead	--	--	--	--	--	--	--				
4312-23	3.1% " " "	180	1.3	A	.19	.38	.44	Dead	--	--	--	--	--	--	--		.22	.34	.42
				B	.19	.33	.38	.43	Dead	--	--	--	--	--	--	14			
				C	.15	--	--	--	.42	Dead	--	--	--	--	--				
4631-12	" " " "	"	"	A	.16	.315	.375	.41	Dead	--	--	--	--	--	--		.26	.39	.45
				B	.15	.28	.34	.38	.45	Dead	--	--	--	--	--	18			
				C	.145	--	--	--	--	.42	Dead	--	--	--	--				

(1) Reduction of Pt salt with carbon monoxide, followed by activation step.
(2) Sintered Carbon-Teflon electrode prepared using Teflon 41 BX emulsion (7.5-15%).
(3) A. Butane performance before oxygen treat.
B. " " after oxygen treat.
C. " " " overpolarization.
(4) Highest specific current density, ma/mg, at 0.4 volts polarized.

APPENDIX A-3 (CONT'D)

SUPPORTED PLATINUM CATALYSTS

Reference	Catalyst[1]	Carbon Surface Area, m^2/g	Pt Loading[2] mg/cm^2	Run Type[3]	Butane Performance, 14.7 M H_3PO_4, 150°C — Polarization from Theory at Indicated ma/cm^2, volts											Pt Utilization[4]	O_2 Performance: Polarization from Theory at Ind. ma/cm^2, volts		
					0	5	10	15	20	25	30	35	40	45	50		0	50	100
4630-4	2.5% Pt on C-10% Cab-O-Sil	192	1.0	A	.17	.32	.38	.41	.45	Dead	--	--	--	--	--		.24	.34	.41
				B	.17	.30	.35	.38	.41	Dead	--	--	--	--	--	23			
				C	--	--	--	--	--	.42	Dead	--	--	--	--				
4630-9	2.6% Pt on C-10% Alumino-silicate	"	1.1	A	.10	.28	.36	.41	Dead	--	--	--	--	--	--		.28	.41	.49
				B	.16	.26	.31	.34	.37	.40	Dead	--	--	--	--	27			
				C	.15	--	--	--	--	--	.40	Dead	--	--	--				
4565-47	" " " "	"	"	A	.17	.30	.38	.415	Dead	--	--	--	--	--	--		.22	.40	.71
				B	.165	.315	.37	.41	Dead	--	--	--	--	--	--	14			
				C	--	--	--	--	.445	Dead	--	--	--	--	--				
3943-45	4.3% Pt on C-10% Ca SiO_3	110	1.8	A	.15	.29	.35	.395	.42	.47	Dead	--	--	--	--		.29	.56	.80
				B	.11	.24	.295	.34	--	.435	Dead	--	--	--	--	13			
				C	.10	--	--	--	--	--	.47	Dead	--	--	--				
3934-10	2.7% Pt on C-10% Acid-Treated Vermiculite	180	1.1	A	.18	.37	.42	Dead	--	--	--	--	--	--	--		.26	.35	.42
				B	.19	.32	.37	.41	.435	Dead	--	--	--	--	--	15			
				C	.17	.33	.365	.39	.415	Dead	--	--	--	--	--				
4630-16	1.7% Pt on C-20% Tungsten Bronze	192	0.7	B	.15	Dead	--	--	--	--	--	--	--	--	--	10	.28	.56	---
				C	--	.365	Dead	--	--	--	--	--	--	--	--				
3934-24	~2.5% Pt-1Ir on C-5% SiO_2	180	~1.0	A	.19	.28	.33	.37	.40	.395	Dead	--	--	--	--		.24	.34	.41
				B	.19	.28	.32	.36	.39	.42	Dead	--	--	--	--	~25			
				C	.17	--	--	--	--	--	.42	.44	Dead	--	--				
4631-13	" " " "	"	"	A	.15	.305	.375	.47	Dead	--	--	--	--	--	--		.23	.43	.66
				B	.13	.28	.35	.45	Dead	--	--	--	--	--	--	~13			
3934-27	~3% Pt-10 Ru on C-5% SiO_2	"	~1.2	A	.165	.29	.385	Dead	--	--	--	--	--	--	--		.24	.38	.44
				B	.15	.25	.335	(.42)	Dead	--	--	--	--	--	--	~10			
3934-29	~3% Pt-10 Rh on C-5% SiO_2	"	"	A	.17	.29	.395	Dead	--	--	--	--	--	--	--		.24	.37	.42
				B	.12	.275	.34	Dead	--	--	--	--	--	--	--	~15			
				C	.11	--	--	.36	Dead	--	--	--	--	--	--				
3943-35	4.9% Colloidal Pt on C-10% SiO_2	"	2.0	A	.165	.29	.35	.39	.405	.43	.45	.47	Dead	--	--		.25	.32	.37
				B	.15	.26	.30	.325	--	.37	.40	Dead	--	--	--	20			
				C	.12	--	--	--	--	--	--	--	.41	.42	Dead				

(1) Reduction of Pt salt with carbon monoxide, followed by activation step.
(2) Sintered Carbon-Teflon electrode prepared using Teflon 41 BX emulsion (7.5-15%).
(3) A. Butane performance before oxygen treat.
B. " " after oxygen treat.
C. " " " overpolarization.
(4) Highest specific current density, ma/mg, at 0.4 volts polarized.

APPENDIX A-3 (CONT'D)

SUPPORTED PLATINUM CATALYSTS

Reference	Catalyst[1]	Carbon Surface Area, m^2/g	Pt Loading[2] mg/cm^2	Run Type[3]	Butane Performance, 14.7 M H_3PO_4, 150°C — Polarization from Theory at Indicated ma/cm^2, volts											Pt Utilization[4]	O_2 Performance: Polarization from Theory at Ind. ma/cm^2, volts		
					0	5	10	15	20	25	30	35	40	45	50		0	50	100
4312-8	4.9% Colloidal Pt on C-10% SiO_2	180	2.0	A	.19	.335	.385	.42	.455	Dead	--	--	--	--	--		.24	---	.38
				B	.155	.295	.34	--	.395	.43	.45	Dead	--	--	--	18			
				C	.15	--	.31	--	.34	--	--	.40	Dead	--	--				
4630-21	~5% " " "	192	~2.1	A	.14	.31	.37	.40	.41	Dead	--	--	--	--	--		.26	.37	.42
				B	.12	.255	.305	.34	.37	.42	Dead	--	--	--	--	~13			
				C	.12	--	--	--	--	.39	Dead	--	--	--	--				
4630-31	" " " "	"	"	A	.13	.30	.34	.365	.39	.41	Dead	--	--	--	--		26	.33	.40
				B	.14	.26	--	.32	--	.35	--	.40	Dead	--	--	~20			
				C	.13	--	--	--	--	--	--	--	.385	Dead	--				
4312-15	3.2% Colloidal Pt on C	110	1.3	B	.22	.35	.39	.45	Dead	--	--	--	--	--	--		.24	.37	.40
				C	.19	--	--	--	.425	Dead	--	--	--	--	--	11			
4312-26	~3% Colloidal Pt on C-10% SiO_2	"	~1.2	A	.20	.43	.49	Dead	--	--	--	--	--	--	--		.23	.44	.62
				B	.17	.385	.42	Dead	--	--	--	--	--	--	--	8			
				C	.15	--	--	Dead	--	--	--	--	--	--	--				
4630-19	6.1% Colloidal Pt on Tungsten Bronze	--	2.5	A	.21	Dead	--	--	--	--	--	--	--	--	--		.30 (.55 @ 10 ma/cm^2)		
				B	.18	Dead	--	--	--	--	--	--	--	--	--	~1			
3943-10	2.8% Pt on C-10% SiO_2[11]	180	1.2	A	.10	.33	.40	.45	Dead	--	--	--	--	--	--	8			

(1) Reduction of Pt salt with carbon monoxide, followed by activation step.
(2) Sintered Carbon-Teflon electrode prepared using Teflon 41 BX emulsion (7.5-15%).
(3) A. Butane performance before oxygen treat.
B. " " after oxygen treat.
C. " " " overpolarization.
(4) Highest specific current density, ma/mg, at 0.4 volts polarized.
(11) Run on decane fuel, porous Teflon barrier.

APPENDIX A-4

SURFACE AREA AND PORE VOLUME DISTRIBUTIONS OF PLATINIZED CARBONS

In view of the correlation found between carbon surface area and activity of platinum catalysts (Phase 3, Part d), it was of interest to ascertain the effect of platinum and of the SiO_2 co-support on the surface areas of the final catalysts. Therefore, surface areas were determined (B.E.T. method) for a series of supported platinum catalysts, using the same carbon support throughout.

The results indicated that introduction of platinum by adsorption of a salt had practically no effect on surface area while adsorption of colloidal Pt resulted in about a 15% area reduction. This area decrease is probably related to blocking of pores by the relatively large particles of the colloidal Pt (100-300 Å).

Inclusion of 10% silica (as silicic acid gel) gives about a 25% increase in surface area. Assuming that the surface areas are additive, the silica contributes about 600 m^2/g, which is a typical value for a high-area silica gel. See Table A-1.

Table A-1

Relation of Catalyst Surface Areas to Support and Catalyst Type

Material	Surface Area, m^2/g
Carbon	179
3% Adsorbed Pt on C	176
3% Adsorbed Pt on C - 10% SiO_2	214
5% Colloidal Pt on C	152
5% Colloidal Pt on C - 10% SiO_2	202

It is conceivable that the beneficial effect of silica is related to this surface area increase. Other possible benefits are discussed in Phase 3, Part f.

Pore size distribution data was obtained on several carbon supports by the mercury porosimeter method. The pore distribution for three of these supports is shown in Figure A-1. The ordinate is the derivative, dA/d log D, obtained by graphically determining the slope of a plot of cumulative surface area, A, versus the logarithm of the pore diameter, D.

Figure A-1

Pore Volume Distribution of Carbon Supports

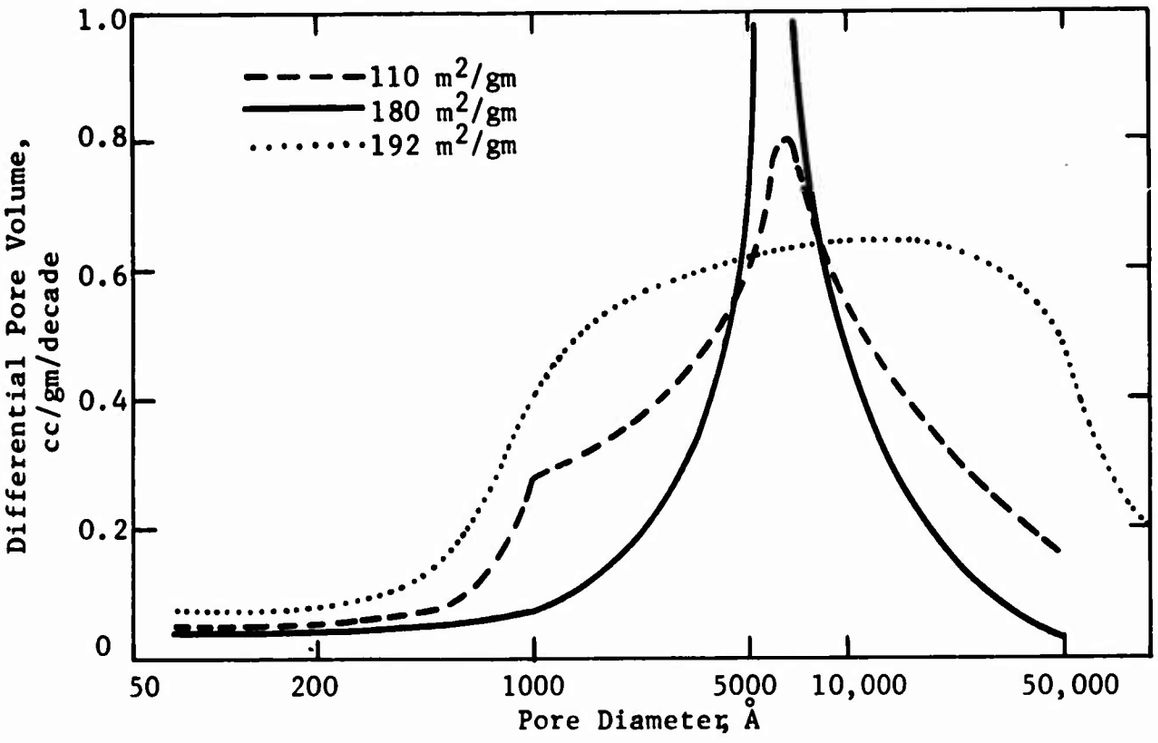

The pore distribution curves differ considerably in the region of > 500 Å diameter pores, despite the fact that these carbons have been similarly prepared. Thus, the carbons of 110 and 180 m^2/g surface area consisted of different batches of FC-30 carbon that had been treated with CO_2 for seven hours at 1000°C. The carbon with a surface area of 192 m^2/g was obtained by retreatment of the 110 m^2/g carbon with CO_2 for five hours.

Unlike the results with bulk Pt, performance of catalysts prepared with these carbons did not correlate with increasing pore volume.

In view of the correlation of performance with increasing carbon surface area, it was of interest to ascertain the surface area distribution of the carbon. This data is shown in Figure A-2 as calculated from the equation,

$$\frac{dA}{d \log D} = \frac{4}{D} \frac{dV}{d \log D}$$

where A is the cumulative surface area, cm^2/gm
D is the pore diameter, cm, and
V is the cumulative pore volume cm^3/gm.

Figure A-2

Surface Area Distribution of Carbon Supports

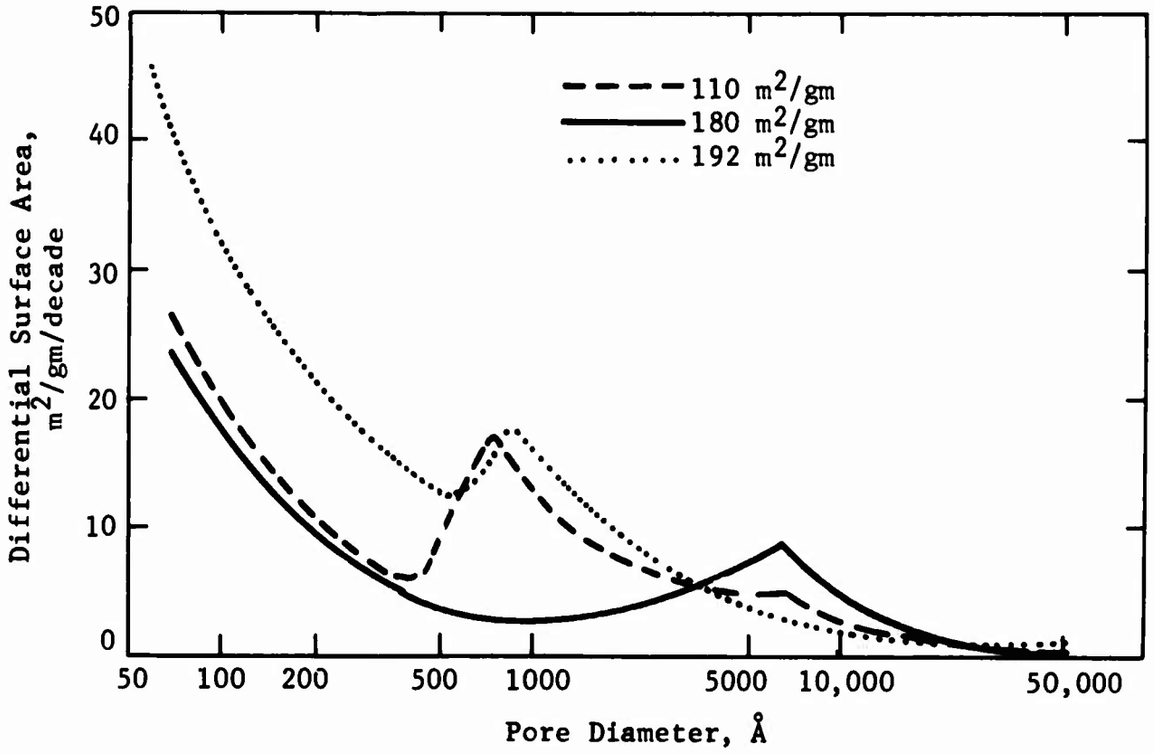

It can be seen that only about 10% of the surface area is located in the pores of >200 Å diameter. Furthermore, there is no correlation of surface area variations with performance variations in this macropore region. Accordingly the most active surface lies in the micropore region (< 200 Å diameter). Transport limitations would appear to rule out activity in very small pores. By suitable selection and treatment of carbon supports or by blocking of the smallest pores, it may be possible to favor Pt adsorption in the desired pore region, as a route to higher activities.

APPENDIX A-5

LIQUID DECANE PERFORMANCE - SINTERED PLATINUM TEFLON STRUCTURES

Electrolyte: 14.7 MH_3PO_4 - 150°C

Reference No.	Fabrication Conditions: Sintering Temp., °C	Fabrication Conditions: Pressure	Barrier Description	TFE Batch No.	Polarization from Decane Theory at Indicated ma/cm², volts: 0	1	10	20	40	60	80	100	125	150	200	300	Fuel Transport Rate, cm³/min	Thickness, Mils	Pt Lot No.	Remarks
Electrode Composition: 85 wt. % Platinum, 15 wt. % Teflon, 50 mg/cm²																				
3444-44-1	620	1100-1 min	Standard 9μ Porous TFE	4002 6/15/65	0.10	0.19	0.33	0.38	0.45	0.50	--	--	--	--	--	--	0.17	8	10,004	
3444-44-2	640	1100-1 min	"	"	0.09	0.16	0.32	0.38	0.50	0.56	0.62	Dead					0.16	8.5	"	
3444-44-3	650	1100-1 min		"	0.09	0.17	0.26	0.39	0.50	0.56	0.60	0.62	--	--	--	--	0.13	9.0	"	
3444-44-4	660	1100-1 min	"	"	0.08	0.12	0.29	0.37	0.42	0.45	0.52	0.54	0.53	0.60	0.61	--	0.138	8.5	"	
3444-44-4A	660	1100-1 min	"	"	0.08	0.10	0.26	0.34	0.36	0.40	0.41	0.40	0.41	0.42	0.45	0.46	0.14	8.5	"	
3444-44-4A	660	1100-1 min	"	"	--	--	--	0.26	0.32	0.36	0.38	0.50	(1 hr. per point)						"	
3444-45-1	680	1100-1 min	"	"	0.09	0.13	0.30	0.36	0.47	0.53	0.57	0.60	0.63				0.11	9.3	"	
3444-46-4	600	1100-2 min	"	"	0.06	0.08	0.27	0.32	0.22	0.30	0.34	0.35	--	0.39	0.40	--	0.17	--	"	
3444-46-3	660	1100-1 min	"	"	0.08	0.14	0.32	0.35	0.41	0.48	0.54	0.57	0.60	--			0.16		"	
3444-46-8	660	8800-2 min	"	"	0.08	0.15	0.38	0.44	0.45	--	0.46	0.55	--				--		"	
4465-3-1	660	1100-1 min	"	4665 9/15/65	0.06	--	--	0.40	0.42	0.55	0.60	0.60	--	--	--	--	--	--	"	
4665-3-2	660	1100-1 min	"	"	0.08	0.14	0.29	0.32	0.40	0.44	0.47	0.51	--						11,909	
4665-3-3	660	1100-1 min	"	"	0.07	0.15	0.26	0.30	0.39	0.47	0.50	0.57	--						11,909	
4665-4-1	660	1100-1 min Clad at 8000 psi	3.5 Mil, 10μ Barrier	4002 7/15	0.07	0.17	0.27	0.32	0.40	0.42	0.49	0.55	--						10,004	Clad Barrier
4665-5-1	660	1100-1 min		4665 10/15/65	0.09	0.18	0.33	0.36	0.48	0.52	0.56	0.60	--						11,909	New Emulsion
4665-6-1	660	1100-1 min	Standard 9μ Porous TFE	"	0.08	0.14	0.27	0.37	0.45	0.53	0.58	0.65	Stored 30 Days						"	
4665-6-2	660	1100-1 min	"	"	0.01	0.14	0.27	0.40	0.50	0.60	0.66	Dead	Filtered and NH_3 Treated						"	
4665-6-3	660	1100-1 min	"	"	0.08	0.17	0.32	0.42	0.50	0.65	--		NH_3 Treated						"	
4665-6-4	660	1100-1 min	"	4665 11/24/65	0.07	0.10	0.30	0.37	0.41	0.49	0.52	0.56							11,907	
4665-6-5	660	1100-1 min	"	4665 10/15/65	0.08	0.11	0.26	0.34	0.42	0.52	0.58	0.72							10,004	
4665-7-1	660	1100-1 min	"	4002 8/15/65	0.05	0.14	0.28	0.31	0.32	0.40	0.42	0.48							11,909	
4665-7-2	660	1100-1 min	"	"	0.12	0.26	0.37	0.47	0.58	0.64			Filtered and NH_3 Treated						"	
4665-8-1	660	1100-1 min	Special Cladding Procedure	"	0.05	0.12	0.23	0.27	0.33	0.36	0.42	0.45	-- Dead						"	
Electrode Composition: 90% Platinum - 10% Teflon - 50 ma/cm²																				
3444-46-1	600	1100-1 min	Standard 9μ Porous TFE	4002	0.04	0.08	0.18	0.22	0.30	0.35	0.44	0.48	0.52	0.57	0.56	--	0.15		10,004	
3444-46-2	660	1100-2 min	"	"	0.09	0.12	0.22	0.29	0.44	0.53	0.57	0.58	0.58	--			0.17			
3444-46-5	600	8800-2 min	"	"	0.05	0.10	0.22	0.26	0.34	0.38	0.44	0.56	--							
3444-46-6	349	8800-1 min	"	"	0.07	--	0.33	0.42	0.49	0.59	0.62	--								

APPENDIX A-6

CHARACTERIZATION OF ALLOYS

	Alloy, at %	Preparation	Heat Treatment	Chemical Analysis[1]	X-Ray Diffraction
3942-37a	60Fe-40Au	Raney Technique	As Cast	--	Mixture of Fe_3O_4 and Au (Au probably contains small amount of Fe)
3942-37a	40Fe-60Au	"	"	--	Mixture of Fe_3O_4 and Au (This alloy contains a greater percentage of Au than 3942-37a. Au probably contains small amount of Fe)
	50Ni-50Au	"	"	--	Mixture of Au (contains about 10% Ni in solid solution and Ni (contains about 2% Au in solid solution)
	50Fe-50Cu	"	"	--	Mixture of Fe_3O_4, Cu_2O and small amount of Cu
	50Ni-50Cu	"	"	--	Cu-Ni Alloy (20-45% Cu in solid solution) and a small amount of NiAl
	50Co-50Cu	"	"	--	Mixture of Cu and Co
	50Mo-50Cu	"	"	--	Mixture of Cu and Mo
	50Fe-50Ag	"	"	--	Mixture of Ag, Fe_3O_4 and some Ag_2Al
	100Ni	"	"	--	Ni and a trace of NiAl
4469-4-1c	60Au-40Fe	"	Anneal at 1050°C water quench	--	Approx 50% solid solution of Fe (about 7%) in Au and approx 50% unidentified phase (may be $AuFe_3$)
4469-5-1c	40Au-60Fe	"	Anneal at 1100°C water quench	--	Approx 25% solid solution of Fe (about 15%) in Au and approx 75% unidentified phase (may be $AuFe_3$)
4469-33	90Ni-10Pt	"	Anneal at 1350°C water quench	--	---
4469-28	90Ni-10Pt	"	Anneal at 1100°C water quench	--	---
4469-16	25V-75Cr	Commercial	As Received	25.0% V 74.2% Cr	Solid solution of V in Cr. Separate phase of V probably present because the amount of V in solid solution was not sufficient to account for 25%
4469-16	99Ti-1Pt	"	"	0.99% Pt	Appeared as pure Ti. Amount of Pt too small to be detected by X-ray
4469-16	98Co-2Pt	"	"	99.1% Co 0.92% Pt	Neither Co nor Co-Pt alloy. Sample unidentifiable
4469-16	90Ni-10Ti	"	"	--	Solid solution of Ti (about 4%) in Ni and a separate phase of Ti
4469-16	90W-10Ag	"	"	--	Mixture of W and Ag
4469-12	90Ni-10Pt	"	"	9.61% Pt	Mixture of Ni and Pt

(1) Analyses are in weight %.

APPENDIX A-7

EVALUATION OF ALLOY CATALYSTS

Test No.	Catalyst No.	Catalyst Composition at %	Electroylte	Temp, °C	Fuel	Polarization from H_2 Theory at Indicated ma/cm^2, volts						Current Density at Indicated volts Polarization from H_2, ma/cm^2		
						0	1	2	10	50	100	0.57	0.61	0.73
4469-10	4469-5-1C	Raney annealed 40 Au-60Fe	3 M KOH	96	N_2	--	0.59	--	--	--	--	1.0	--	--
"	"	"	"	"	C_4H_{10}	--	0.62	--	--	--	--	0.9	--	--
"	"	"	"	"	H_2	--	--	0.59	--	--	--	2.0	--	--
4469-11	"	"	85% H_3PO_4	150	N_2	--	0.30	0.62	--	--	--	--	--	--
"	"	"	"	"	C_4H_{10}	--	--	0.62	--	--	--	--	--	--
"	"	"	"	"	H_2	--	--	0.22	0.62	--	--	--	--	--
4469-11	"	"	85% H_3PO_4	150	H_2	--	0.05	--	0.61	--	--	--	10	--
"	"	"	"	"	C_4H_{10}	--	--	--	--	--	--	--	1.2	--
"	"	"	"	"	N_2	--	--	--	--	--	--	--	1.4	--
4469-8	4469-4-1C	Raney annealed 60 Au-40Fe	85% H_3PO_4	150	N_2	--	--	--	--	--	--	--	--	2.0
"	"	"	"	"	C_4H_{10}	--	--	--	--	--	--	--	--	2.0
"	"	"	"	"	H_2	--	--	--	--	--	--	--	--	25.0
2669-16	Commercial	Raney Ni(1)	3 M KOH	80	H_2	--	--	--	0.00	0.08	0.19	--	--	--
3942-28	3942-28	Raney Ni(1)	3 M KOH	94	H_2	--	--	--	0.00	0.06	0.15	--	--	--
3942-30	3942-30	Raney 50 Ni-50 Au(1)	3 M KOH	94	H_2	--	--	--	0.00	0.02	0.05	--	--	--
3942-32	3942-32	Raney 50 Ni-50 Cu(1)	3 M KOH	97	H_2	--	--	--	0.03	0.03	--	--	--	--
4469-29	3942-41	Raney 50 Ti-50 Au	3 M KOH	100	H_2	--	--	--	--	--	--	<0.05	--	--
4469-17	Commercial	99 Ti-1 Pt	3 M KOH	100	H_2	--	--	--	--	--	--	0.70	--	--
"	"	"	"	"	N_2	--	--	--	--	--	--	0.70	--	--
"	"	"	"	"	C_4H_{10}	--	--	--	--	--	--	0.55	--	--
4469-30	Commercial	90 Ni-10 Ti	3 M KOH	100	H_2	--	--	--	--	--	--	0.08	--	--
"	"	"	"	"	N_2	--	--	--	--	--	--	0.08	--	--
"	"	"	"	"	C_4H_{10}	--	--	--	--	--	--	0.08	--	--
3942-48	Commercial	98 Co-2 Pt	30% H_2SO_4	100	N_2	--	--	--	--	--	--	Completely Dissolved		
4469-31	Commercial	75 Cr-25 V	3 M KOH	100	N_2	--	--	--	--	--	--	1.2	--	--
"	"	"	"	"	C_4H_{10}	--	--	--	--	--	--	1.2	--	--
"	"	"	"	"	H_2	--	--	--	--	--	--	0.7	--	--
4469-46	4469-33	Raney annealed (1350°C) 90 Ni-10 Pt	3 M KOH	105	N_2	--	--	--	--	--	--	1.2	--	--
"	"	"	"	"	C_4H_{10}	--	--	--	--	--	--	1.2	--	--
"	"	"	"	"	H_2	--	--	--	--	--	--	80.0	--	--
4469-40	3942-42	Raney gold	3 M KOH	102	N_2	--	--	--	--	--	--	0.4	--	--
"	"	"	"	"	C_4H_{10}	--	--	--	--	--	--	0.5	--	--
"	"	"	"	"	H_2	--	--	--	--	--	--	6.0	--	--
4469-34	4469-28	Raney annealed (1100°C) 90 Ni-10 Pt	"	102	N_2	--	--	--	--	--	--	0.05	--	--
"	"	"	"	"	C_4H_{10}	--	--	--	--	--	--	0.02	--	--
"	"	"	"	"	H_2	--	--	--	--	--	--	2.0	--	--
4469-22	4469-19-1C	Raney 99 Ni-1 Pt	3 M KOH	100	C_4H_{10}	--	--	--	--	--	--	3.0	--	--
"	"	"	"	"	H_2	--	--	--	--	--	--	52.0	--	--

(1) Not tested according to the procedures specified in the text, Task C, Phase 4, Part b.

APPENDIX A-8

PREPARATION AND PROPERTIES OF Mn- AND Cr-DOPED PEROVSKITES (OXIDIZED STATES)

Reference	Nominal Formula	Starting Materials	Firing Conditions: Atmosphere	Firing Conditions: Time, hrs	Firing Conditions: Temp, °C	Product Formula(1)	A.C. Conductance, mhos/cm	Acid Stability Test(2): Percent Metal	Acid Stability Test(2): Test Time, hrs	Acid Stability Test(2): A.C. Conductance, mhos/cm	Acid Stability Test(2): Percent Change in Weight	X-Ray Spectrum(14)
						A. Cobalt Compounds						
3952-30	$SrCo^{II}_{0.25}Mn^{IV}_{0.25}Ta_{0.50}O_3$	SrO, CoO, MnO_2, Ta_2O_5	Air	18	1205	--(5)	4.2×10^{-6}	107.1(Co)(6)	24	4.2×10^{-7}	+15.1	--
3951-28	$SrCo^{II}_{0.15}Mn^{IV}_{0.55}Ta_{0.30}O_3$	SrO, CoO, MnO_2, Ta_2O_5	Air	24	1205	--(5)	8.8×10^{-5}	57.6(Co) 145.5(Co)(6)	96.8 24	9.2×10^{-6} 3.7×10^{-6}	+42.0 +30.0	-- --
3952-45	$SrCo^{II}_{0.167}Mn^{III}_{0.167}Mn^{IV}_{0.167}Ta_{0.50}O_3$	$SrCO_3$, CoO, MnO_2, Ta_2O_5	Air	65	1205	$SrCo_{0.167}Mn_{0.333}Ta_{0.50}O_{2.76}$	3.7×10^{-6}	89.6(Co)	24.1	4.1×10^{-8}	+14.0	--
3952-36	$SrCo^{II}_{0.25}Mn^{IV}_{0.45}Ta_{0.30}O_{2.90}$	$SrCO_3$, CoO, $MnCO_3$, Ta_2O_5	Air	24.5	1260	$SrCo_{0.25}Mn_{0.45}Ta_{0.30}O_{2.41}$	4.3×10^{-5}	73.3(Co)	24.1	1.2×10^{-5}	+27.5	B (a = 7.909 Å).
	First Preparation											
	Same Refired	--	Air	20	1370	--	1.5×10^{-4}	80.1(Co)	24	1.6×10^{-5}	+23.6	A (a = 7.849 Å).
3952-48	$SrCo^{II}_{0.25}Mn^{IV}_{0.45}Ta_{0.30}O_{2.90}$(a)	$SrCO_3$, CoO, $MnCO_3$, Ta_2O_5	Air	62.5	1260	$SrCo_{0.25}Mn_{0.45}Ta_{0.30}O_{2.77}$	4.7×10^{-5}	--	--	--	--	--
	Second Preparation											
	Same Refired	--	Air	20	1370	--	1.5×10^{-4}	--	--	--	--	--
	Same Refired	--	Air	20	1480	--	8.8×10^{-7}	48.2(Co)	24	3.4×10^{-7}	+1.9	B (a = 7.939 Å).
3952-37	$SrCo^{II}_{0.25}Mn^{IV}_{0.45}Ta_{0.30}O_{2.90}$	$SrCO_3$, CoO, MnO_2, Ta_2O_5	Air	24.5	1260	$SrCo_{0.25}Mn_{0.45}Ta_{0.30}O_{2.83}$	4.3×10^{-5}	62.1(Co)	24.1	1.3×10^{-5}	+27.5	A (a = 8.003 Å)(15).
	Same Refired	--	Air	20	1370	--	3.4×10^{-4}	44.8(Co)	24	1.2×10^{-5}	+23.6	--
3952-42	$SrCo^{II}_{0.35}Mn^{IV}_{0.15}Ta_{0.50}O_{2.90}$	$SrCO_3$, CoO, MnO_2, Ta_2O_5	Air	24	1260	$SrCo_{0.35}Mn_{0.15}Ta_{0.50}O_{2.62}$	1.1×10^{-6}	87.1(Co)	24.1	5.1×10^{-8}	+27.0	--
3952-38	$SrCo^{II}_{0.35}Mn^{IV}_{0.35}Ta_{0.30}O_{2.80}$	$SrCO_3$, CoO, MnO_2, Ta_2O_5	Air	24	1260	$SrCo_{0.35}Mn_{0.35}Ta_{0.30}O_{2.54}$	1.6×10^{-5}	68.6	24.1	8.1×10^{-6}	+30.7	--
	Same Refired	--	Air	15.5	1095	--	7.5×10^{-6}	--	--	--	--	--
3952-39	$(Sr_{0.8}La^{III}_{0.2})Co^{II}_{0.35}Mn^{IV}_{0.35}Ta_{0.30}O_{2.30}$	$SrCO_3$, La_2O_3, CoO, MnO_2, Ta_2O_5	Air	24	1260	$(Sr_{0.8}La_{0.2})Co_{0.35}Mn_{0.35}Ta_{0.30}O_{2.27}$	5.8×10^{-5}	91.3(Co)	24.1	1.45×10^{-6}	+19.7	--
3952-43	$(Sr_{0.8}Ce^{IV}_{0.2})Co^{II}_{0.45}Mn^{IV}_{0.25}Ta_{0.30}O_{2.30}$	$SrCO_3$, CeO_2, CoO, MnO_2, Ta_2O_5	Air	23	1260	$(Sr_{0.8}Ce_{0.2})Co_{0.45}Mn_{0.25}Ta_{0.30}O_{2.57}$	1.2×10^{-5}	78.4(Co)(7) 77.8(Co)(7)	24.1 24.1	0.91×10^{-6} 1.87×10^{-6}	+16.7 +17.5	-- --
	Same Refired	--	Air	15.5	1095	--	7.0×10^{-6}	--	--	--	--	--
3952-49	$(Sr_{0.8}Pr^{3-3/4}_{0.2})Co^{II}_{0.417}Mn^{IV}_{0.283}Ta_{0.30}O_{2.90}$	$SrCO_3$, Pr_6O_{11}, CoO, MnO_2, Ta_2O_5	Air	62.5	1260	$(Sr_{0.8}Pr_{0.2})Co_{0.417}Mn_{0.283}Ta_{0.30}O_{2.68}$	1.1×10^{-4}	72.8(Co)	24	1.5×10^{-6}	+4.3	B (a = 7.986 Å)(15).
3952-41	$SrCo^{II}_{0.25}Mn^{IV}_{0.45}W_{0.30}O_{2.90}$	$SrCO_3$, CoO, MnO_2, V_2O_5	Air	24	1260	$SrCo_{0.25}Mn_{0.45}W_{0.30}O_{2.21}$	2.1×10^{-8}	--	--	--	--	B (a = 7.53 Å).
3952-40	$SrCo^{II}_{0.25}Mn^{IV}_{0.45}Nb_{0.30}O_{2.90}$	$SrCO_3$, CoO, MnO_2, Nb_2O_5	Air	24	1260	$SrCo_{0.25}Mn_{0.45}Nb_{0.30}O_{2.81}$	4.4×10^{-5}	62.9(Co)	24.1	2.9×10^{-6}	+20.9	--
4571-5	$SrCo^{II}_{0.25}Mn^{IV}_{0.45}Sb_{0.30}O_{2.90}$	$SrCO_3$, CoO, MnO_2, Sb_2O_5	Air	22.3	1205	$SrCo_{0.25}Mn_{0.45}Sb_{0.30}O_{2.89}$	6.4×10^{-5}	48.4(Co)	24	1.3×10^{-6}	+33.0	B (a = 7.844 Å).
3952-44	$SrCo^{II}_{0.25}Cr^{IV}_{0.45}Ta_{0.30}O_{2.90}$-First Prep.	$SrCO_3$, CoO, Cr_2O_3, Ta_2O_5	Air	65.5	1205	$SrCo_{0.25}Cr_{0.45}Ta_{0.30}O_{2.99}$	7.7×10^{-7}	0.0(Co)(8a)	24.1	2.7×10^{-8}	+10.9	C
	Same Refired	--	Air	19	1370	--	4.3×10^{-6}	--	--	--	--	--
	Same Refired	--	Air	19.5	1480	--	2.0×10^{-5}	90.2(Co)(8)	24	3.6×10^{-7}	+5.9	B (a = 7.910 Å).
4571-3	$SrCo^{II}_{0.25}Cr^{IV}_{0.45}Ta_{0.30}O_{2.90}$-Second Prep.	$SrCO_3$, CoO, Cr_2O_3, Ta_2O_5	Air	24	1590	$SrCo_{0.25}Cr_{0.45}Ta_{0.30}O_{2.79}$	1.7×10^{-5}	69.2(Co)(9)	24	4.2×10^{-7}	+1.1	B (a = 7.890 Å).
3952-50	$SrCo^{II}_{0.35}Cr^{IV}_{0.35}Ta_{0.30}O_{2.80}$	$SrCO_3$, CoO, Cr_2O_3, Ta_2O_5	Air	24	1590	$SrCo_{0.35}Cr_{0.35}Ta_{0.30}O_{2.67}$	6.2×10^{-6}	81.6(Co)(10)	24	1.7×10^{-7}	-2.2	B (a = 7.925 Å).
3951-29	$SrCo^{II}_{0.60}Mn^{IV}_{0.40}Mo^{VI}_{0.30}O_3$	SrO, CoO, MnO_2, MoO_3	Air	24	1205	--(5)	8.6×10^{-6}	51.6(Co) 154.9(Co)(6)	95.8 24	2.1×10^{-7} 2.6×10^{-8}	+10.1 +14.3	D (a = 7.988 Å). D (a = 7.84 Å).
3952-35	$SrCo^{II}_{0.375}Mn^{IV}_{0.25}Mo^{VI}_{0.375}O_3$	SrO, CoO, MnO_2, MoO_3	Air	30	1260	--(5)	1.0×10^{-5}	94.8	24	8.8×10^{-10}(13)	-3.0	D (a = 7.891 Å).
3951-26	$SrCo^{II}_{0.4}Mn^{IV}_{0.10}Mo^{VI}_{0.30}O_3$	SrO, CoO, MnO_2, MoO_3	Air	23.3	1150	--(5)	8.7×10^{-6}	121.4(Co)(6)	24	2.9×10^{-10}	+3.4	--
3951-24	$SrCo^{II}_{0.40}Mn^{IV}_{0.30}Mo^{VI}_{0.30}O_{2.90}$	SrO, CoO, MnO_2, MoO_3	Air	23.8	1150	--(5)	4.7×10^{-4}	--	--	--	--	B (a = 7.81 Å)(15).
	Same Refired	--	Air	15.3	1205	--	6.0×10^{-4}	22.9(Co) 104.3(Co)(6)	95.8 24	4.8×10^{-7} 9.4×10^{-8}	+7.1 +10.4	-- --
3952-31	$SrCo^{II}_{0.50}Mn^{IV}_{0.20}Mo^{VI}_{0.30}O_{2.80}$	SrO, CoO, MnO_2, MoO_3	Air	18	1205	--(5)	1.0×10^{-4}	61.5(Co)(6)	24	1.86×10^{-9}(13)	+3.5	--
3952-34	$SrCo^{II}_{0.30}Cr^{IV}_{0.40}Mo^{VI}_{0.30}O_3$	SrO, CoO, Cr_2O_3, MoO_3	Air	30	1260	--(5)	9.2×10^{-6}	55.8(Co)(11)	24	2.5×10^{-10}(13)	-1.4	B (a = 7.935 Å).
	Same Refired	--	Air	19.5	1480	--	6.0×10^{-5}	63.4(Co)(12)	24	3.1×10^{-8}	+1.7	--
						B. Compounds of Nickel, Iron and Copper						
3952-47	$SrNi^{II}_{0.35}Mn^{IV}_{0.35}Ta_{0.30}O_{2.80}$	$SrCO_3$, NiO, MnO_2, Ta_2O_5	Air	21.5	1205	$SrNi_{0.35}Mn_{0.35}Ta_{0.30}O_{2.63}$	7.0×10^{-6}	75.6(Ni)	24	3.3×10^{-6}	+22.8	A (a = 7.953 Å).
	Same Refired	--	Air	19.8	1370	--	3.3×10^{-5}	93.2(Ni)	24	5.1×10^{-6}	+21.5	--
	Same Refired	--	Air	22.5	1480	--	2.7×10^{-5}	92.3(Ni)	24	4.5×10^{-6}	+9.3	A (a = 7.917 Å).
3952-46	$SrFe^{III}_{0.30}Mn^{IV}_{0.40}Ta_{0.30}O_3$	$SrCO_3$, Fe_2O_3, MnO_2, Ta_2O_5	Air	21.5	1205	$SrFe_{0.30}Mn_{0.40}Ta_{0.30}O_{2.90}$	3.5×10^{-6}	98.9(Fe)	24	4.5×10^{-6}	+22.3	B (a = 7.962 Å).
	Same Refired	--	Air	22.5	1370	--	1.2×10^{-6}	98.6(Fe)	24	3.4×10^{-6}	+12.8	--
4571-4	$SrCu^{II}_{0.35}Mn^{IV}_{0.35}Ta_{0.30}O_{2.80}$	$SrCO_3$, CuO, MnO_2, Ta_2O_5	Air	22.3	1205	$SrCu_{0.35}Mn_{0.35}Ta_{0.30}O_{2.60}$	5.3×10^{-6}	17.1(Cu)	24	2.3×10^{-8}	+1.3	B (a = 7.933 Å).

(1) Calculated from weight changes during firing.
(2) Acid stability tests run with 3.7 N H_2SO_4 for specified number of hours unless otherwise stated.
(3) Conductance of solid recovered from acid stability test by filtering, water washing and finally drying overnight in oven under air at 235°F.
(4) Change in weight of solid recovered from acid stability tests (see 3).
(5) When SrO used as starting material, calculated product formulas are not reliable.
(6) 0.83 molal CoSO4 in 2.9 N H_2SO_4 used as corroding medium (instead of 3.7 N H_2SO_4) in acid stability test.
(7) Duplicate acid stability tests.
(8) 6.2% of chromium originally in solid found as chromate in acid.
(8a) 53.3% - - - - - - - - - -
(9) 14.2% - - - - - - - - - -
(10) 16.1% - - - - - - - - - -
(11) 20.9% - - - - - - - - - -
(12) 18.6% - - - - - - - - - -
(13) Conductance determined with d.c. bridge.
(14) X-Ray powder diagram of fired solid. Code A--All reflection maxima assigned to cubic perovskite structure; no detectable impurity phases.
B--All major reflection maxima assigned to cubic perovskite structure; small to moderate amounts of impurity phases present.
C--Major reflection maxima assigned to tetragonal perovskite structure.
D--Ordered cubic perovskite structure; relatively small amounts of impurity phases present.
(15) These spectra indicate some tetragonal distortion of cubic structure.

Note: Cr analysis in (8a) indicates some Cr is in valence state above IV, since the maximum percent of Cr^{IV} that can arise from the disproportionation of dissolved CrIV is 33.3% of the total chromium ($3Cr^{IV} \rightarrow Cr^{VI} + 2Cr^{III}$). In notes 8-12, if all Cr^{VI} is produced by the above disproportionation, then the total chromium that dissolved is threefold larger than the chromate values given.

APPENDIX A-9

PREPARATION AND PROPERTIES OF REDUCED-STATE PEROVSKITES (MIXED MOLYBDENUM VALENCIES)

Reference	Nominal Formula	Starting Materials	Firing Conditions[1] Temp, °C	Time, hrs	Conductance[5] mho/cm	Acid Stability Test[2] Percent Metal Retained	Test Time, hrs	Conductance[3] mho/cm	Percent Change in Wt[4]	X-Ray Spectrum
3951-25	$SrCo^{II}_{0.417}Mo^{V}_{0.333}Mo^{VI}_{0.250}O_3$	SrO, Co, CoO, MoO_3	1150	23.7	2.9×10^{-7}	--	--	--	--	--
	Same Refired	--	1205	87.5	9.8×10^{-10}(8)	92.9	24	1.9×10^{-8}	+2.2	Ordered cubic perovskite structure (a = 7.887 A).
3951-27	$SrCo^{II}_{0.375}Mo^{V}_{0.50}Mo^{VI}_{0.125}O_3$	SrO, Co, CoO, MoO_3	1150	23.3	6.3×10^{-6}	55.5(9)	96	7.0×10^{-8}	-16.5	Ordered cubic perovskite structure (a = 7.893 A).
3952-32	$SrCo^{II}_{0.323}Mo^{IV}_{0.431}Mo^{V}_{0.246}O_{2.80}$ (from MoO_2)	SrO, Co, CoO, MoO_2, MoO_3[6]	1260	3.8	1.1×10^{-8}	--	--	--	--	Ordered cubic perovskite structure (a = 7.904 A).
	Same Refired	--	1260	21	3.8×10^{-10}(8)	81.3(10)	24	5.2×10^{-7}	+4.6	Ordered cubic perovskite structure (a = 7.899 A).
3952-33	$SrCo^{II}_{0.323}Mo^{IV}_{0.431}Mo^{V}_{0.246}O_{2.80}$ (from Mo metal)	SrO, Co, Mo, MoO_3(7)	1260	3.8	3.8×10^{-6}	--	--	--	--	Ordered cubic perovskite structure (a = 7.901 A).
	Same Refired	--	1260	21	8.1×10^{-9}	89.6(11)	24	1.1×10^{-7}	+3.1	Ordered cubic perovskite structure (a = 7.905 A).
3952-12	$SrCo^{II}_{0.5}Mo^{VI}_{0.5}O_3$ (12)	SrO, CoO, MoO_3	1260	23	5.2×10^{-9}	--	--	--	--	Ordered cubic perovskite structure (a = 7.904 A).

(1) Mixtures of starting materials fired as powders in open zircon boats in LECO tube furnace under stream of H_2 specially treated (manganous hydroxide slurry) to remove traces of oxygen and dried by sulfuric acid. Cooling of products to room temperature was conducted under same atmosphere.
(2) Run with 3.7 N H_2SO_4 at 86°C for times specified. Analyses for cobalt carried out polarographically.
(3) 60 cycle a.c. values, (unless otherwise specified), on solid recovered from acid stability test by filtering, water washing, and drying overnight in air oven at 235°F.
(4) Change in weight of solid recovered from acid stability test.
(5) 60 cycle a.c. values unless otherwise specified.
(6) Conductance of mixture before firing--6.2×10^{-1} $ohm^{-1}cm^{-1}$.
(7) Conductance of mixture before firing--5.5×10^{-10} $ohm^{-1}cm^{-1}$.
(8) d.c. values.
(9) Acid contained a large amount of reduced molybdenum and was deep blue in color. Oxidation of this soluble molybdenum with H_2O_2 resulted in precipitation of MoO_3. Cobalt analyses before and after H_2O_2-treatment were in agreement.
(10) Acid was green in color at end of test due to reduced molybdenum in solution. Formed a brownish-green precipitate on neutralization.
(11) Acid was blue-green in color at end of test due to reduced molybdenum in solution.
(12) Older sample described in earlier reports.

APPENDIX A-10

PREPARATION AND PROPERTIES OF SIMPLE AND "MODIFIED" TUNGSTEN BRONZES

Reference	Nominal Composition	Starting Materials	Firing Conditions[1] Temp. °C	Time, hrs	Conductance[2] mho/cm	X-Ray[3] Data	Acid Stability[4] Test 1 Time, hrs	Test 1 Percent Metal Dissolved	Test 2 Time, hrs	Test 2 Percent Metal Dissolved	Conductance[5] mho/cm	Percent[6] Change in Weight
					A. Simple Tungsten Bronzes							
4571-12	$Na_{0.35}W^{V}_{0.35}W^{VI}_{0.65}O_3$	Na_2WO_4, WO_3, WO_2	950	24	1.23	$A^{(11)}$	--	--	--	--	--	--
4571-6	$Na_{0.80}W^{V}_{0.80}W^{VI}_{0.20}O_3$ Prep. 1	Na_2WO_4, WO_3, W	900	24	11.8	$A^{(12)}$	--	--	--	--	--	--
4571-6	$Na_{0.80}W^{V}_{0.80}W^{VI}_{0.20}O_3$ Prep. 2	Na_2WO_4, WO_3, W	900[7]	24	6.07	$A^{(12)}$	--	--	--	--	--	--
4571-7	$Na_{0.80}W^{V}_{0.80}W^{VI}_{0.20}O_3$ Prep. 3	Na_2WO_4, WO_3, WO_2	900	24	3.36	$A^{(12)}$	--	--	--	--	--	--
4571-30	$Pb_{0.20}W^{V}_{0.40}W^{VI}_{0.60}O_3$	PbO, WO_3, W	925	24	23.1	--	--	--	9[8]	--	6.89	-0.4
4571-19	$Pb_{0.35}W^{V}_{0.70}W^{VI}_{0.30}O_3$	PbO, WO_3, WO_2	980	24	6.09	$B^{(17)}$	--	--	--	--	--	--
4571-32	$Pb_{0.45}W^{V}_{0.90}W^{VI}_{0.10}O_3$	PbO, WO_3, W	925	24	1.65	--	--	--	97	--	6.9×10^{-2}	+7.9
4571-35	$Pb_{0.80}W^{IV}_{0.60}W^{V}_{0.40}O_3$	Pb, WO_3	925	24	1.77	$C^{(18)}$	--	--	97	--	2.1×10^{-2}	+11.1
					B. Bronzes Modified With Nickel							
4571-13	$Na_{0.35}Ni^{II}_{0.0583}W^{V}_{0.117}W^{VI}_{0.825}O_3$	Na_2WO_4, NiO, WO_3, WO_2	955	24	5.2×10^{-2}	$B^{(13)}$	25.5	1.4	97.3	57.7	6.3×10^{-5}	-2.0
4571-14	$Na_{0.35}Ni^{II}_{0.070}W^{V}_{0.07}W^{VI}_{0.86}O_3$	Na_2WO_4, NiO, WO_3, WO_2	955	84	7.9×10^{-2}	$B^{(13)}$	25.7	6.8	98.4	35.8	6.8×10^{-4}	-1.9
4571-15	$Na_{0.35}Ni^{II}_{0.0778}W^{V}_{0.0389}W^{VI}_{0.883}O_3$	Na_2WO_4, NiO, WO_3, WO_2	955	84	6.1×10^{-2}	$B^{(13)}$	25.7	3.6	98.4	46.4	4.0×10^{-4}	-2.5
4571-8	$Na_{0.80}Ni^{II}_{0.133}W^{V}_{0.267}W^{VI}_{0.600}O_3$	Na_2WO_4, NiO, WO_3, WO_2	925	24	4.2×10^{-6}(10)	$C^{(14)}$	66.1	19.3	114.1	26.0	5.6×10^{-7}(10)	-7.2
4571-9	$Na_{0.80}Ni^{II}_{0.16}W^{V}_{0.16}W^{VI}_{0.68}O_3$	Na_2WO_4, NiO, WO_3, WO_2	925	24	9.4×10^{-7}(10)	$D^{(15)}$	66.1	13.0	114.1	33.2	7.7×10^{-7}(10)	-6.8
4571-10	$Na_{0.80}Ni^{II}_{0.178}W^{V}_{0.0889}W^{VI}_{0.733}O_3$	Na_2WO_4, NiO, WO_3, WO_2	900	24	(I)[9] 2.4×10^{-7}(10) (II)[9] 2.8×10^{-7}(10)	$C^{(16)}$ $C^{(16)}$	66.1 66.1	3.2 34.5	114.1 114.1	13.0 51.7	7.9×10^{-7}(10) 8.8×10^{-7}(10)	-7.2 -8.4
4571-11	$Cu^{I}_{0.80}Ni^{II}_{0.133}W^{V}_{0.267}W^{VI}_{0.600}O_3$	Cu_2O[10], NiO, WO_3, WO_2	955	24	2.8×10^{-8}	C	25.5	37.6	97.3	67.4	2.5×10^{-8}	-13.7
4571-29	$Pb_{0.20}Ni^{II}_{0.0667}W^{V}_{0.133}W^{VI}_{0.80}O_3$	PbO, NiO, WO_3, W	925	24	0.508	--	24.1	7.2	96.2	80.9	2.2×10^{-2}	+3.1
4571-20	$Pb_{0.35}Ni^{II}_{0.117}W^{V}_{0.233}W^{VI}_{0.65}O_3$	PbO, NiO, WO_3, WO_2	955	24	0.11	$B^{(17)}$	25.7	20.3	98.4	96.4	2.0×10^{-3}	+5.6
4571-22	$Pb_{0.35}Ni^{II}_{0.14}W^{V}_{0.14}W^{VI}_{0.72}O_3$	PbO, NiO, WO_3, WO_2	955	24	5.2×10^{-2}	$B^{(17)}$	25.7	13.0	98.4	69.1	8.8×10^{-6}(10)	+7.1
4571-21	$Pb_{0.35}Ni^{II}_{0.156}W^{V}_{0.0778}W^{VI}_{0.767}O_3$	PbO, NiO, WO_3, WO_2	955	24	1.7×10^{-2}	$B^{(17)}$	25.7	13.2	98.4	40.2	4.7×10^{-6}(10)	+7.8
4571-27	$Pb_{0.35}Ni^{II}_{0.17}W^{V}_{0.02}W^{VI}_{0.81}O_3$	PbO, NiO, WO_3, W	925	24	1.5×10^{-4}	--	24.1	3.1	96.2	36.6	1.1×10^{-5}(10)	+8.9
4571-31	$Pb_{0.50}Ni^{II}_{0.167}W^{V}_{0.333}W^{VI}_{0.50}O_3$	PbO, NiO, WO_3, W	955	24	2.1×10^{-2}	--	24	38.8	96.3	57.0	1.3×10^{-6}(10)	+9.1
4571-40	$Pb_{0.80}Ni^{II}_{0.15}W^{IV}_{0.15}W^{V}_{0.70}O_3$	Pb, PbO, Ni, WO_3	925	24	2.5×10^{-10}	--	24.4	65.1	96.5	90.5	1.7×10^{-5}(10)	+15.9
4571-28	$Pb_{0.80}Ni^{II}_{0.22}W^{V}_{0.72}W^{VI}_{0.06}O_3$	PbO, NiO, WO_3, W	955	24	2.1×10^{-3} (2.1×10^{-11})(10)	--	24.1	65.0	96.2	71.3	1.5×10^{-5}(10)	+12.9
4571-16	$Pb_{0.80}Ni^{II}_{0.267}W^{V}_{0.533}W^{VI}_{0.200}O_3$	PbO, NiO, WO_3, WO_2	955	64	4.3×10^{-10}	--	25.5	74.8	97.3	82.5	4.5×10^{-8}	+13.7
4571-17	$Pb_{0.80}Ni^{II}_{0.32}W^{V}_{0.32}W^{VI}_{0.36}O_3$	PbO, NiO, WO_3, WO_2	955	64	5.3×10^{-10}	--	25.5	49.3	97.3	85.9	4.1×10^{-8}	+11.0
4571-18	$Pb_{0.80}Ni^{II}_{0.356}W^{V}_{0.178}W^{VI}_{0.467}O_3$	PbO, NiO, WO_3, W	955	24	5.5×10^{-10}	--	25.7	19.1	98.4	54.2	2.8×10^{-2} (8.4×10^{-2})(10)	+11.2
					C. Bronzes "Modified" By Other Metals (Co, Fe, Mn, Cr, Cu)							
4571-33	$Pb_{0.35}Co^{II}_{0.117}W^{V}_{0.233}W^{VI}_{0.65}O_3$	PbO, CoO, WO_3, W	925	24	0.373	--	24	84.0	96.3	79.5	1.9×10^{-3}	+5.4
4571-36	$Pb_{0.34}Fe^{II}_{0.117}W^{V}_{0.233}W^{VI}_{0.65}O_3$	PbO, Fe_2O_3, Fe, WO_3, W	925	24	0.656	--	24	83.3	96.5	82.3	2.1×10^{-4}	+5.7
4571-38	$Pb_{0.35}Fe^{III}_{0.14}W_{0.28}W^{VI}_{0.58}O_3$	PbO, Fe_2O_3, WO_3, W	925	25	5.0×10^{-2}	--	24.4	31.2	96.3	70.6	4.7×10^{-9}(10)	+7.1
4571-34	$Pb_{0.35}Mn^{II}_{0.117}W^{V}_{0.233}W^{VI}_{0.65}O_3$	PbO, MnO, WO_3, W	925	24	0.683	--	24	83.7	96.3	82.7	3.5×10^{-3}	+5.7
4571-39	$Pb_{0.35}Cr^{III}_{0.14}W^{V}_{0.28}W^{VI}_{0.58}O_3$	PbO, Cr_2O_3, WO_3, W	925	25	0.78	--	24.4	37.2	96.5	10.1	7.4×10^{-3}	+7.8
4571-37	$Pb_{0.35}Cu^{II}_{0.117}W^{V}_{0.233}W^{VI}_{0.65}O_3$	PbO, CuO, WO_3, W	925	24	8.0×10^{-5}	--	24.4	78.6	96.5	70.5	1.6×10^{-8}	+9.2

(1) Firing Procedure: oven-dried pills of firing mixtures were wrapped in platinum foil and placed in fused silica tubes. The latter were then evacuated and sealed. Sealed tubes were placed in hot zone of LECO furnace.
(2) Direct current values unless otherwise specified.
(3) Code: A - Strong maxima for Bronze phase with only small amounts of other phases present.
B - Strong maxima for Bronze structures together with moderate amounts of other phases
C - X-Ray Spectrum very complex--some indications of Bronze phases.
D - X-Ray Spectrum very complex--presence of Bronze Phases doubtful.
(4) Run with 3.7 M H_2SO_4 at 86°C for time specified. Analyses for "modifying" metals run polarographically.
(5) Conductance of solid recovered from acid stability tests (end of Test 2) by filtering, water washing, and drying in air oven overnight at 235°F. Direct current values unless otherwise specified.
(6) Change in weight of solid due to acid treatment.
(7) Fired in unsealed silica tube connected to laboratory vacuum pump.
(8) Due to an error, CuO may have been used. Preparation to be repeated.
(9) All "modified" materials in the $Na_{0.80}$ melted during firing. Silica was attacked causing tube to shatter on cooling. Part I is portion which flowed out of the Pt foil wrapping onto silica surface. Part II is portion remaining in Pt foil wrapper.
(10) Values with 60 cycle a.c.
(11) Small amounts of impurity phases present not identified. Average value of a for cubic bronze lattice = 3.8097 Å. Product deep blue in color.
(12) Only small amounts of impurities, mostly Na_2WO_4 present. Strong reflection peaks from 100 to 222 planes. Cubic lattice. Average a value = 3.8147 Å. Products bronze color.
(13) Two bronze phases, at least one of which is tetragonal, are indicated to be present.
(14) Cubic bronze phase (a = 3.817 Å) appears to be present.
(15) A small 100 reflection suggests presence of a small amount of cubic bronze phase with a = 3.78 Å.
(16) Cubic bronze phase present has a = 3.79 Å.
(17) Two cubic bronze phases present (a = 3.87 Å and 3.78 Å) along with fairly large amounts of $PbWO_4$ (stolzite).
(18) A comparison X-ray spectra before and acid treatment shows (1) $PbWO_4$ (large amounts present) is almost completely destroyed in the acid stability test; (2) one bronze phase (a = 3.87), and possibly another (a = 3.80), are present and persist through acid treatment. The presence of other acid-stable, non-perovskitic phases is also indicated.

APPENDIX A-11

RESULTS OBTAINED ON SIMPLE CARBIDES AND BORIDES AS CATALYSTS

		30% H_2SO_4		30% KOH	
		Corrosion	Hydrogen Activity	Corrosion	Hydrogen Activity
1.	Tungsten carbide (WC)	No	No	No	No
2.	Tungsten carbide about 95% WC + about 5% W_2C	No	No(1)	No	No(1)
3.	Tantalum carbide (TaC)	No	No(1)	No	No(1)
4.	Zirconium carbide ZrC	Yes	No(1)	Not Tested	Not Tested
5.	Titanium carbide TiC	No	No(1)	Yes	No
6.	Chromium carbide Cr_3C_2 + some $Cr_{23}C_6$	Yes	No(1)	Not Tested	Not Tested
7.	Tantalum Hafnium carbide ($HfTa_4C_5$)	No	No(1)	Not Tested	Not Tested
8.	Chromium diboride (CrB_2)	Yes	No	Yes	No
9.	Tungsten-nickel-carbide (WC + small amount of Ni_3C and Ni_2W_4C)- after removal of Ni_3C	No	No	No	No
10.	Tungsten-manganese carbide WC + small amount of Mn_3C and Mn_2W_4C	No	No(1)	Yes	No
11.	Chromium aluminum carbide (Cr_2AlC)	Severe	Not Tested	Severe	Not Tested
12.	Zirconium tin carbide (Zr_2SnC)	Severe	Not Tested	Severe	Not Tested
13.	Niobium indium carbide Nb_2InC	Severe	Not Tested	Severe	Not Tested
14.	Niobium tin carbide (Nb_2SnC)	Severe	Not Tested	Severe	Not Tested

(1) No activity on oxygen.

APPENDIX A-12

LIQUID PHASE REFORMING

Pilot Unit 861C, Run Sequence No. 194

Condition Period	1	2	3	4	5	6	7	8	9	10
Feed	Hexane	Hexane	Hexane	Hexane	Hexane	Hexane	Hexane	Hexane	Decane	Decane
Temp, °C	155	149	207	204	226	227	226	226	228	227
Press, psig	185	925	615	925	925	917	925	925	922	500
Feed Rate, W/W/hr	2.25	2.01	1.64	2.07	2.19	.30	15.45	2.19	1.83	2.62
Water Rate, W/W/hr	.00	.00	1.01	1.11	1.20	1.11	1.11	23.50	1.11	1.66
Conversion, W/W/hr x 10^4	6.63	4.94	4.81	13.8	17.4	0.00	106	119	10.8	12.3
Feed Reacted from Gas Made, Pct x 10^2	2.93	2.45	2.92	6.68	7.91	0.00	6.89	54.2	5.92	4.70
Water Reacted from Gas Made, Pct x 10^2	∞	∞	0.772	1.37	1.41	0.00	16.8	0.934	2.15	1.42
H_2 + HC in Gas Sample, Mole Pct	.97	1.11	64.00	4.55	2.20	.68	8.26	15.64	1.04	1.91
Ffact H_2 + CH_4 in Total H_2 + HC	.83	.86	.94	.59	.21	.32	.12	.05	.22	.27
H_2/CH_4 Mole Ratio	80.0	95.0	5.0	1.6	1.1	--	6.5	7.9	22.0	9.6

Pilot Unit 861C Run Sequence No. 195

Condition Period	3	4	5	6	7	8	9	10	11	12	13	14	15
Feed	Decane	Decane	Decane	Decane	Decane	Decane	Decane	Decane	Decane	Decane	Decane	Decane	Decane
Temp, °C	149	149	151	151	151	228	227	227	261	261	260	259	227
Press, psig	925	75	75	75	75	500	500	925	925	925	925	925	550
Feed Rate, W/W/hr	1.83	2.13	3.60	7.63	1.95	1.77	3.48	1.89	1.83	4.15	15.14	1.83	2.01
Water Rate, W/W/hr	1.20	2.03	1.20	1.29	25.16	.92	.83	1.20	1.11	1.11	1.11	23.68	.92
Conversion, W/W/hr x 10^4	6.75	9.49	43.2(1)	27.8	107	7.91	23.3	16.7	17.6	45.9	77.5	87.4	15.4
Feed Reacted from Gas Made, Pct x 10^2	3.68	4.44	12.0	3.64	54.7	4.47	6.69	8.83	9.64	11.0	5.12	47.7	7.66
Water Reacted from Gas Made, Pct x 10^2	1.15	0.362	1.88	2.68	0.387	1.04	2.72	1.41	2.28	3.14	9.81	0.473	2.31
H_2 + HC in Gas Sample, Mole Pct	1.21	19.81	.49	4.30	.84	6.50	.21	.22	.43	.46	2.86	2.94	.73
Ffact H_2 + CH_4 in Total H_2 + HC	.85	.45	.20	.59	.77	.42	.61	.31	.81	.80	.95	.89	.89
H_2/CH_4 Mole Ratio	13.7	.5	.0	2.2	.9	2.1	1.1	1.3	3.3	.5	3.1	2.4	3.0

(1) When corrected for a 2.2 mole ratio of H_2/CH_4 the conversion x 10^4 becomes 20.0.

APPENDIX B-1

LIQUID DECANE HYDROCARBON TOTAL CELL

Anodes: 50 mg/cm^2 S.P.T.E. Electrodes with 1/16" 9 Porous Teflon Barriers
Electrolyte: 14.7 M H_3PO_4, Flow Rate 5 cc/min
Temperature: 150-155°C
Oxidant: 10 x Stoichiometric

Run No.	Cathode Description	Test Period, hrs	Cumulative Time on Current, hrs	Number of Cells	Oxidant	Assembly Voltage at Indicated Current Density ma/cm^2, volts 0	5	10	15	20	25	30	40	50	60	80	Total, hrs	Remarks
B-1	50 mg/cm^2 S.P.T.E.	0-72	24	1	O_2	0.83	0.64	0.58	--	0.50	0.46	0.42	0.37	0.30	0.32	0.22	72	Terminated at 72 hrs due to excessive cathode leakage--cathode checking noted.
					Air	0.78	--	0.56	0.47	0.38	0.30	0.21	--	--	--	--		
B-2	50 mg/cm^2 S.P.T.E. 6-5 mg/cm^2 Teflon spray coated	2	0	1		---------- Exploded on startup with oxygen ----------												
B-3	50 mg/cm^2 S.P.T.E. 6-8 mg/cm^2 Spray Teflon on air side	0-69	17	1	O_2	0.82	0.60	0.56	0.50	0.44	--	0.38	0.34	0.29	0.22	0.18	--	
					Air	0.81	0.50	0.44	--	0.38	--	0.36	0.33	0.30	0.22	--	69	
		133-205	36		O_2	0.83	0.53	0.47	--	0.40	--	0.34	0.29	0.26	0.20	--	--	
					Air	0.81	0.50	0.45	0.41	0.38	0.30	0.28	0.20	0.16	--	--	206	Cathode leakage noted.
		206-227	45	1	O_2	0.81	0.59	0.50	--	0.36	--	0.26	--	--	--	--		Cathode leaking badly. Test terminated--checking of cathode noted.
					Air	0.81	0.51	0.44	--	0.33	--	0.22	--	--	--	--	227	
B-5	50 mg/cm^2 S.P.T.E. 6-8 mg/cm^2 Teflon spray on air side	0-89	25	3	O_2	2.3	1.81	1.65	--	1.55	1.3	1.15	1.05	0.96	0.69	--		70 ma/cm^2 = 0.90.
					Air	2.25	1.8	1.5	--	1.16	--	1.02	0.92	0.85	0.75	--	89	Terminated due to cathode failure.
B-6	50 mg/cm^2 S.P.T.E. 3.5 mil, 10 micron porous Teflon film	0-70	20	3	O_2	2.35	--	1.65	--	1.3	--	1.05	0.9	--	0.75	0.65		
					Air	2.3	--	1.5	--	1.1	--	0.96	0.88	--	0.70	--	20	
		70-101	32	3	Air	--	--	--	--	1.06	1.03	--	--	--	--	--	101	Steady current run.
		101-102	33	3	Air	--	--	--	--	--	--	0.95	--	--	--	--	102	No performance curve obtained.
		166-174	41	3	Air	--	--	--	--	--	1.05	--	--	--	--	--	174	
		182-187	46	3	Air	--	--	--	--	--	--	0.84	--	--	--	--	187	
		187-189	48	3	Air	--	--	--	--	--	1.10	--	--	--	--	--	189	
		189-190	49	3	Air	--	--	--	--	--	--	--	0.85	--	--	--	190	
		190-196	55	3	Air	--	--	--	--	0.76	--	--	--	--	--	--	196	Cathode separated from barrier--observed on disassembly.
B-7	10 mg/cm^2 Cyanamid AA-1 laminated to 3.5 mil 10μ porous Teflon film	3-50	18	3	O_2	2.35	--	1.64	--	1.25	1.16	--	1.0	1.0	0.9	0.85		
					Air	2.25	--	1.40	--	1.1	1.0	0.9	0.8	0.65	--	--	50	
		70-99	29	3	Air	--	--	--	--	0.90	--	--	--	--	--	--		
		164-165	30	3	Air	--	--	--	--	0.7	--	--	--	--	--	--		Decane appeared in air condenser.
		165-167	32	3	O_2	--	--	--	--	--	1.16	--	--	--	--	--	167	Test terminated decane presence at cathode.
B-8	2.5 mg/cm^2 S.C. T.E.	0-8	6	2	O_2	1.28	--	0.66	--	0.54	--	0.46	--	--	--	--	6	2 cells.
						---------- Initial O_2 Performance Too Poor System Abandoned ----------												Cell 1 current collectors failed was bypassed.
						Butane Performance												
B-7	10 ma/cm^2 Cyanamid AA-1 laminated to 3.5 mil 10 porous Teflon	0-3	3	3	O_2	2.4	--	1.95	--	1.74	--	--	1.5	1.35	1.25	1.05		
					Air	2.38	--	1.8	--	1.55	--	--	1.2	1.0	0.95	0.70		
					IR Measured	--	--	0.050	--	0.090	--	--	0.130	0.150	0.180	0.280		Gas buildup.

APPENDIX B-2

LIQUID DECANE PERFORMANCE - MULTICELL STACK

180 cm^2, 14.7 M H_3PO_4, 150°C - 9 μ Porous Teflon Anode Barrier

Run No.	Anode	Cathode	Time at Temp, hrs	Time on Load, hrs	No. of Cells	Oxidant	Assembly Voltage at Indicated Current, amps. 0	0.5	1	1.5	2	2.5	3.0	3.5	4.0	5.0	Remarks
C-1	50 mg/cm^2 S.P.T.E. on Gold Plated Ta Screen	Cyanamid AA-1 Laminated to 3.5 mil porous Teflon film	8	8	5	O_2	3.85	3.0	2.5	2.25	2.0	1.85	1.60	1.5	1.45	1.2	
						Air	3.5	2.7	2.2	1.85	1.55	1.30	1.10	1.0	--	--	
			24	24	5	Air	---------- 1.66 amps - 1.5 volts ----------										16 hrs unattended operation.
			53	34	5	Air	3.6	2.4	1.8	1.4	--	--	--	--	--	--	
			75	54	5	Air	---------- 1.66 amps - 1.2-1.4 volts ----------										16 hrs unattended operation. Temperature over ran to 168°C.
			99	78	5	Air	---------- 1.66 amps - 1.2 volts ----------										24 hrs unattended operation. Temperature runaway to 168°C.
			103	81	5	O_2	---------- 1.66 amps - 1.5 volts ----------										
			107	85	5	Air	---------- 1.3 amps - 1.0 volts ----------										
			178	93	5	Air	---------- 1-1.2 amps - 1.4 volts ----------										Weekend not on load.
			192	101	5	Air	---------- 1.0 amps - 1.2-1.5 volts ----------										
			216	109	5	Air	---------- 1.0 amps - 1.3 volts ----------										
			240	117	5	Air	---------- 1.0 amps - 1.3 volts ----------										Test terminated cathode leaked. Decane in air condenser.
							Operating System Test Unit										
C-2	50 mg/cm^2 S.P.T.E. Gold Plated Ta Screen	Cyanamid AA-1 Laminated to 3.5 mil porous Teflon Film	3(1)	3	5	Air	3.6	--	--	2.2	2.0	--	1.25	--	0.7	--	
			78	6	5	Air	3.25	--	2.20	1.75	1.30	--	--	--	--	--	Temperature controller failed intermittently 200°C attained, electrolyte turned red due to Pt.
			92	14	5	--	---------- 2.00 amps - 0.8 volts ----------										Second control failure cells melted together platinum dissolved.
							---------- Test Terminated ----------										
							Operating System Test Controller Replaced, Safety Installed										
C-3	50 mg/cm^2 S.P.T.E. on Au Plated Ta Screen Laminated to Porous Teflon Film	50 mg/cm^2 S.P.T.E. on Au Plated Ta Screen Laminated to Porous Teflon Film Cold Pressed at 8000 psi	6	4	3	O_2	2.40	--	1.8	1.65	1.48	--	1.20	--	0.8	--	
						Air	2.25	--	1.65	1.40	1.1	--	0.90	0.55	--	--	
			8	6	3	Air	---------- 2.00 amps at 1.0 volts ----------										
			26	8	3	O_2	2.3	1.95	1.70	1.40	1.15	0.90	0.65	--	--	--	
						Air	2.2	1.95	1.65	1.20	0.9	--	--	--	--	--	
			32	14	3	Air	---------- 1.4 amps - 1.0 volts ----------										
			56	22	3	Air	---------- 1.4-1.8 amps - 1.0 volts ----------										Removed from test assembly and installed in lab test unit after seven days cold shutdown.
			64	30	3	O_2	2.4	1.85	1.50	1.35	1.20	1.1	1.0	--	--	--	
						Air	2.2	1.75	1.40	1.20	1.00	0.80	0.65	--	--	--	
			80	30	3		---------- **Test on OTF-90 Fuel** ----------										
C-3			88	38	3	Air	---------- 1.50 amps - 1.0 volts ----------										1.5 watts
			112	46	3	Air	---------- 1.2-1.5 amps - 1.0 volts ----------										1.2-1.6 watts
			136	54	3	Air	---------- 1.0-1.2 amps - 1.0-1.15 volts ----------										1.2-1.36 watts
			160	62	3	Air	---------- 1.0 amps - 1-1.15 volts ----------										1-1.15 watts
			184	70	3	Air	---------- 1.0 amps - 1.0 volts ----------										1.0 watts
							---------- Cold Shutdown, 96 hrs ----------										
			192	78	3	Air	---------- 1.1 amps - 1.0 volts ----------										1.1 watts
			216	86	3	Air	---------- 1.0 amps - 1.0 volts ----------										1.0 watts
			240	94	3	Air	---------- 1.2 amps - 1.0 volts ----------										Cathode leaking due to cold shutdown.
			264	102	3	Air	---------- 1.0 amps - 1.0 volts ----------										
			288	110	3	Air	---------- 0.95 amps - 1.0 volts ----------										
							---------- Cold Shutdown 72 hrs ----------										
			296	118	3	Air	---------- 1-1.1 amps - 0.9-1.25 volts ----------										
			324	126	3	Air	---------- 1.0 amps - 0.95 volts ----------										
			348	134	3	Air	---------- 1.0 amps - 1.0 volts ----------										
			372	142	3	Air	---------- 1.5 amps - 0.85 volts ----------										
							---------- 1.2 amps - 1.0 volts ----------										
			396	150	3	Air	---------- 1.0 amps - 1.0 volts ----------										

(1) Butane run first three hours.

APPENDIX B-3

PERFORMANCE ON OTF-90
THREE CELL LIQUID HYDROCARBON CELL

Run No.	Anode	Cathode	Time at Temp, hrs	Time on Load, hrs	No. of Cells	Oxidant	Assembly Voltage at Indicated Current, amps. 0	0.4	0.8	1.0	1.2	1.4	1.6	Remarks
C-3	50 mg/cm^2 S.P.T.E. on Au Plated Ta Screen Laminated to Porous Teflon Film	50 mg/cm^2 S.P.T.E. on Au Plated Ta Screen Laminated to Porous Teflon Film Cold Pressed at 8000 psi	85	35	3	O_2	2.25	1.65	1.30	1.10	0.9	0.7	0.6	Air performance deteriorated to 0.5 volts at 1.0 amps in three hours due to fuel transport to the cathode.
						Air	2.25	1.60	1.40	0.8	0.7	0.6	0.5	

APPENDIX B-3

DESCRIPTION OF THE INDIVIDUAL CELLS

4" x 4" Multicell Assembly

Each cell of this stack accommodates a nominal 4" x 4" electrode with an effective area of 80 cm^2[(1)]. The anodes are the standard 50 mg/cm^2 sintered platinum-Teflon emulsion electrodes laminated to 3.5 mil porous Teflon sheet (10 micron pores). Two cathode systems are available for use with the five cell assembly, a commercial cathode prepared by cladding 10 mg/cm^2 Cyanamid AA-1 electrode with porous Teflon film and a laminated sintered 50 mg/cm^2 platinum Teflon structure described previously. The cell is constructed of Rulon LD[(2)] with inlet manifolding and exit control weirs in the side walls to permit circulation of fuel, air and electrolyte. Exhaust gases are removed through vent manifolds which can be nitrogen purged.

The single cell shown in Appendix Figure B-1 is actually a three chamber assembly consisting of an electrode support-cell partition ① a liquid fuel chamber ② an electrolyte chamber ③, and an air chamber ④. As indicated in Figure B-1, air is fed into the top of the cathode chamber and exhausted at the bottom removing product water. Liquid decane is pumped in at the bottom of the fuel chamber--it then percolates through a porous Teflon barrier to the anode. At the anode, part of the fuel is consumed electrochemically, the remainder is transported into the electrolyte space. The electrolyte (14.7 M H_3PO_4) is also fed from entry weirs at the bottom of the cell via a constant displacement (Buchler) pump. The electrolyte level is controlled by an exit weir at the top of the electrolyte chamber, which provides a decane residence space above the operating electrodes to minimize chemical oxidation at the cathode. Consideration of carbon dioxide evolution and decane transport dictate electrolyte chamber thickness and volumetric flow.

In addition, both the fuel and electrolyte chambers are fitted with gas vent chambers to facilitate safe removal of combustion products and vaporized fuel. These vents may be purged with nitrogen when operating with oxygen as the oxidant. This vent system insures that any contact between fuel and oxygen will occur in the nitrogen purged space above the electrodes, not at the catalyst surface.

The interface between the reactant streams (fuel-electrolyte, electrolyte-air) is maintained by the individual fuel or air electrode. At the cathode this function is performed by a thin porous Teflon cladding or laminate on the air side of the cathode. At the anode, the electrode and auxiliary barrier perform this interface control function. Positive seals between chambers are maintained by using oversized electrodes and expendable seal gaskets designed to assure a 1 to 3 mil interference fit at all seal and support surfaces.

---

(1) The loss of 20 cm^2 is due to required support and seal surfaces within the cell, and the volume occupied in maintenance of a positive electrolyte head.

(2) Trademark of low distortion silica-filled Teflon manufactured by Dixon Corporation.

Figure B-1

DIAGRAM OF INDIVIDUAL CELL UNIT

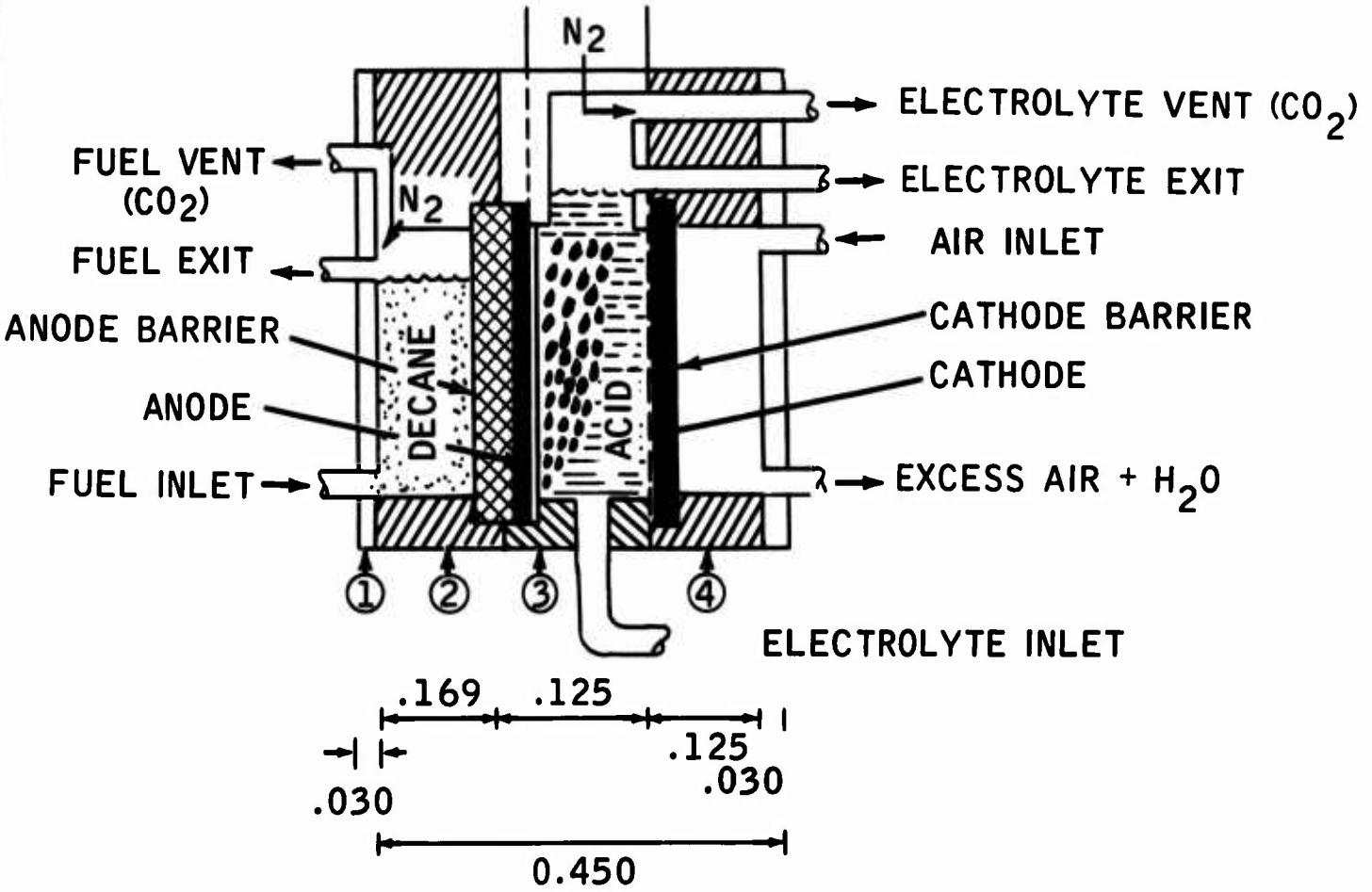

An exploded view of the unit cell is shown in Appendix Figure B-2, and the details of the entrance and exit weir configuration required to prevent fuel poisoning at the cathode is shown in Appendix Figure B-3, in which the electrolyte chamber is viewed from the air electrode side.

Figure B-2

COMPONENTS OF DECANE-AIR UNIT CELL

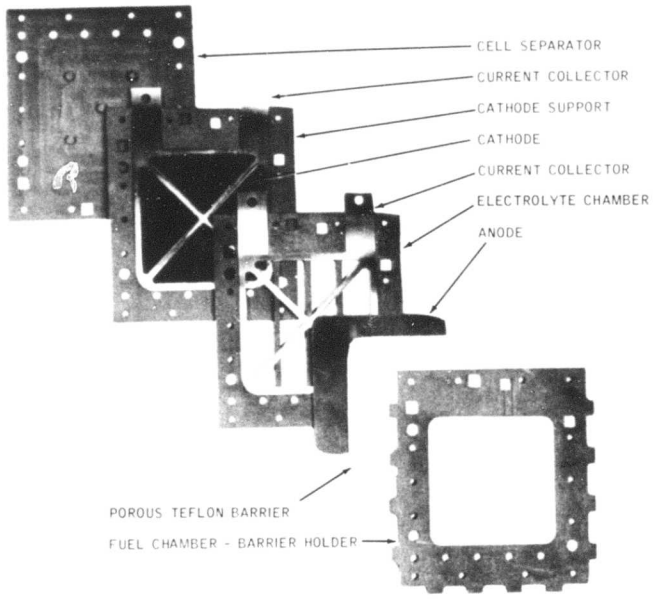

Figure B-3

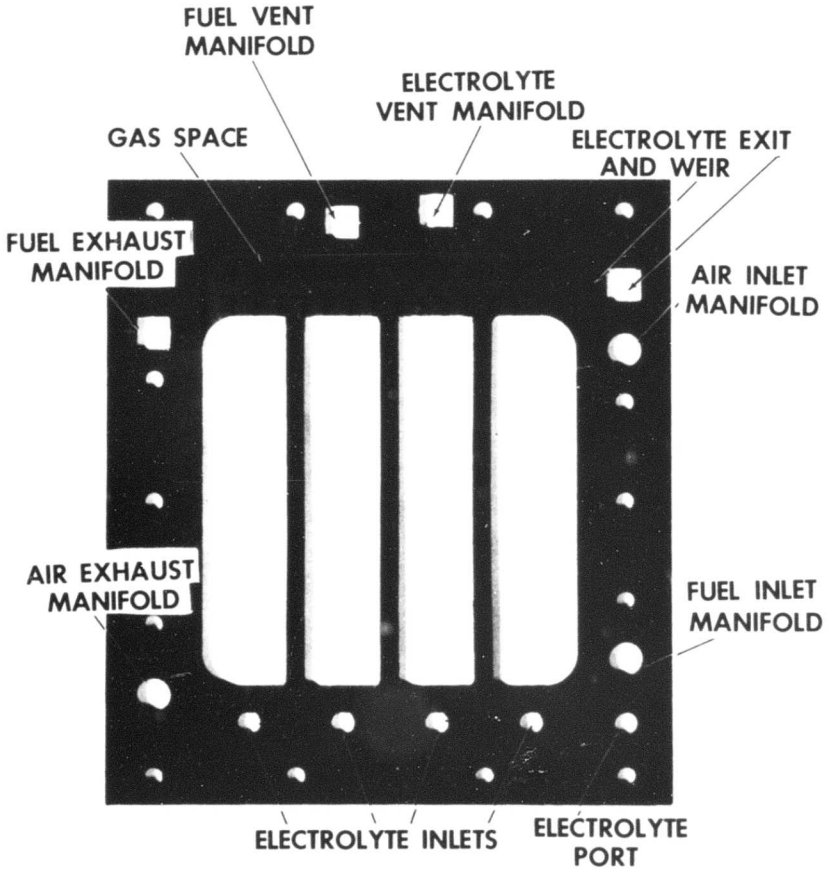

APPENDIX B-4

DESCRIPTION OF OPERATING SYSTEM

The liquid decane-air multicell assembly operating system includes: temperature control, safety and monitoring equipment, air and nitrogen rotometers, a combined electrolyte and fuel preheater, a water recovery unit, and the requisite electrolyte and fuel circulation and recovery equipment.

Electrical equipment shown in Appendix Figure B-4 includes a 1.5 ohm resistive load (consisting of a 1.0 ohm and a 0.5 ohm, 50 watt (Rheostat), a ten amp ammeter and a five volt voltmeter for cell operation.

Figure B-4

ELECTRICAL CIRCUIT FOR HYDROCARBON TOTAL CELL OPERATING SYSTEM

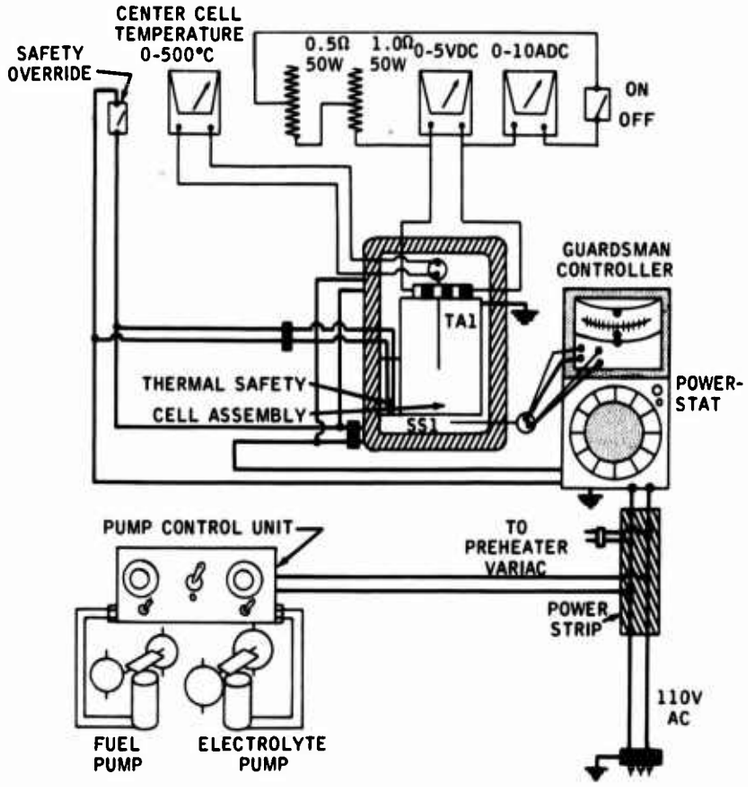

SS1 - Stainless clad IC couple.
TA1 - Tantalum clad IC couple.

Part a - Electrolyte Circulation System

The salient features of the electrolyte circulation system are illustrated in Appendix Figure B-5. Electrolyte is fed from a two liter reservoir through a flow director valve (F) and pump feed splitter (P) to both sides of a Buchler pump (Capacity: 30 cc/min) and then to a combined fuel-electrolyte preheater where the electrolyte temperature is raised to 150°C. The preheated electrolyte is then fed to the cell through valve E, where it loses water. The spent electrolyte returns to the electrolyte reservoir carrying any decane which has been transported through the anode. To prevent electrolyte discoloration, a nitrogen sparge is provided in the electrolyte storage tank.

Part b - Fuel Recovery and Feed

Fuel transported through the anode into the electrolyte space is swept from the system by flowing electrolyte into the electrolyte reservoir. This fuel is automatically separated from this electrolyte by gravity and is passed over an exit weir to the fuel-electrolyte expansion tank(1). The decane overflow from this column is pumped back into the fuel feed tank through one half of the (Buchler) fuel feed pump. The other half of the fuel pump pumps decane from the five hundred milimeter reservoir through the combined electrolyte-fuel preheater into the anode chamber. Flow director valve D (4 way) provides for venting the preheater, draining the anode chamber, and purging the fuel chamber with nitrogen during shutdown. Fuel exits from the anode chamber at a level below that of the electrolyte exit and returns to the fuel tank for re-use. Notice that only the fuel which has resided in the electrolyte is passed through the silica gel recovery unit.

Figure B-5

HYDROCARBON TOTAL CELL OPERATING SYSTEM-PIPING DIAGRAM

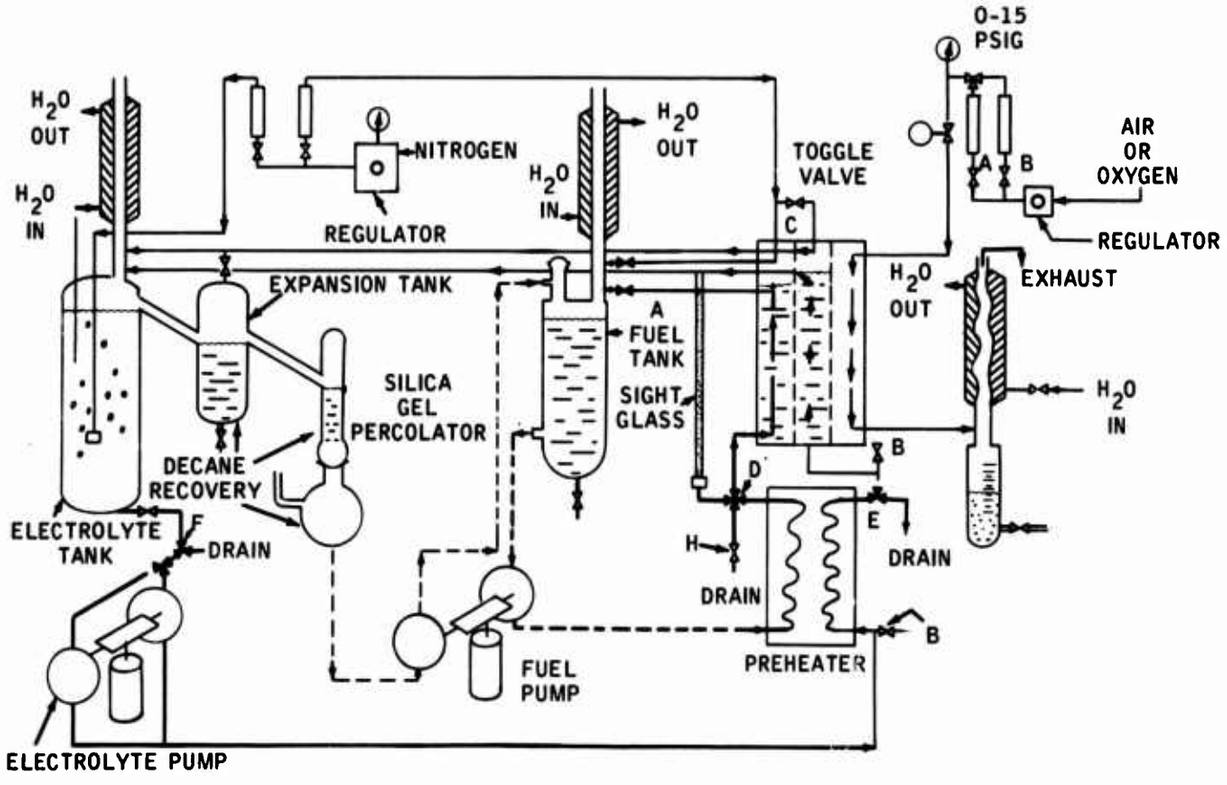

(1) The electrolyte-fuel expansion tank serves two functions. First, it provides additional settling volume to prevent acid from reaching the silica gel column, and second, it allows for expansion of the electrolyte due to gas buildup in the stack.

Part c - Inert Gas Supply

Nitrogen is supplied to three areas in the stack (1) the electrolyte tank as a sparge to prevent electrolyte discoloration and decane oxidation, (2) the fuel and electrolyte exhaust vents as a safety precautions when operating on oxygen and (3) the fuel chamber to provide a purge on shutdown.

APPENDIX C-1

BUTANE PERFORMANCE WITH CATALYZED CARBON ELECTRODES IN PYROPHOSPHORIC ACID

Catalyst Density: 5 mg/cm^2
Electrolyte Temperature: 275°C

Electrode Type	Relative Porosity	Number of Catalyst Impregnations	Carbon Catalyst Content, wt %	Water Bath Temp, °C	Polarization From Butane Theory at Indicated ma/cm^2, volts							
					5	10	25	50	100	150	200	250
CT	Low	2	12	80	0.32	0.34	0.46	0.48	--	--	--	--
CT	High	2	12	80	0.30	0.34	0.39	0.42	0.46	0.47	0.48	0.54-0.66
CT	High	2	12	95	0.21	0.26	0.29	0.32	0.39	0.46-0.51	--	--
CT	Low	1	12	80	0.26	0.29	0.44	0.46	0.52	--	--	--
CT	High	1	12	80	0.18	0.23	0.28	0.35	0.40	0.43	0.44	--
CT(1)	High	2	8	80	0.26	0.30	0.43	0.45	0.49	--	--	--
Carbon-Teflon Emulsion	--	1	12	80	0.16	0.27	0.30	0.33	--	--	--	--

(1) Catalyst density, 2.5 mg/cm^2.

APPENDIX C-2

OXYGEN PERFORMANCE WITH CATALYZED CARBON ELECTRODES IN PYROPHOSPHORIC ACID

Catalyst Density: 5 mg/cm^2
Electrolyte Temperature: 275°C

Electrode Type	Relative Porosity	Number of Catalyst Impregnations	Carbon Catalyst Content, wt %	Polarization From Oxygen Theory at Indicated ma/cm^2, volts							
				5	10	25	50	100	200	300	500
CT	High	2	12	0.11	0.13	0.17	0.23	0.30	0.36	--	--(1)
CT	High	2	12	--	0.15	--	0.21	0.28	0.30	0.33	0.38
CT	High	2	12	--	0.15	--	0.24	0.28	0.32	0.35	--(2)

(1) Not tested beyond 200 ma/cm^2.

(2) Not tested beyond 300 ma/cm^2.

APPENDIX C-3

BUTANE ACTIVITY IN ALKALI METAL BISULFATE MELTS

Electrode	Water Bath Temp, °C	Electrolyte	Electrolyte Temp, °C	Polarization from Butane Theory at Indicated ma/cm^2, volts					
				5	10	25	50	100	200
Pt-Teflon	(--) (1)	$KHSO_4$	275	0.58	-	-	-	-	-
Pt-Teflon	25	$KHSO_4$	275	0.49	0.53	0.60	0.67	-	-
Pt-Teflon	60	$KHSO_4$	275	0.46	0.48	0.54	0.55	-	-
Pt-Teflon	80	$KHSO_4$	275	0.30	0.31	0.36	0.42	0.44	0.47
Pt-Teflon	90	$KHSO_4$	275	0.26	0.26	0.34	0.40	-	-
Pt-Teflon	80	Eutectic (2)	150	0.27-0.31	0.37-0.43	-	0.42-0.47	0.50-0.56	0.44-0.56
Pt-Teflon	80	$KHSO_4$	350	0.33	0.40	0.75	-	-	-

(1) No H_2O sparge, fuel fed dry.
(2) Eutectic consists of 53.5% $NaHSO_4$, 46.5% $KHSO_4$.

APPENDIX C-4

OXYGEN ACTIVITY IN ALKALI METAL BISULFATE MELTS

Electrode	Electrolyte	Electrolyte Temp, °C	Polarization from Oxygen Theory at Indicated ma/cm^2, volts					
			0	5	10	25	50	100
Pt-Teflon	$KHSO_4$	275	0.48	0.59	0.67	0.76	--	--
" "	"	"	0.08	0.14	0.18	0.24	0.34	0.41
" "	"	"	0.12	0.26	0.30	0.33	0.36	0.37
" "(1)	"	"	0.07	0.15	0.19	0.27	0.33	0.37
" "	"	350	0.20	0.26	0.29	0.36	0.43	0.64(2)
" "(1)	"	"	0.23	0.30	0.32	0.38	0.44	0.48

(1) Cold pressed, unsintered.
(2) Electrode started to leak.

APPENDIX C-5

PERFORMANCE OF NON-PLATINOID CATALYSTS IN BASIC ELECTROLYTES

Test No.	Electrode	Sintering Temp, °C	Electrolyte	Fuel	Test Temp, °C	Polarization at Indicated ma/cm^2, volts									
						0	1	5	10	50	100	500	1000	1500	2000
4209-44	Au-PdO	400	6.9 M KOH	4 vol % CH_3OH	90	0.00	0.04	--	0.17	0.26	0.32	--	--	--	--
4209-44	Au-PdO	400	6 M K_2CO_3	"	105	0.06	0.17	--	0.36	0.56	0.66	--	--	--	--
4629-4	Ag-PdO	No Sintering	6.9 M KOH	None	90	0.90	0.96	1.09(1)	--	--	--	--	--	--	--
4629-4	Ag-PdO	No Sintering	6 M K_2CO_3	None	105	0.93	0.99	1.09(1)	--	--	--	--	--	--	--
3942-50	Ag-PdO	"	6.9 M KOH	4 vol % CH_3OH	90	0.00	--	--	0.03	0.09	0.12	0.23	0.32	0.45	0.54
3942-50	Ag-PdO	"	6 M K_2CO_3	"	105	0.03	--	--	0.10	0.34	0.44	--	--	--	--
4629-5	Ag-PdO	500	6.9 M KOH	"	90	0.00	--	0.02	0.05	0.09	0.12	0.22	0.35	0.42	0.57
4629-5	Ag-PdO	500	6 M K_2CO_3	"	105	0.06	--	--	0.16	0.38	0.50	--	--	--	--
4209-46	Ag-PdO	400	6.9 M KOH	"	90	0.00	--	--	0.04	0.11	0.15	0.29	0.44	--	--
4209-46	Ag-PdO	400	6 M K_2CO_3	"	105	0.05	--	--	0.17	0.38	0.49	--	--	--	--
4469-49	Ag-PdO	500	6 M K_2CO_3	H_2	120	0.01(2)	--	--	--	--	--	--	--	--	--
4469-49	Ag-PdO	"	6 M K_2CO_3	C_4H_{10}	120	0.05(2)	--	--	--	--	--	--	--	--	--
4469-48	Ag-PdO	No Sintering	6 M K_2CO_3	"	120	--	0.00	0.02	--	--	--	--	--	--	--
4629-6	Ag-PdO	500	6.9 M KOH	$C_{10}H_{22}$	110	0.02	0.06	0.30	--	--	--	--	--	--	--
4469-43	Ag-PdO	No Sintering	15 M KOH	C_4H_{10}	140	0.00	0.00	--	0.17	--	--	--	--	--	--
4469-45	Ag-PdO	No Sintering	15 M KOH	$C_{10}H_{22}$	150	0.00	0.00	--	0.61	--	--	--	--	--	--
4209-43	Raney annealed 40 Au-60Fe		6.9 M KOH	4 vol % CH_3OH	90	0.16	0.40	0.70	0.88	--	--	--	--	--	--
4209-43	" " "		6 M K_2CO_3	"	105	0.23	0.63	0.88	--	--	--	--	--	--	--
4469-41	Raney Gold		6.9 M KOH	"	90	0.12	0.25	--	0.36	0.44	0.50(3)	--	--	--	--
4209-41	Commercial Ni-3.5 Pt		6.9 M KOH	"	90	0.25	0.29	--	0.41	--	0.56	--	--	--	--

(1) Polarization from methanol theory.
(2) Polarization from hydrogen theory.
(3) 0.56 volts at 200 ma/cm^2; 0.65 volts at 300 ma/cm^2.

APPENDIX C-6

PERFORMANCE OF SLURRY SYSTEM ON LIQUID DECANE

Test No	Stationary Collector Area cm^2	Stirrer	Electrolyte	Catalyst	Non Catalytic Solid	Temp °C	Polarization at Indicated Amperes, Volts										
							0.05	0.10	0.15	0.20	0.30	0.50	0.60	1.0	1.5	2.0	4.8
3677-49b	75	Helical Glass	85% H_3PO_4	3.5 g Pt	None	150	--	--	--	--	--	0.31	--	--	--	--	--
"	50	"	"	"	"	"	--	--	--	--	--	0.35	--	--	--	--	--
"	25	"	"	"	"	"	--	--	--	--	--	0.61	--	--	--	--	--
3677-49d	75	"	85% H_3PO_4	3.5 g Pt	"	150	0.4	0.16	0.19	0.23	0.28	--	0.36	--	--	--	--
"	50	"	"	"	"	"	--	0.17	0.21	0.25	0.30	--	0.40	--	--	--	--
"	25	"	"	"	"	"	--	0.25	0.31	0.37	0.49	--	0.75	--	--	--	--
3677-50b	75	"	30% H_2SO_4	3.5 g Pt	"	100	0.08	0.14	0.19	0.27	0.34	--	0.46	--	--	--	--
"	50	"	"	"	"	"	0.08	0.15	0.20	0.29	0.37	--	0.52	--	--	--	--
"	25	"	"	"	"	"	0.09	0.19	0.27	0.40	0.53	--	0.78	--	--	--	--
3677-50c	75	"	"	"	"	"	--	--	--	--	0.39	--	--	--	--	--	--
"	75	"	"	"	"	"	--	--	--	--	0.40	--	--	--	--	--	--
3677-50d	75	Plain Rectangular	"	"	"	"	--	0.20	0.24	0.29	0.39	--	0.59	--	--	--	--
"	50	"	"	"	"	"	--	0.23	0.27	0.33	0.48	--	0.72	--	--	--	--
"	25	"	"	"	"	"	--	0.31	0.41	0.53	0.70	--	0.10	--	--	--	--
3677-50f	75	"	"	"	"	107	--	--	--	--	0.34	--	--	--	--	--	--
"	75	Helical Glass	30% H_2SO_4	3.5 g Pt	Carbon	100	--	--	--	--	--	--	--	0.54	0.60	0.66	--
3677-49a	75	"	85% H_3PO_4	"	None	175	--	--	--	--	--	0.12	--	0.19	--	0.27	0.46

APPENDIX C-7

STIRRING POWER CONSUMPTION IN THE SLURRY SYSTEM

Test No. 3677-47

35 cc 3.7 M H_2SO_4, 35 cc Decane, 3.5 gm Pt black

	Power Consumption (watts) at Indicated r.p.m.		
	1200	1800	3000
Frictional Power[1]	1.91	2.58	4.5
Stirring Power[2]	0.43	0.43	1.08
Total Power[3]	2.34	3.01	5.58

(1) Frictional Power consumption was determined by operating the system without the liquid, the stirrer spinning in air.

(2) The difference between total power consumption and frictional power consumption.

(3) Measured with the system under operating conditions such that the stirrer stirs up the liquid containing suspended solid catalyst particles.

APPENDIX D-1

SUMMARY OF LIFE TESTING ON RUTHENIUM MODIFIED P-TYPE CATALYST

Half Cell No.	Run No.	Current Density, ma/cm^2	Starting Date	Final Date	Test Duration, Hours	Polarization, volts: Initial	Polarization, volts: Before Final Activation	Polarization, volts: After Final Activation	Comments
1	2	44	4/14/65	10/15/65	4,400	0.26	0.29	0.28	
2*	1	46	7/2/64	10/14/65	11,000	0.35	0.375	0.36	
3*	1	48	7/2/64	10/14/65	11,000	0.35	0.40	0.37	
4	2	46	4/14/65	10/14/65	4,400	0.26	0.28	0.27	
4	2a	48	10/14/65	10/15/65	24	0.27	0.38	--	3.3 grams copper added to run 2.
5	1a	46	3/17/65	6/24/65	2,400	0.355	0.385	0.38	Distilled (not deionized) water in electrolyte.
5	2	46	6/24/65	7/1/65	170	0.29	0.29	--	
5	2a	46	7/1/65	8/20/65	1,200	0.29	0.31	0.29	Distilled (not deionized) water in electrolyte.
5	2b	46	8/20/65	10/14/65	1,350	0.295	0.315	0.295	1.3 grams aluminum added to 2a.
5	2c	46	10/14/65	10/15/65	24	0.295	0.43	--	4 gram $CuSO_4$ added to 2b.

* Potassium borohydride reduced catalyst. All others reduced with hydrogen.
5 cm^2 electrode on tantalum screens. About 20 mg/cm^2 catalyst.

Total Cell No.	Run No.	Current Density, ma/cm^2	Starting Date	Final Date	Test Duration, Hours	Cell Voltage: Initial	Cell Voltage: Before Final Activation	Cell Voltage: After Final Activation	Comments
1	2	43	12/17/64	6/25/65	4,700	0.44	0.35	0.39	High IR at termination.
2	2	46	12/17/64	6/25/65	4,700	0.43	0.39	0.42	
3	2	46	5/21/65	11/1/65	4,000	0.34	0.38	--	Storage test. Run 30 min twice a
4	2	46	5/21/65	11/1/65	4,000	0.37	0.38	--	week at room temperature.

10 cm^2 anodes on platinum screens. About 20 mg/cm^2 catalyst.
Permion 1010 - clad American Cyanamid AA-1 cathode.
5 x stoichiometric air rate.

APPENDIX D-2

PERFORMANCE OF RU-MODIFIED P-TYPE CATALYST AT HIGH CURRENT DENSITIES

Notebook 3629-46

Methanol Concentration, M	Current Density, ma/cm^2	Polarization vs Theory, volts
0.5	0	0.047
"	10	0.261
"	20	0.283
"	40	0.302
"	100	0.332
"	200	0.365
"	400	0.406
"	1000	0.505
"	2000	0.670
"	2400	0.860
1.0	2000	0.455
"	1000	0.422
"	400	0.380
"	200	0.368

Conditions: 60°C, 3.7 M H_2SO_4, 20 mg/cm^2 catalyst loading

APPENDIX D-3

PERFORMANCE OF CARBON SUPPORTED CATALYSTS

Catalyst: Ruthenium Modified P-type
Test Conditions: 3.7 M Sulfuric Acid, 1 M Methanol, 60°C
Electrodes: 4 cm^2 Flag Type

Electrode Ident.	Catalyst Preparation	Catalyst Content on Support, wt %	Electrode Preparation	Catalyst Loading on Electrode, mg/cm^2	Polarization from Methanol Theory at Indicated ma/cm^2, volts						Polarization Decrease on Adding Methanol to 2 M, volts	Current Density at 0.35 volts Polarization, ma/cm^2	Catalyst Utilization at 0.35 volts Polarization, ma/mg	Remarks
					0	0.25	1	10	40	80				
4265-16-1	10% SiO_2 on Carbon Batch B Red. with KBH_4 at room temp .01 N KOH wash.	2.3	Pressed at 5000 lb, with 0.5% Teflon emulsion	0.26	0.52	0.58	0.74	--	--	--	0.290	0	0	
4265-16-2	10% SiO_2 on Carbon Batch B Red. with KBH_4 at room temp 5% H_2SO_4 wash.	2.3	Pressed at 5000 lb, with 0.5% Teflon emulsion	0.14	0.61	0.80	1.09	--	--	--	0.003	0	0	
4265-16-3	10% SiO_2 on Carbon Batch B Red. with KBH_4 at room temp .01 N KOH wash.	5.7	Pressed at 5000 lb, with 0.5% Teflon emulsion	0.54	0.51	0.59	0.77	--	--	--	0.020	0	0	
4265-16-4	10% SiO_2 on Carbon Batch B Red. with KBH_4 at room temp 5% H_2SO_4 wash.	5.7	Pressed at 5000 lb, with 0.5% Teflon emulsion	0.48	0.51	0.57	0.70	--	--	--	0.295	0	0	
4265-16-5	10% SiO_2 on Carbon Batch B Red. with H_2, 2 hrs at 225°C .01 N KOH wash.	2.3	Pressed at 5000 lb, with 0.5% Teflon emulsion	0.30	0.38	0.44	0.54	--	--	--	0.040	0	0	
4265-16-6	10% SiO_2 on Carbon Batch B Red. with H_2, 2 hrs at 225°C 5% H_2SO_4 wash.	2.3	Pressed at 5000 lb, with 0.5% Teflon emulsion	0.21	0.42	0.48	0.58	--	--	--	0.070	0	0	
4265-16-7	10% SiO_2 on Carbon Batch B Red. with H_2, 2 hrs at 225°C .01 N KOH wash.	5.7	Pressed at 5000 lb, with 0.5% Teflon emulsion	0.67	0.38	0.42	0.49	--	--	--	0.110	0	0	
4265-18-1	Carbon Batch A Red. with H_2, 2 hrs at 225°C .01 N KOH wash.	20	Pressed at 5000 lb, with 1.0% Teflon emulsion	4.5	0.21	0.22	0.26	0.39	0.47	0.55	--	5.6	1.2	Catalyst stored under H_2O for six months.
4265-18-2	Carbon Batch A Red. with H_2, 2 hrs at 225°C .01 N KOH wash.	20	Pressed at 5000 lb, with 0.5% Teflon emulsion	4.5	0.24	0.28	0.33	0.42	0.53	0.64	0.020	1.9	0.42	Electrode in cell overnight between runs.
4265-18-3	Carbon Batch B Red. with H_2, 2 hrs at 225°C .01 N KOH wash.	20	Pressed at 5000 lb, with 0.5% Teflon emulsion	4.5	0.18	0.24	0.30	0.48	--	--	--	2.4	0.53	75% of catalyst fell off at 0.25 ma/cm^2.
4265-18-4	Carbon Batch B Red. with H_2, 2 hrs at 225°C .01 N KOH wash.	20	Pressed at 5000 lb, with 0.5% Teflon emulsion	4.5	0.09	0.16	0.22	0.32	0.41	0.48	--	20.0	4.5	Gas evolution starts an electrode surface breakup at 40 ma/cm^2.

APPENDIX D-3 (CONT'D)

PERFORMANCE OF CARBON SUPPORTED CATALYSTS

Catalyst: Ruthenium Modified P-type
Test Conditions: 3.7 M Sulfuric Acid, 1 M Methanol, 60°C
Electrodes: 4 cm^2 Flag Type

Electrode Ident.	Catalyst Preparation	Catalyst Content on Support, wt %	Electrode Preparation	Catalyst Loading on Electrode, mg/cm^2	Polarization from Methanol Theory at Indicated ma/cm^2, volts 0	0.25	1	10	40	80	Polarization Decrease on Adding Methanol to 2 M, volts	Current Density at 0.35 volts Polarization, ma/cm^2	Catalyst Utilization at 0.35 volts Polarization, ma/mg	Remarks
4265-18-4	Carbon Batch B Red. with H_2, 2 hrs at 225°C .01 N KOH wash.	20	Pressed at 2500 lb, with 1.0% Teflon emulsion	4.5	0.11	0.16	0.26	0.36	0.44	0.49	--	9	2.0	
4265-18-4	Carbon Batch B Red. with H_2, 2 hrs at 225°C .01 N KOH wash.	20	Pressed at 2500 lb, with 1.0% Teflon emulsion	4.5	0.13	0.21	0.30	0.38	0.46	0.52	0.010	6.5	1.5	Electrode in cell overnight between runs.
4265-18-5	Carbon Batch B Red. with H_2, 2 hrs at 225°C .01 N KOH wash.	20	Pressed at 10,000 lb, with 1.0% Teflon emulsion	4.5	0.10	0.15	0.22	0.35	0.44	0.49	0.010	10	2.2	
4265-18-6	Carbon Batch B, burned out twice, Red. with H_2, 2 hrs at 225°C, .01 N KOH wash.	20	Pressed at 2500 lb, with 1.0% Teflon emulsion	4.5	0.12	0.17	0.21	0.31	0.41	0.45	0.000	17.5	4.4	Electrode in cell one week before run.
4265-18-7	Blank No Catalyst.	--	Only flag support No catalyst	--	0.65	1.16	1.76	--	--	--	--	--	--	
4265-23-B	10% SiO_2 on carbon Batch A Red. with H_2, 2 hrs at 225°C Two washes with H_2O.	20	Pressed at 5000 lb, with 1.0% Teflon emulsion	4.5	0.32	0.28	0.63	--	--	--	0.000	0.12	0.024	Slow voltage oscillation with 10 mv max amplitude.
4265-23-C	10% SiO_2 on carbon Batch A Red. with H_2, 2 hrs at 225°C One fast wash with 0.001 N KOH.	20	Pressed at 5000 lb, with 1.0% Teflon emulsion	4.5	0.24	0.34	0.40	0.65	--	--	0.005	0.4	0.080	Slow voltage oscillation with 25 mv max amplitude.
4265-23-D	10% SiO_2 on carbon Batch A Red. with H_2, 2 hrs at 225°C Two washes in 90% sat. K_2SO_4.	20	Pressed at 5000 lb, with 1.0% Teflon emulsion	4.5	0.27	0.31	0.38	0.50	--	--	0.000	0.6	0.12	Slow voltage oscillation with 40 mv max amplitude.
4265-23-D	10% SiO_2 on carbon Batch A Red. with H_2, 2 hrs at 225°C Two washes in 90% sat. $KClO_4$.	20	Pressed at 5000 lb, with 1.0% Teflon emulsion	4.5	0.27	0.32	0.40	0.63	--	--	0.000	0.45	0.09	Slow voltage oscillation with 15 mv max amplitude.

APPENDIX D-4

PERFORMANCE OF B_4C SUPPORTED CATALYSTS

Catalyst: Ruthenium Modified P-type
Test Conditions: 3.7 M Sulfuric Acid, 1 M Methanol, 60°C
Electrodes: 4 cm^2, Flag Type

Electrode Ident.	Catalyst Preparation	Catalyst Content on Support, wt %	Electrode Preparation	Catalyst Loading on Electrode, mg/cm^2	Polarization from Methanol Theory at Indicated ma/cm^2, volts 0	0.25	1	10	40	80	Low Tafel Slope, b	High Tafel Slope, b	Polarization Decrease on Adding Methanol to 2 M, volts	Current Density at 0.35 volts Polarization, ma/cm^2	Catalyst Utilization at 0.35 volts Polarization, ma/mg	Remarks
4265-20-1	Red. KBH_4 at room temp 0.01 N KOH wash.	20	Pressed at 5000 lb, with 1% Teflon emulsion	5.45	0.18	0.22	0.27	0.35	0.43	0.46	0.08	0.13	0.020	11	2.0	
4265-20-2	Red. with H_2, 2 hrs at 120°C 0.01 N KOH wash.	20	Pressed at 5000 lb, with 1% Teflon emulsion	5.82	0.14	0.19	0.24	0.32	0.41	0.45	0.08	0.14	0.015	17	2.9	
4265-20-3	Red. with H_2, 2 hrs at 250°C 0.01 N KOH wash.	20	Pressed at 5000 lb, with 1% Teflon emulsion	4.84	0.09	0.16	0.22	0.30	0.37	0.44	0.08	0.16	0.010	23	4.7	
4265-20-4	Red. KBH_4 at room temp 0.01 N KOH wash.	5	Pressed at 5000 lb, with 1% Teflon emulsion	1.25	0.24	0.30	0.35	0.49	0.57	--	0.08	0.16	0.030	1.2	0.96	Catalyst started coming off at 40 ma/cm^2.
4265-20-5	Red. with H_2, 2 hrs at 120°C 0.01 N KOH wash.	5	Pressed at 5000 lb, with 1% Teflon emulsion	1.14	0.25	0.30	0.36	0.42	--	--	0.10	--	0.005	0.8	0.70	Catalyst started coming off at 20 ma/cm^2.
4265-20-6	Red. with H_2, 2 hrs at 250°C 0.01 N KOH wash.	5	Pressed at 5000 lb, with 1% Teflon emulsion	1.27	0.24	0.30	0.36	0.64	--	--	0.11	--	0.000	0.8	0.66	
4265-20-6B	Red. with H_2, 2 hrs at 250°C 0.01 N KOH wash.	5	Pressed at 5000 lb, with 1% Teflon emulsion	0.87	0.21	0.26	0.33	0.49	--	--	0.10	0.25	0.005	1.8	2.1	Voltage oscillation 10 mv at 20 ma/cm^2.
4265-20-7	Red. KBH_4 at room temp 0.01 N KOH wash.	1	Pressed at 5000 lb, with 1% Teflon emulsion	0.20	0.32	0.41	0.48	--	--	--	0.11	--	0.000	0.09	0.45	Voltage oscillation 20 mv at 1 ma/cm^2.
4265-20-8	Red. with H_2, 2 hrs, 120°C 0.01 N KOH wash.	1	Pressed at 5000 lb, with 1% Teflon emulsion	0.28	0.31	0.38	0.45	--	--	--	0.11	--	0.000	0.15	0.54	
4265-20-9	Red. with H_2, 2 hrs, 250°C 0.01 N KOH wash.	1	Pressed at 5000 lb, with 1% Teflon emulsion	0.35	0.37	0.44	0.50	--	--	--	0.11	--	0.000	0.04	0.114	

APPENDIX E-1

TEST APPARATUS FOR LIFE TESTING CATHODE STRUCTURES

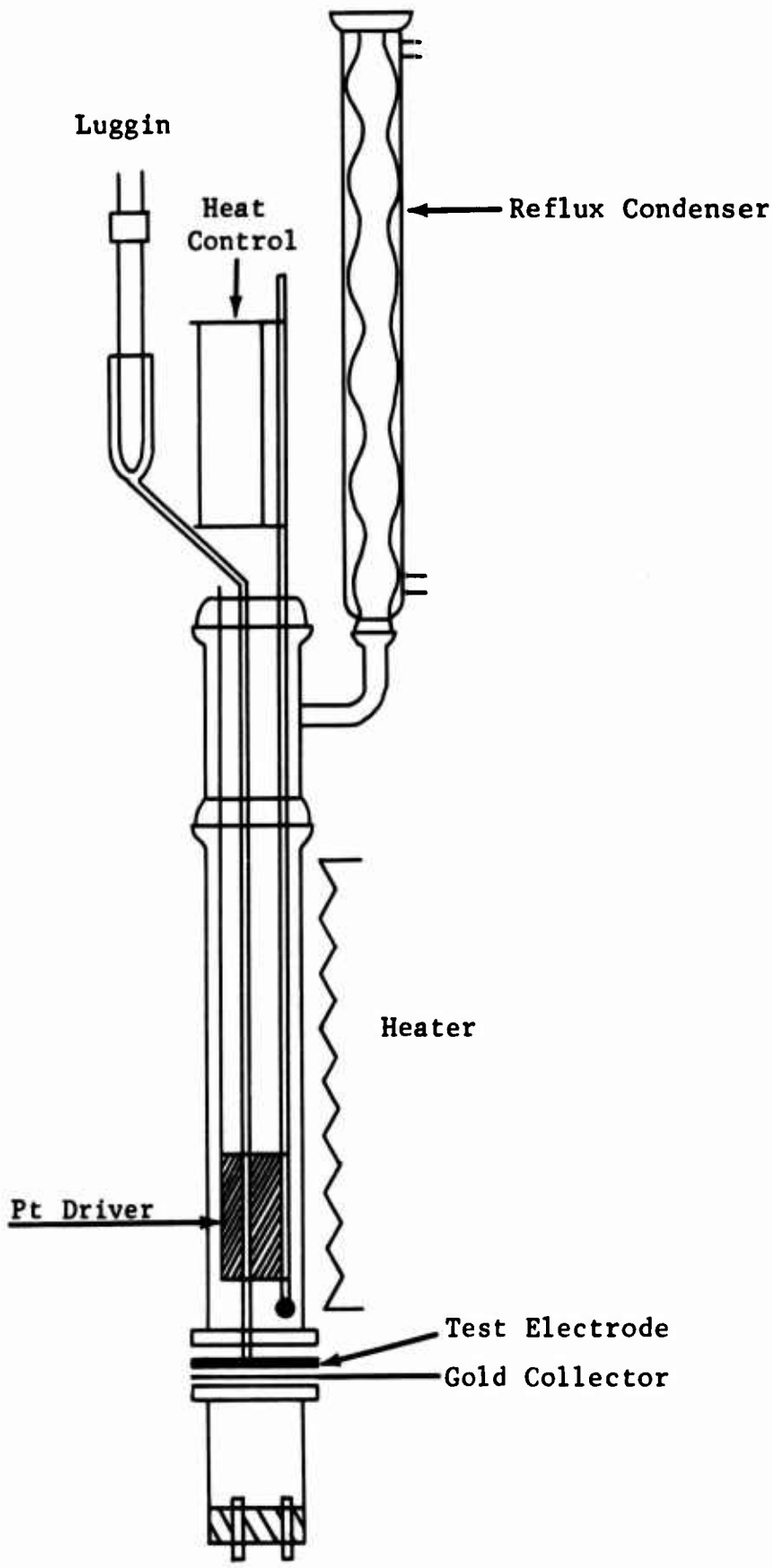

APPENDIX E-2

APPARATUS FOR TESTS ON SCALED-UP 7.5 INCH DIAMETER CATHODES

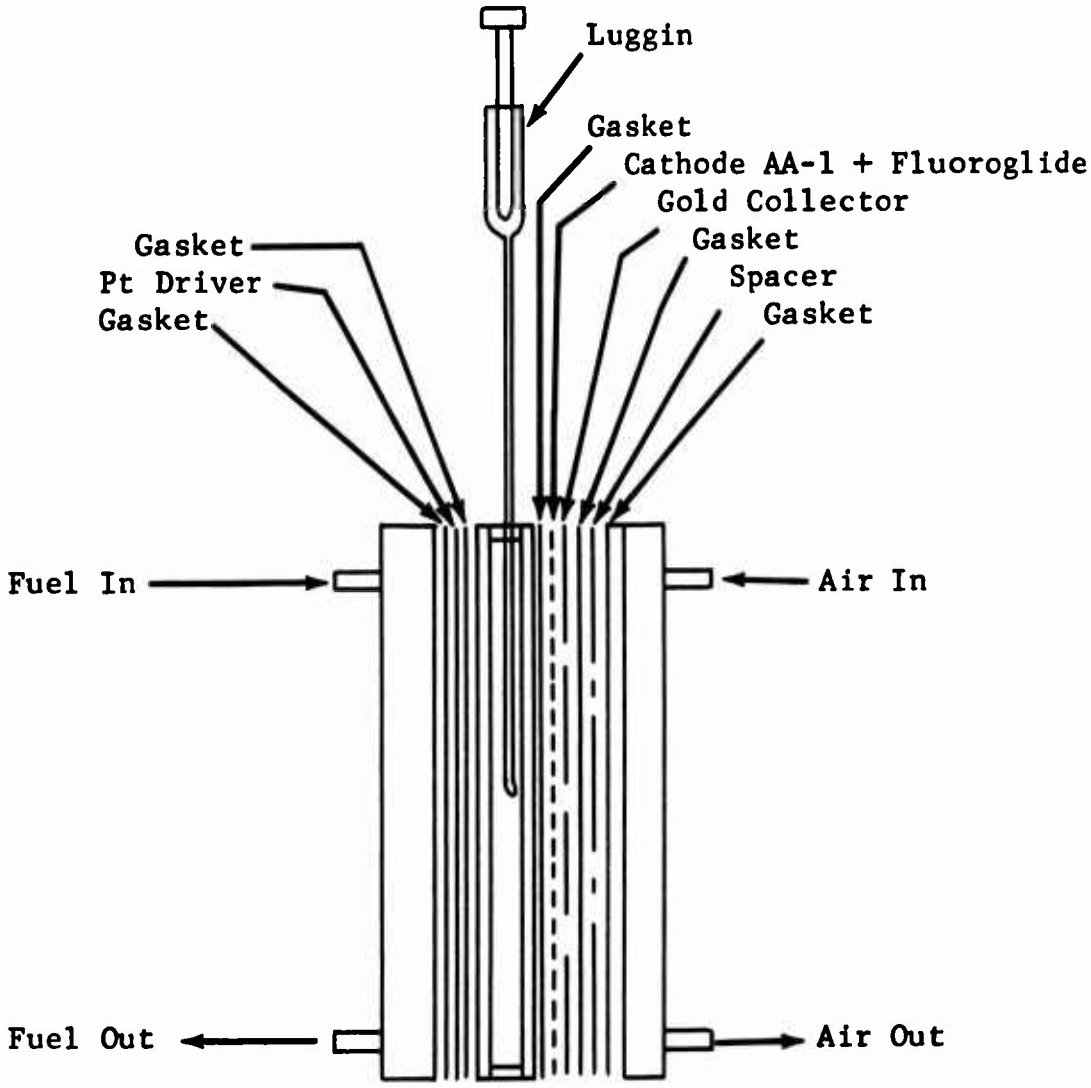

APPENDIX E-3

ELECTROCHEMICAL PERFORMANCE OF SODIUM ALGINATE BARRIER ELECTRODES

Electrode Description	Electrolyte Composition, Vol %	Polarization at Indicated ma/cm^2, volts		
		0	50	100
Sodium alginate 26 wt % in H_2O pressed to Cyanamid AA-1	0	0.33	0.49	--
	4	0.47	0.49	0.54
Sodium alginate 17 wt % in H_2O pressed to Cyanamid AA-1	0	0.25	0.45	0.52
	4	0.45	0.47	0.52
Conventional permion Cyanamid clad AA-1	0	0.22	0.47	0.51
	4	0.42	0.53	0.55
Teflon spray coated Cyanamid AA-1	0	0.25	0.48	0.53
	4	0.52	0.56	0.56

Electrodes tested in 30 wt % H_2SO_4 at 60°C using air at 10 x stoichiometric rate

APPENDIX E-4

CATHODE STUDIES - BARRIER SYSTEM EXPLORATORY STUDY

Reference No.	Fabrication Conditions: Sintering Temp., °C	Fabrication Conditions: Pressure	Cladding Conditions: Pressure, psi	Cladding Conditions: Temp., °C	Cladding Conditions: Time, Min	Loading, mg Pt/cm²	Oxidant	Polarization at Indicated ma/cm², volts: 0	10	20	40	60	80	100	Cladding: Type	Cladding: Pore Size
4355-16-2	American Cyanamid AA-1		0	Placed - Not Pressed		10	O_2	0.15	0.22	0.25	0.29	0.31	0.33	0.35	Chem. Plast	10μ, 3.5 Mil
4355-16-2				Placed - Not Pressed		10	Air	0.13	0.26	0.30	0.35	0.38	0.41	0.44		
4355-16-1			1500	Room	1	10	O_2	0.16	0.22	0.24	0.26	0.28	0.28	0.29	Chem. Plast	10μ, 55% Porous
4355-16-1			1500	Room	1	10	Air	0.16	0.24	0.29	0.33	0.34	0.35	0.37		
4355-19-2			1500	Room	1	10	O_2	0.19	0.26	0.28	0.30	0.31	0.33	0.34	E610-1218B	5 Microns, 55% Porous
4355-19-2			1500	Room	1	10	Air	0.23	0.30	0.34	0.36	0.38	0.40	0.42		
4355-19-3			1500	Room	1	10	O_2	0.14	0.23	0.25	0.28	0.29	0.31	0.32	K233-1220A	40-60μ, 78% Porous
4355-19-3			1500	Room	1	10	Air	0.19	0.27	0.30	0.33	0.36	0.38	0.40		
4355-20-2			1500	Room	1	10	O_2	0.24	--	--	--	--	--	0.35	D10-122A	250-500μ, 90% Porous
4355-20-2			1500	Room	1	10	Air	0.23	--	--	--	--	--	0.45		
4355-20-1			1500	Room	1	10	O_2	0.21	--	--	--	--	--	0.36	K120-1220A	50-100μ, >90% Porous
4355-20-1			1500	Room	1	10	Air	0.24	--	--	--	--	--	0.47		
4355-20-3			1500	Room	1	10	O_2	0.22	--	--	--	--	--	0.38	C180-1120B	200 Mesh, Percale
4355-20-3			1500	Room	1	10	Air	0.26	--	--	--	--	--	0.47		
4355-21-1			1500	Room	1	10	O_2	0.16	0.22	0.25	0.26	0.28	0.29	0.30	W4-1218B	20μ, 58% Porous
4355-21-1			1500	Room	1	10	Air	0.22	0.27	0.30	0.34	0.36	0.38	0.40		
4355-21-2			1500	Room	1	10	O_2	0.17	0.24	0.26	0.29	0.31	0.33	0.34	H107-2218B	50μ, 70% Porous
4355-21-2			1500	Room	1	10	Air	0.21	0.29	0.32	0.35	0.38	0.41	0.43		
4355-14-3	349	1100-1 Min	1100	Room	1	50	O_2	0.17	0.18	0.19	0.22	0.23	0.25	0.26	Cladding laminated to screen side of electrode.	
			1100	Room	1	50	Air	0.17	0.21	0.22	0.26	0.28	0.29	0.30		
4355-24	349	1100-1 Min	4500	Room	1	50	Air	0.21	0.22	0.24	0.26	0.28	0.29	0.29	Cladding laminated to screen side of electrode.	
4355-25	349	1100-1 Min	500	349	0.25	50	Air	0.17	0.20	0.23	0.25	0.28	0.33	0.40	Cladding to Ta side of electrode Cold press at 8000 psi preceeding lamination.	

APPENDIX E-5

CATHODE STUDIES - SINTERED CARBON TEFLON SYSTEM

12% PLATINIZED CARBON CATALYST (1)
14.7M H_3PO_4 - 100°C.

Reference No.	Fabrication Conditions: Sintering Temp., °C.	Sintering Pressure	Sintering Time, Min.	% Teflon	Loading mg Pt/cm²	Oxidant	Thickness, Mils	Polarization at Indicated ma/cm², volts: 0	10	20	40	60	80	100	Remarks
4355-6	349	2200	2	15	5	O_2	17	0.21	0.30	0.35	0.40	0.45	0.48	0.52	
4355-6	349	2200	2	15	5	Air	17	0.26	0.40	0.49	0.64	0.87	--	0.85	
4355-7	349	2200	2	15	5	O_2	18	0.21	0.30	0.33	0.38	0.41	0.41	0.43	113 mg Sprayed TFE.
4355-7	349	2200	2	15	5	Air	18	0.23	0.35	0.41	0.45	0.50	0.52	0.56	
4355-9-1	349	2200	2	10	5	O_2	19	0.19	0.55	- - - - - -		Dead	- - - - - -		
4355-9-2	349	2200	1	10	5	O_2	19	0.21	0.27	0.31	0.36	0.39	0.40	0.44	
4355-9-2	349	2200	1	10	5	Air	19	0.23	0.31	0.36	0.42	0.48	0.53	0.57	
4355-13-1	313	2200	1	10	5	O_2		0.21	0.26	0.32	0.47	0.65	0.81	--	
4355-13-1	313	2200	1	10	5	Air		0.25	0.65						
4355-13-2	326	2200	1	10	5	O_2		0.28	0.32	0.36	0.42	0.47	0.51	0.53	
4355-13-2	326	2200	1	10	5	Air		0.31	0.39	0.43	0.53	0.60	0.66	0.72	
4355-14-1	338	2200	1	10	5	O_2		0.19	0.24	0.29	0.32	0.35	0.38	0.40	
4355-14-1	338	2200	1	10	5	Air		0.23	0.30	0.36	0.43	0.49	0.55	0.58	
4355-14-2	343	2200	1	10	5	O_2		0.23	0.30	0.34	0.40	0.43	0.45	0.47	
4355-14-2	343	2200	1	10	5	Air		0.28	0.37	0.41	0.49	0.53	0.57	0.61	
4355-15-1	349	2200	1	10	5	O_2		0.23	0.31	0.35	0.39	0.42	0.43	0.44	
4355-15-1	349	2200	1	10	5	Air		0.26	0.38	0.41	0.46	0.485	0.51	0.53	
4355-15-2	354	2200	1	10	5	O_2		0.24	0.29	0.32	0.37	0.43	0.47	0.53	
4355-15-2	354	2200	1	10	5	Air		0.27	0.45	0.64	--				
4355-22-1	349	2200	1	10	10	O_2	15.3	0.19	0.21	0.24	0.27	0.29	0.31	0.33	) 24% Platinization
4355-22-1	349	2200	1	10	10	Air		0.19	0.27	0.32	0.38	0.42	0.46	0.50	)
4355-22-2	349	2200	1	10	5	O_2	15.3	0.19	0.23	0.26	0.31	0.34	0.36	0.39	
4355-22-2	349	2200	1	10	5	Air		0.19	0.29	0.33	0.38	0.43	0.47	0.50	
4355-22-3	349	2200	1	10	2.5	O_2		0.20	0.27	0.28	0.31	0.35	0.38	0.39	) 6% Platinization
4355-22-3	349	2200	1	10	2.5	Air		0.21	0.33	0.38	0.43	0.47	0.50	0.54	)
4355-23-1	349	2200	1	10	5	O_2	7.9	0.20	0.25	0.29	0.33	0.36	0.38	0.41	) 24% Platinization
4355-23-1	349	2200	1	10	5	Air		0.21	0.32	0.36	0.40	0.45	0.48	0.50	)
4355-23-2	349	2200	1	10	2.5	O_2	9.8	0.18	0.24	0.28	0.33	0.35	0.37	0.30	
4355-23-2	349	2200	1	10	2.5	Air		0.20	0.29	0.34	0.37	0.42	0.44	0.40	
4355-23-3	349	2200	1	10	1.25	O_2	9.8	0.20	0.28	0.32	0.38	0.43	0.46	0.50	) 6% Platinization
4355-23-3	349	2200	1	10	1.25	Air		0.20	0.36	0.41	0.46	0.52	0.55	0.56	)

(1) Unless indicated.

APPENDIX F-1

HALF CELL TESTS: CATHODE DIFFUSION BARRIERS

Notebook	Barrier	Methanol Conc, Vol %	Air Rate x Stoichiometric	Current Density, ma/cm^2	Cathode volts vs Theory	Direct Oxidation, ma/cm^2
3629-43	None	0	∞	0	--	0
	"	"	4.3	80	0.405	"
	"	"	4.3	60	0.39	"
	"	"	4.3	40	0.37	"
	"	"	4.3	20	0.335	"
	"	"	4.3	10	0.235	"
	"	"	4.3	80	0.41	"
	"	2	4.3	80	0.465	53
	"	"	4.3	60	0.455	54
	"	"	4.3	40	0.445	50
	"	"	4.3	20	0.430	--
	"	"	4.3	10	0.70	--
	"	"	35	10	0.385	45
	"	"	∞	0	0.375	--
3629-44	#5290 Troy Dacron Felt(1)	0	∞	0	0.21	0
	"	"	4.3	80	0.41	"
	"	"	4.3	60	0.395	"
	"	"	4.3	40	0.375	"
	"	"	4.3	20	0.34	"
	"	"	4.3	10	0.315	"
	"	"	∞	0	0.20	"
	"	2	∞	0	0.38	34
	"	"	4.3	80	0.45	38
	"	"	4.3	60	0.435	37
	"	"	4.3	40	0.42	38
	"	"	4.3	20	0.405	42
	"	"	4.3	10	0.44	28
	"	"	35	10	0.385	28
3629-48	#54 Troy Dacron Felt(2)	0	∞	0	0.21	0
	"	"	4.3	80	0.425	"
	"	"	4.3	60	0.41	"
	"	"	4.3	40	0.39	"
	"	"	4.3	20	0.355	"
	"	"	4.3	10	0.325	"
	"	2	∞	0	0.375	28
	"	"	4.3	80	0.46	35
	"	"	4.3	60	0.445	37
	"	"	4.3	40	0.425	32
	"	"	4.3	20	0.405	27
	"	"	4.3	10	0.415	30
	"	"	35	10	0.385	30
3629-37	None	0	∞	0	0.22	0
	"	"	5.3	80	0.44	"
	"	"	5.3	60	0.42	"
	"	"	5.3	40	0.40	"
	"	"	5.3	20	0.365	"
	"	"	5.3	10	0.33	"
	"	2	5.3	80	0.515	80
	"	"	5.3	60	0.495	81
	"	"	5.3	40	0.485	64
	"	"	∞	0	0.43	75
	Permaplex C_20	0	5.3	40	0.405	0
	"	"	5.3	80	0.455	"
	"	"	5.3	60	0.425	"
	"	"	5.3	40	0.405	"
	"	"	5.3	20	0.36	"
	"	"	5.3	10	0.335	"
	"	"	∞	0	0.225	"
3629-38	"	4	5.3	80	0.515	32
	"	"	5.3	60	0.505	29
	"	"	5.3	40	0.495	32
	"	"	5.3	20	0.465	22
	"	"	5.3	10	0.465	15
	"	"	∞	0	0.435	15
	"	2	∞	0	0.39	6.8
	"	"	5.3	80	0.51	15.5
	"	"	5.3	60	0.49	15.3
	"	"	5.3	40	0.43	14.3
	"	"	∞	40	0.43	11.0
	"	"	5.3	20	0.40	9.6
	"	"	5.3	10	0.38	7

Conditions: 60°C, 3.7 M H_2SO_4
American Cyanamid AA-1 cathode.

(1) 14 oz/sq yd, 0.072" thick.
(2) 19 oz/sq yd, 0.070" thick.

APPENDIX F-2

EFFECT OF FELT BARRIERS IN METHANOL TOTAL CELL

Notebook	Barrier	Methanol Conc, vol %	Electrolyte Flow Rate cc/hr	Current Density, ma/cm^2	Cell Voltage	IR volts	Anode Polarization, volts	Cathode Polarization, volts	Direct Oxidation, ma/cm^2
4388-3	None	4	48	40	0.45	0.05	0.28	0.42	28
"	"	"	32	"	0.45	0.05	0.293	0.407	12
"	"	"	30	"	0.45	0.05	0.28	0.42	9.6
"	"	"	29.25	"	0.45	0.05	0.29	0.41	8.0
4388-4	"	2	72	40	0.44	0.025	0.345	0.39	8.4
"	"	"	78	"	0.46	0.025	0.315	0.40	8.8
"	"	"	76	"	0.475	0.025	0.315	0.385	8.4
"	"	"	62	"	0.465	0.025	0.32	0.39	6.8
"	"	"	62	"	0.460	0.025	0.31	0.405	6.8
"	"	"	56	"	0.43	0.025	0.335	0.41	5.2
4388-5	Dacron	4	60	40	0.44	0.035	0.28	0.445	11.6
"	Felt	"	32	"	0.44	0.04	0.305	0.415	4.8
"	"	"	32	"	0.43	0.04	0.315	0.415	4.8
"	"	2	32	"	0.31	0.04	0.515	0.335	2.8(1)
"	"	"	60	"	0.32	0.04	0.435	0.415	1.6(2)
"	"	"	60	"	0.29	0.04	0.435	0.435	1.6
4388-6	"	"	60	"	0.45	0.045	0.315	0.39	6.0

(1) Not steady state.
(2) Very definite anode starvation. Probably not steady state.

APPENDIX F-3

INTERNAL MODIFICATION OF 9" x 5-3/4" CELLS

Cell Configuration	MeOH Conc, vol %	% Conc, Per Pass	Cell Voltage	Polarization at 40 ma/cm^2 Anode	Polarization at 40 ma/cm^2 Cathode	IR volts	Equivalent Chemical Oxidation, ma/cm^2
Glass Beads in Anode Chamber	1	12.5	0.40	0.31	0.44	0.048	20
		25	0.34	0.41	0.40	"	12
		5.0	0.10	0.52	0.53	"	7
	2	12.5	0.40	0.33	0.42	"	44
		25	0.34	0.41	0.40	"	24
		50	0.22	0.45	0.48	"	13
	3	12.5	0.38	0.35	0.42	"	44
		25	0.38	0.35	0.42	"	26
		50	--	--	--	"	--
Dacron Baffles in Anolyte Chamber	2	50	0.40	0.37	0.36	0.073	18
	3	50	0.39	0.37	0.37	0.069	34
Multified Insert Configuration A*	2	12.5	0.36	0.37	0.39	0.080	40
		25	0.38	0.37	0.37	"	32
		50	0.38	0.38	0.36	"	18
	3	25	0.37	0.34	0.41	"	39
		50	0.40	0.34	0.38	"	29
Multified Insert Configuration B*	1	12.5	0.35	0.39	0.38	0.080	30
		25	0.37	0.38	0.37	"	26
		50	0.36	0.40	0.36	"	15
	2	12.5	0.34	0.35	0.43	"	45
		25	0.35	0.37	0.40	"	33
		50	0.38	0.37	0.38	"	19
	3	12.5	0.30	0.36	0.46	"	54
		25.0	0.32	0.37	0.44	"	43

* See Figures

APPENDIX F-3 (CONT'D)

INTERNAL MODIFICATION OF 9" x 5-3/4" CELLS

Cell Configuration	MeOH Conc, vol %	% Conc, Per Pass	Cell Voltage	Polarization at 40 ma/cm^2 Anode	Polarization at 40 ma/cm^2 Cathode	IR volts	Equivalent Chemical Oxidation, ma/cm^2
Double Anode-- Portless Second Anode	3	12.5	0.40	0.34	0.38	0.095	--
		25	0.40	0.35	0.38	0.095	--
		50	0.40	0.33	0.37	0.094	--
	2	12.5	0.40	0.34	0.37	0.089	--
		25	0.39	0.34	0.37	0.010	--
		50	0.36	0.37	0.37	0.010	--
	3	33	0.37	0.34	0.40	0.089	--
		48	0.37	0.34	0.40	0.095	--
		63	0.28	0.44	0.39	0.091	--
	3*	50	0.28	0.39	0.42	0.11	--

* Using 40 wt % H_2SO_4

APPENDIX F-4

SCHEMATIC OF BARRIER STUDY SETUPS

Dacron Felt

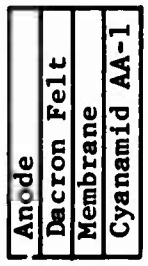

Dacron Felt + Spacer

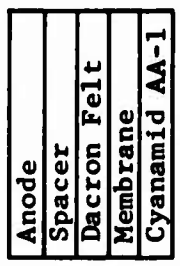

Dacron Felt + Nalfilm + Spacer

APPENDIX F-5

INCORPORATING BARRIERS INTO THE 9" x 5-3/4" CELL

Added Barrier	MeOH Conc, vol %	% Conc, Per Pass	Cell Voltage	Polarization at 40 ma/cm^2 Anode	Polarization at 40 ma/cm^2 Cathode	IR volts	Equivalent Chemical Oxidation, ma/cm^2
Dacron Felt	3	50	0.34	0.42	0.34	0.10	17
Dacron Felt + Spacer	3	50	0.37	0.39	0.33	0.11	57
	2		0.35	0.41	0.33	0.11	14
	1		0.35	0.41	0.33	0.11	14
	3	50	0.35	0.37	0.37	0.110	8
		25	0.34	0.35	0.40	"	22
		12.5	0.33	0.35	0.41	"	28
	2	50	0.34	0.40	0.35	"	10
		25	0.33	0.40	0.36	"	13
		12.5	0.31	0.40	0.38	"	21
Two Permion Membranes	1	12.5	0.23	0.40	0.45	0.120	10
		25	0.24	0.40	0.43	"	7
		50	0.24	0.43	0.41	"	6
	2	25	0.25	0.39	0.44	"	15
		50	0.27	0.35	0.48	"	17

APPENDIX G-1

VARIATION OF SIXTEEN CELL STACK PERFORMANCE WITH TIME

(Notebook #-4485)

Time On Current, hrs	Current Density, ma/cm^2(1)	Stack Potential, volts	Average Cell Potential, volts
0-1	0	11.6	0.72
	20	8.5	0.53
	33.3	7.75	0.48
	40	7.3	0.46
	50	6.6	0.41
	60	6.0	0.38
	70	5.6	0.35
60	0	11.2	0.70
	10	8.8	0.55
	40	6.9	0.43
	50	6.0	0.38
	80	4.6	0.29
235	20	8.0	0.50
	40	6.6	0.41
	80	4.4	0.27
275	0	11.3	0.71
	3.3	9.7	0.61
	10	9.0	0.56
	20	8.05	0.50
	40	6.8	0.42
	60	5.85	0.37
	80	4.95	0.31
350	40	6.0	0.38
	60	4.5	0.26
384	40	6.4	0.40
	50	5.7	0.36
400	40	6.58	0.41
	60	5.25	0.32
	80	4.3	0.27
485	10	8.1	0.51
	20	7.3	0.46
	40	5.2	0.33
	60	3.8	0.24
	80	2.5	0.16

(1) Once-through 0.75 M CH_3OH, 50% Conversion per pass, 8.4 times stoichiometric air rate.

APPENDIX G-2

VARIATION OF OHMIC LOSSES IN SIXTEEN CELL STACK WITH TIME

(Notebook #4485)

Time on Current, hrs	Ohmic Losses at 100 ma/cm^2, mv(1)	
	Total Stack	Cell Average(2)
1	1818	114
20	1868	117
45	2016	126
94	2020	126
163	2020	126
213	2020	126
233	2020	126
321	2222	139
365	2703	169
384	2480	155
485	2808	176

(1) Measured with AC technique (6).

(2) Calculated from measured value for total stack.

Figure G-1

Effect of Time on Ohmic Losses

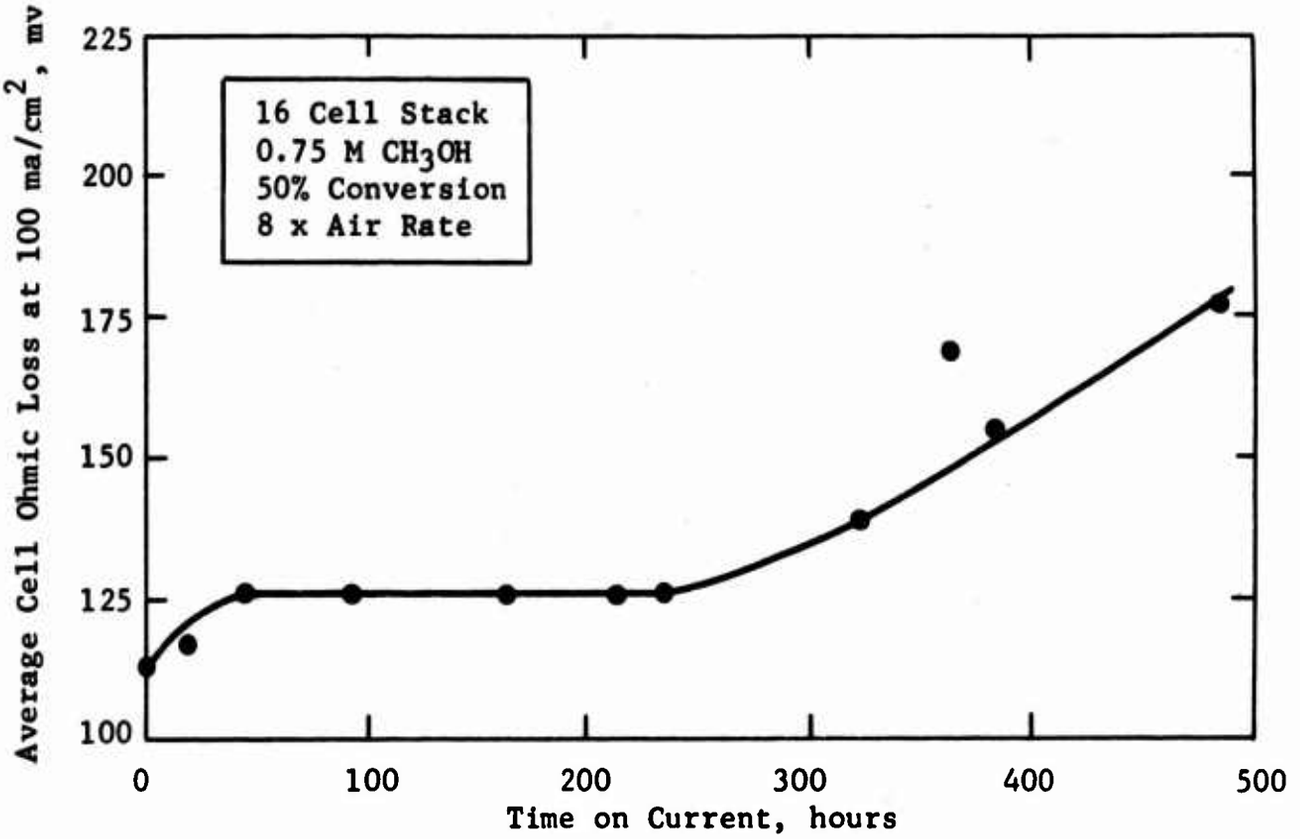

APPENDIX G-3

EFFECT OF TIME ON CELL PERFORMANCE

Run No.[1]	65-2-10(4)				65-11-18(1)			
Time on Load, hrs	1				485			
Cell No.	Cell Voltage	Polarization, volts Anode	Cathode	Ohmic Losses, volts	Cell Voltage	Polarization, volts Anode	Cathode	Ohmic Losses, volts
1	0.38	0.36	0.42	0.04	0.33	0.42	0.39	0.06
2	0.40	0.33	0.42	0.04	0.29	0.43	0.38	0.10
3	0.46	0.31	0.39	0.04	0.34	0.42	0.38	0.06
4	0.42	0.32	0.41	0.04	0.30	0.38	0.42	0.10
5	0.43	0.23	0.49	0.05	0.31	0.35	0.45	0.09
6	0.50	0.35	0.31	0.04	0.35	0.40	0.37	0.08
7	0.47	0.31	0.37	0.05	0.33	0.39	0.42	0.06
8	0.43	0.21	0.52	0.05	0.33	0.36	0.43	0.08
9	0.46	0.26	0.43	0.05	0.34	0.40	0.40	0.06
10	0.44	0.27	0.45	0.04	0.36	0.38	0.40	0.06
11	0.48	0.30	0.37	0.05	0.34	0.41	0.39	0.06
12	0.48	0.17	0.50	0.04	0.36	0.40	0.38	0.06
13	0.39	0.29	0.48	0.04	0.33	0.43	0.38	0.06
14	0.46	0.26	0.44	0.04	0.36	0.39	0.39	0.06
15	0.42	0.31	0.43	0.04	0.35	0.35	0.45	0.05
16	0.44	0.30	0.41	0.05	0.34	0.42	0.38	0.06
Average	0.44	0.29	0.43	0.05	0.34	0.40	0.40	0.07
Std. Deviation	0.03	0.05	0.05	0.00	0.02	0.03	0.03	0.02

(1) 40 ma/cm^2 once-through 0.75 M CH_3OH in 3.7 M H_2SO_4; 8.4 times stoichiometric air rate; 60-65°C.

APPENDIX G-4

EFFECT OF ALTERING FEED INLET MANIFOLD ON STACK TEMPERATURE

Run No. 65-	8-24(2)	8-24(3)	8-25(4)
Current Density, ma/cm^2	40	50	80
Air Rate, Stoichiometric multiple	8.4	8.4	4.2
Inlet Electrolyte Temperature, °C	49	51	49
Inlet Air (Humid) Temperature, °C	42	43	46
Temperature, °C			
Cell No. 1	63	63	73
5	66	67	79
6	68	69	87
7	68	68	82
9	67	68	77
10	68	69	87
14	67	68	88
15	65	67	86
16	57	58	75

N.B. (1) 8 times stoichiometric air rate. 0.62 M Methanol at 50% conversion.

(2) Electrolyte feed to stack split; cells 1 to 8 and 9 to 16 fed separately.

APPENDIX G-5

EFFECT OF ALTERING FEED INLET MANIFOLD ON STACK PERFORMANCE

Run: 65-8-24(2)
Current Density: 40 ma/cm^2
Air Rate: 8.4 x Stoichiometric
Methanol Concentration: 0.62 M

Conversion: 50%
Electrolyte Inlet Temperature: 49°C
Air (Humid) Inlet Temperature: 42°C

Cell No.(1)	Cell Voltage	Anode Polarization, volts
1	0.39	0.41
2	0.39	0.38
3	0.40	0.37
4	0.38	0.35
5	0.36	0.40
6	0.42	0.40
7	0.36	0.43
8	0.38	0.37
9	0.38	0.41
10	0.41	0.37
11	0.40	0.40
12	0.44	0.42
13	0.40	0.39
14	0.42	0.37
15	0.40	0.38
16	0.42	0.36

Cell Group	Average Cell Voltage	Average Anode Polarization, volts
1 to 8	0.38 ± 0.05	0.40 ± 0.03
9 to 16	0.41 ± 0.04	0.39 ± 0.02

(1) Split inlet feed manifold. Cells 1 to 8 and 9 to 16 fed separately.

APPENDIX G-6

ELECTROLYTE DISPLACEMENT VOLUMES

The oxidation of methanol within the fuel cell stack produces gaseous carbon dioxide. This evolving gas displaces electrolyte within the stack, in the manner of a conventional co-current gas-liquid contactor. The following data were obtained to define both the volume of displaced electrolyte at steady state, and the rate at which the displacement occurs. The sixteen cell stack was operated at electrolyte flow rates equivalent to 50% nominal conversion per pass. The stack electrolyte volume at rest was 1870 cc at 24°C.

Current Density, ma/cm^2	Time, min	Displaced Electrolyte Volume, cc	Current Density, ma/cm^2	Time, min	Displaced Electrolyte Volume, cc
3.3	0	0	40	0	0
	7	15		5	150
	12	35		10	225
	17	35		15	225
	22	50		20	235
	27	75			
10	0	0	60	0	0
	6	60		3	165
	11	85		8	225
	16	120		13	220
	21	140		18	225
	26	150			
20	0	0	80	0	0
	5	70		2	150
	10	142		7	210
	15	180		12	210
	20	195		17	245
	25	250			
20	0	0	80	0	0
	5	80		4	200
	11	140		9	270
	15	170		14	275
	20	185			
	25	200			
40	0	0			
	5	115			
	10	160			
	15	190			
	20	210			
	25	220			

APPENDIX G-7

PHOTOGRAPHS OF HARDWARE UNITS USED IN METHANOL FUEL CELL BATTERY DEMONSTRATOR

A. Electrolyte Pump and Metering Assembly

Figure G-2

Electrolyte Pump and Metering Assembly

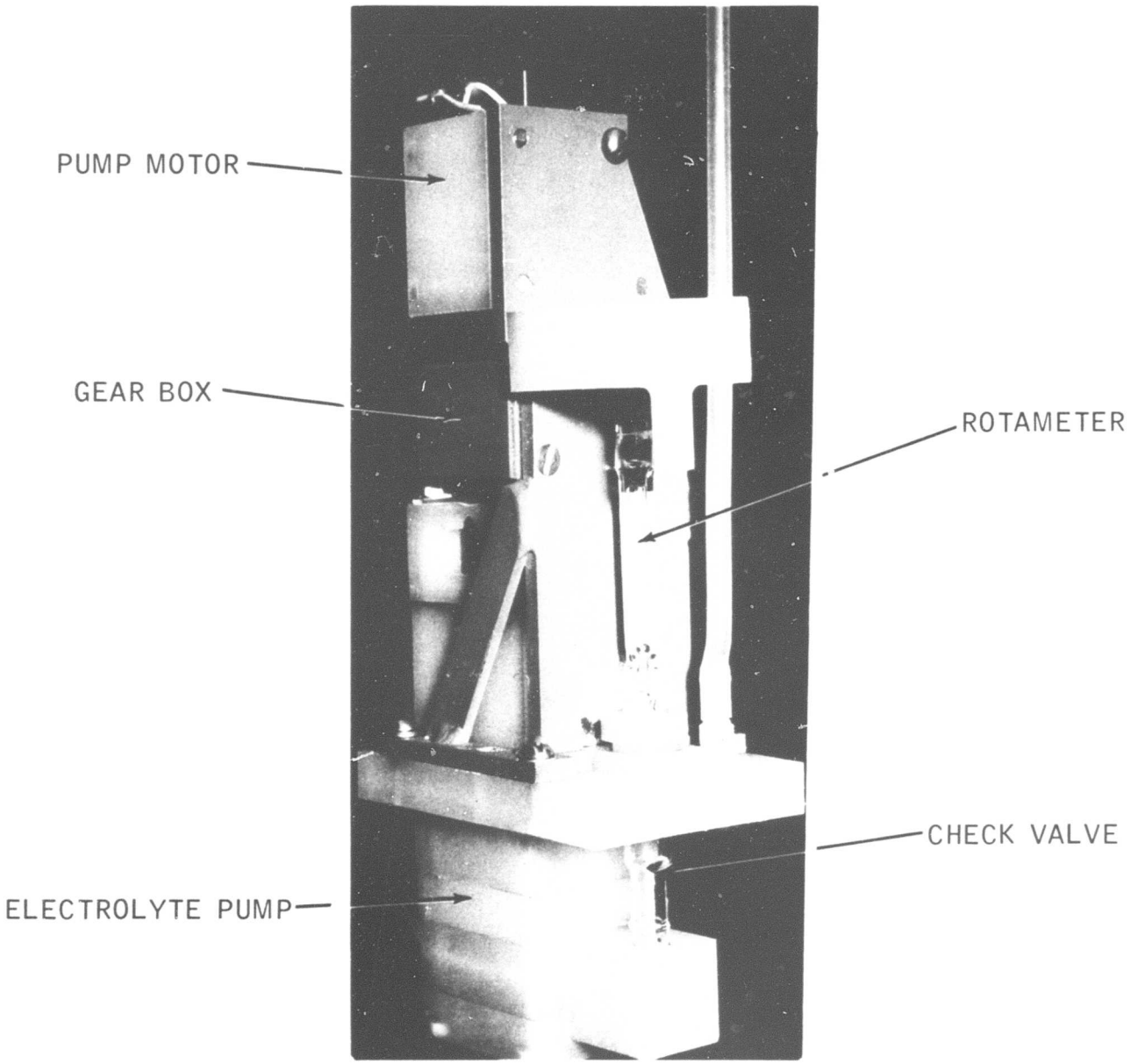

B. Hydrometer Float Assembly

Figure G-3

Hydrometer Float Assembly

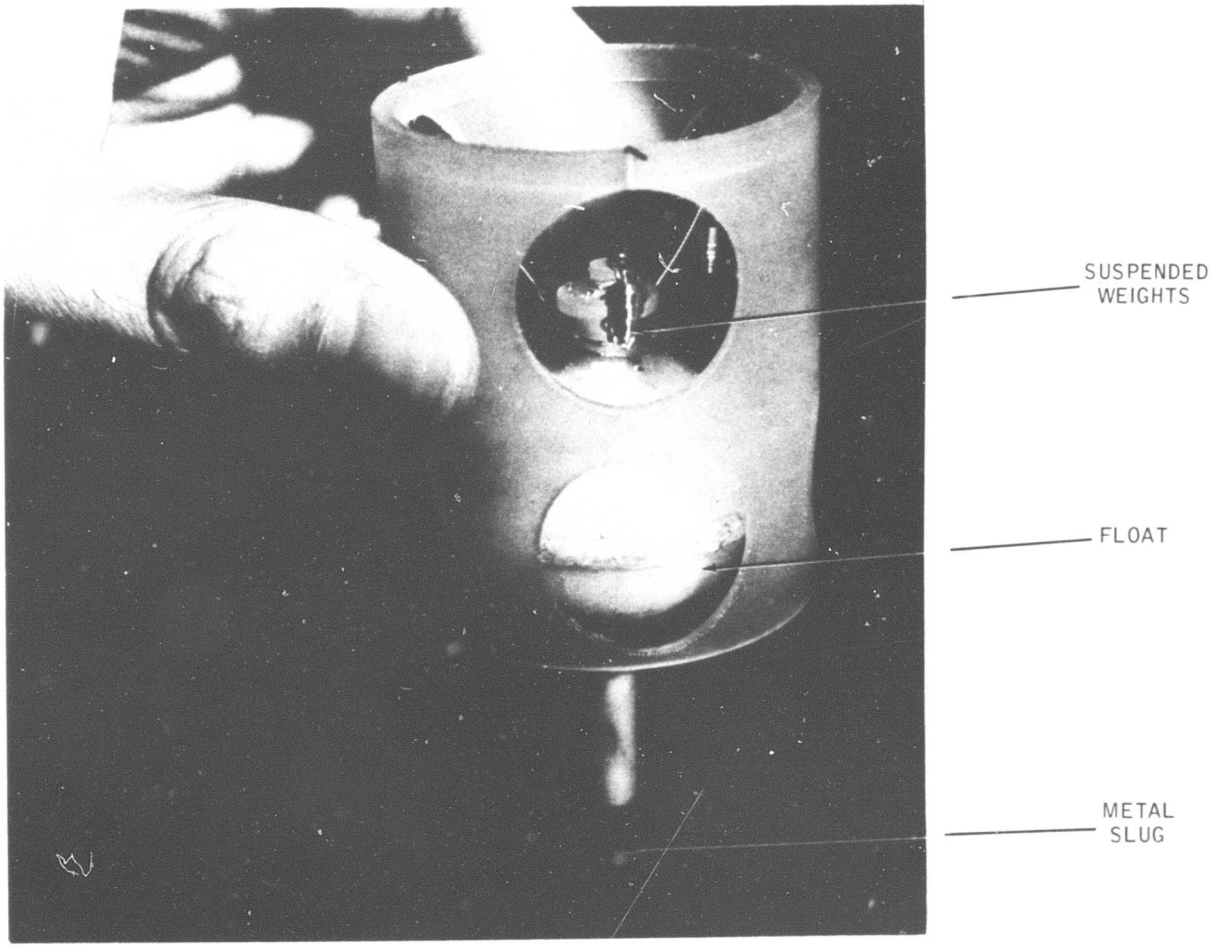

C. Air Condenser

Figure G-4

Air Condenser

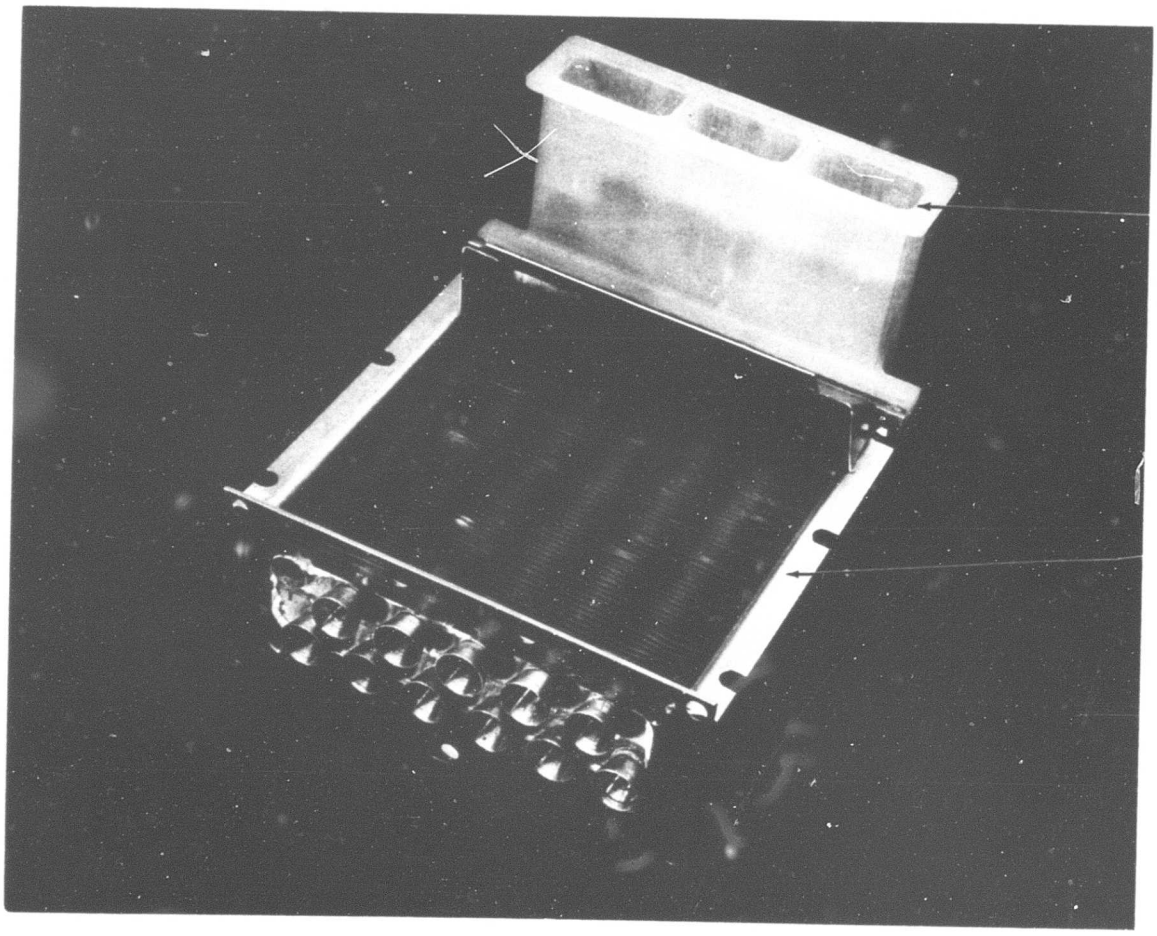

D. Air System Transition Ducts

Figure G-5

Air System Transition Ducts

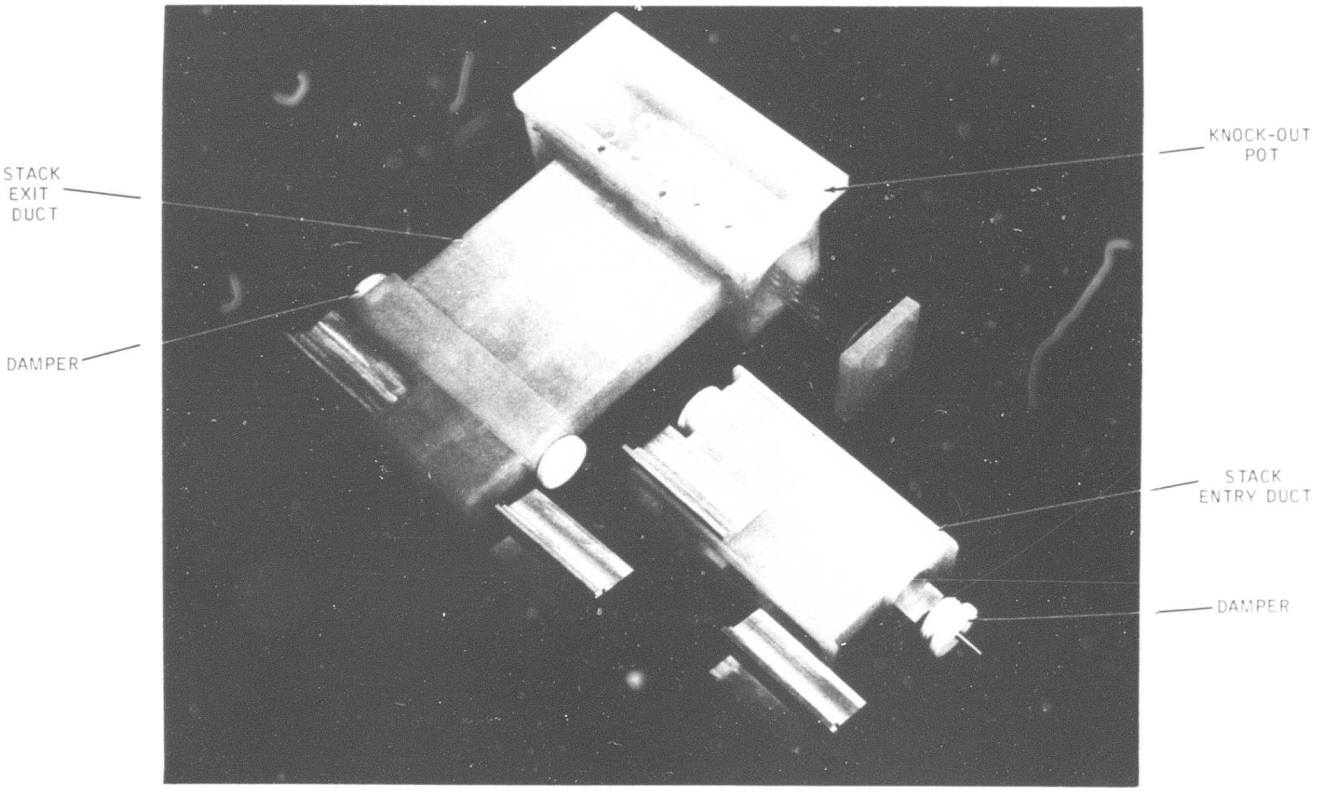

E. Electrolyte Cooler

Figure G-6

Electrolyte Cooler

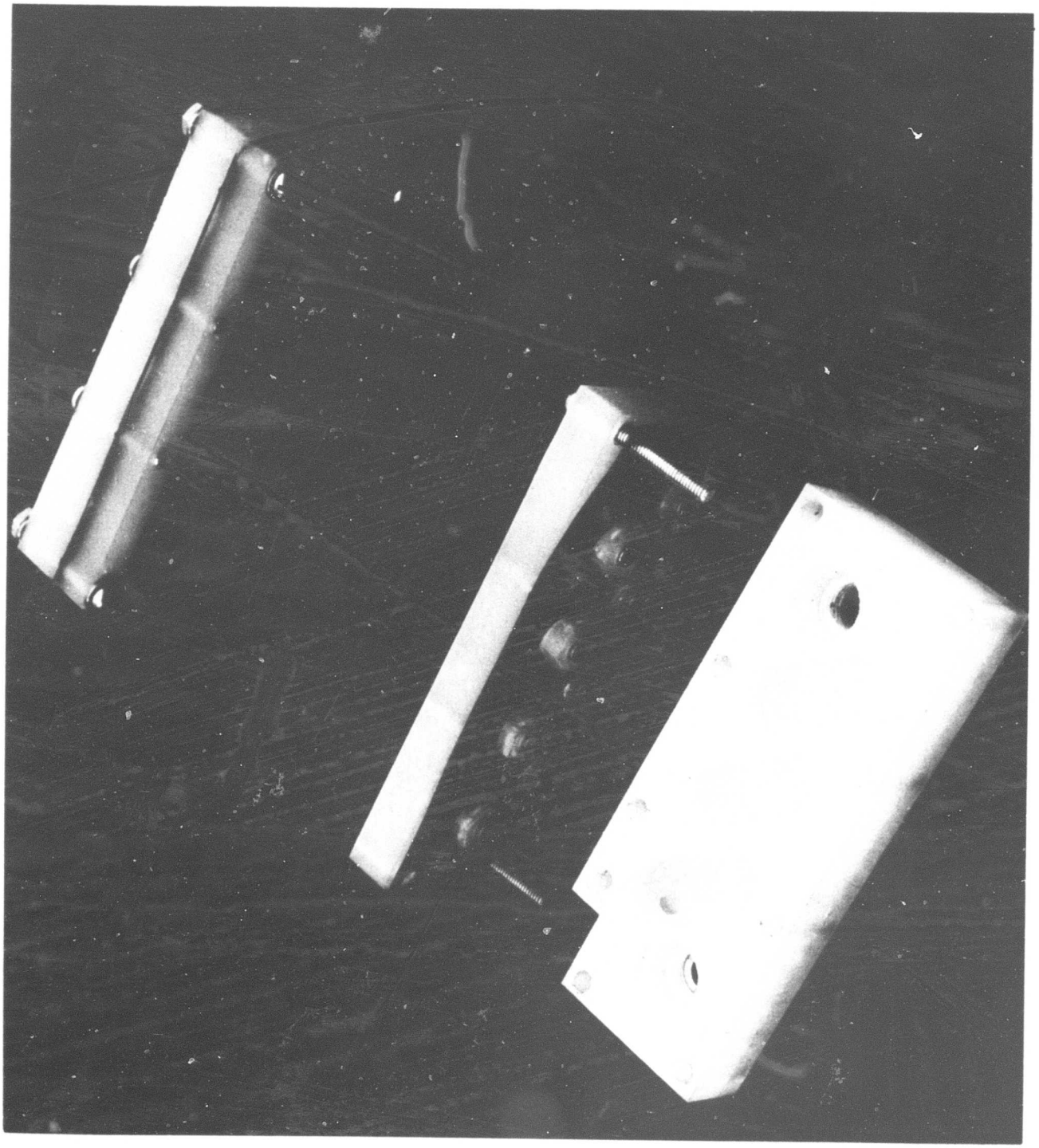

F. Valve Assemblies

Figure G-7

Valve Assemblies

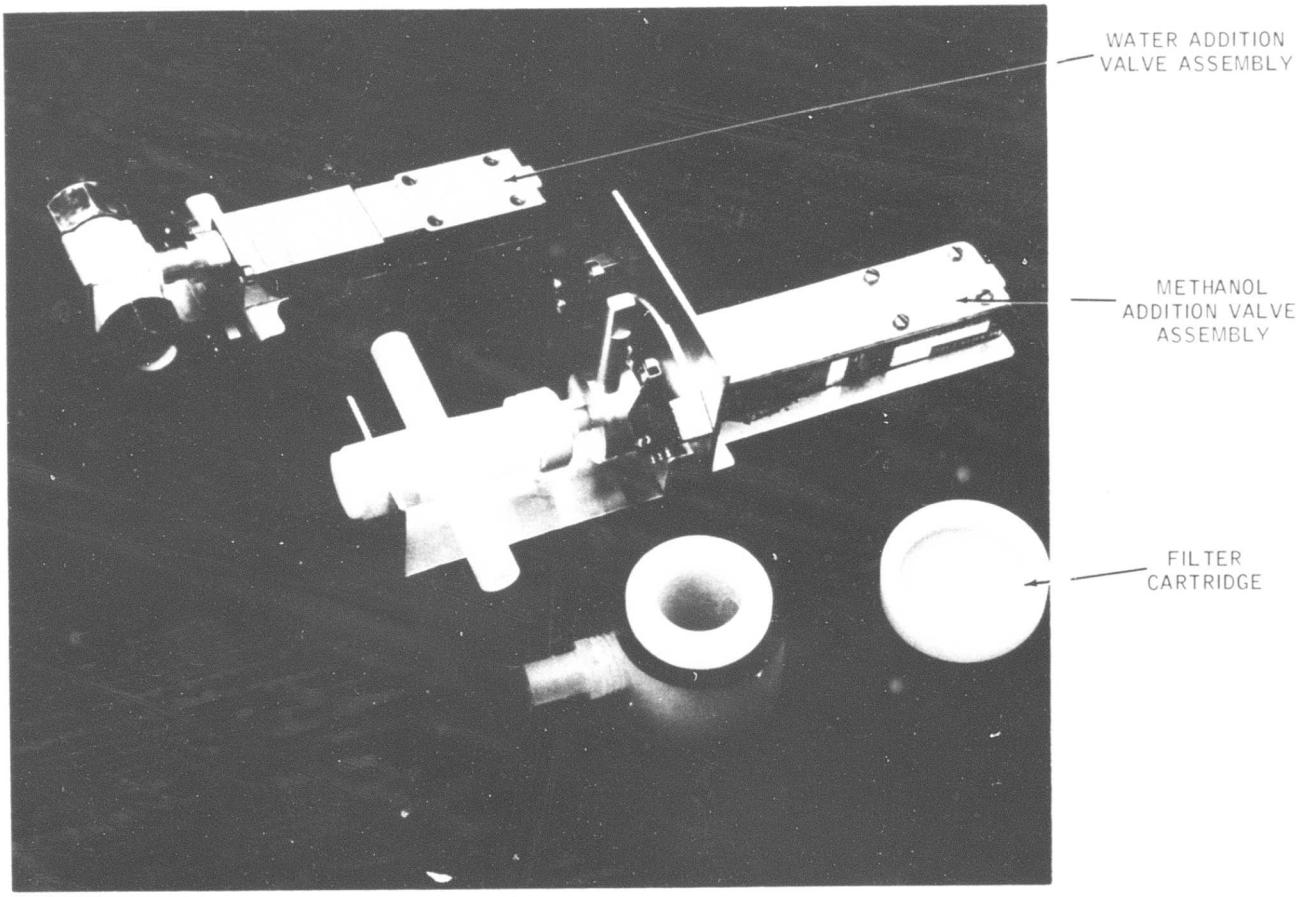

G. Manifolds

Figure G-8

Manifolds for Twenty Cell Stack

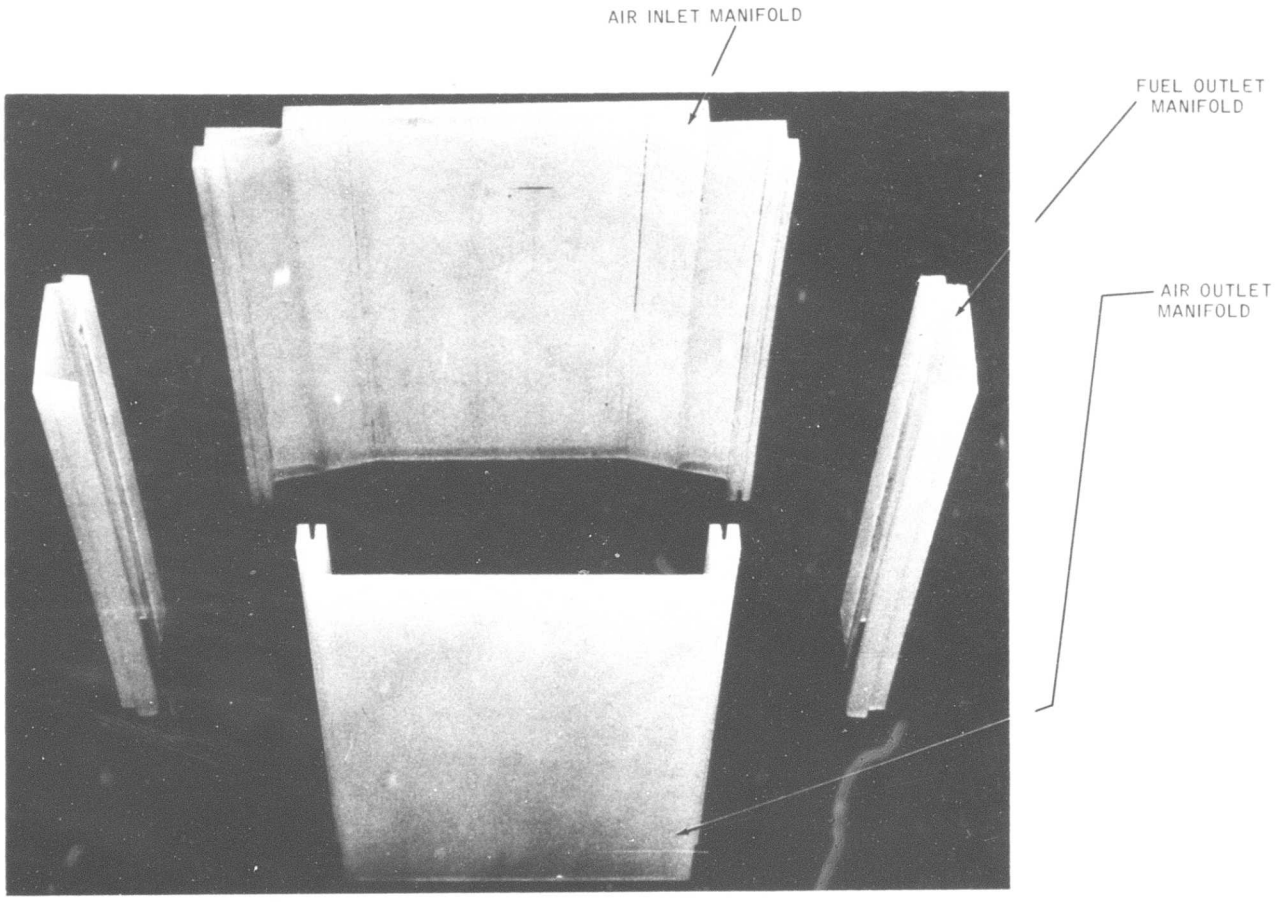

APPENDIX G-8

ELECTROLYTE CIRCULATION SYSTEM

A. Pump and Hydrometer Assembly Drawing

Figure G-9

Pump and Hydrometer Assembly Drawing

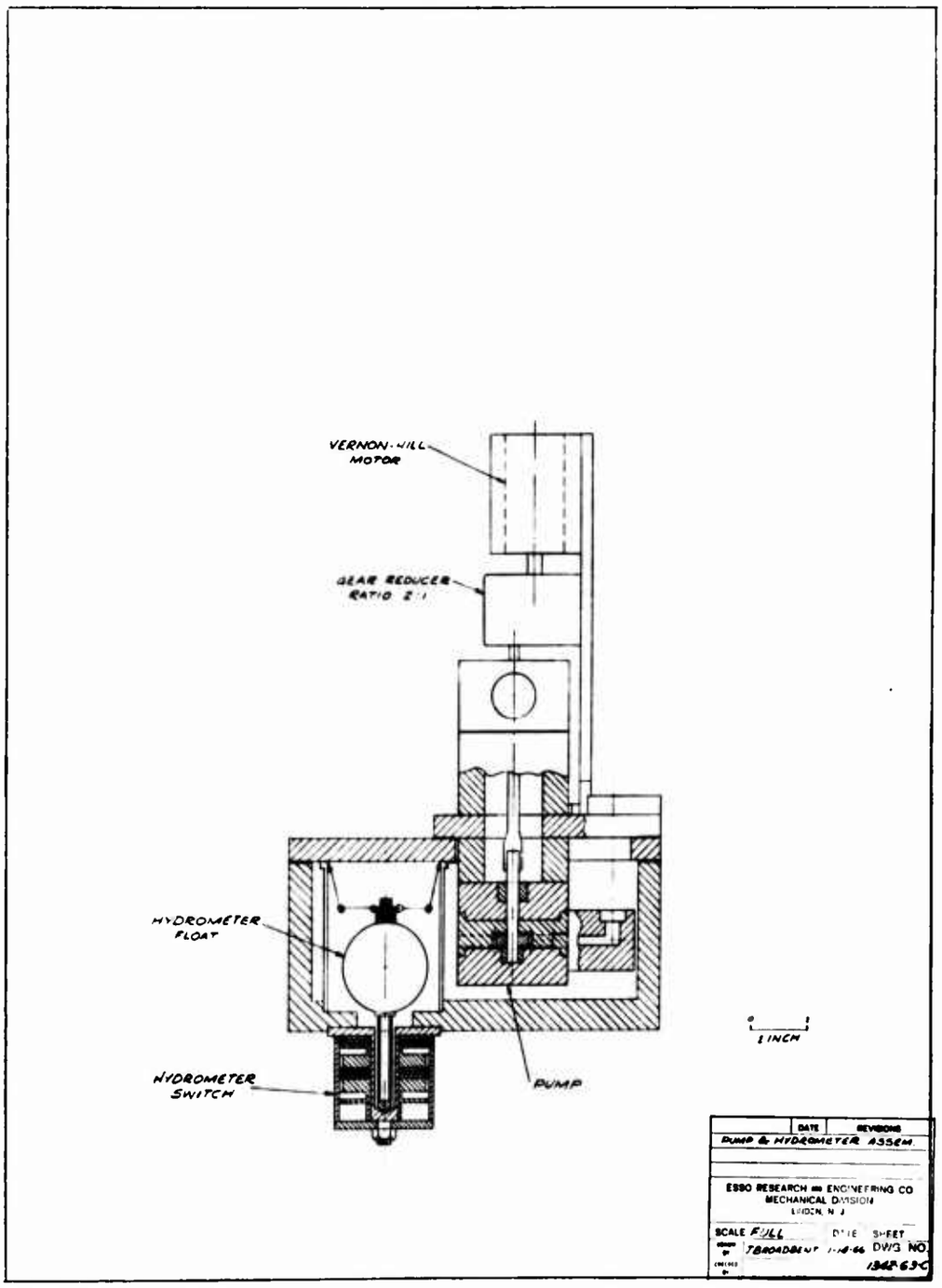

B. Calibration Charts

Figure G-10

Electrolyte Pump Calibration

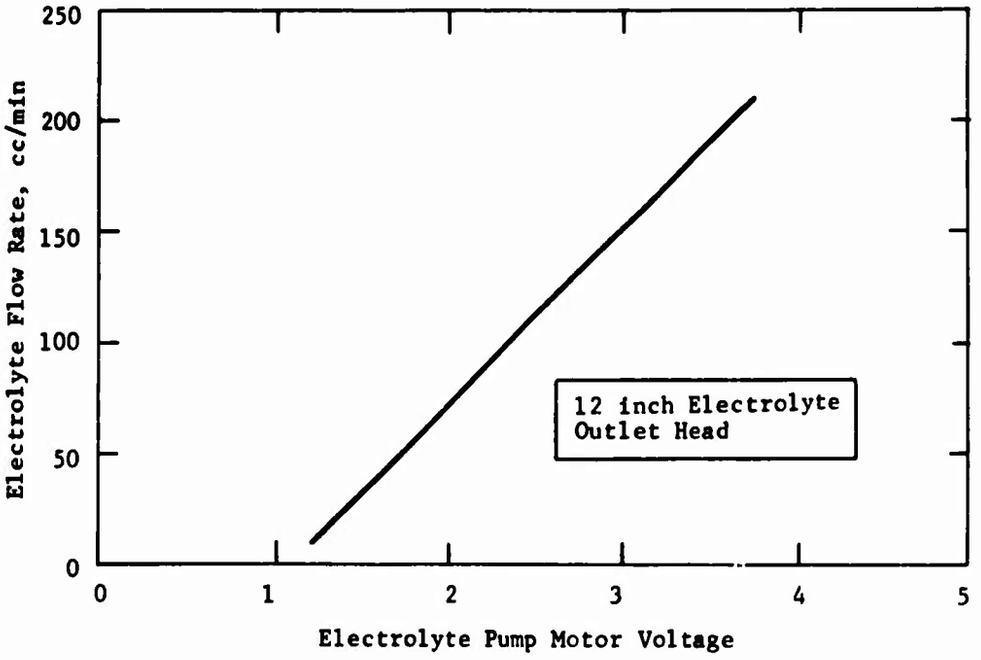

Figure G-11

Electrolyte Rotameter Calibration

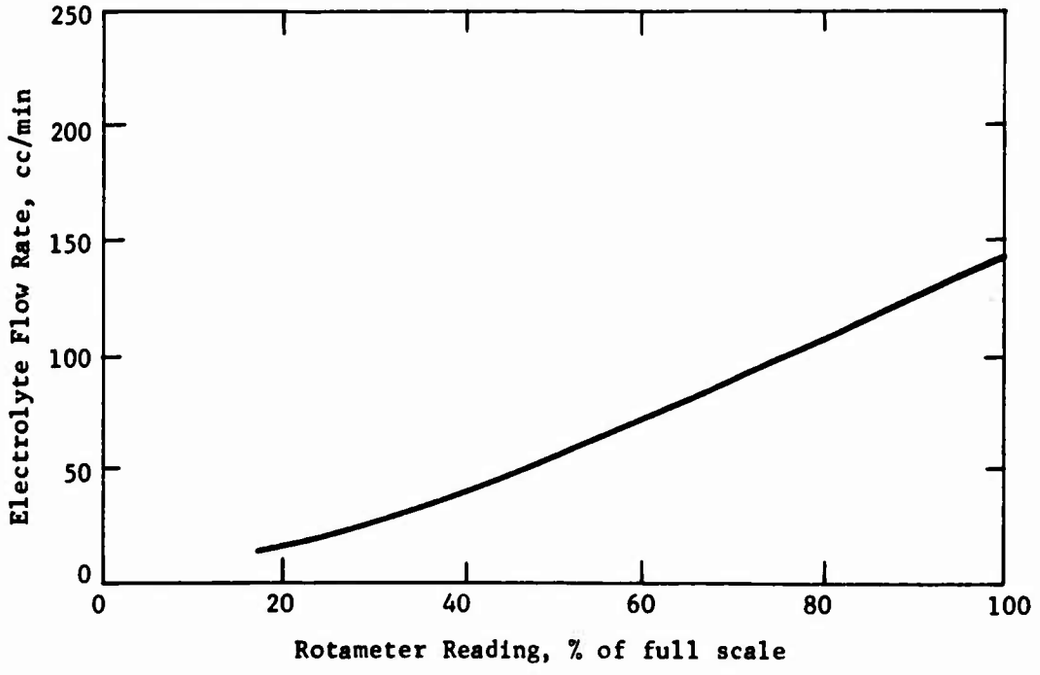

APPENDIX G-9

ASSEMBLY DRAWINGS FOR COMPONENTS IN BATTERY DEMONSTRATOR

A. Water Tank

Figure G-12

Water Tank Assembly

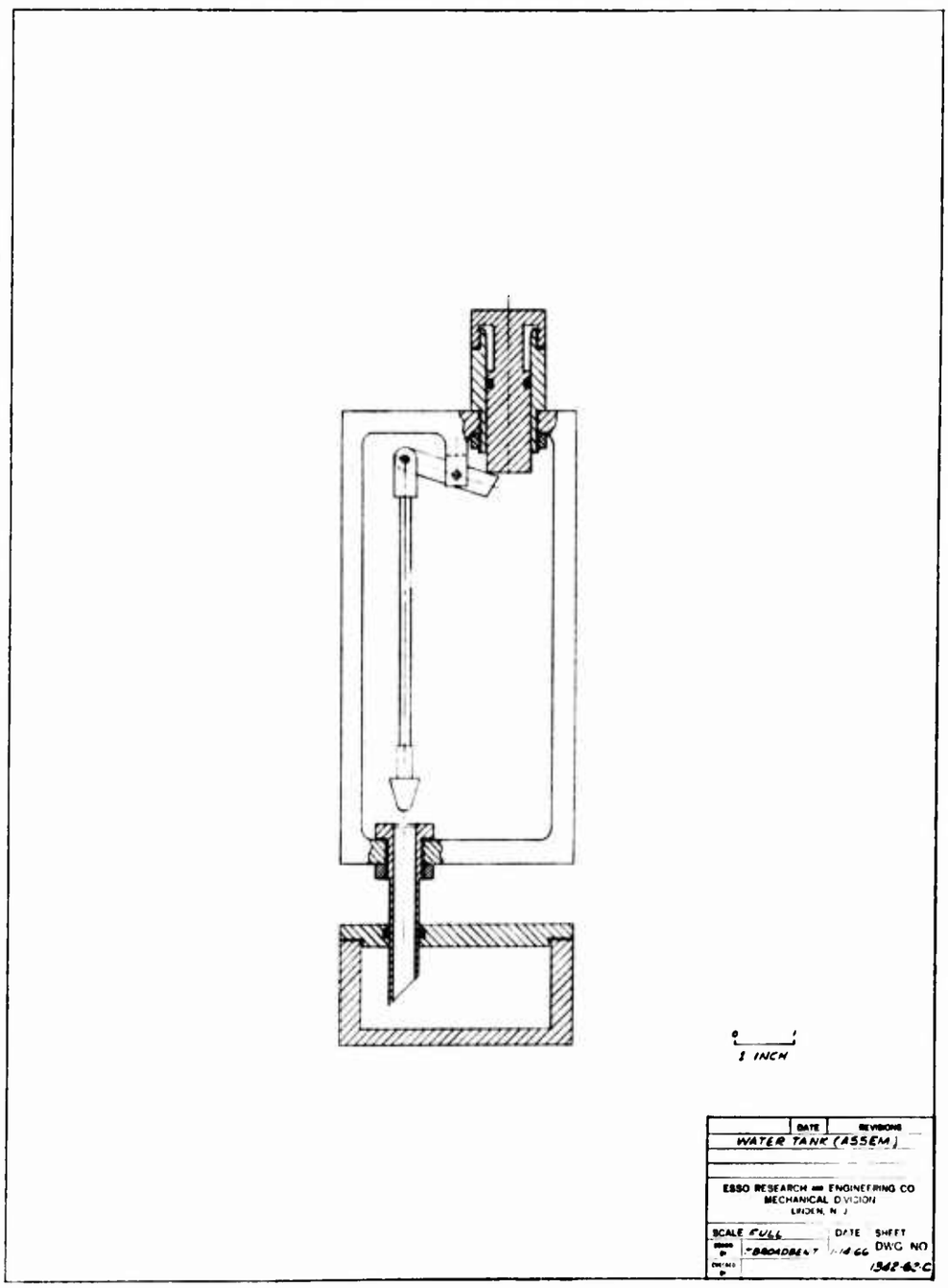

B. Water Economy Unit

Figure G-13

Water Economy Unit

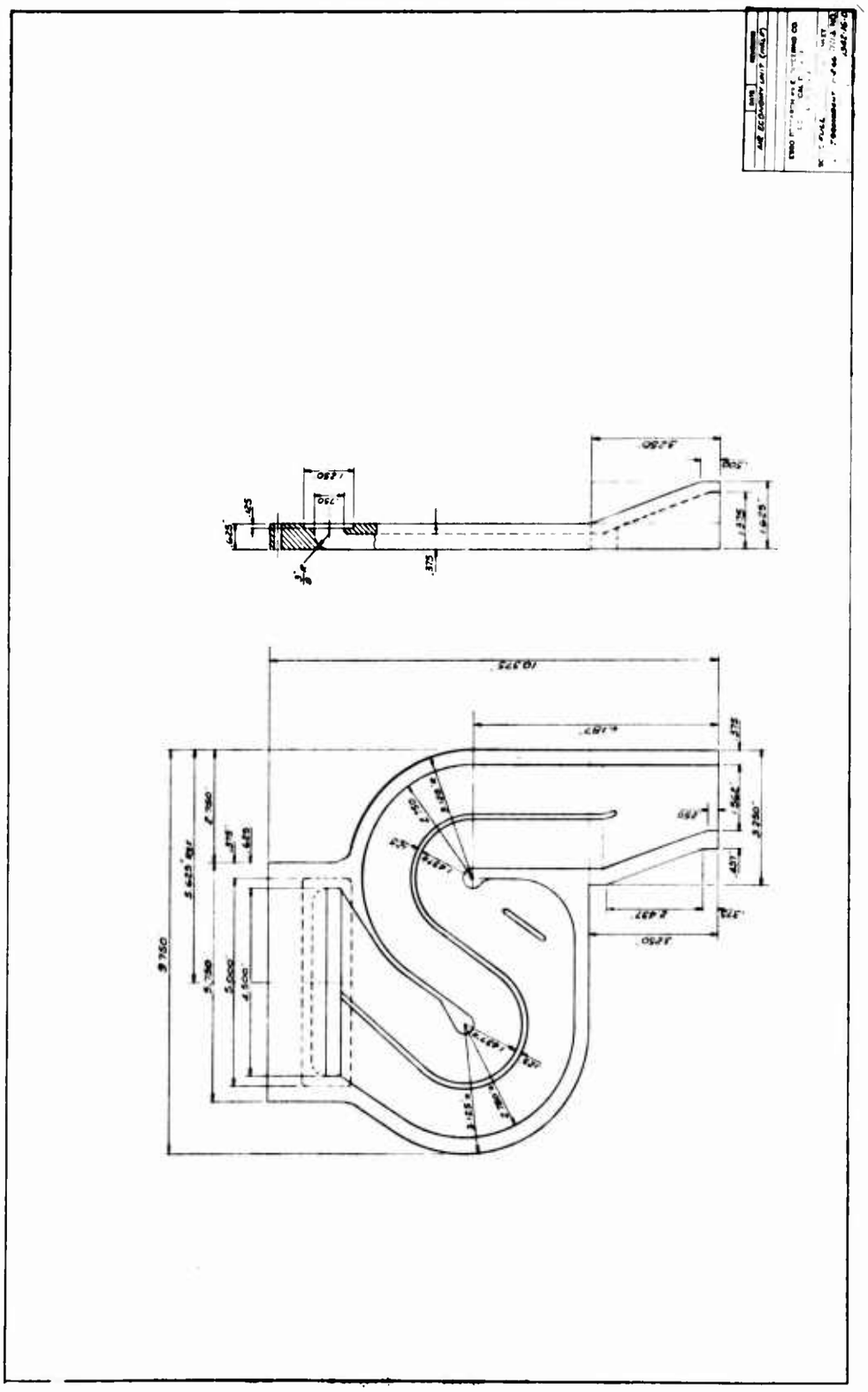

C. Electrolyte Cooler

Figure G-14

Electrolyte Cooler

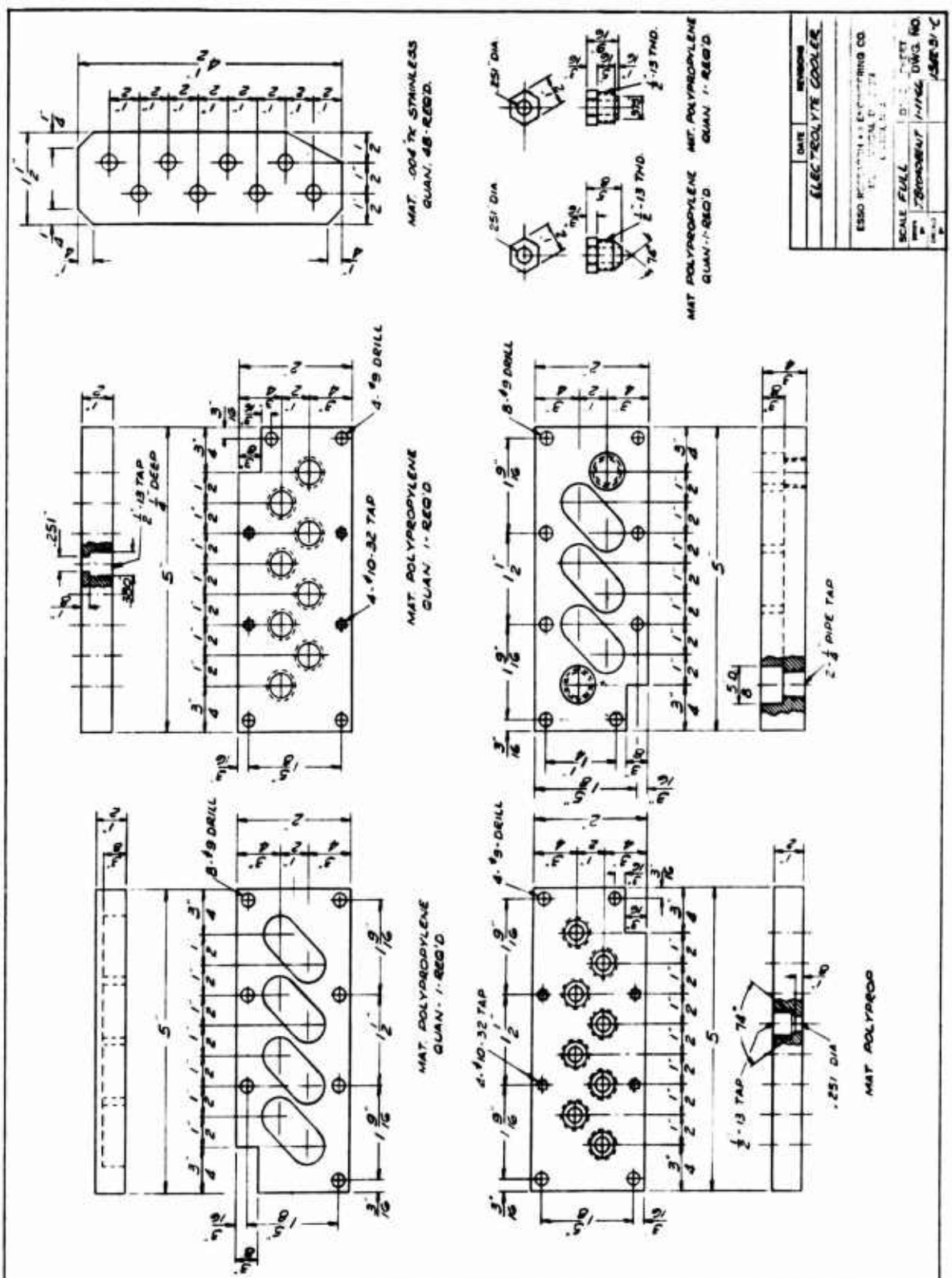

D. Methanol Analyzer Housing

Figure G-15

Methanol Analyzer Housing

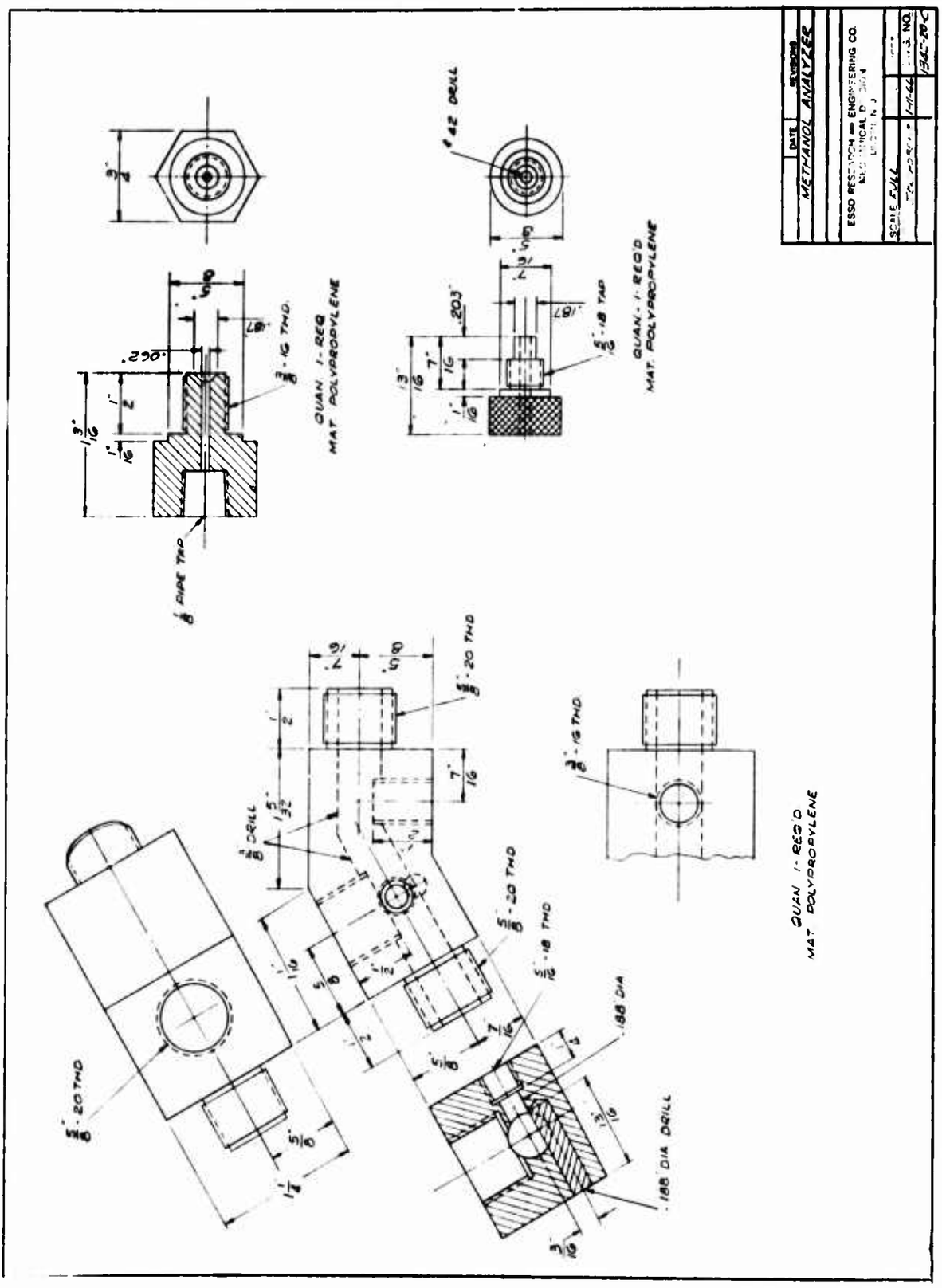

E. Methanol Analyzer Anode Holder

Figure G-16

Methanol Analyzer Anode Holder

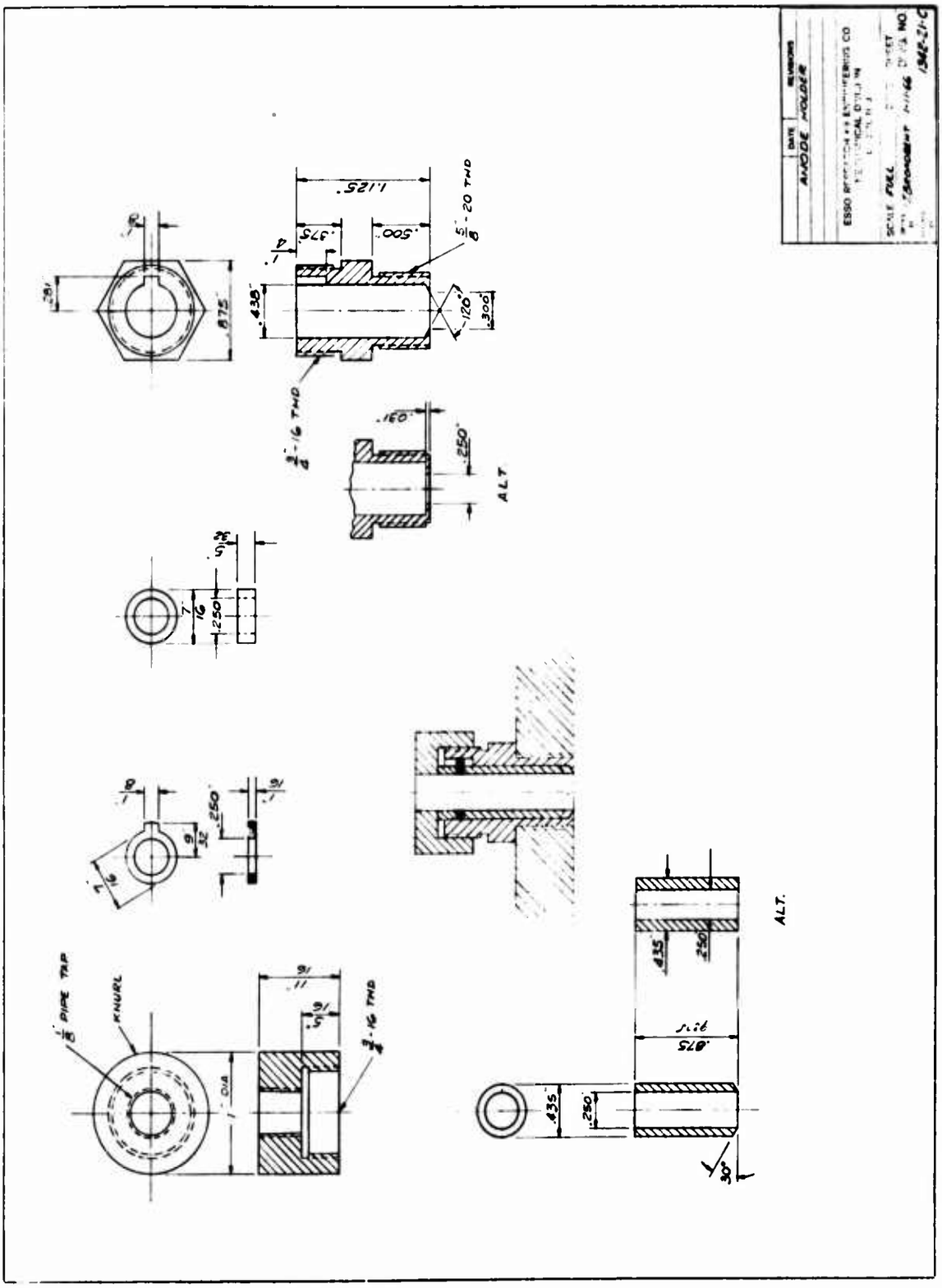

APPENDIX G-10

PERFORMANCE OF AIR CONDENSER

Simulated Stack Effluent[1]		
Flow Rate, cc/min at STP	Temp, °C	Condenser Effluent Temp, °C[2]
20,000	52	31
27,000	52	36
40,000	52	39
60,000	52	43
20,000	56	33
27,000	56	39
40,000	56	43

(1) Presaturated at indicated temperature.

(2) Ambient temperature was 26°C. Cooling fan operated at 4 volts and 18 ma.

APPENDIX G-11

PERFORMANCE OF WATER ECONOMY UNITS

A. Evaluation of Low Pressure Drop Unit for Use in Battery Demonstrator

Inlet Air Temp, °C(1)	Air Flow Rate, cc/min at STP	Water Recovery, wt %
43	20,000	20
	30,000	16.5
	40,000	12.6
	50,000	9
	60,000	5
52	20,000	20
	30,000	15
	40,000	10
	50,000	5.6
	60,000	1

(1) Presaturated at indicated temperature.

B. Evaluation of High Pressure Drop Unit

Inlet Air Temp, °C	Air Flow Rate, cc/min at STP	Water Recovery, wt %
46	36,000	52.3

APPENDIX G-12

THE METHANOL CONTROL SYSTEM

The methanol control system consists of a detecting analyzer and the associated electronic circuitry required to control the addition rate of methanol to the circulating electrolyte stream entering the fuel cell stack. Studies were made to define the response characteristics of this system and to define the best means for incorporating the system into the Methanol Fuel Cell Battery Demonstrator.

Methanol Analyzer

The methanol analyzer measures the current of a small anode under conditions where methanol transport to this detecting electrode is limited by a membrane rather than by the catalyzed reaction. In this situation, the current is essentially independent of factors causing changes in catalyst activity or electrode performance.

The basic analyzer element consists of a diffusion-restricting membrane pressed tightly to the surface of a platinum electrode. The potential of the electrode is maintained at about 0.85 volts versus a hydrogen-evolving cathode, a level where methanol oxidation is diffusion limited. Under these conditions, all the fuel reaching the electrode is oxidized to carbon dioxide, and the current is directly proportional to the methanol concentration on the other side of the membrane. The current is temperature dependent, with an apparent energy of activation of about 4 Kcal/mole. Additional details of the principles involved were presented in an earlier report (7). Drawings of the polypropylene analyzer housing and the electrode holders used in these studies are given in Appendix G-9.

Analyzer Anode Study

The initial analyzer anodes, fabricated from Permion 1010 membrane and Cyanamid AA-1 electrodes, had poor life characteristics. Failure occurred primarily as a result of membrane detachment. Therefore, a study was made of alternative components and fabrication procedures.

Nalfilm 3C membrane was found to be an effective substitute, particularly when a thin coating of gold was electrodeposited on one face. As shown in Figure G-17, Nalfilm electrodes were more permeable to methanol and gave higher analyzer currents than the Permion membrane anodes. The response to concentration, however, was still linear up to about 1.75 M methanol. The gold-coated Nalfilm membrane was chosen for further study because of its stability to high temperature. The pressing procedure was also modified by using a porous Teflon platen face to equalize pressure distribution.

Figure G-17

Effect of Methanol Concentration on Analyzer Anode Response

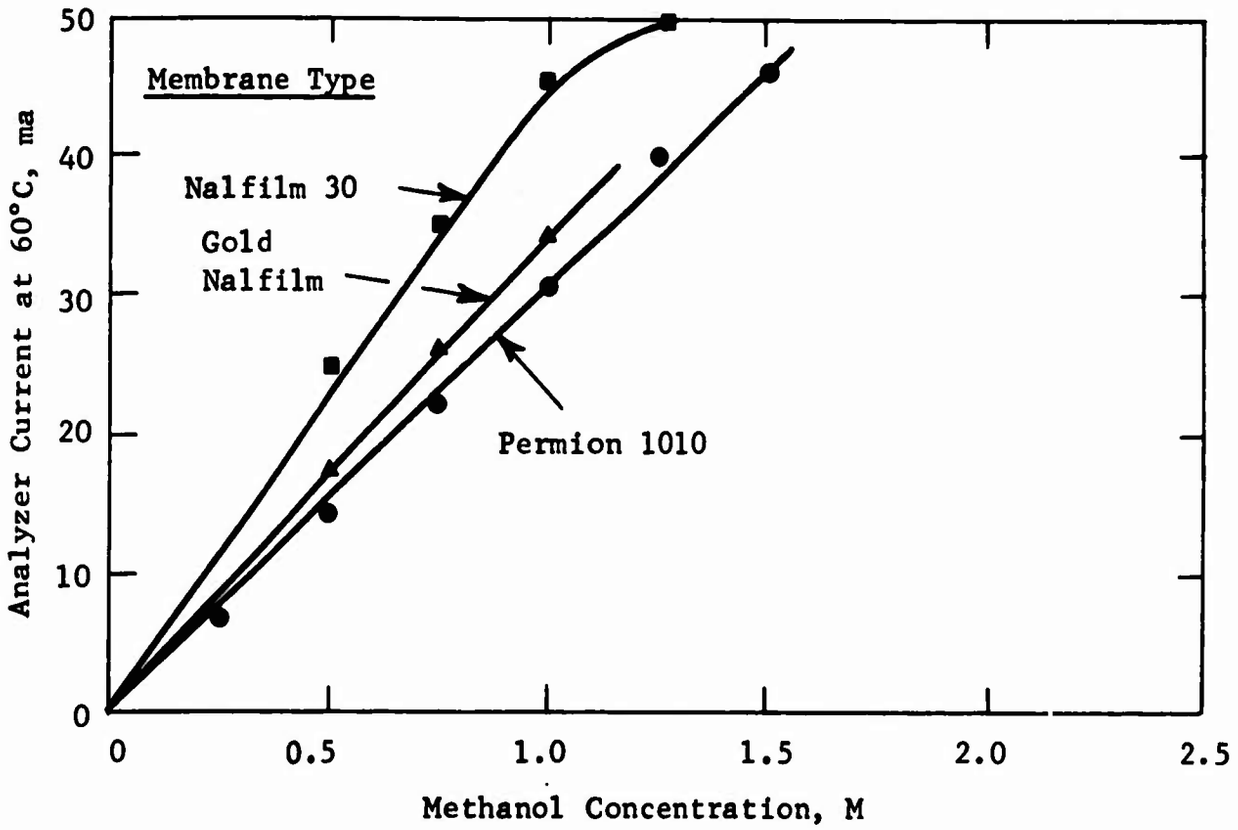

A number of anodes were fabricated and evaluated, primarily in static test units. Occasional testing was done in flowing electrolyte systems. Test conditions ranged from 25 to 70°C and 0.25 to 1.5 M methanol. High concentrations of methanol were used to accelerate the effect of stresses on the membrane-electrode bond caused by carbon dioxide evolution. Average life of the gold-coated Nalfilm anodes exceeded 500 hours, as shown in Table G-1.

Table G-1

Life Testing of Methanol Analyzer Anodes

Status	Number	Comments
Operative(1)	10	Age distribution: 1000 + hrs 3 500-1000 hrs 3 500 hrs 4
Nonlinear Concentration Dependence	2	Tests terminated after 600-1000 hrs stable operation
Failed	3	Failed after 400-600 hrs

(1) Gold-coated Nalfilm 30 membrane anodes tested primarily in static systems at 25-70°C and 0.25-1.5 M CH_3OH in 3.7 M H_2SO_4.

Additional quality control studies showed that anode fabrication variables were in reasonable control. Anode current usually ranged from 10 to 15 ma at 38°C for 0.75 M methanol, as shown in Table G-2. Variations in the current level were probably caused by variations in the membrane porosity and the thickness of gold coating. Also, the temperature response characteristics of the anodes were quite consistent.

Table G-2

Methanol Analyzer Anode Quality Control

Current Range for 0.75 M CH_3OH at 38°C, ma(1)	Number of Anodes	Temperature Coefficient Range(2)	Number of Anodes
5-9.9	1	1.5-1.69	3
10-14.9	6	1.7-1.89	9
15-19.9	3	1.9-2.09	2
20-24.9	5	2.1-2.29	1
25-29.9	0		

(1) Gold-coated Nalfilm membrane.

(2) Temperature coefficient = $\frac{\text{Current at 60°C for 0.75 M } CH_3OH, \text{ ma}}{\text{Current at 38°C for 0.75 M } CH_3OH, \text{ ma}}$

Open-Loop Control Study

The response characteristics of the methanol analyzer were evaluated in a simulation loop, shown schematically in Figure G-18. Electrolyte, containing low concentrations of methanol, flowed through the analyzer. Programmed amounts of methanol were periodically injected into the electrolyte ahead of the analyzer, and the response of the analyzer current was noted.

These studies showed that the analyzer gave essentially instantaneous response to step changes in methanol concentration. Initial results with Permion membrane anodes indicated only moderate increases in analyzer current due to increased flow rate at constant methanol concentration. Subsequent studies with the more permeable Nalfilm membrane showed greater sensitivity to flow rate. Here the film diffusion resistance is apparently a significant portion of the overall diffusion path resistance from the bulk electrolyte through the membrane to the anode surface.

Figure G-18

Schematic Flow Diagram of Analyzer Simulation Loop

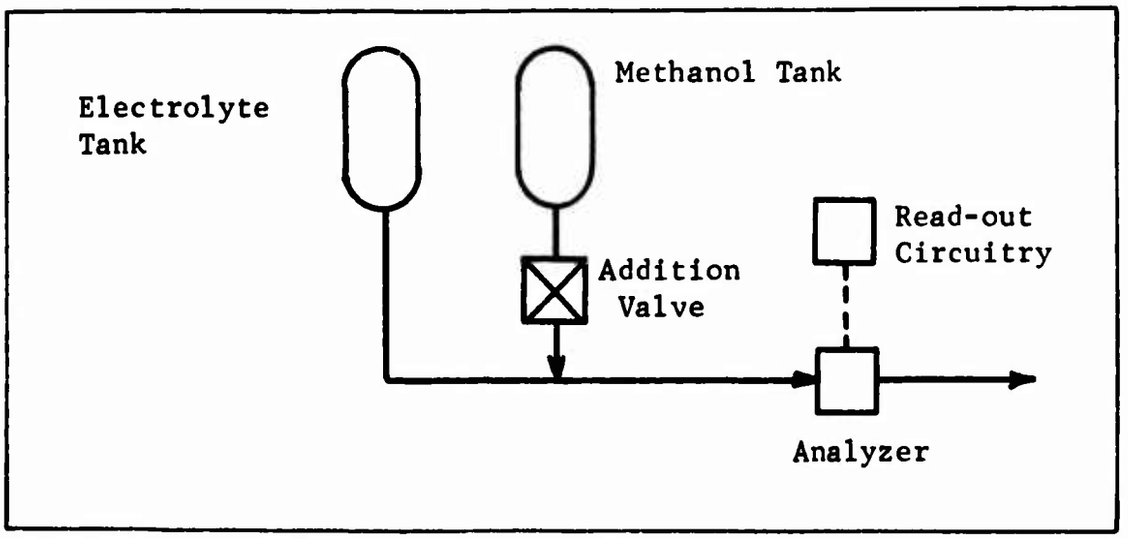

Closed Loop Control

The methanol analyzer was evaluated in conjunction with the sixteen cell stack containing 9" x 5-3/4" electrodes. The signal current from the analyzer was used to control the action of a motor-driven addition valve so as to maintain methanol concentration at 0.75 M, a level found optimum in previous studies (7).

A number of factors causing control instability were found. These are listed in Table G-3 together with the corrective action taken.

Table G-3

Causes of Control Instability

Cause	Remedy
• Large dead time between injection and detection points.	• Minimize distance between points.
• Lack of electrolyte flow during decreasing stack load, caused by changes in electrolyte displacement volume.	• Insertion of upper electrolyte sump or reservoir between stack and analyzer so that some electrolyte continually flows past analyzer at low loads.
• Back-flow of electrolyte up methanol addition line.	• Insertion of methanol-wetted porous polypropylene plug at injection point.
• Valve motor inertia at low operating voltages.	• Use of time-sequenced pulses of high constant voltage. See Figure G-19.
• Large over and under-riding of valve travel, resulting in over or under-feeding pulses.	• Micro-limit switches added to motor circuitry to limit travel and hence flow rates to desired maximum and minimum values. See Appendix G-7, Figure G-7.
• Flow-dependent analyzer current signal.	• Lowering analyzer cell voltage at high flow rate to compensate for higher transport rates, based on data in Figure G-20.

Figure G-19

Voltage Characteristics of Methanol Addition Valve Motor

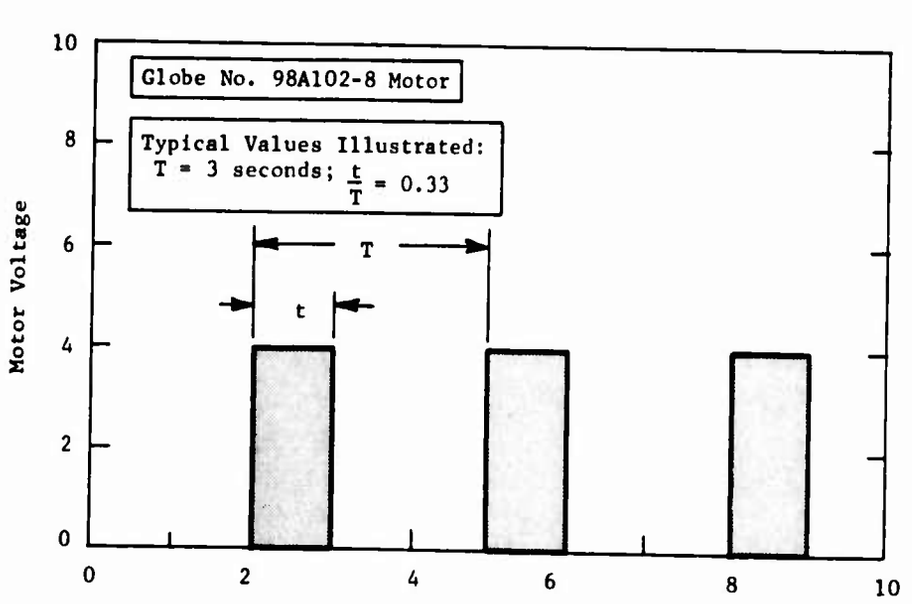

Figure G-20

Effect of Cell Voltage on Analyzer Current

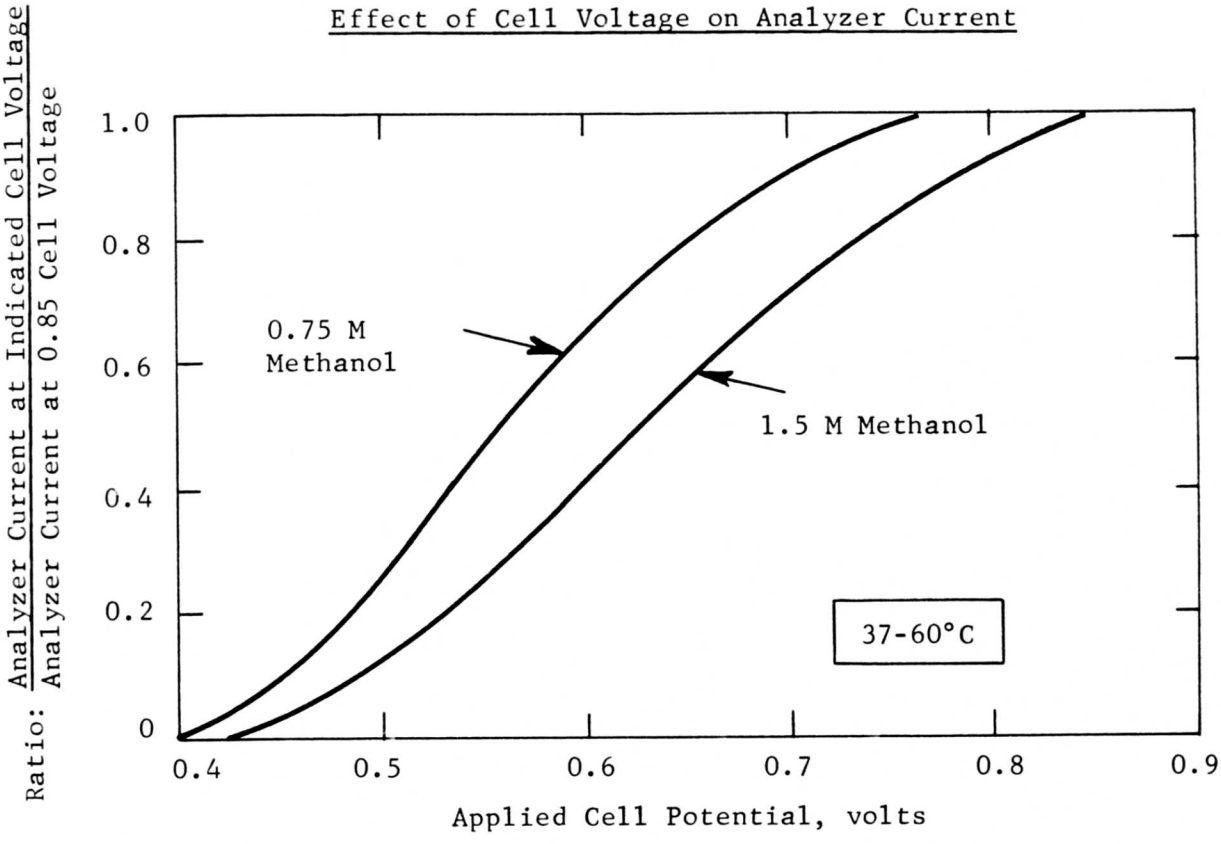

The control system provided compensation for the effect of temperature on the diffusion properties of the membrane anode. A thermistor placed in series with the analyzer cell was used. The effects of temperature on the analyzer current and thermistor resistance are shown in Figure G-22; complete details are given in Appendix G-13.

Tests with the sixteen cell stack showed that stable operation could be achieved, with methanol concentration ranging up to ± 0.1 M about the 0.75 M control point.

The final control system was tested only briefly in the Battery Demonstrator. Stable operation was not achieved during tests in our laboratories.

Figure G-21

Effect of Temperature on
Analyzer Current and Thermistor Resistance

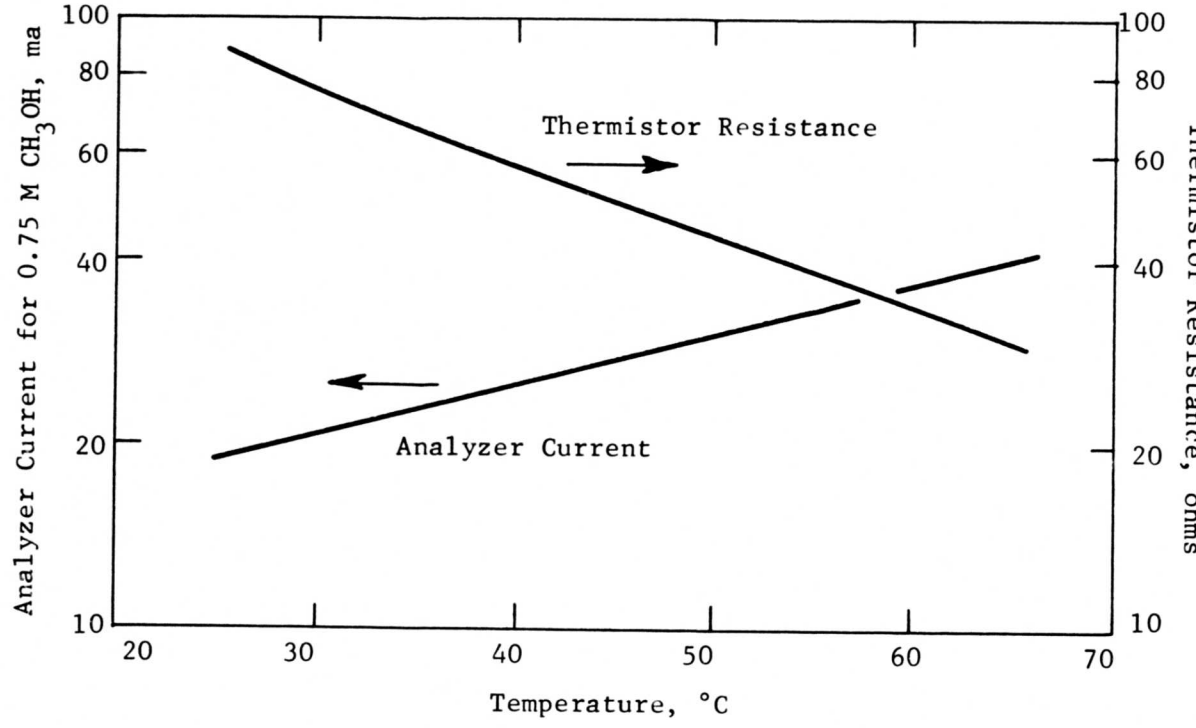

Figure G-22

Simplified Schematic of Analyzer Circuitry

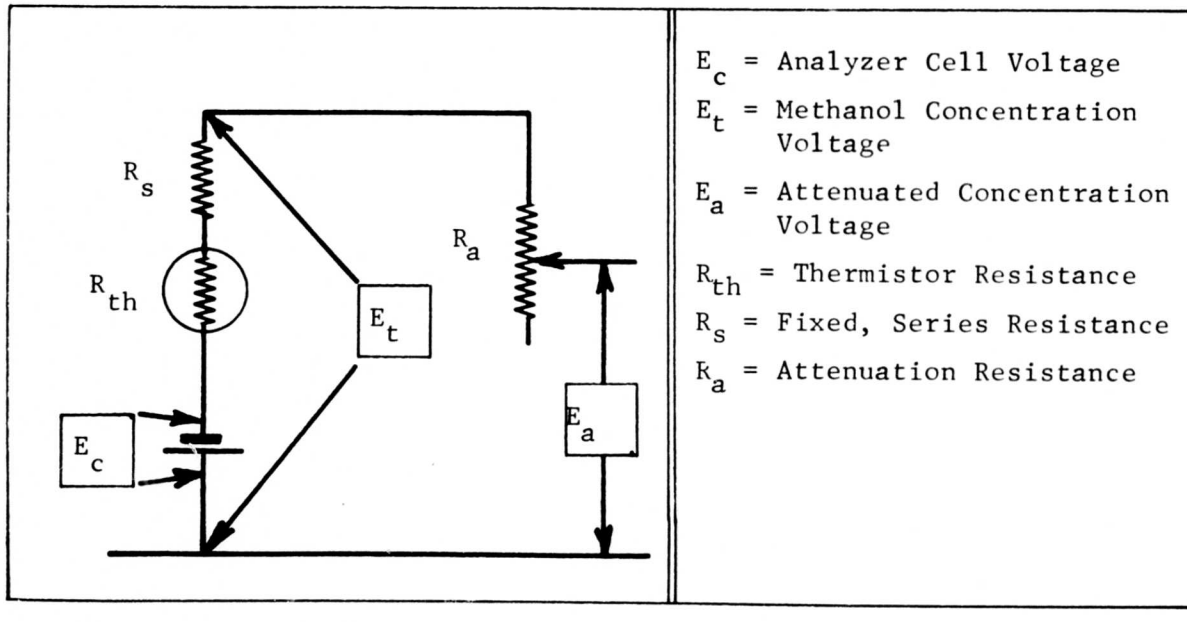

APPENDIX G-13

ELECTRICAL CONTROL SYSTEM FOR METHANOL FUEL CELL BATTERY DEMONSTRATOR

The electrical control system includes means for main power switching, load and voltage indication, output voltage regulation, process control, visual alarm indication, and detailed performance monitoring. All electrical equipment is contained within the Battery Demonstrator, except the performance monitoring facility.

Main Power Switching

The main power system is activated in two steps; STAND-BY and REGULATED. Switches driven along with the process block valves connect the fuel cell stack to the auxiliary circuits and the output regulator when the control handle is moved from OFF to STAND-BY. Small mercury batteries are connected to the electrolyte pump and air blower by the same action. No power is available at the output plug until the control handle is rotated to the REGULATED position. In this position the mercury batteries are disconnected from the pump and blower circuit. All power is supplied by the fuel cell stack. A block diagram of the electrical system is shown in Figure G-23.

Load and Voltage Indication

Two small meters on the front panel indicate regulated output voltage and current under normal conditions. Small push button switches associated with each meter allow the meters to also indicate the stack voltage and total current from the stack.

Voltage is indicated by a 0-15 volt 1000 ohm/volt meter. Current is indicated on a 50 millivolt meter calibrated 0-25 amperes. This meter reads the voltage drop across either the regulated output 50 mv shunt or an Esterline-Angus 100 mv shunt in series with the stack. Circuit details are shown in Figure G-24.

Voltage Regulator

Output voltage is maintained at a constant level of 6.0 ± 0.1 volts by a series type regulator. The regulator will start under a full load of 16 amperes and pass up to 20 amperes at voltages lower than the regulating level. Circuit details are shown in Figure G-25.

Process Controls

Transistorized electronic circuitry is provided to control process air rate, electrolyte flow rate, cooling air rate, acid concentration, and methanol concentration.

The process air rate is controlled by varying the DC blower motor speed. A DC amplifier and series regulator varies the DC voltage applied to the blower motor in a feedback loop where the command signal is obtained from the total current shunt in series with the stack. Circuit adjustments are provided to set the zero level and maximum motor voltage level of the blower. Circuit details are shown in Figure G-25.

A duplicate of the air blower control is used to regulate the electrolyte flow rate with a DC motor driving the pump. Circuit details are shown in Figure G-25.

Cooling air for the electrolyte heat exchanger is supplied by a fan driven with a DC motor. The fan operates at a fixed preset speed determined by a pulse width type voltage regulator which supplies a fixed voltage to the motor regardless of stack voltage. Circuit details are shown in Figure G-26.

Acid concentration is controlled by adding fresh water to the electrolyte stream through a small motor driven valve. This valve is actuated by a controller which detects the position of the hydrometer in the lower sump. Detection is accomplished by the use of radio frequency coils around the keel of the hydrometer which contains a metal slug. The upper coil controls the water addition circuit. The lower coil actuates the low acid concentration alarm light. Circuit details are shown in Figure G-27.

A small DC motor-driven positioning valve controls the rate of flow of methanol into the electrolyte stream depending on the methanol concentration in the stream. The signal from the methanol analyzer cell is compared to a present reference signal. Any error between these two signals is amplified by the circuitry and actuates the positioning valve motor so as to hold the methanol concentration at a fixed value. Proportioning control features are included in the circuitry to vary the rate of action of the positioning motor depending on the concentration error and the load on the main stack. Circuit details are shown in Figure G-28.

These electronic controls are mounted in compact trays mounted along the lower periphery of the Demonstrator, as shown in Figure G-29.

Visual Alarms

Three visual alarm lights are provided on the front panel. One, as described, for low acid concentration indication; one for indicating high temperature and one for indicating that regulator output voltage is below the regulation range.

The high temperature alarm is actuated by a resistance change in the thermistor in cell 6. Alarm indication occurs at 91°C $\pm$ 2°C.

Low voltage alarm conditions occur at regulator output voltages below 5.9 volts. The alarm circuit compares the regulator output with a fixed voltage reference. Circuit details for the high temperature and low voltage alarms are shown in Figure G-26.

Performance Data Monitor

A 32 terminal connector behind the lower front trim strip provides the means for connecting to a performance data monitoring device. This device is enclosed in a metal box and contains read-out meters, meter switches, process control switches and mercury batteries.

Four meters and four meter switches provide read-out of 26 data points. These include motor currents and voltages, controller voltages, temperature, and anode polarization.

The process control toggle switches on the performance data monitor provide means for over-riding the normal process control systems. This is accomplished by connecting the mercury batteries in the monitor directly to the control devices through the over-ride switches.

Details of the meter and switch functions on the data monitor are presented in Figure G-30. Circuit details are shown in Figures G-31 and G-32. Data readout calibrations are presented in Figure G-33 through G-39. A photograph of the performance monitor is given in Figure G-40.

Electronic Circuitry

The location of the various electronic cards and the identification of adjustment potentiometers are shown in Figures G-41 and G-42.

Connection details for the motors, thermistors, methanol analyzer cell, alarm lamps, and reference electrodes are shown in Figure G-43.

Terminal board location and identification numbers along with the battery box connections are shown in Figure G-44.

Figure G-23

Electrical System

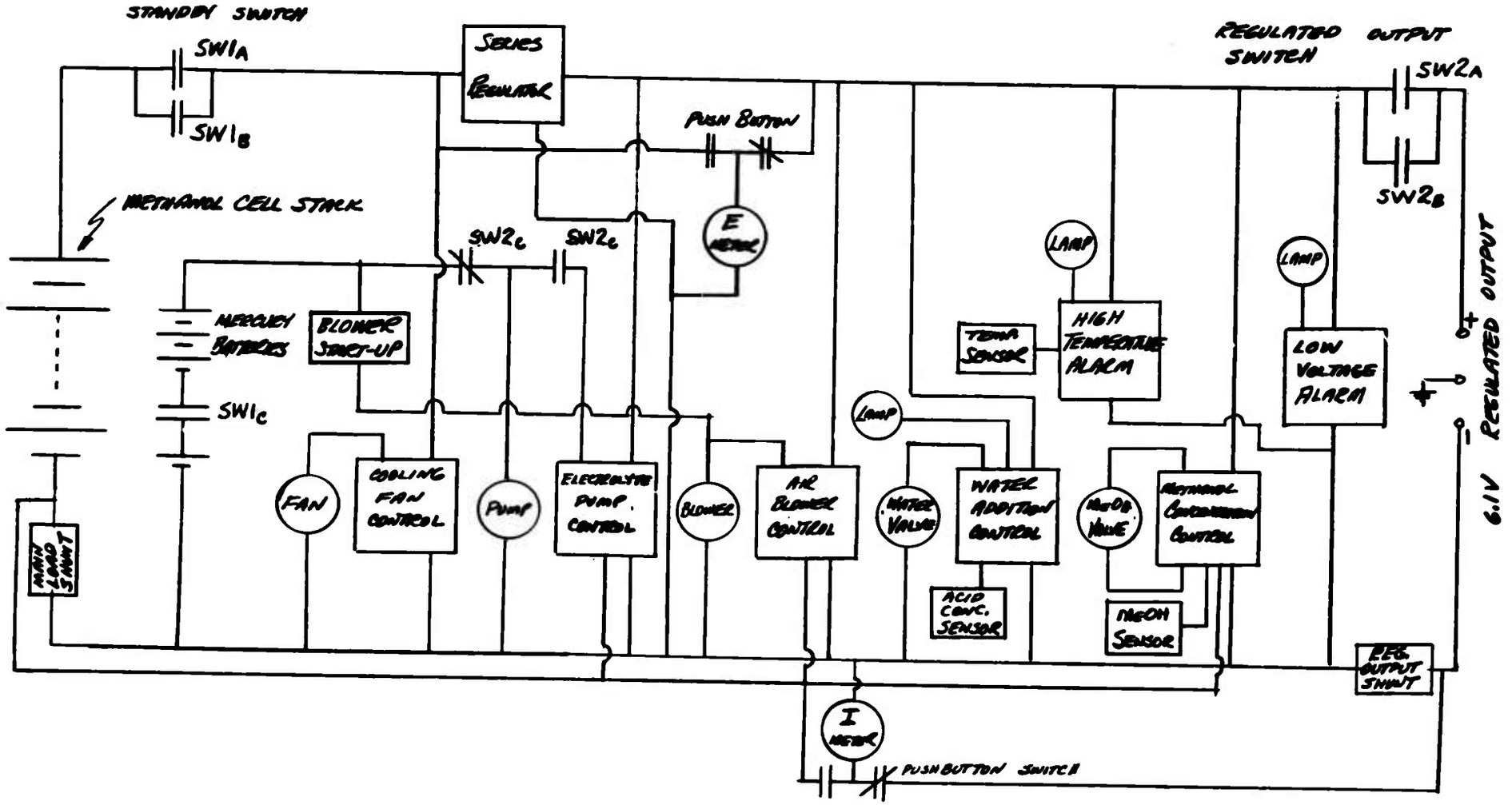

Figure G-24

Bottom Deck Electrical Wiring

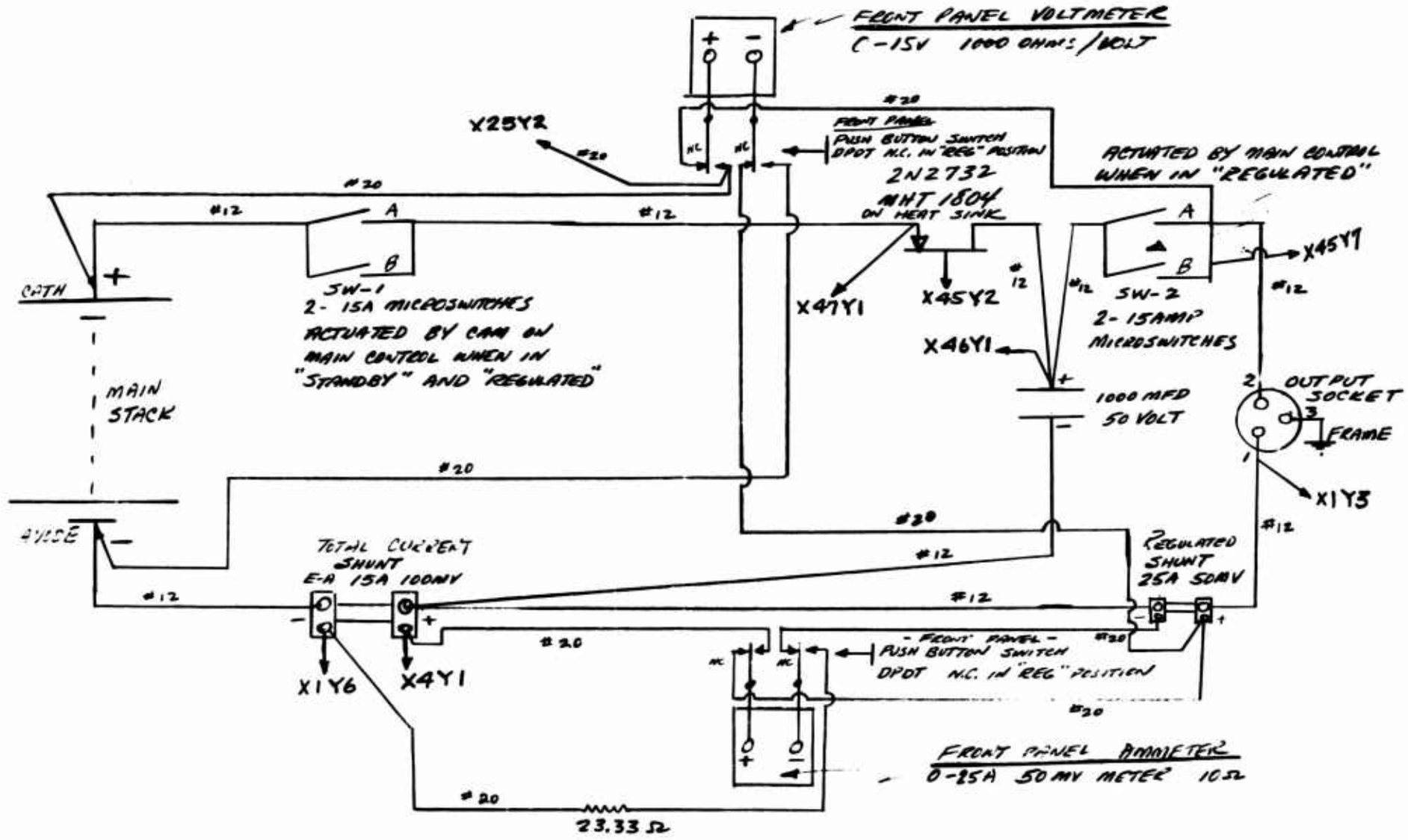

Figure G-25

Electronics - Card "B"

Air Blower Control - Electrolyte Pump Control - Series Regulator Amplifier

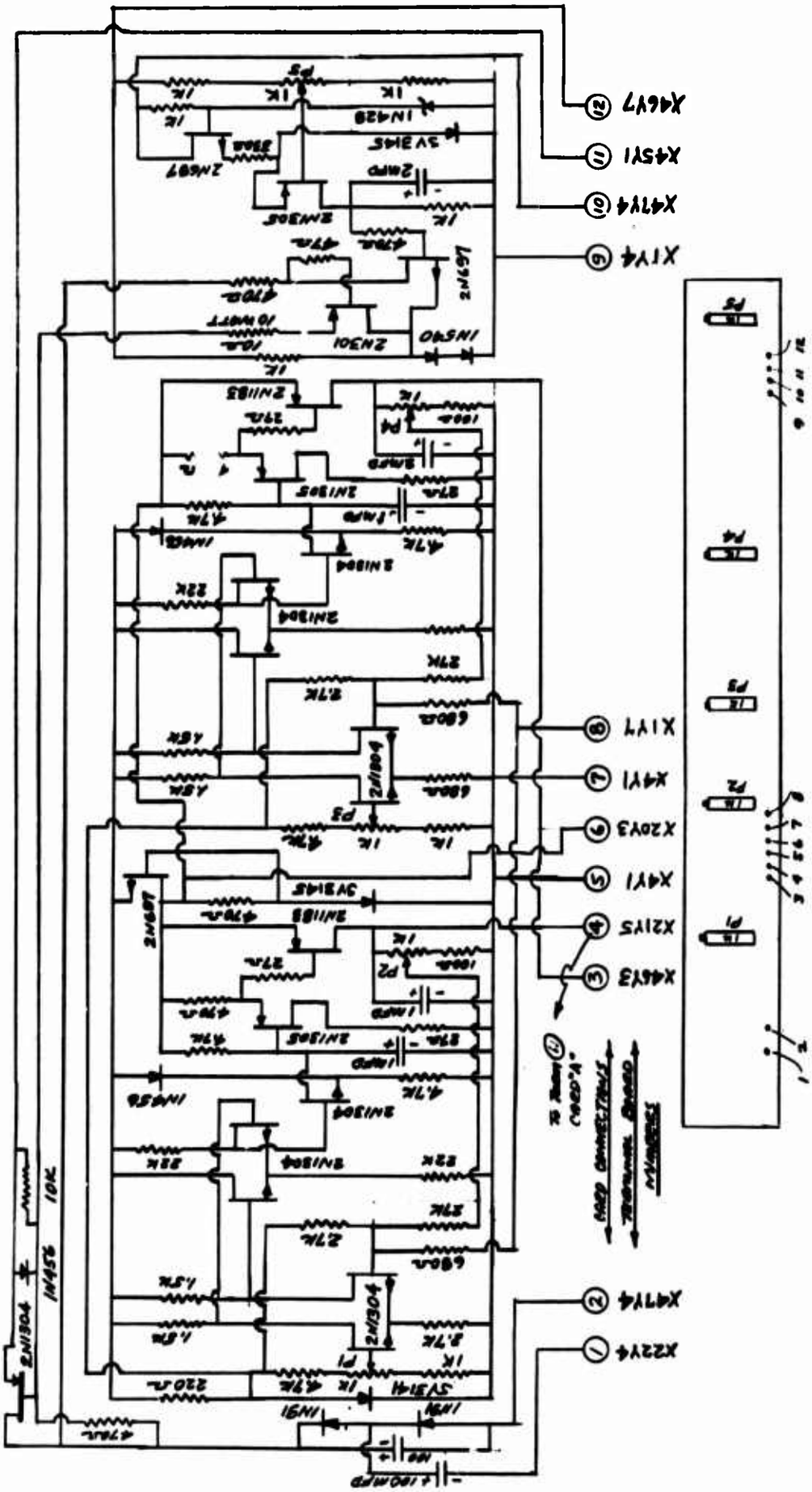

Figure G-26

Electronics - Card "C"

Cooling Fan Regulator, High Temperature and Low Voltage Alarm

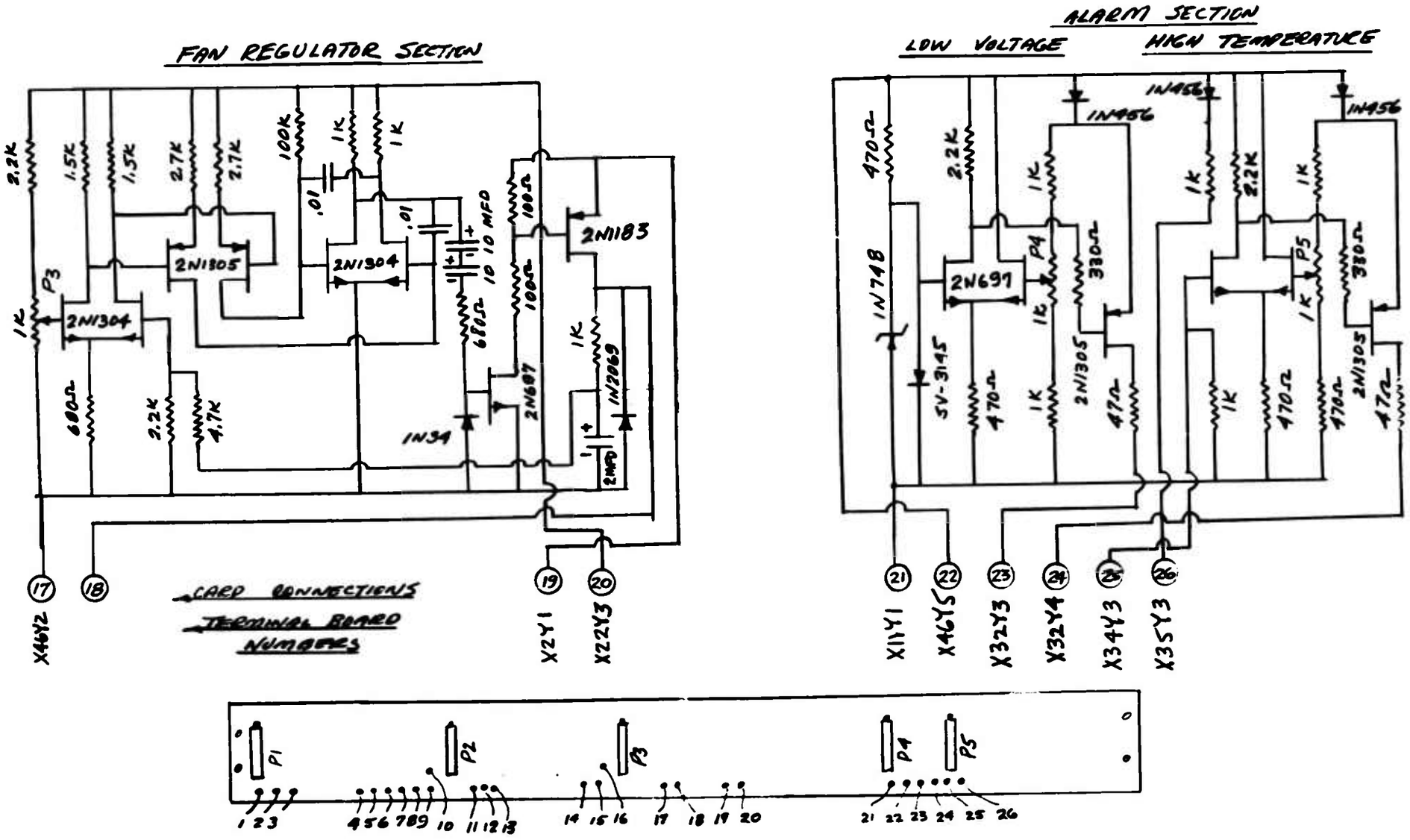

Figure G-27

Electronics - Card "C" (Cont'd)

Acid Concentration Controller

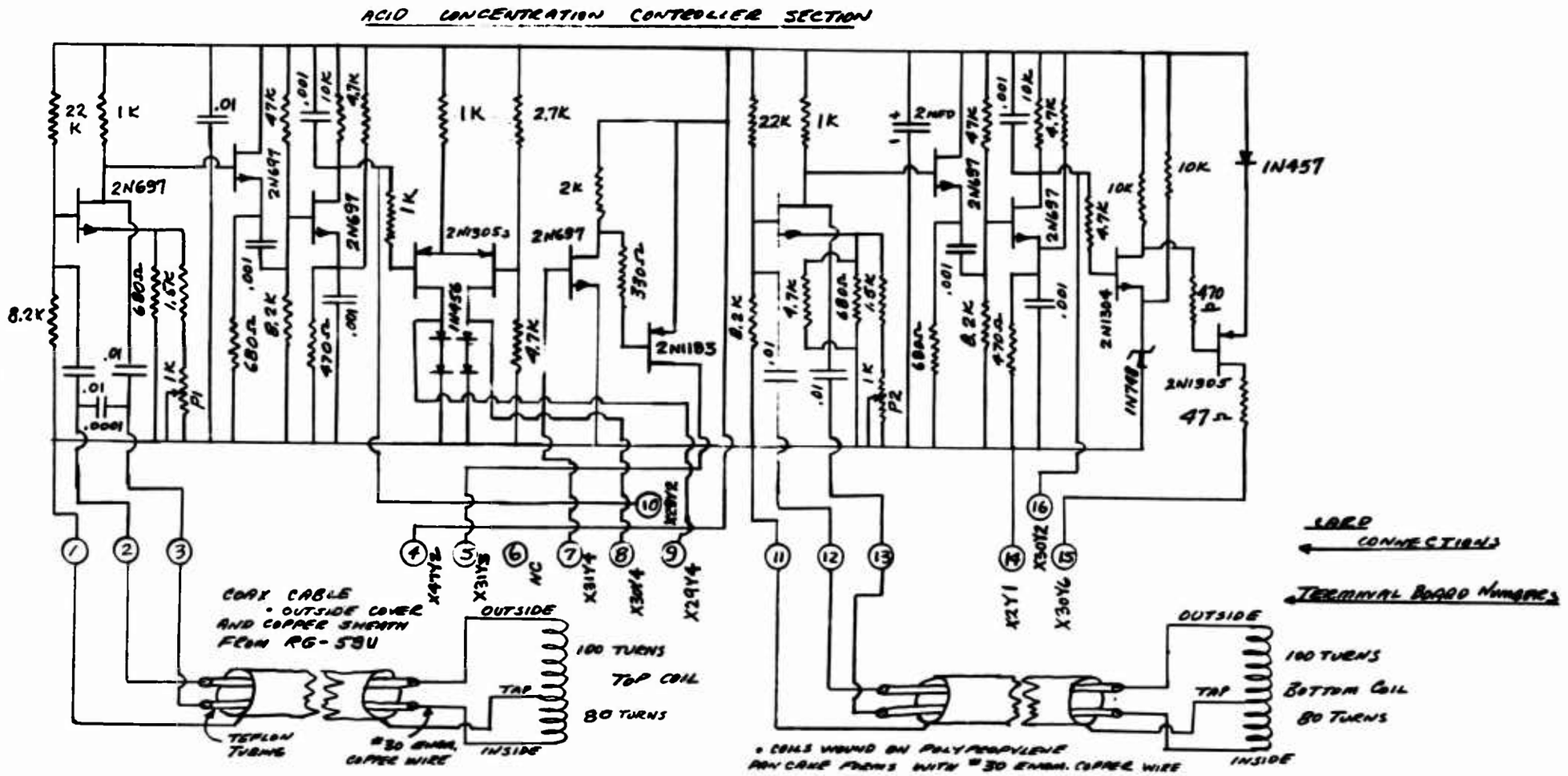

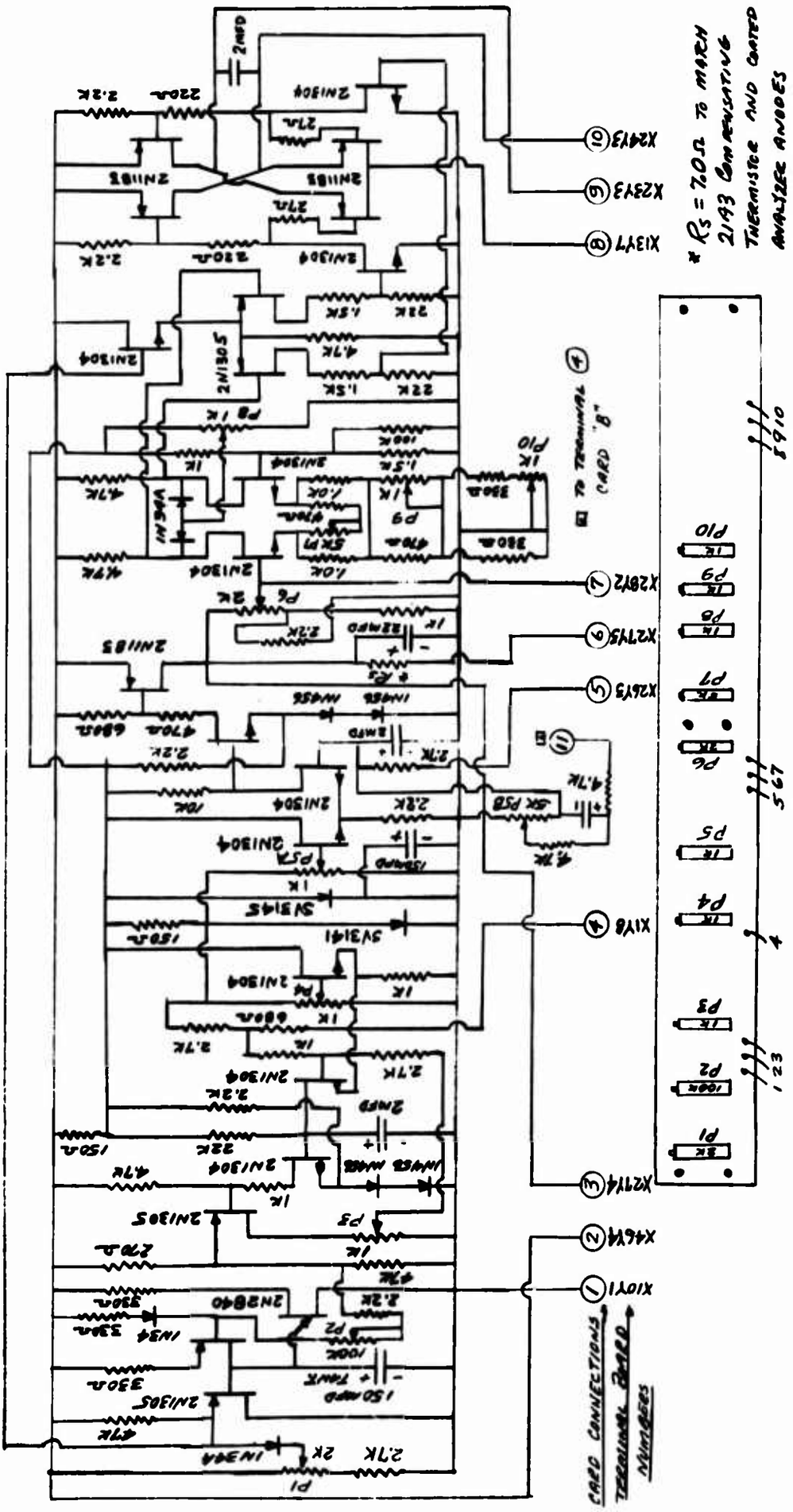

Figure G-28

Electronics - Card "A"

Methanol Analyzer and Controller

Figure G-29

Side View of Battery Demonstrator

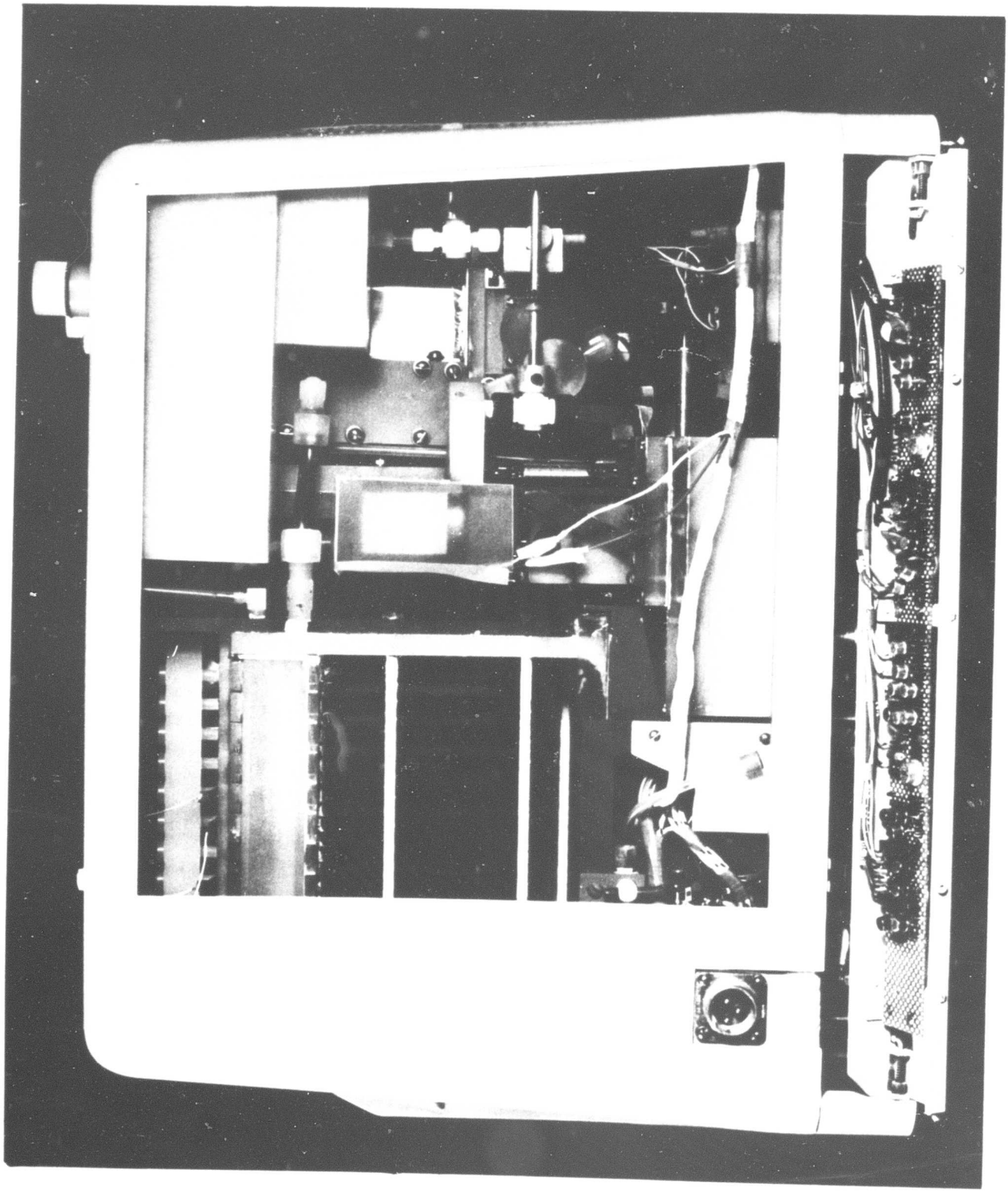

Figure G-30

Battery Performance Monitor

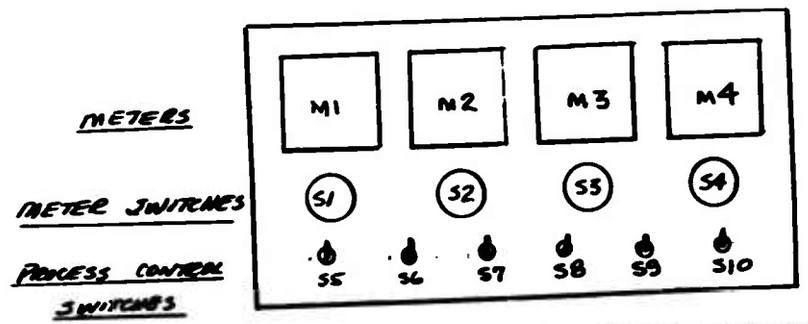

METER AND METER SWITCH FUNCTIONS

METER No. 1

POS.	FUNCTION	RANGE
1	BLOWER MOTOR CURRENT	300mA
2	PUMP MOTOR CURRENT	300mA
3	FAN MOTOR CURRENT	1A
4	METHANOL ADDITION VALVE MOTOR CURRENT	300mA
5	WATER ADDITION VALVE MOTOR CURRENT	300mA
6	START-UP CURRENT (LOAD ON MERCURY BATTERIES)	2A

METER No. 2

POS.	FUNCTION	RANGE
1	BLOWER MOTOR VOLTAGE	10V
2	PUMP MOTOR VOLTAGE	10V
3	FAN MOTOR VOLTAGE	10V
4	METHANOL ADDITION VALVE MOTOR VOLTAGE (−)	10V
5	" (+)	10V
6	CELL STACK VOLTAGE	15V

METER No. 3

POS.	FUNCTION	RANGE
1	METHANOL ANALYZER CELL VOLTAGE	1V
2	METHANOL ANALYZER CONCENTRATION VOLTAGE	3V
3	METHANOL ANALYZER ATTENUATED CONCENTRATION VOLTAGE	2V
4	HYDROMETER FLOAT POSITION DETECTOR VOLTAGE - NOT UP	7V
5	" - NOT DOWN	5V
6	WATER ADDITION VALVE ACTION - CLOSED PROPERLY	3V

METER No. 4

POS.	FUNCTION	RANGE
1	ANODE POLARIZATION CELL 5	1V
2	" CELL 9	1V
3	" CELL 11	1V
4	" CELL 16	1V
5	TEMPERATURE CELL 10	70-220°F
6	" CELL 12	70-220°F
7	" EXHAUST AIR	70-220°F
8	" CELL 6	70-220°F

READOUT FROM HIGH TEMP. ALARM CIRCUIT

NOTE: SWITCH TO BE IN POS. 8 WHEN MONITOR IS NOT CONNECTED TO BATTERY SIMULATOR.

PROCESS CONTROL SWITCH FUNCTIONS

S5
- ↓ NORMAL CONTROL
- ↑ 5.4 VOLTS DIRECTLY TO BLOWER MOTOR

S6
- ↓ NORMAL CONTROL
- ↑ 4.2 VOLTS DIRECTLY TO PUMP MOTOR

S7
- ↓ NORMAL CONTROL
- ↑ 5.0 VOLTS DIRECTLY TO FAN MOTOR

S8
- — NORMAL CONTROL
- ↑ DECREASE METHANOL ADDITION RATE
- ↓ INCREASE RATE

S9
- ↓ NORMAL CONTROL
- ↑ OPEN WATER ADDITION VALVE

S-10
- SPACE

Figure G-31

Battery Performance Monitor Wiring Diagram

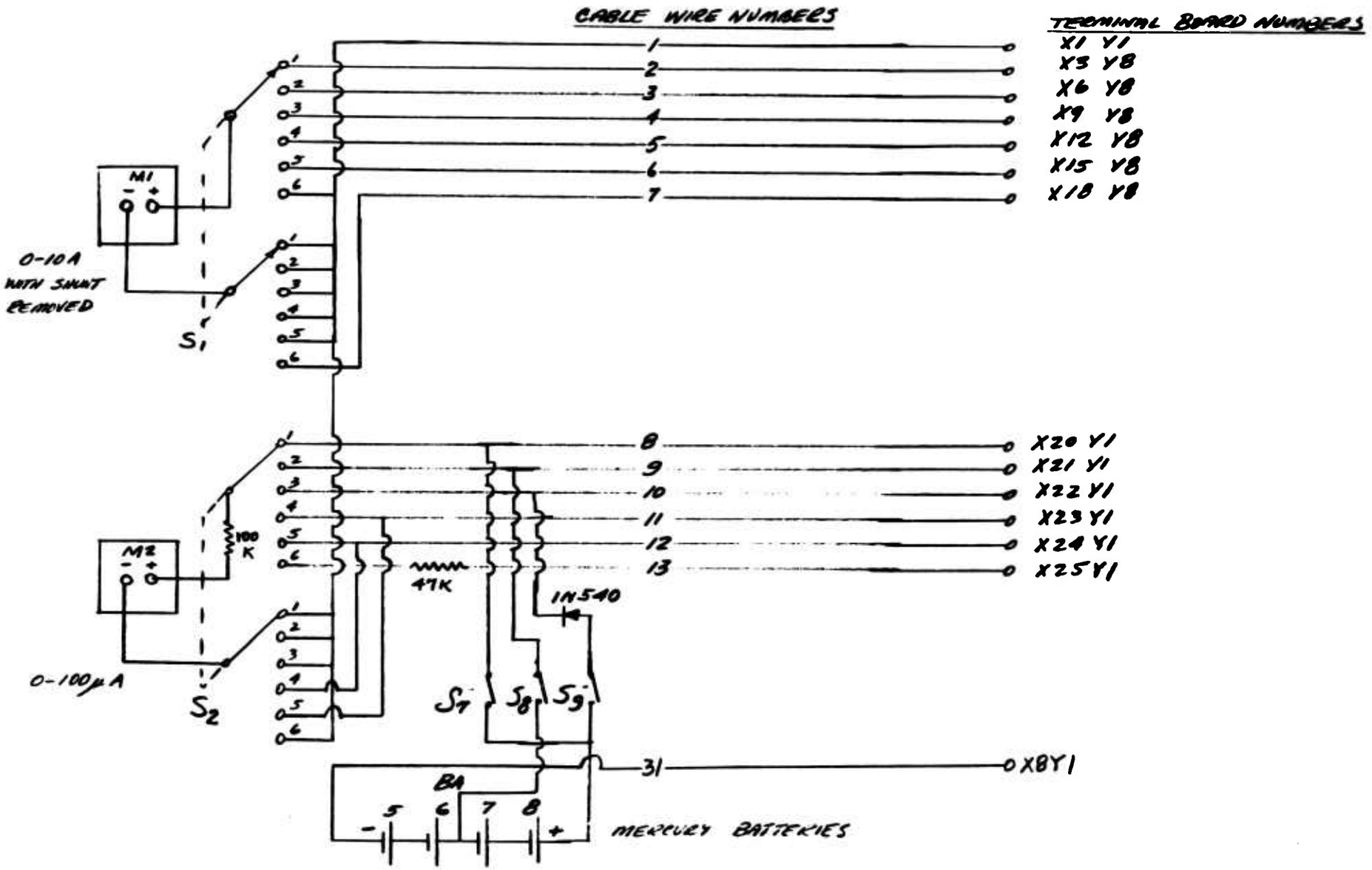

Figure G-32

Battery Performance Monitor Wiring Diagram (Cont'd)

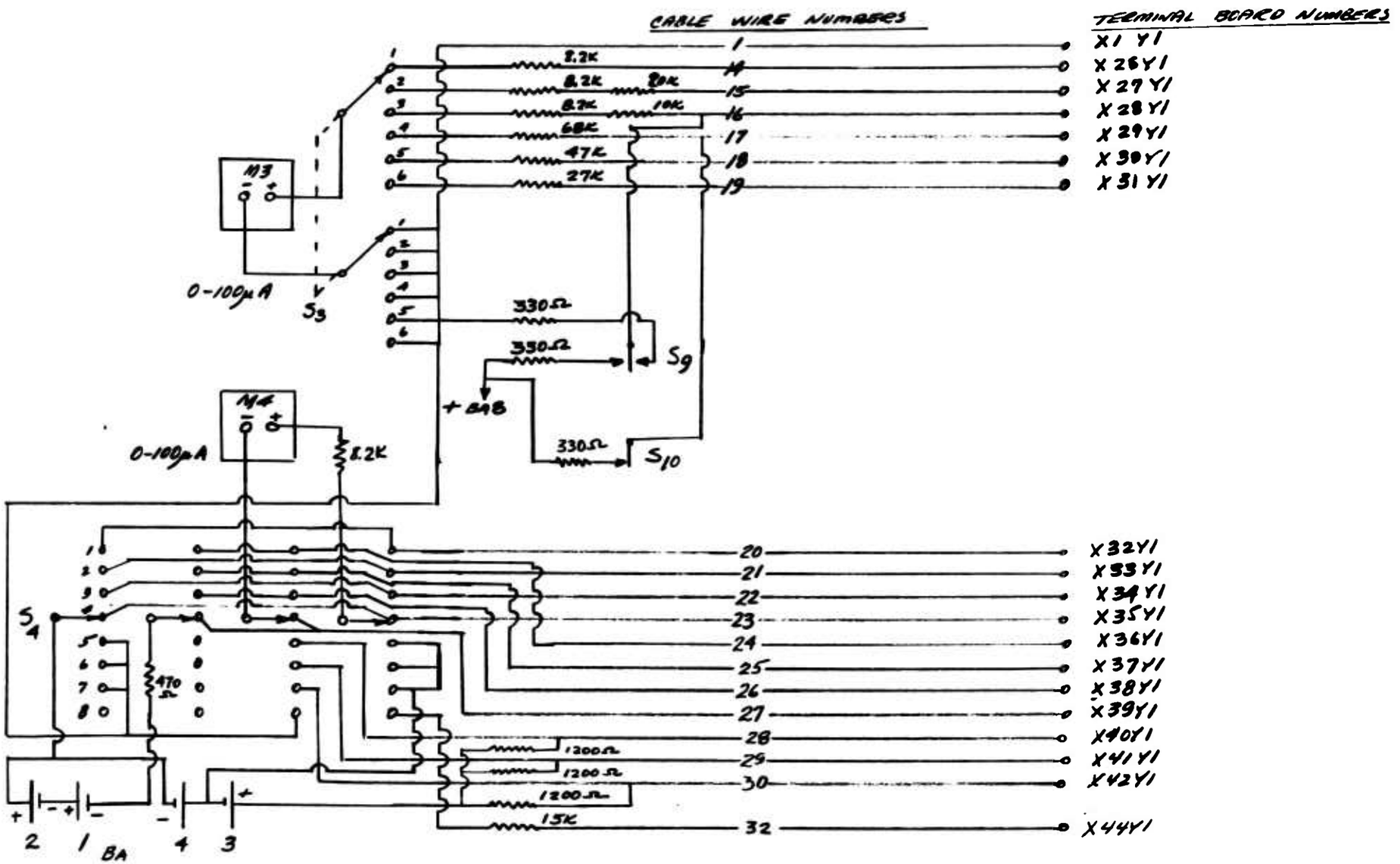

Figure G-33

Battery Performance Monitor Meter Calibration

Meter No. 2

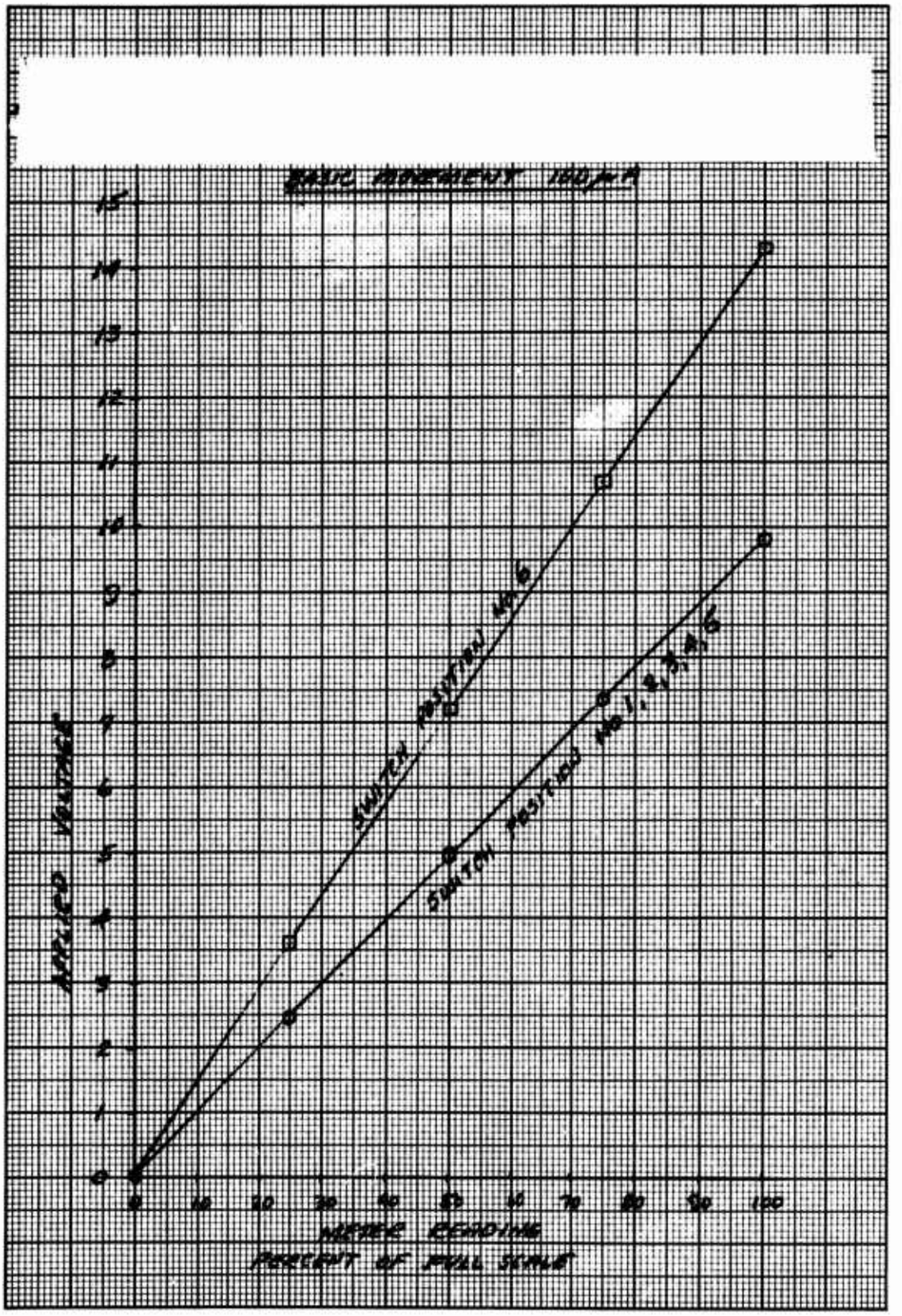

Figure G-34

Battery Performance Monitor Meter Calibration

Meter No. 3

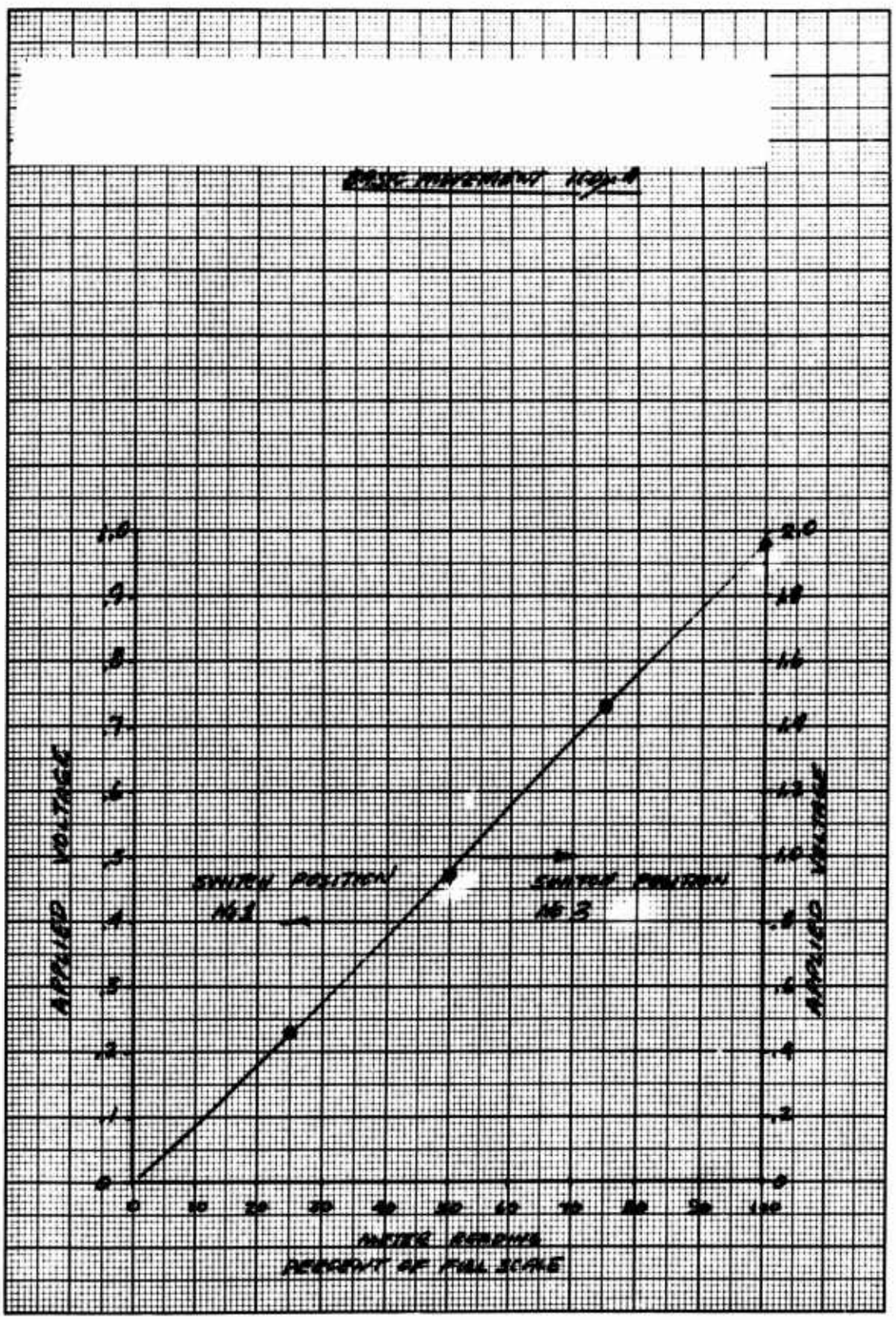

Figure G-35

Battery Performance Monitor Meter Calibration

Meter No. 3 (Cont'd)

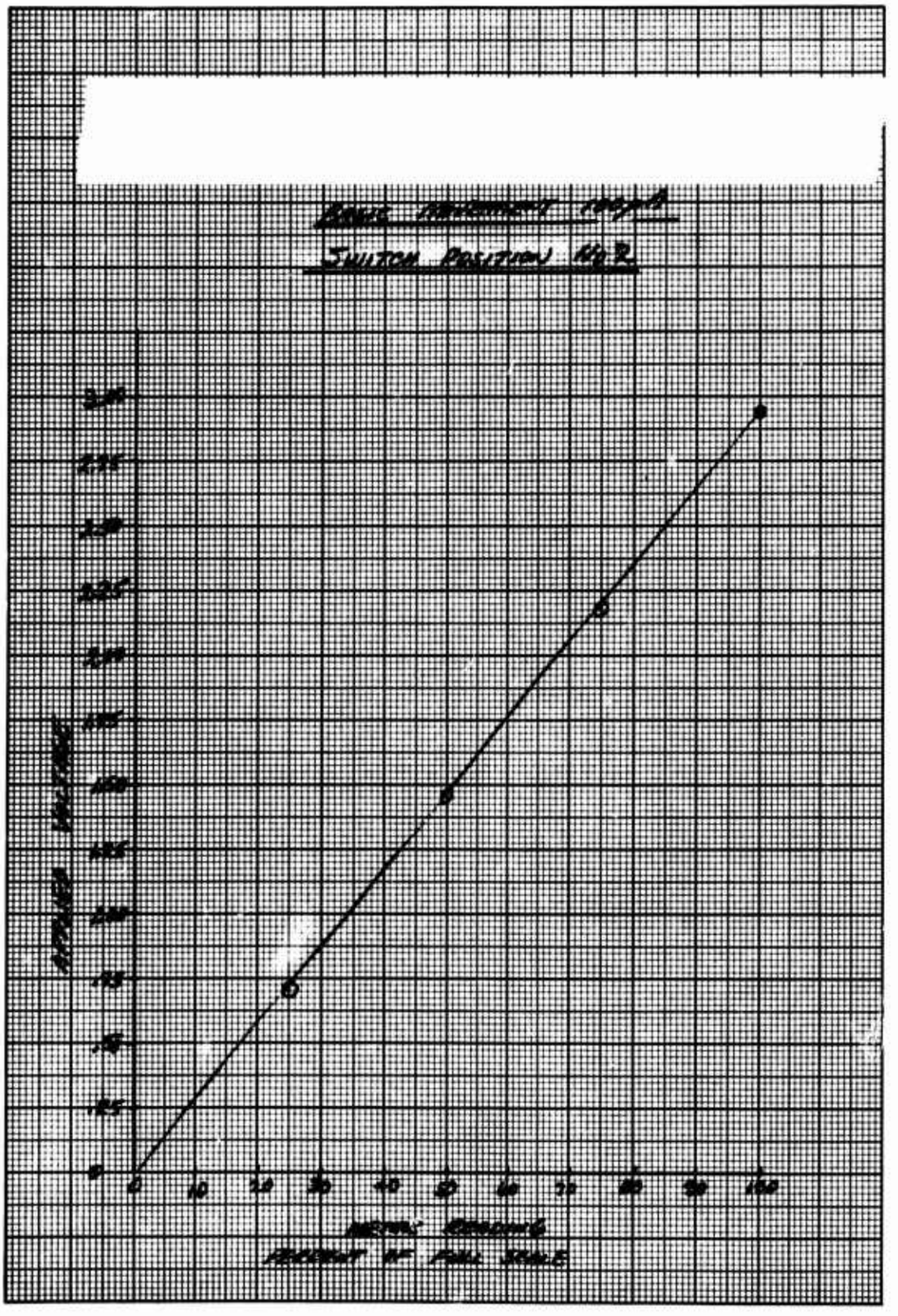

Figure G-36

Battery Performance Monitor Meter Calibration

Meter No. 3 (Cont'd)

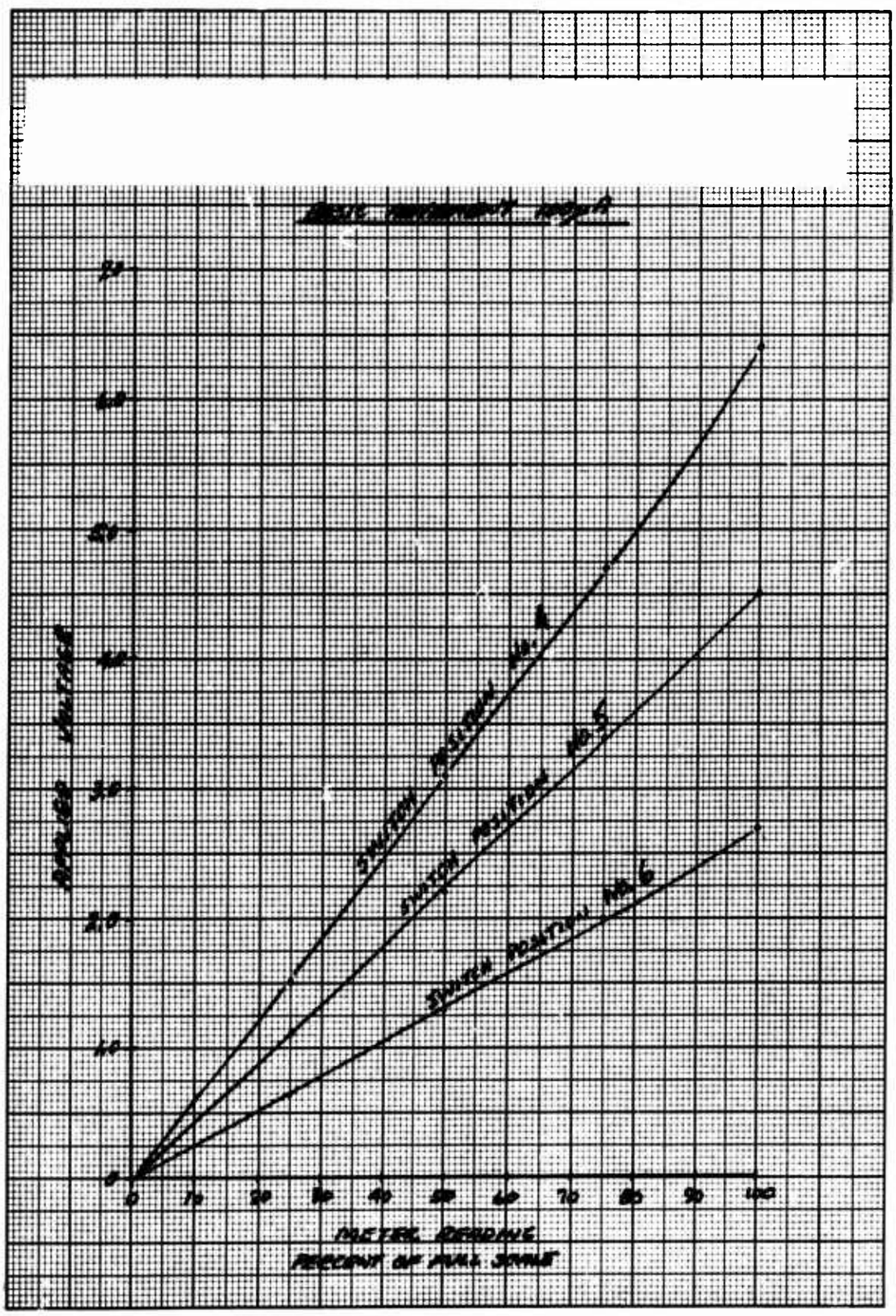

Figure G-37

Battery Performance Monitor Meter Calibration

Meter No. 4

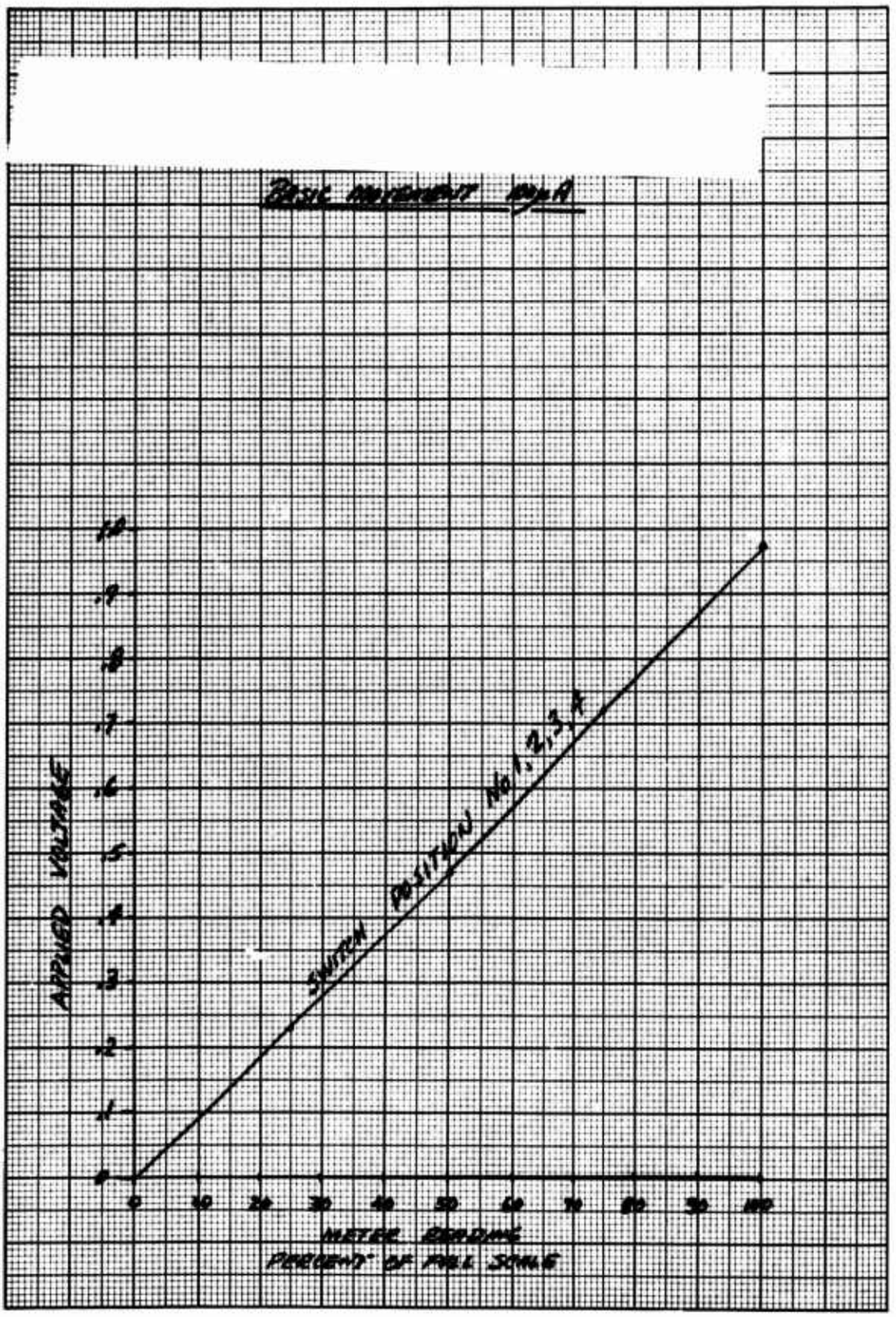

Figure G-38

Battery Performance Data Monitor

Meter No. 4

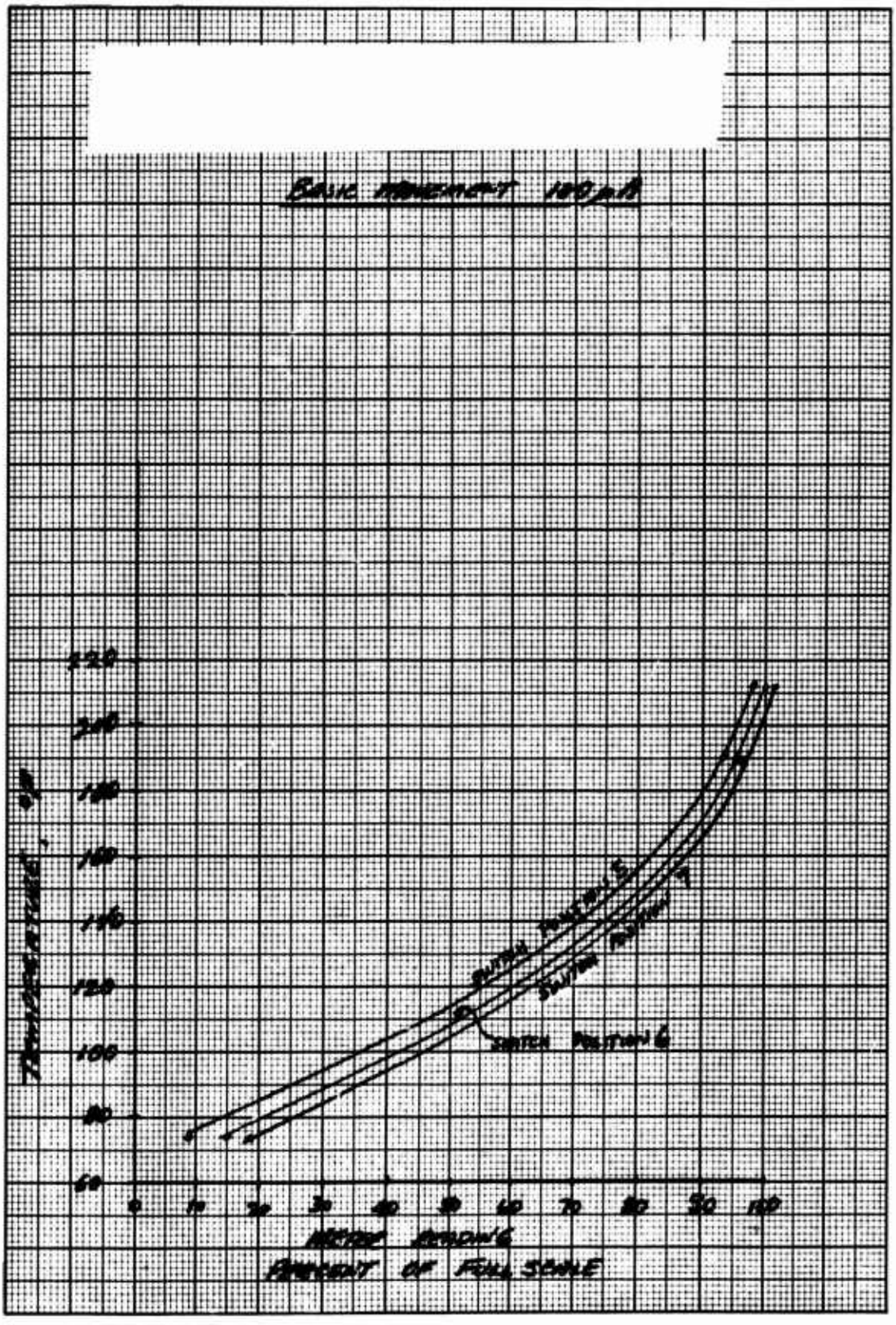

Figure G-39

Battery Performance Monitor Meter Calibration

Meter No. 4 (cont'd)

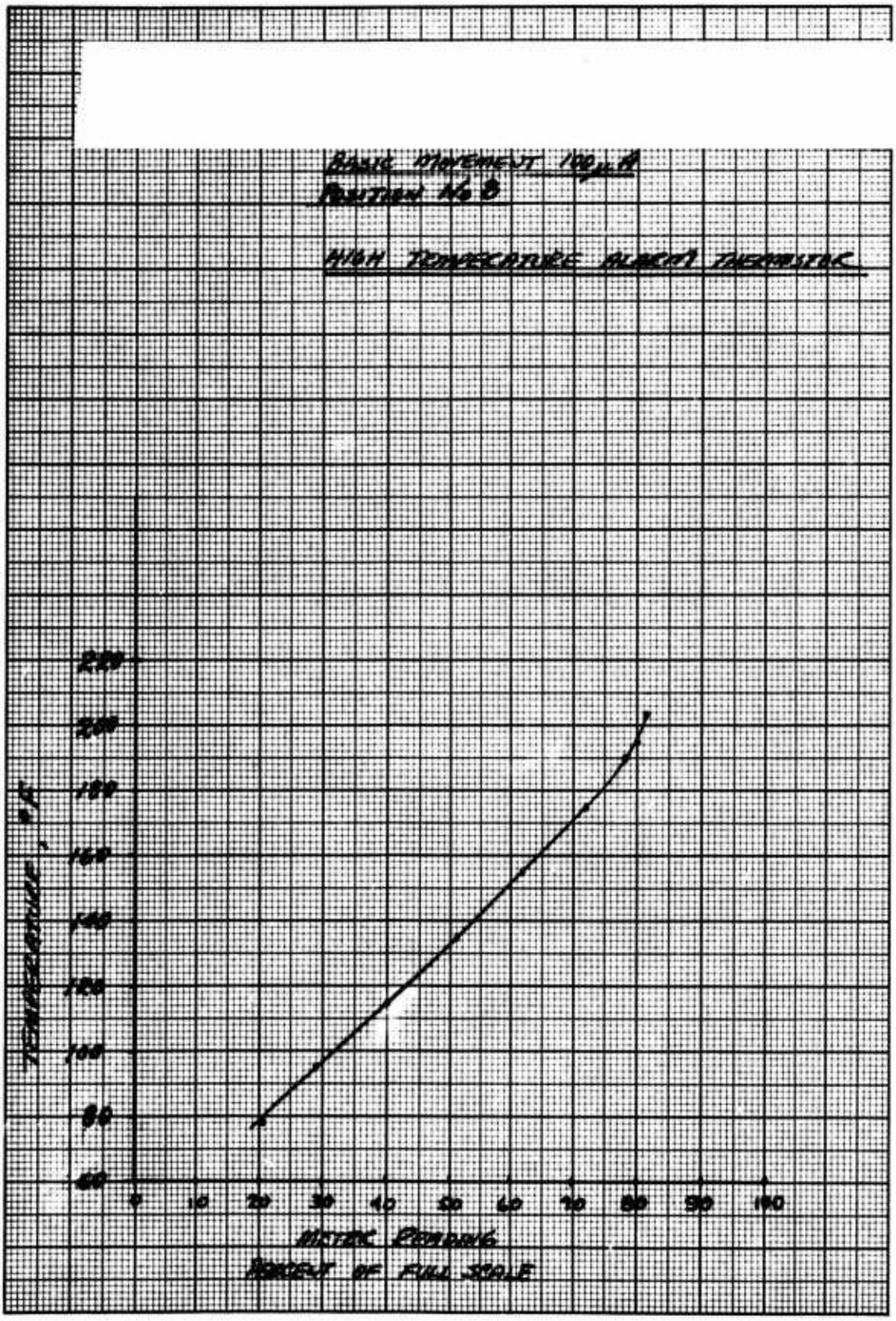

Figure G-40

Battery Demonstrator and Performance Monitor

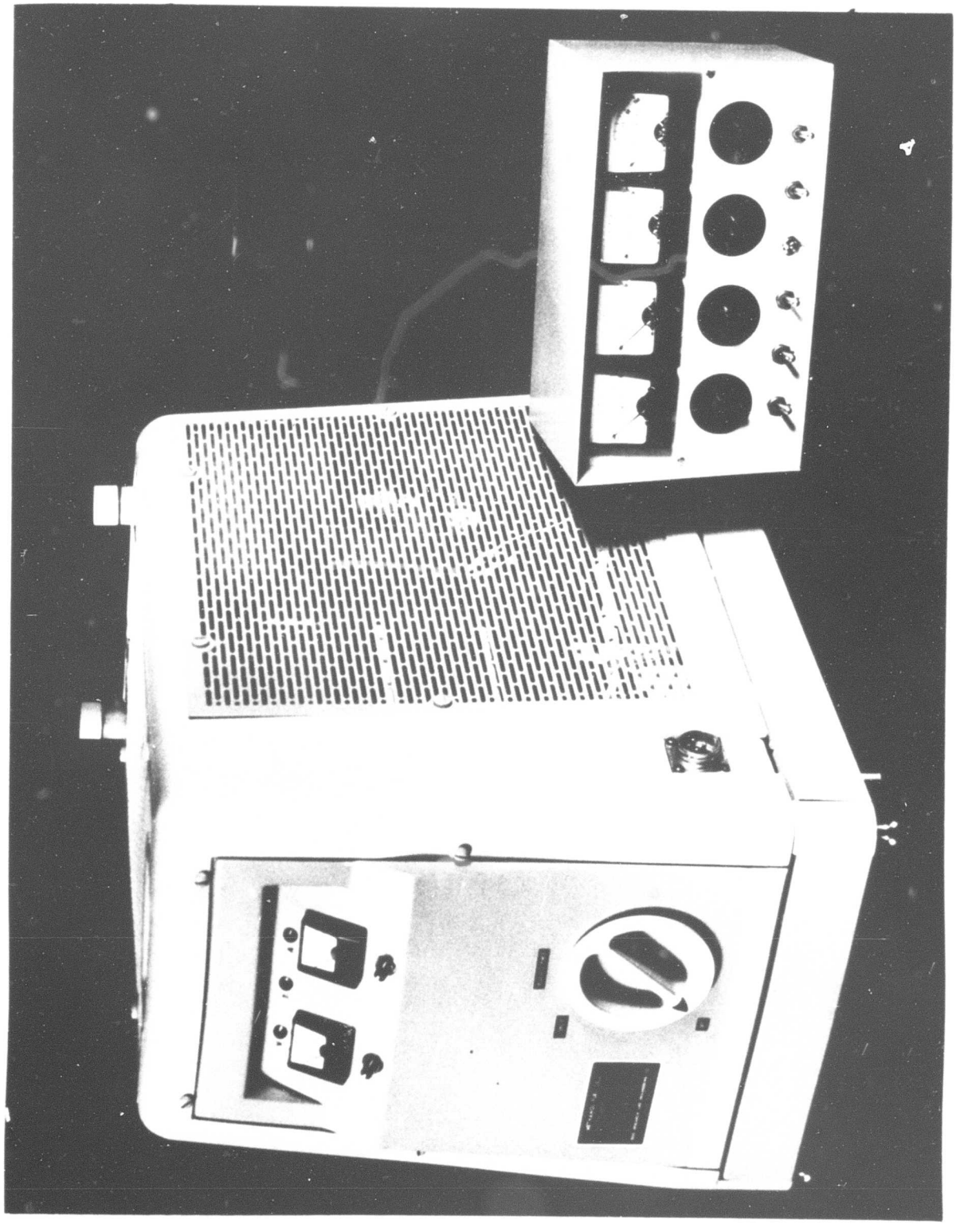

Figure G-41

Electronic Card Layout

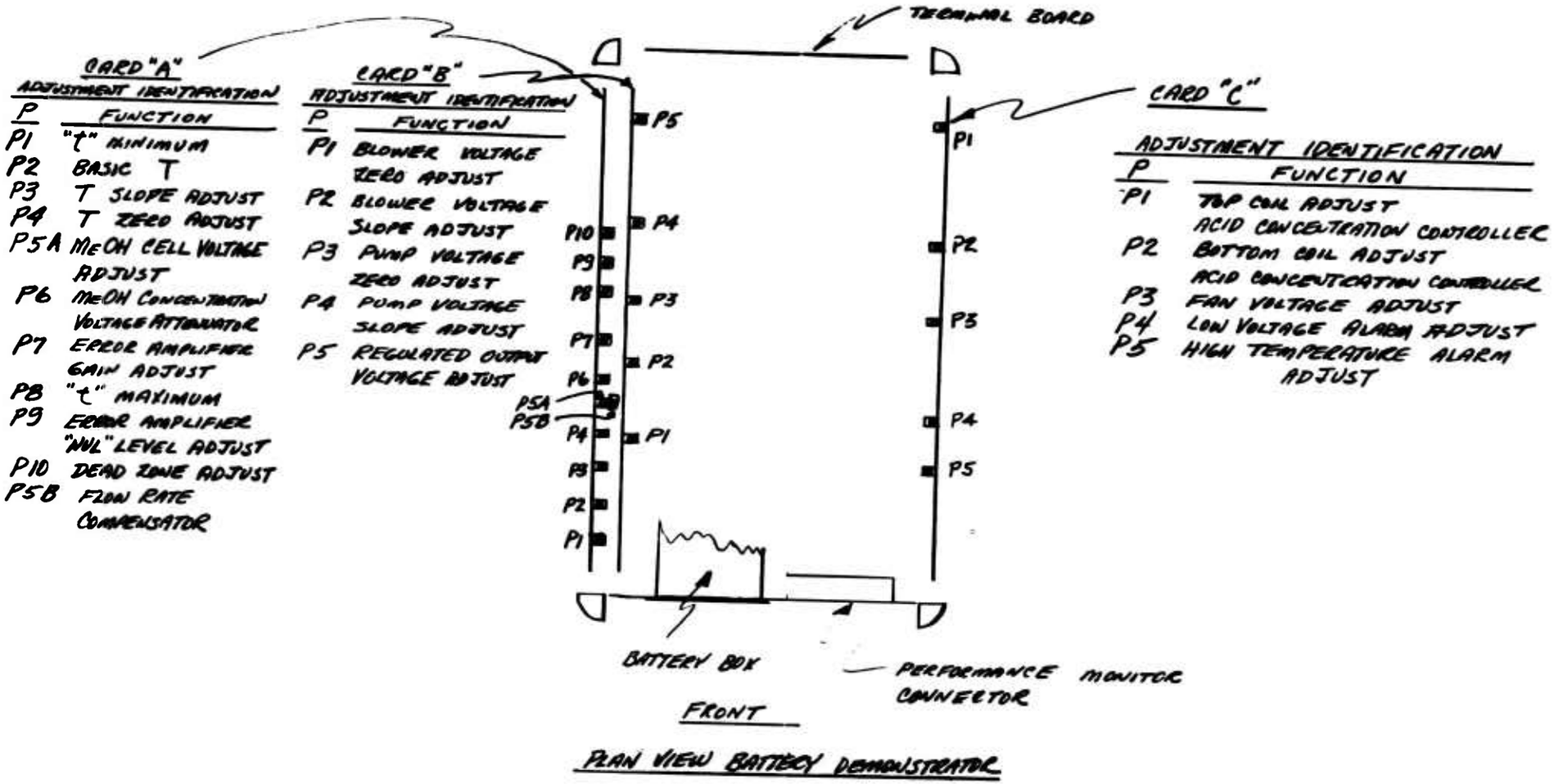

PLAN VIEW BATTERY DEMONSTRATOR

Figure G-42

Potentiometer Adjustment Chart

Card A

P10  Lower Dead Zone

P9  Balance With Meter

P8  Raise Max "t"

P7  Lower Error Amp Gain

P6  Raise Atten. Factor

P5A  Raise MeOH Cell E

P5B  Increase Feedback To Use E Pump To Correct E Cell

P4  Raise T Zero

P3  Lower T Slope

P2  Lower T

P1  Lower "t"

Card B

P5  Raise Regulated Voltage

P4  Lower Pump Slope

P3  Raise Pump Zero

P2  Lower Blower Slope

P1  Raise Blower Zero Voltage

Card C

P1  Bring Top Coil OSC "On"

P2  Bring Bottom Coil OSC "On"

P3  Raise Fan Volts

P4  Raise Low Voltage Alarm Set Point

P5  Raise High Temp. Set.

Figure G-43

Connection Details

Thermistors, Methanol Analyzer, Cell, Reference Electrodes, Alarm Lamps and Motors

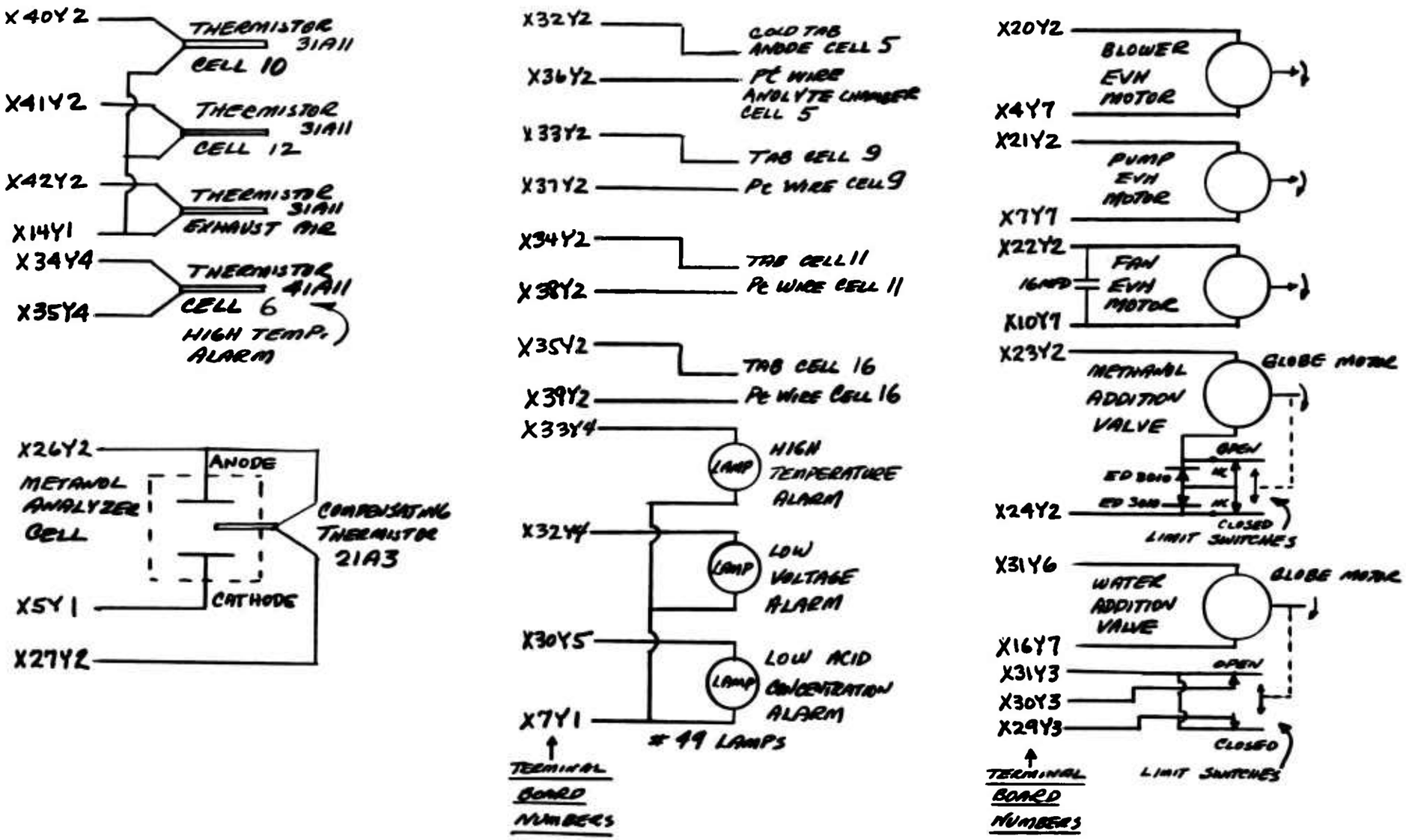

Figure G-44

Terminal Board Connection Identification
and Battery Box Detail

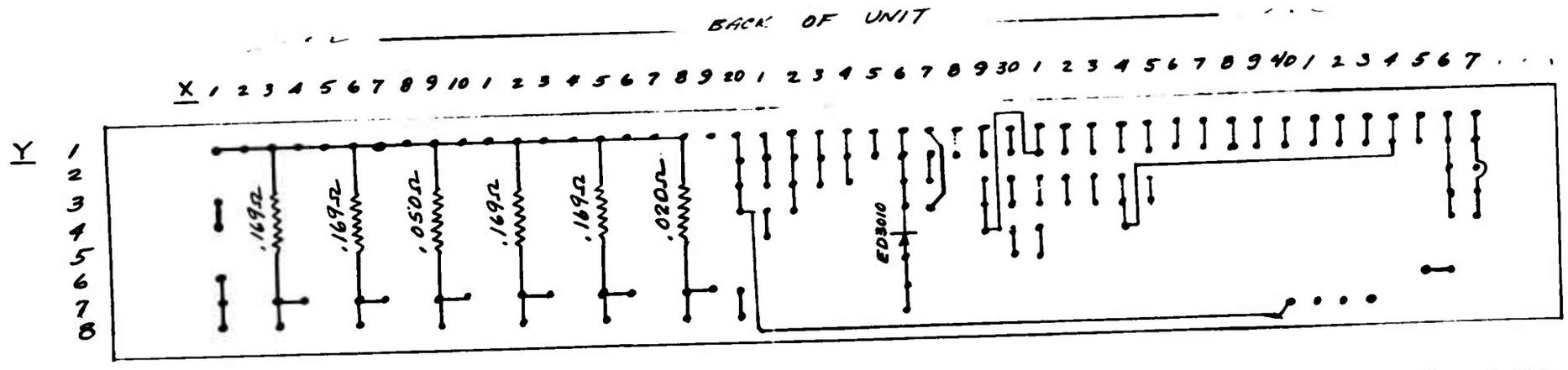

- AS VIEWED LOOKING AT BACK OF COMPLETE BATTERY ASSEMBLY WITH TERMINAL BOARD ASSEMBLY IN "OPEN" POSITION

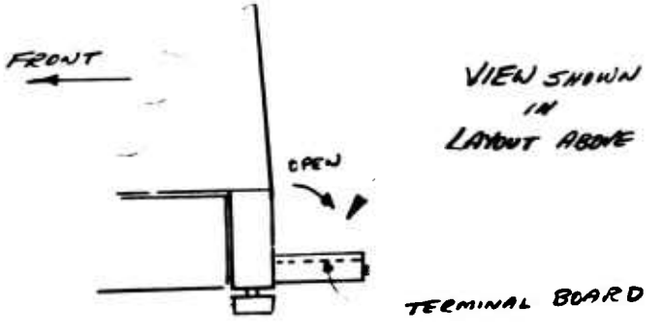

RIGHT SIDE VIEW

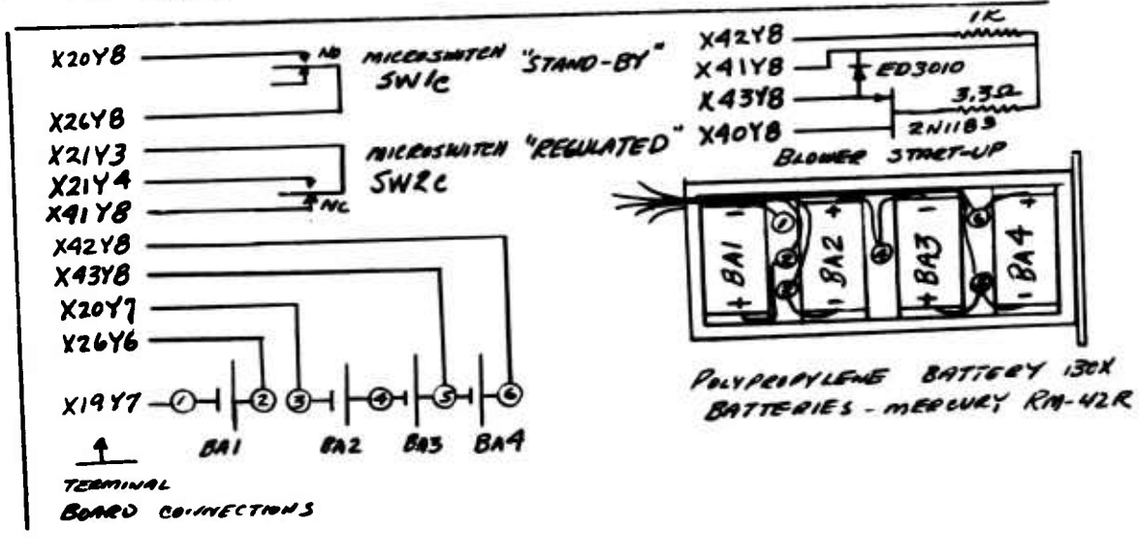

APPENDIX G-14

FLOW DIAGRAMS FOR METHANOL FUEL CELL BATTERY DEMONSTRATOR

Figure G-45

Schematic Electrolyte Flow Diagram

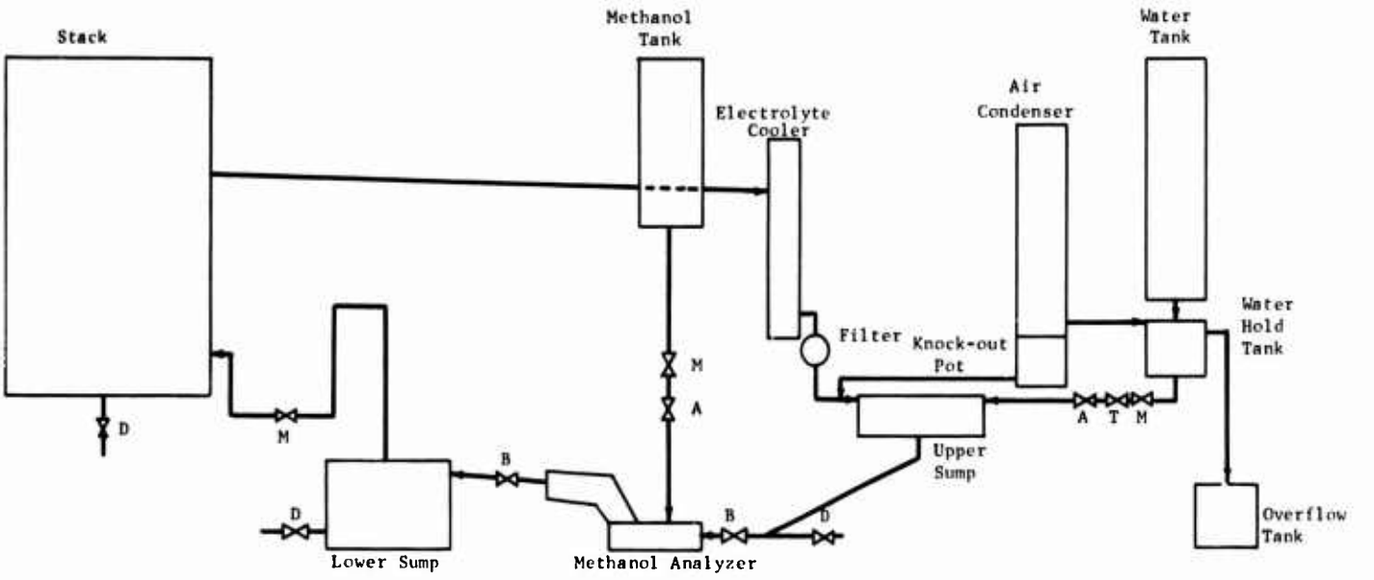

Valve Designations	Activating Force
A = Automatic	Controlled Motor
B = Block	Manual
D = Drain	Manual
M = Mechanical	Master Switch
T = Throttle	Manual

APPENDIX G-14 (CONT'D)

FLOW DIAGRAMS FOR METHANOL FUEL CELL BATTERY DEMONSTRATOR

Figure G-46

Schematic Air Flow Diagram

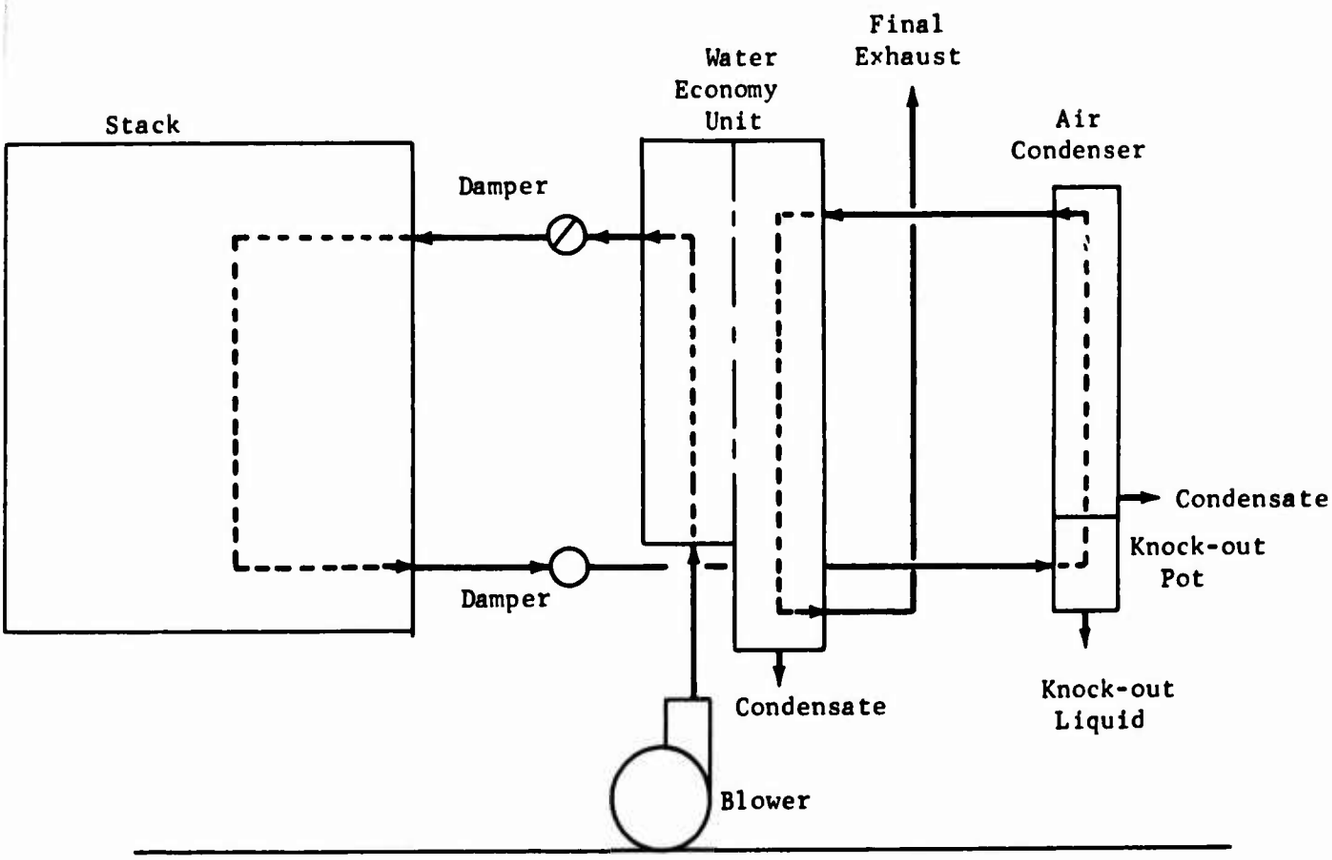

Figure G-47

Schematic Arrangement of Demonstrator Sump Drain System

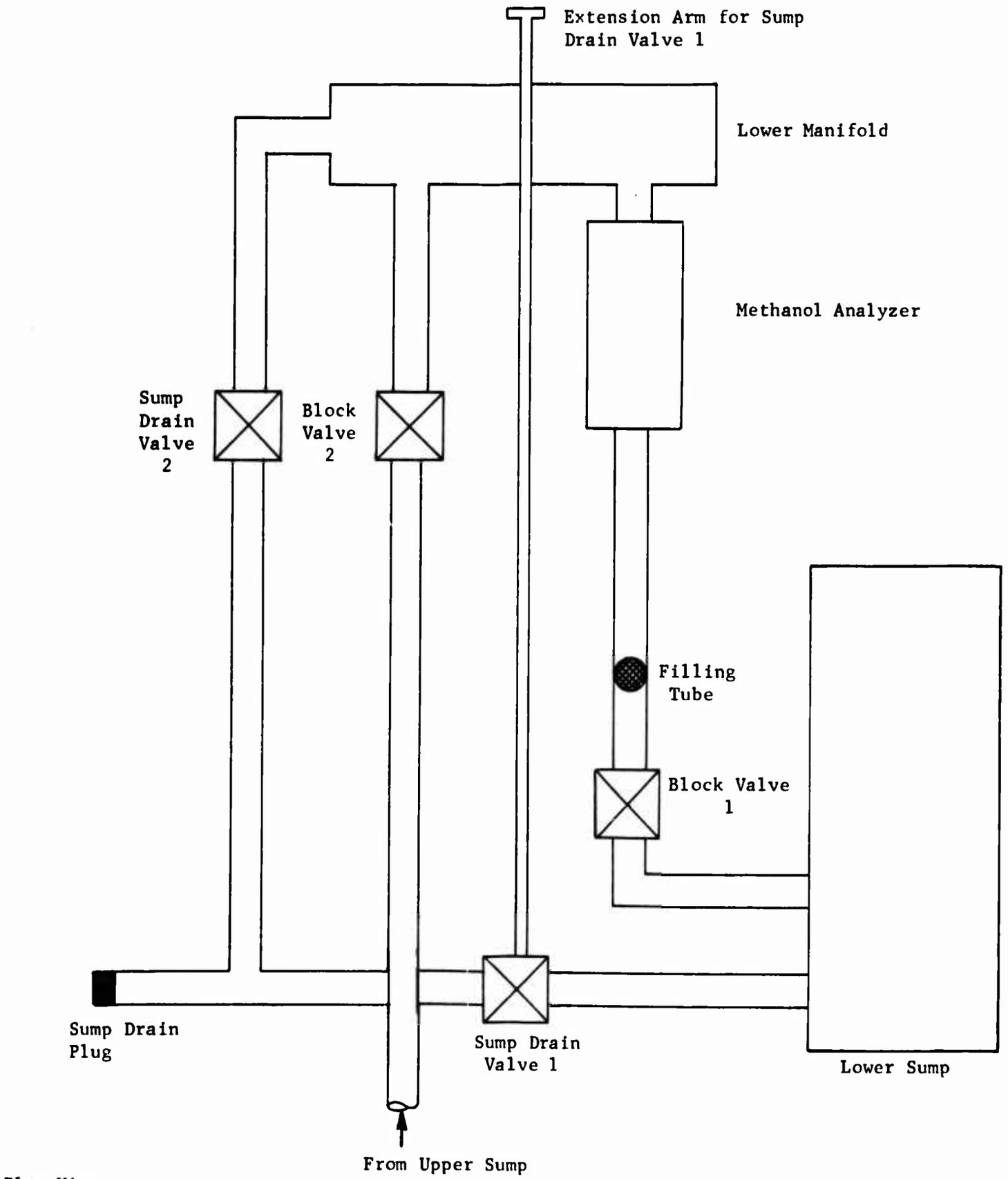

Plan View

APPENDIX G-15

INITIAL PERFORMANCE OF TWENTY CELL STACK

Current Density, ma/cm^2	Stack[1] Potential, volts	Stack[1] Power watts	Stack[1] Ohmic Loss, volts	Average Anode Polarization, volts	Average Cell Potential, volts
0	13.7	0	--	0.24	0.68
1	13.2	4	--	0.26	0.66
5	12.3	18	--	0.28	0.62
10	11.5	34	--	0.31	0.58
20	10.0	60	--	0.34	0.50
30	9.0	81	--	0.36	0.45
40	8.2	98	1.085	0.37	0.41
50	7.6	114	--	0.38	0.38
60	6.8	123	--	0.39	0.34
80	5.5	132	--	0.40	0.28
100	4.3	129	2.304	0.41	0.22

(1) Run 66-1-3, stack only, 70-80°C, 0.75 M CH_3OH in 3.7 M H_2SO_4, 50% conversion per pass, once-through via Mace pump. House air at about 8 times stoichiometric.

APPENDIX G-16

OPERATION OF THE METHANOL FUEL CELL BATTERY DEMONSTRATOR

The Methanol Fuel Cell Battery Demonstrator is a self-contained six volt power supply operating on methanol as the fuel and atmospheric air. The complete assembly includes a fuel supply, make-up water supply, all the necessary process controls, a voltage regulator, and a small start-up battery.

The twenty cell stack within the Demonstrator is a proven unit, with several comparable units with favorable test histories over the past two years. However, the combination of the stack and the auxiliaries is largely untested. Their designs, as well as those of the associated electronics, are based on operating data obtained on the individual components not integrated together, but under test conditions as close to projected operation conditions as was possible. Therefore, the entire unit is a research device, and it is expected that its operation will reflect problems inherent in an untried first assembly.

The following are the recommended procedures for storing, activating, operating, evaluating, and trouble shooting the Demonstrator. Several process monitors have been incorporated directly into the Demonstrator. To further aid in the evaluation, a Performance Monitor also has been supplied, which can be used in evaluating the operation of all the critical components. The instructions are broad rather than detailed and do not cover in depth the modes of operation of these components. Instead, general operating and diagnostic procedures are discussed. It is suggested that those evaluating the Demonstrator acquaint themselves with the response characteristics of the Demonstrator, that are displayed on the Performance Monitor, particularly meters 3 and 4 to understand the operating characteristics of this unit.

- Storage

1. The Master Switch must be OFF during Storage.
2. During prolonged storage, check twice weekly for electrolyte leakage. Find and repair leaks, when necessary. For ease of maintenance, remove top case.
3. Check for electrolyte discoloration, by draining a 50 cc sample of electrolyte from the stack, using stack drain valve on the right hand side as you face the front panel. If electrolyte is green or a dark brown, drain stack and replace via the drain with 2200 cc of fresh 3.7 M sulfuric acid containing 0.75 M methanol using graduating glass filling tank provided.
4. Depress voltage push-button switch to read stack voltage. Proper value in storage is about 1 volt. Over 2 volts is high. Check whether air dampers are closed.
5. Attach Performance Monitor to plug under front panel. Read anode reference voltages by setting dial to positions 1 through 4 on the fourth meter of the Performance Monitor (see Appendix G-13). If any anode reads over 0.6 volts, replace electrolyte in stack.

- Activation

1. Drain stack through valve on right side.
2. Drain sumps through valve on drain line.
3. Refill stack immediately with 2200 cc of 3.7 M sulfuric acid containing 0.75 M methanol.
4. Fill lower sump with 300 cc of electrolyte mixture through fill line located on top on the right side.
5. Fill upper sump with 300 cc of electrolyte mixture through fill line located in top on the left side.
6. Fill fuel tank, marked F, with commercial grade methanol. Replace cap.
7. Fill water tank, marked W, with demineralized water. Replace cap. Cap must be in place to permit water addition.

- Operation

1. Turn Master Switch to STAND-BY. Operate in this position for five minutes. Check stack voltage by depressing voltage push-button switch beneath front panel voltmeter. Voltage should exceed 10 volts. If not, refer to subsystems C, D and E.
2. Check for gas blockage in methanol fuel line using vacuum bulb and line. Evacuate fuel tank (F) to degass the bubbles in feed line, repressurize with several squeezes, then replace.
3. Turn Master Switch to REGULATED POWER.
4. Connect load into receptacle. Suggested loads include the load panel delivered in 1965 and the electric drill delivered with the Demonstrator.
5. Monitor Demonstrator voltage and current. Do not operate at currents higher than 15 amps.
6. If voltage drops below 5.9 volts, depress push-button switches to check stack voltage. Remove or reduce load if stack voltage has dropped below 6.8 volts. Move Master Switch to STAND-BY for five minutes, then return control to load under REGULATED POWER. If trouble persists, see Evaluation and Trouble Shooting Section, below.
7. Refill fuel and water tanks when required.
8. To shutdown Demonstrator, remove load and turn Master Switch to STAND-BY for three minutes. Then turn switch to OFF.

- Evaluation and Trouble Shooting

- With Master Switch set at STAND-BY.

1. Check electrolyte circulation using rotometer located near the pump. Rotometer should read at least 100.
2. Check operation of air blower by placing hand over top stack exhaust to feel whether air is exiting from the unit. If no air is felt, check rotation of blower rotor.
3. Recheck for gas blockage in methanol fuel line.
4. Check position of methanol control valve between its microswitch set points.

5. Check acid concentration by removing electrolyte sample and measuring gravity with hydrometer.

With Master Switch at STAND-BY or REGULATED POWER.

1. Check red lights marked V and T. If designated lights are on, check stack voltage. Using Performance Monitor, check readings from positions 1 through 8 on the fourth meter. See calibration curves in Appendix G-13. Ignore flickering red light marked A. If continuously on for more than two hours, check acid concentration. Refer to subsystem B in Table G-4.
2. Red light, T is high temperature indicator. High temperatures generally means excess methanol. Check subsystems A, D, and E.
3. High anode polarizations generally mean anode starvation. Check subsystems A. If O.K. check subsystems D, and E.
4. Expected ranges for the observed Performance Monitor readings are given in Table G-5.

Table G-4

DIAGNOSTIC PROCEDURE

Approach: Systems ←Diagnosis→ Causes ←→ Corrective Action

Subsystems:
A. MeOH Addition System
B. Water Addition System
C. Electrolyte Circulation System
D. Air Auxiliaries
E. Stack

Possible Causes:

A. MeOH Addition System
   1. Closed MeOH line valve
   2. Clogged MeOH line
      a. Bubble bound
      b. Filter plugged
      c. P.P. plug fouled
   3. Empty MeOH tank
   4. Inoperative MeOH valve/Motor
      a. Decoupled Motor Shaft-Valve Shaft
      b. Motor failure
      c. Electrical wiring
      d. Inoperative limit switches
   5. Inoperative Analyzer
      a. Faulty anode
      b. Faulty cathode
      c. Electrical wiring
      d. Electrolytic path (gas-filled)

Table G-4 (Cont'd)

DIAGNOSTIC PROCEDURE

e. Improper tuning
   + Set point
   + Dead zone
   + Error gain
   + Current gain
   + Pulse frequency
   + Limit switch position
f. Faulty thermistor

6. Leaks in line

7. Plugged vent hole in cap

8. Loose cap

B. Water Addition System

1. Closed water line valve

2. Clogged water line

   a. Filter plugged

3. Empty Main Water Tank

   a. Improperly tightened filling cap

4. Defective hydrometer float

   a. Leading float
   b. Distorted links on float

5. Improperly tuned sensing coil positions

6. Low electrolyte level in lower sump

7. Electrical connections

8. Faulty limit switches

9. Inoperative water valve/motor

   a. Decoupled motor-valve shafts
   b. Detuned limit switch/cam relation
   c. Inoperative motor

10. Inoperative feeding mechanism in Main Water Tank

11. Improperly positioned throttle valve

12. Leaks in line

C. Electrolyte Circulation System

1. Bound pump

   a. Pump unprimed
   b. Dirt in impellers
   c. Clogged screen
   d. Stuck check valve
   e. Stuck rotometers float
   f. Misaligned shafts

Table G-4 (Cont'd)

DIAGNOSTIC PROCEDURE

2. Plugged filter cartridges
3. Low electrolyte level in lower sump
4. Pump motor shaft/gear box shaft/pump shaft decoupled
5. Jammed gear box
6. Electrical connections
7. Pump stuck on BATTERY power position
8. Leaking system
   a. Tanks and sumps leak
   b. Lines leak
   c. Drain valve open
9. MeOH analyzer block valves closed
10. Electrolyte line valve closed
11. Stack overflow ports clogged
12. System vents clogged
13. Pump motor voltage insufficient
    a. Load-voltage relation incorrect
14. Inoperative electrolyte cooler

D. Air Auxiliaries

1. Inoperative Blower
   a. Motor defective
   b. Motor/impeller uncoupled
   c. Friction between impeller and walls
   d. Blocked air intake
   e. Electrical wiring
2. Blower motor voltage insufficient
   a. Load-voltage relation incorrect
3. Blower stuck on BATTERY power position
4. System Pressure Drop too High
   a. Plugged air lines
   b. Pampers closed
   c. Condensate and drippage drain lines plugged
   d. Blocked air exhaust
   e. Misaligned demister screens in knock-out pot
5. Inoperative Water Economy Unit
   a. Ruptured membrane
   b. Plugged internal condensate drain line
6. Plugged knock-out pot

Table G-4 (Cont'd)

DIAGNOSTIC PROCEDURE

7. Fouled air condenser tubes
8. Assembly leaks between auxiliary units
9. Inoperative cooling fan
    a. Inoperative motor
    b. Improper motor voltage
    c. Motor/fan uncoupled
    d. Friction between fan blades and housing
    e. Blocked air intake
    f. Electrical wiring

E. Stack

1. Leaking assembly
    a. Between frames
    b. Overflow manifolds
    c. Electrolyte inlet system
    d. Between frames and end plates
    e. Thermister and reference electrode wells
2. Improperly tensioned external current collector system
3. Gas buildup
    a. Incorrectly positioned anode notches
    b. Plugged overflow ports
4. Non-level stack
5. Leaking cathode/membrane assembly
6. Loose electrical connections
7. Plugged feed manifold
8. Plugged air manifold

Table G-5

Expected Ranges for Performance Monitor Readings

Meter No.	Position No.	Function	Expected Range, % of Scale
1	1	Blower motor current	10-20
	2	Pump motor current	20-40
	3	Fan motor current	20-30
	4	Methanol addition valve motor current	10-40
	5	Water addition valve motor current	10-40
	6	STANDBY current (load on Hg batteries)	10-30
2	1	Blower motor voltage	40-50
	2	Pump motor voltage	10-40
	3	Fan motor voltage	40-50
	4	Methanol addition valve motor voltage: Opening	40-60
	5	Same Closing	40-60
	6	Stack voltage	0-100
3	1	Methanol analyzer cell voltage	75-85
	2	Methanol analyzer concentration voltage	70-80
	3	Methanol analyzer attenuated concentration voltage	70-80
	4	Hydrometer float position detector: Upper Coil	Rest 20-40 Activated 65-80
	5	Same Lower Coil	Rest 20-40 Activated 50-85
	6	Water addition valve action detector: Closing	5-20
		Closed	50-80
4	1,2,3,4	Anode polarization	10-50
	5,6,7,8	Temperature	10-100

APPENDIX G-17

INITIAL PERFORMANCE OF INTEGRATED BATTERY SYSTEM

Maximum Cell Temp, °C	Stack Performance[1]			Regulated Output		
	Current, amps	Potential, volts	Power, watts	Current, amps	Potential, volts	Power, watts
54	0.6	12.2	7	0	6.1	0
54	3.4	10.4	35	2.7	6.1	16
68	3.4	11.4	39	2.7	6.1	16
55	6.8	9.0	61	6.0	6.1	36
58	10.2	8.3	84	9.3	6.1	57
62	12.3	7.9	97	11.8	6.0	71
69	12.3	8.1	99	11.8	6.0	71
--	14.1	7.0	99	13.3	6.0	82
64	16.0	7.0	113	14.7	5.9	86

(1) Integrated process system, electronics mounted external to unit. Short duration runs only.

APPENDIX G-18

CELL VOLTAGE DISTRIBUTION IN TWENTY CELL STACK

Cell No.	Cell Potential at Indicated ma/cm^2, volts[1]	
	13	38
1	0.51	0.40
2	0.48	0.32
3	0.50	0.39
4	0.52	0.40
5	0.52	0.40
6	0.55	0.41
7	0.52	0.40
8	0.53	0.39
9	0.50	0.36
10	0.52	0.34
11	0.50	0.38
12	0.53	0.37
13	0.52	0.40
14	0.51	0.37
15	0.52	0.38
16	0.49	0.36
17	0.53	0.41
18	0.54	0.42
19	0.51	0.38
20	0.46	0.24

(1) Run 66-1-18, integrated system, temperature distribution:

Cell 6	67°C
Cell 10	62°C
Cell 12	58°C
Stack Exhaust	58°C
Final Air Exhaust	34°C

APPENDIX G-19

PERFORMANCE OF ASSEMBLED BATTERY DEMONSTRATOR

Stack Performance[1]			Regulated Output		
Current, amps	Potential, volts	Power, watts	Current, amps	Potential, volts	Power, watts
0.6	10.5	6	--	6.0	--
7.0	8.5	60	--	6.0	--
10.0	7.9	79	--	6.0	--
11.4	7.4	87	10.9	6.0	65
14.1	6.6	93	13.0	5.6[2]	72

(1) Completely integrated system. Cells 19 and 20 connected in parallel electrically. Performance not stable with time.

(2) Off regulation.

Unclassified
Security Classification

DOCUMENT CONTROL DATA - R&D

(Security classification of title, body of abstract and indexing annotation must be entered when the overall report is classified)

1. ORIGINATING ACTIVITY (Corporate author)	2a. REPORT SECURITY CLASSIFICATION
Esso Research and Engineering Company Process Research Division Linden, New Jersey	Unclassified
	2b GROUP

3. REPORT TITLE

HYDROCARBON-AIR FUEL CELL

4. DESCRIPTIVE NOTES *(Type of report and inclusive dates)*

Semi-Annual - 1 July 1965 - 31 December 1965

5. AUTHOR(S) *(Last name, first name, initial)* Heath, Carl E.; Horowitz, Hugh H.; Tarmy, Barry L.; Morrell, Charles E.; Wilson, James A.; Asher, William J.; Beltzer, Morton, Broyde, Barret; Ciprios, George; Feng, I-Ming; Lieberman, Martin; Matsen, John M.; Okrent, Eugene H.; Shropshire, Joseph A.; Vickers, Herbert H.; Vogelfanger, Elliot A.; Zimmerman, Abraham A.

6. REPORT DATE	7a. TOTAL NO. OF PAGES	7b. NO. OF REFS
June 1966	255	21

8a. CONTRACT OR GRANT NO.	9a. ORIGINATOR'S REPORT NUMBER(S)
DA 36-039 AMC-03743(E) b. [redacted] AMC Code: 7900.21.903.01.00 c. d.	Report No. 8
	9b. OTHER REPORT NO(S) *(Any other numbers that may be assigned this report)*

10. AVAILABILITY/LIMITATION NOTICES

Distribution of this document is unlimited.

11. SUPPLEMENTARY NOTES	12. SPONSORING MILITARY ACTIVITY
	Commanding General U.S. Army Electronics Command Fort Monmouth, N.J. ATTN: AMSEL-KL-PB

13. ABSTRACT

Task A, Hydrocarbon Electrode

Work on the direct hydrocarbon electrode has continued to concentrate on studies of mechanism, catalysis and structure, aimed at improving the utilization of platinum or finding non-noble substitutes for it.

The mechanism studies were based on the finding during the previous period that the adsorption of saturated hydrocarbons occurred only on one of the two types of sites on the surface of platinum. Researchers at Baylor University had reported that it was possible to vary the ratio of the two types of sites by electrodepositing platinum from solutions containing different amounts of lead acetate. However, attempts to repeat this here produced no obvious effects on the relative sizes of the hydrogen peaks corresponding to the two types of sites in voltammetric scans. The total number of sites did vary, and the amount of butane adsorbed varied correspondingly. The ratios of the hydrogen, oxygen and butane peaks on the different electrodeposited blacks changed in a complex manner, but no pronounced advantage was found for any of the catalysts. More work would have to be done to learn how to vary the two kinds of sites and what affect this would have on butane performance.

Butane adsorption measurements were also made in phosphoric acid at 140° to determine whether the higher temperatures might not lead to stronger adsorption. It was found that adsorbed butane did cover a higher fraction of the sites available to hydrogen at the higher temperature. It was also more difficult to desorb by

(Continued on Attached Sheet)

DD FORM 1 JAN 64 1473

Unclassified
Security Classification

14. KEY WORDS	LINK A		LINK B		LINK C	
	ROLE	WT	ROLE	WT	ROLE	WT
Hydrocarbon Oxidation						
Adsorption Mechanism						
Catalyst Utilization						
Electrochemical Activity						
Non-Noble Catalysts						
Stability						
Single and Multicells						
Buffer Electrolytes						
Limiting Currents						
Noble Metal Alloy Catalysts						
Electrode Structure						
Catalyst Supports						
Auxiliary Fuel Cell Components						
Self-Sustained Operation						
Prototype Units						

INSTRUCTIONS

1. **ORIGINATING ACTIVITY:** Enter the name and address of the contractor, subcontractor, grantee, Department of Defense activity or other organization *(corporate author)* issuing the report.

2*a*. **REPORT SECURITY CLASSIFICATION:** Enter the overall security classification of the report. Indicate whether "Restricted Data" is included. Marking is to be in accordance with appropriate security regulations.

2*b*. **GROUP:** Automatic downgrading is specified in DoD Directive 5200.10 and Armed Forces Industrial Manual. Enter the group number. Also, when applicable, show that optional markings have been used for Group 3 and Group 4 as authorized.

3. **REPORT TITLE:** Enter the complete report title in all capital letters. Titles in all cases should be unclassified. If a meaningful title cannot be selected without classification, show title classification in all capitals in parenthesis immediately following the title.

4. **DESCRIPTIVE NOTES:** If appropriate, enter the type of report, e.g., interim, progress, summary, annual, or final. Give the inclusive dates when a specific reporting period is covered.

5. **AUTHOR(S):** Enter the name(s) of author(s) as shown on or in the report. Enter last name, first name, middle initial. If military, show rank and branch of service. The name of the principal author is an absolute minimum requirement.

6. **REPORT DATE:** Enter the date of the report as day, month, year; or month, year. If more than one date appears on the report, use date of publication.

7*a*. **TOTAL NUMBER OF PAGES:** The total page count should follow normal pagination procedures, i.e., enter the number of pages containing information.

7*b*. **NUMBER OF REFERENCES:** Enter the total number of references cited in the report.

8*a*. **CONTRACT OR GRANT NUMBER:** If appropriate, enter the applicable number of the contract or grant under which the report was written.

8*b*, 8*c*, & 8*d*. **PROJECT NUMBER:** Enter the appropriate military department identification, such as project number, subproject number, system numbers, task number, etc.

9*a*. **ORIGINATOR'S REPORT NUMBER(S):** Enter the official report number by which the document will be identified and controlled by the originating activity. This number must be unique to this report.

9*b*. **OTHER REPORT NUMBER(S):** If the report has been assigned any other report numbers *(either by the originator or by the sponsor)*, also enter this number(s).

10. **AVAILABILITY/LIMITATION NOTICES:** Enter any limitations on further dissemination of the report, other than those imposed by security classification, using standard statements such as:

(1) "Qualified requesters may obtain copies of this report from DDC."

(2) "Foreign announcement and dissemination of this report by DDC is not authorized."

(3) "U. S. Government agencies may obtain copies of this report directly from DDC. Other qualified DDC users shall request through _____."

(4) "U. S. military agencies may obtain copies of this report directly from DDC. Other qualified users shall request through _____."

(5) "All distribution of this report is controlled. Qualified DDC users shall request through _____."

If the report has been furnished to the Office of Technical Services, Department of Commerce, for sale to the public, indicate this fact and enter the price, if known.

11. **SUPPLEMENTARY NOTES:** Use for additional explanatory notes.

12. **SPONSORING MILITARY ACTIVITY:** Enter the name of the departmental project office or laboratory sponsoring *(paying for)* the research and development. Include address.

13. **ABSTRACT:** Enter an abstract giving a brief and factual summary of the document indicative of the report, even though it may also appear elsewhere in the body of the technical report. If additional space is required, a continuation sheet shall be attached.

It is highly desirable that the abstract of classified reports be unclassified. Each paragraph of the abstract shall end with an indication of the military security classification of the information in the paragraph, represented as *(TS)*, *(S)*, *(C)*, *or (U)*.

There is no limitation on the length of the abstract. However, the suggested length is from 150 to 225 words.

14. **KEY WORDS:** Key words are technically meaningful terms or short phrases that characterize a report and may be used as index entries for cataloging the report. Key words must be selected so that no security classification is required. Idenfiers, such as equipment model designation, trade name, military project code name, geographic location, may be used as key words but will be followed by an indication of technical context. The assignment of links, rules, and weights is optional.

BLANK PAGE

cathodization than it was at 80-90°C. These results explain why butane has poorer open circuit values but higher limiting currents in hot phosphoric acid than in sulfuric acid at the lower temperature: the butane adsorbs more strongly at the higher temperature but blocks some of the sites otherwise available for water discharge. Measurements of actual adsorption rates in hot phosphoric acid have not yet been successful, however.

The program to improve the utilization of platinum by using a support made considerable progress during this period. Butane limiting currents as high as 40 ma per mg of platinum were achieved at 150°C using a support of carbon treated with silica. Platinum black or platinum on untreated carbon gave only about 8 ma/mg under the same conditions. Part of the improvement was due to the impregnation procedure, which involves adsorption by the carbon of a surprisingly small amount of the platinum in the impregnating solution. Another factor was the silica content of the carbon, which was optimum at ten percent. The surface area of the carbon was also important since adsorption is being relied upon to implant the platinum. A low surface area carbon yielded a low activity catalyst. When oxidized with CO_2, however, the surface area increased, the platinum uptake rose and the catalytic activity improved. Raising the operating temperature to 190° increased the limiting current to over 80 ma/mg of platinum. Overall a tenfold improvement has been achieved, thus making the outlook for this program bright.

Some work was also done on the structure or fabrication of platinum black electrodes for use on liquid hydrocarbons, although most of the effort available had to be devoted to preparation of a demonstration cell stack. Fuel transport through decane electrodes is a recurring problem. The rate of fuel transport was found to be independent of the activity of the electrode, varied by changing the Teflon sintering conditions. Thus, it is hoped to be able to reduce fuel transport without adversely affecting performance. Another structure problem had to do with separation of the fuel side Teflon barrier used to prevent fuel flooding. This problem was solved by finding a means of laminating a 3.5 mil porous Teflon film to the electrode without collapsing thepores. Variability in the quality of Teflon emulsion is a structural problem which remains to be faced in the future.

The non-noble catalyst program featured alloys, oxides, carbides and steam reforming catalysts. The alloy program concentrated on the development of a method for producing high surface area metals, which were truly alloyed in the sense of having altered lattice spacings in their X-ray patterns. A chemical reduction technique was found to be unsatisfactory as were initial attempts at making Raney alloys. After extraction of the aluminum the residues were found to be mixtures of the unalloyed metals or their oxides. However, true high surface area alloys could be prepared by annealing the Raney alloy, before extraction at a temperature at which the binary phase diagram indicates a solid solution or intermetallic compound, and then quenching in water to retain the alloy in a metastable condition. While some of the alloys are active with hydrogen, none so far has shown activity on hydrocarbons. The method, however, appears to be very promising for future use.

In the oxide program the work on perovskites has been concluded and attention has been directed toward the closely related tungsten bronzes. Perovskites containing nickel and cobalt had been rendered conductive via the incorporation of vacancies in the oxide positions of the lattice. This conductivity, however, was lost rapidly on acid treatment. By analogy with the conductivity of lithiated nickel oxide, it was concluded that the conductivity of oxide deficient perovskites was due to oxidized species such as Co^{+++} which are known to be much less stable than the divalent ions. Hence the rapid conductivity loss as the unstable ions are extracted. Elements with more stable higher valence states such as manganese and chronium would be expected to form perovskites whose conductivity was acid stable. This proved to be the case. A good combination of acid stability and corrosion resistance was obtained with chromium and manganese perovskites. However, no catalytic activity toward hydrogen, oxygen, or hydrocarbons could be detected.

An attempt was made, therefore, to use achieve conductivity using the lower-than-normal valence states of the element molybdenum. However, there is apparently too little overlap between molybdenum orbitals in the perovskite struture. Satisfactory conductivity was not achieved and the approach was dropped.

The bronzes, however, look much more promising. These materials, utilizing the lower valence states of tungsten ina perovskite-like structure, are very acid resistant and have metallic conductivity. Unmodified they have no catalytic activity. It has been found possible to incorporate nickel into them, with some sacrifice in conductivity and acid stability, but with generally with a good combination of properties. The X-ray diagrams of these materials were extremely complex, indicating both mixed bronze phases and impurities. Therefore, improved compositions or means of preparation will have to be developed before an accurate assessment of their potential is possible. So far they have shown no catalytic activity, but only Ni^{++} ions have been incorporated. These do not have the d-10 configuration, which appears desirable for catalytic activity.

Mixed transition metal carbides are being investigated as fuel cell catalysts because they are more metallic in nature than the oxides, are highly conductive and in certain cases are corrosion resistant. It was first verified that commercially available grinding tool carbides were not catalytic, and that some "H" phase carbides available at the University of Pennsylvania, and other simple carbides were not corrosion resistant. However, the so-called eta carbides appeared much more interesting. These combine group V and VI metals, which yield acid resistant carbides, and the first row transition elements into single phase carbides. A purchased sample of nickel-tungsten-carbide proved to be very impure, but the nickel in the actual eta phase was resistant to acid. Various apparatus are being set up to custom make these compounds at the desired compositions, stoichiometries and degrees of purity. It appears that a vacuum-induction furnace with a water cooled shield will be required.

Abstract (DA 36-039 AMC-03743(E)) (Contd)

Some time ago a means was found for fabricating non-noble steam reforming catalysts into conductive electrodes. These were active with hydrogen fuel but not with hydrocarbons. It was hypothesized that the presence of the reactants in the liquid phase might have inhibited the steam reforming function of the catalyst. To test this hypothesis steam reforming runs were carried out non-electrochemically in a pressure reactor, where the reactants, hexane or decane and water, could be main- in the liquid phase. Appreciable activity was obtained, limited only by diffusion rates. Thus, the presence of the reactants in the liquid phase did not damage the electrochemical performance of the catalysts. The presence of ions or the lower pressure must have been responsible.

Task B, Hydrocarbon Fuel Cell

Total cell studies were conducted to assess the engineering feasibility and system requirements of a direct liquid fuel-air fuel cell system. A liquid decane-air fuel cell was constructed with sufficient capability to allow evaluation of anticipated problem areas related to fuel transport and carbon dioxide rejection in the electrolyte space.

Tests in small (10 cm^2) single and multicell units indicated that cathode cracking and anode barrier separation could limit stack life. However, this problem was solved by laminating porous Teflon film directly to the sintered platinum-Teflon electrodes. Satisfactory life and performance were thus obtained. Unfortunately, chemical oxidation and cathode deterioration due to decane transport was observed in some multicell units. In addition, the small cell tests indicated a need for improved electrolyte venting to minimize carbon dioxide buildup and reduce cell resistive losses. Despite these problems, performance levels were quite satisfactory yielding 17-21 mw/cm^2 and 14-17 mw/cm^2 on oxygen and air respectively.

Based upon the information developed in the small scale cell tests a large (80 cm^2) five cell liquid decane-air multicell assembly and operating system was designed and constructed. Initial oxygen performance with Cyanamid AA-1 cathodes laminated to porous Teflon film agreed with that obtained in small cells. However, air performance showed an 80 mv debit due to decane transport to the cathode and system life was limited. Improvements in performance and life were obtained by using laminated porous Teflon film on sintered platinum-Teflon anodes and cathodes. A three cell assembly with these improved components has been run for over 400 hours. This same three cell assembly was run on a wide boiling range isoparaffinic jet fuel, yielding only about one third the liquid decane activity.

Task C, New Systems

The new systems effort has concentrated on intermediate temperature and buffer electrolytes, catalysts for buffer electrolytes and the catalyst-electrolyte slurry system.

Abstract (DA 36-039 AMC-03743(E)) (Contd)

The intermediate temperature electrolytes examined were pyrophosphoric and molten bisulfate mixtures. Work with low catalyst content electrodes in pyrophosphoric acid at 275°C has shown that high catalyst utilizations can be obtained. Butane could sustain 200 ma/cm^2 at 0.44 volts polarized, and oxygen, 500 ma/cm^2 at 0.38 volts polarized, on electrodes containing 5 mg/cm^2 of platinum. These activities are considerably greater than that attained by the equivalent electrode structures in 85% phosphoric acid at 150°C. The usefulness of an electrolyte that can operate at higher temperatures as a means of effecting higher catalyst utilizations has thus been demonstrated. Electrodes of still lower catalyst content, 2.5 mg/cm^2, exhibited a disproportionate activity decrease due to structural problems. It is anticipated that when suitable low catalyst density electrode structures are available, still further catalyst utilizations will be obtained using pyrophosphoric acid.

Molten alkali metal bisulfate electrolytes were studied to ascertain whether a system operating in the same temperature range as pyrophosphoric, but not as corrosive, was available. Hydrocarbon and oxygen activities in this medium on massive platinum electrodes were considerably lower than that obtained in pyrophosphoric acid. In addition, the electrolyte was not invariant, losing SO_3 at high temperatures and generating H_2S at reducing potentials. Molten salt fuel cell electrolytes must have anions which equilibrate with non-volatile and non-reducible oxides.

Silver cathodes exhibit appreciable activity in carbonate solutions, but the activity decreases with decreasing pH. A study was carried out to determine whether a carbonate solution could be kept above its equilibrium pH value when used as the electrolyte in a fuel cell where CO_2 is an anodic oxidation product. It was shown that carbon dioxide rejection from a carbonate solution into a flowing gas stream, such as would be available in an air electrode, was too slow to prevent rapid carbonation and return to the equilibrium pH.

Silver-palladium oxide catalyzed electrodes exhibited considerable activity on methanol in potassium hydroxide and potassium carbonate solutions. Limiting currents over 2000 ma/cm^2 were observed. Even butane showed evidence of some activity at these highly alkaline pH values. Raney gold and gold alloys were also shown to have some methanol activity in potassium hydroxide.

Further work with the slurry electrode system has shown that considerable performance improvement could be achieved with decane fuel by increasing the ratio of electrode area to volume and by improving the flow pattern. However, while the current density of the electrode was very high, the specific current density in ma/mg of catalyst was still so low that it is doubtful that catalyst utilizations better than that achieved in static systems could be obtained.

Abstract (DA 36-039-AMC-03743(E)) (Contd)

Task D, Methanol Electrode

Studies on the methanol electrode were continued, concentrating on further establishing the degree of stability and reliability of the ruthenium modified P-type catalyst, and on determining whether catalyst supports could be used to improve catalyst utilization. Single cell and half cell testing of the catalyst was completed. Anodes were tested for as long as 11,000 hours with non-recoverable losses of only 15 mv. In addition, reversible performance losses in cell performance ranging from 10 to 50 mv were found. These were recoverable by open circuiting the cell, changing the electrolyte, and/or overpolarizing the anode in the absence of methanol to 0.8 to 0.9 volts. Storage would not impair performance. However, copper was found to be an undesirable contaminant.

New techniques were developed for employing supports to effect reductions in catalyst loadings. Both silica-on-carbon and boron carbide were tested as supports. Catalyst utilization using the silica-on-carbon support amounted to only 0.12 ma/mg at 0.35 volts polarization. Studies of the impaired performance indicated a need to develop new washing procedures. Catalyst utilizations of 4.7 ma/mg were obtained using boron carbide as a support. Increasing the reduction temperature improved performance, with the best utilization obtained with hydrogen reduction at 225°C. Further improvements may be possible through changes in procedures for making the catalyst.

Task E, Air Electrode

Testing has continued on the development of cathode structures for methanol cells that do not require membrane backings to prevent gross water transport. Experiments were carried out using cathodes that were spray-coated with Teflon on the air side, to evaluate the performance during extended operation, and the effects of scaling them to practical sizes. It was found that these coated electrodes, when not heat-treated would operate for about 900 hours with unimpaired performance. Furthermore, large 7.5 inch diameter electrodes could be prepared with performances comparable to the smaller 1 inch diameter electrodes. However, the electrodes leak electrolyte at small, but still unacceptably high, rates. As an alternative approach, sodium alginate was evaluated as a membrane substitute. Its performance in small electrodes was at least comparable to the conventional cathode. But scaled-up electrodes were 0.1 volt more polarized and also leaked. Thus, more work remains.

Research was also carried out on cathodes suitable for use in the hydrocarbon cell at 150°C in 14.7 M phosphoric acid. Several cathodes were developed. These included 50 and 10 mg/cm^2 sintered platinum-Teflon electrodes laminated to 3.5 mil porous Teflon films, and a carbon supported cathode containing 2.5 mg/cm^2 platinum. The electrode with the highest catalyst loading was polarized only 0.30 volt at 100 ma/cm^2. The 10 and 2.5 mg/cm^2 cathodes exhibit additional 70 and 160 mv polarizations, respectively. In addition, a high performance cathode using the silica-on-carbon support and containing only 1 mg/cm^2 of platinum presently is under test. This electrode exhibits over four times the catalyst utilization of the above mentioned electrodes.

Abstract (DA 36-039 AMC-03743(E)) (Contd)

Task F, Methanol Fuel Cell

Because of the high chemical oxidation rates occurring at the cathode in the 9" x 5-3/4" cells, further studies were carried out on techniques for reducing this loss. Dacron felt and Permaplex C-20 membrane barriers, installed between the electrodes in 4" x 4" half-cells and total cells, were found to substantially reduce chemical oxidation at the cathode. Performance was also improved. However, no improvements were obtained in the 9" x 5-3/4" cells using the same techniques. Baffling the anode chamber and the use of multiple injection ports were also tested in the 9" x 5-3/4" cell because this cell was not able to operate at low methanol concentrations at performance comparable to those obtained in 4" x 4" cells. However, no significant improvements were obtained.

A simplified cell was also tested using a wicking system to supply fuel, and natural breathing to supply air. The cell operated virtually unattended for 3000 hours. Thus, simplified cell operation without electrolyte circulation is feasible.

Task G, Prototype Development

A self-contained Methanol Fuel Cell Battery Demonstrator was designed, constructed, and tested briefly prior to delivery to the U.S. Army Electronics Command. Miniaturized, automatically controlled devices were developed to provide the essential auxiliary facilities required by the fuel cell module, with low parasitic power consumption. These include a corrosion-free high output pump for circulating sulfuric acid electrolyte, a low pressure drop system for supplying ambient air, facilities to provide adequate heat removal and recovery of product water and a simple acid concentration detector and controller. Also included was a methanol concentration controller to ensure an optimum addition rate of methanol. Power levels of about 80 watts at 6.0 volts regulated output were obtained during initial short-term testing of the integrated system. Subsequent testing of the fully-assembled Demonstrator gave power levels of 65 watts, but performance was not consistent, due to instability of the methanol control system. (Author)